Removal of Polycyclic Aromatic Hydrocarbons (PAHs) from Contaminated Media Using Magnetized Activated Carbon Composites

Ehsan Mirzaee

A thesis submitted to the University of Ottawa in partial fulfillment of the requirements for the Doctorate in Philosophy degree in Civil Engineering

Department of Civil Engineering
Faculty of Engineering
University of Ottawa

© Ehsan Mirzaee, Ottawa, Canada, 2022

Abstract

Among current technologies used for the treatment of polycyclic aromatic hydrocarbons (PAHs) -contaminated media, adsorption has been reported to offer relatively high PAH removal efficiency while being rapid and cost-effective. Therefore, the main goal of this research was to assess and optimize the adsorption process for the removal of PAHs from contaminated water and soil using recoverable magnetic activated carbon-based composites.

In the first phase, 6 different composites, 3 magnetic powder activated carbon (MPAC) composites and 3 magnetic granular activated carbon (MGAC) composites, were synthesized, and then, characterized using XRD, FE-SEM, EDS, and FTIR methods. The adsorption experiments revealed that all the recoverable MPACs and MGACs were capable of removing the PAHs from water, with removal percentages ranging from 87.2 to 99.3%. The PAH-loaded MPAC and MGAC with the highest PAH removal efficiency were also subjected to a series of desorption studies. The results indicated that the PAHs desorption was in the range 38.1-60.1% for low molecular weight (LMW) PAHs and 23.4 to 57.2% for the high molecular weight (HMW) PAHs.

In the second phase, the adsorption kinetics and isotherms studies were performed on MPAC synthesized by a precipitation (MPAC-Prec.) method, which showed the highest PAH removal efficiency among the prepared magnetic activated carbons (MACs). The PAHs adsorption by MPAC-Prec. was rapid, reaching equilibrium in 6 h with the removal efficiency ranging from 95.6 to 100.0% under the conditions of this study. Among the studied kinetics models, pseudo-second order fitted the experimental data very well, implying that all the MPAC adsorption sites had an equal affinity for PAHs. The results of the kinetic studies also indicated that the greater molecular weight PAHs had a slower adsorption rate due to the slower transfer of their molecules to the MPAC adsorption sites. With an R^2 in the range 0.73-0.96, the Langmuir model described the isotherms adsorption of LMW and HMW PAHs better than the other isotherms models. Furthermore, according to the Langmuir model, the maximum adsorption capacity of MPAC-Prec. was determined to be between 8.7 and 11.4 µg/mg for the LMW PAHs, and 8.4 and 20.2 µg/mg for the HMW PAHs.

In the third phase, a series of soil washing tests using MGAC synthesized by co-precipitation (MGAC-CoP) method, were carried out to explore the effect of MAC on the PAHs removal from soil. The employed MGAC was the second most efficient MAC in the PAHs adsorption experiments (first phase of research), and it showed greater recovery from soil washing mixture

compared to the MPAC-Prec. in the preliminary tests. The MGAC-CoP composite had a surface area and total pore volume of 837.9 m^2/g and 0.5 cm^3/g, respectively, which were approximately 10% lower than the bare GAC, according to BET test results. Soil washing parameters were optimized for the treatment of a real contaminated soil, which were MGAC-CoP dose of 2% (w/w), washing time of 24 h, liquid to soil ratio of 15:1, stirring speed of 100 rpm, pH of 8.3, and temperature of 25 ˚C. Under these optimized conditions, an average PAHs removal of 47.4% was obtained. Among the LMW and HMW PAHs, anthracene (ANT), and fluoranthene (FLUO) showed the highest affinity to MGAC during the treatment process, with 57.7% and 67.1% removal from soil, respectively. The thermodynamic studies revealed that the adsorption of the LMW and HMW PAHs onto MGAC in soil washing was non-spontaneous and endothermic as the values of Gibbs free energy ($\Delta G^\circ>0$) and Enthalpy change ($\Delta H^\circ>0$) were positive.

In the fourth phase, the efficiency of MGAC-CoP in surfactant-enhanced soil washing for the PAH removal and the recovery of the surfactant solution was studied. The effective parameters of soil washing with the surfactant (Tween 80) were assessed using a real contaminated soil sample, and the results showed that 5% Tween 80, a liquid to soil ratio of 10:1, and a 72-hour washing time at 20°C were optimum operating conditions. Under these conditions, the average PAHs removal efficiency was 67.6%, which was higher than the 47.4% obtained for the same soil with no surfactant addition in phase 3. The possibility of recycling and reusing the Tween 80 solution was investigated by adding MGAC-CoP to the soil and surfactant solution mixture during the soil washing process. For this purpose, 5% Tween 80 and 2% (w/w) MGAC were used in 7 successive washing cycles, with no regeneration process for the MGAC composite. The results revealed that the combination of surfactant and MGAC was capable of removing 68.6, 70.7, 70.3, 61.6, 55.5, 50.2, and 39.4% of the PAHs from soil in the 7 washing cycles, respectively. Furthermore, the recycled Tween 80 and non-regenerated MGAC did not produce any waste or effluent after 6 times reuse in the treatment process, while successfully recovered and reused. This implies that soil washing with Tween 80 and MGAC is a very affordable, efficient, and practical method for remediation of PAH-contaminated soils.

Keywords: Magnetic activated carbon composites; polycyclic aromatic hydrocarbons; adsorption models; soil washing, surfactant-enhanced soil washing.

Dedication

To my dear parents, Fatemeh and Ayoub

&

My beloved wife, Reyhaneh

Acknowledgement

It is an honour for me to thank those who made this thesis possible, and words fail to appreciate them in the way they should be. First and foremost, I would like to express my sincere gratitude and deepest appreciation to my supervisor Prof. Majid Sartaj for his valuable supervision, contribution and advice. The completion of this thesis would not have been possible without his encouragement, invaluable suggestions and continuous support throughout this research program. My thanks are also extended to the technical officer of the environmental engineering laboratory, Patrick M. D'Aoust, Andrew Sluiter (Environment Canada), Keith Holmes (Golder Associates Inc.), the materials characterization facility manager in the catalyst center of the University of Ottawa, Dr. Yun Liu, for their support and technical assistance. I would like to acknowledge Dr. Ataollah Babakhani and my other friends and colleagues in the Department of Civil Engineering at the University of Ottawa for their help. Finally, my highest appreciation goes to my family for their endless encouragement, especially my dear parents, Fatemeh and Ayoub, for their unconditional love and support during all these years. Special thanks to my wife, Reyhaneh, who has always supported me with patience and encouragement during this long journey.

Table of Contents

List of Figures

List of Tables

Abbreviations

AC: Activated carbon

ACE: Acenaphthene

ACEP: acenaphthylene

ANT: Anthracene

B[a]A: Benz[a]anthracene

B[a]F: Benzo[b]fluoranthene

B[a]P: Benzo[a]pyrene

BET: Brunauer Emmett Teller

B[ghi]P: Benzo[ghi]perylene

B[k]F: Benzo[k]fluoranthene

CCME: Canadian Council of Ministers of the Environment

CHR: Chrysene,

D[a,h]A: Dibenz[a,h]anthracene

DOC: Dissolved organic carbon

D-R: Dubinin–Radushkevich

EDS: Energy-dispersive spectroscopy

EU: European Union

FE-SEM: Field emission scanning electron microscopy

FLU: Fluorene

FLUO: Fluoranthene

FTIR: Fourier transform infrared spectroscopy

GAC: Granular activated carbon

HPLC: High Performance Liquid Chromatography

HMW: High molecular weight

IARC: International Agency for Research on Cancer

IDP: Indeno[1,2,3-cd] pyrene

IEP: Isoelectric point

K-D: Kuderna-Danish

LMW: Low molecular weight

MAC: Magnetic activated carbon

MB: Methylene blue dye

MGAC: Magnetic Granular activated carbon

MPAC: Magnetic powder activated carbon

MO: Methyl orange

NAP: Naphthalene

PAC: Powder activated carbon

PAH: Polyaromatic (Polycyclic aromatic) hydrocarbon

PCB: Polychlorinated biphenyl

PHE: Phenanthrene

POM: Polyoxymethylene

PYR: Pyrene

R-P: Redlich-Peterson

SGE: Nano-sulfonated graphene

SOM: Soil organic matter

TCE: Trichloroethylene

USEPA: US Environmental Protection Agency

XRD: X-ray diffraction

1 Introduction

1.1 General background

The generation of various types of industrial waste has been dramatically elevated during recent decades, leading to the release of organic and inorganic pollutants into soil in large scale [1,2]. There is no doubt that the capacity of soil to cope with all these types of pollutants is limited. On the other hand, the governments' activities to control the release of pollutants from industry and to reduce, recycle, and dispose of all types of waste is not sufficient to protect soil. As a result, soil contamination has become a serious concern around the world.

One of the main sources that spread toxic and persistent organic contaminants into the environment is the petroleum industry. This could happen at oil extraction sites (e.g., offshore oil drilling), refineries, or transport activities [2–5]. There are also some point sources of contaminants that lead to soil pollution on small scale, such as accidental spill of petroleum products and leakage from old storage tanks [5,6]. These point sources have contaminated many commercial and industrial sites in North America, Europe, Russia, and the middle east [7]. For example, there are more than 1300 abandoned contaminated sites, designated as Superfund Sites, in the United States, in which the soil has been contaminated due to oil refinery activities [8]. Similar situations are found in the most populated provinces of Canada, such as Ontario and Quebec. The abandoned coal gas plants and oil refineries in sites categorized as Brownfields have released hazardous contaminants in the soil. Due to development of the metropolitan areas, rehabilitation of these contaminated sites has been considered by the local and federal governments during the past years [9].

Petroleum hydrocarbons found in gasoline, diesel, oil, lubricants, coal, bitumen, and many raw and refined fuels are classified as hazardous organic contaminants by many environmental protection agencies worldwide [10–13]. When soil becomes contaminated with petroleum hydrocarbons, it may then function as a secondary source distributing these contaminants in air, water, groundwater, and other natural resources [14]. According to a report published by the Canadian Council of Ministers of the Environment (CCME), petroleum hydrocarbons, such as polycyclic aromatic hydrocarbons (PAHs), are one of the most widespread groups of soil contaminants in Canada. In 2018, Environment Canada reported that the number of federal sites that are contaminated with PAHs, including different media from groundwater to sediments, has been increased to around 6800 sites (Figure 1.1) [15].

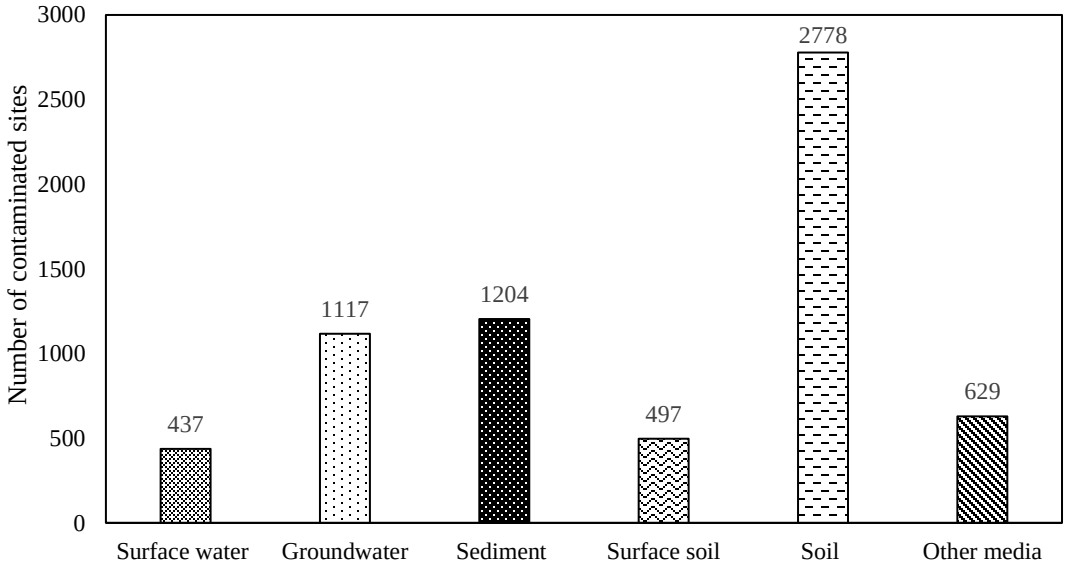

Figure 1.1. PAH-contaminated sites in Canada [15]

The U.S. Environmental Protection Agency (USEPA) considers PAHs as a class of prevalent persistent hydrocarbons that have contaminated many industrial sites across the United States [14,16,17]. PAHs are potentially carcinogenic, mutagenic or allergenic compounds to humans due to the interference with the function of cellular membranes as well as with enzyme systems of the membranes [16,18,19]. They consist of two or more fused benzenoid rings, being distributed in the environment by both human activities and natural resources [19–21]. The major anthropogenic sources of PAHs pollution are various petroleum or coal-derived products, vehicle exhaust, and industrial processes. The other important sources of PAHs are the incomplete combustion of organic material such as coal, oil and wood. PAHs can also be released naturally as a result of forest fires and volcanic eruptions. [14].

Table 1.1 shows the physical characteristics of sixteen PAHs classified as priority pollutants by USEPA (USEPA, 2008). The PAHs are often divided into two groups of low molecular weight (LMW) and high molecular weight (HMW) compounds. Naphthalene (NAP), acenaphthene (ACE), acenaphthylene (ACEN), fluorene (FLU), anthracene (ANT), and phenanthrene (PHE) are known as LMW PAHs, consisting of a core structure of two to three benzenoid rings, while HMW PAHs (fluoranthene (FLUO), benzo[a]pyrene (B[a]P), benzo[b]fluoranthene (B[b]F), pyrene (PYR), benz[a]anthracene (B[a]A), chrysene (CHR), Benzo[k]fluoranthene (B[k]F), benzo[ghi]perylene (B[ghi]P), indeno[1,2,3-cd]pyrene (IDP), and dibenz[a,h]anthracene D[a,h]A)

Table 1.1. Physical and chemical characteristics of the PAH compounds [22]

PAH compound	Structure	Molecular weight(g/mol)	Solubility 25◦ ($mg.dm^{-3}$)	Log K_{ow}	Vapor pressure (Pa)
NAP		128	32	2300	0.0492
ACE		154	3.4 at 25^0 C	21000	$10^{-3} – 10^{-2}$ at 20^0 C
ACEN		152	3.93	12000	$10^{-3} – 10^{-2}$ at 20^0 C
FLU	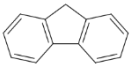	166	1.9	15000	$10^{-3} – 10^{-2}$ at 20^0 C
PHE	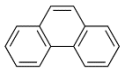	178	1-1.3 at 25^0 C	29000	6.8×10^{-4} at 20^0 C
ANT	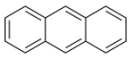	178	0.05-0.07 at 25^0 C	28000	2×10^{-4} at 20^0 C
FLUO	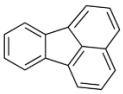	202	0.26 at 25^0 C	340000	$10^{-6} – 10^{-4}$ at 20^0 C
PYR	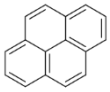	202	0.14 at 25^0 C	2×10^5	6.9×10^{-9} at 20^0 C
B[a]A*	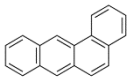	228	0.01 at 25^0 C	4×10^5	5×10^{-9} at 20^0 C
CHR*	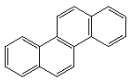	228	0.002 at 25^0 C	4×10^5	$10^{-11} – 10^{-6}$ at 20^0 C
(B[b]F)*	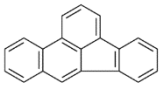	252	-	4×10^5	$10^{-11} – 10^{-6}$ at 20^0 C
(B[k]F)*	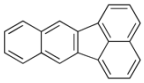	252	-	7×10^6	9.6×10^{-7} at 20^0 C
B[a]P*	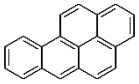	252	0.0038 at 25^0 C	10^6	5×10^{-9}
B[ghi]P		276	0.00026 at25^0 C	10^7	~10^{-9}
IDP*	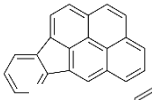	276	-	5×10^7	~10^{-10}
D [a,h]A*	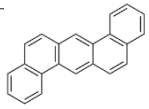	278	0.0005 at 25^0 C	10^6	~10^{-10}

Those indicated with an asterisk (*) are considered carcinogenic

comprise of molecular structures of four or more benzenoid rings [22]. According to Table 1.1, PAHs with higher molecular weight are more stable, lipophilic and hydrophobic than the LMW PAHs. This table also shows that the HMW PAHs are hardly soluble in water, leading them to be more acutely toxic to aquatic organisms and other creatures [14, 23, 24].

Considering the toxicity and carcinogenicity of PAHs, various treatment methods have been proposed to remove these organic compounds from the environment. These treatment methods could be physical, chemical, biological, or combined processes, and include incineration, soil washing/flushing, solvent extraction, soil vapor extraction, , chemical oxidation, bioremediation, and phytoremediation [18,23–26]. However, the application of many of these methods is restricted due to their low efficiency, high cost, water and energy consumption, and slow process [7,27]. For example, the chemical methods may produce some by-products of the PAHs during the treatment process that are more toxic than the PAH compounds themselves [4]. Biological technologies are known to be time-consuming and environmentally friendly. Furthermore, any change in the environmental conditions (e.g., temperature, pH, nutrient element, dissolved oxygen levels) may affect their ability to remove the contaminants from soil, making them operationally intensive [12,25,27,28].

Adsorption by carbon materials, such as activated carbon (AC), is one of the most frequently and cost-effective treatment methods that has been developed for the removal of a variety of contaminants, including PAHs, from the environment [29]. This method is safe, universal, easy to operate, and with no need to use high pressure and thermal energy inputs in the cleanup process [4]. The unique characteristics of AC that play a key role in the adsorption and removal of PAHs from contaminated media are high porosity and hydrophobicity, high specific surface area and activity, the presence of different functional groups on AC surface, thermal stability, high ions adsorption, and resistance against different acids and bases [30,31].

Several studies have reported the high removal efficiency of organic contaminants from the environment using only a few percent by weight of AC [32–36]. However, one of the disadvantages of using bare AC, either granular or powder type, in the adsorption process is that it cannot be readily retrieved from the soil matrix [37]. This issue may lead to the loss of some pollutant-loaded AC particles in the media, helping the pollutants to be released back into the environment [38]. To overcome this potential issue, magnetization of the adsorbent particles can be considered as a practical solution. During recent years, AC magnetization by stable iron oxides

(Fe_2O_3, Fe_3O_4, etc.) has been investigated by some researchers for removal of organic and inorganic pollutants such as petroleum hydrocarbons, arsenic, arsenate, dyes, etc., and most of them have obtained satisfactory results [18,38–45]. Taking advantage of the adsorption capacity of AC and the superparamagnetic properties of iron oxides, it will be possible to achieve high contaminant adsorption removal efficiencies by magnetic AC composite (MAC) as well as rapid recovery of the composite from media using a simple external magnetic field. The adsorption of PAHs by the MAC particles could provide a convenient, cost-effective, and efficient strategy for removing pollutants from water and soil environments that are in urgent need of treatment [41,46].

1.2 Research objectives

In recent years, the application of various types of adsorbents in treatment techniques has received increasing attention since they provide relatively high pollutant removal efficiencies while being fast and cost-effective. However, there are only a few studies on the efficiency of MACs to remove petroleum hydrocarbons, particularly PAHs, from the environment. The PAH compounds consist of extended aromatic rings with a high electronic density allowing them to form supramolecular complexes with complementary receptors such as carbon and graphene. Carbon particles possess strong adsorption capacity and are able to provide extensive hydrophobic surfaces, appropriate to establish noncovalent π–π interactions with the electron-rich aromatic rings of PAHs [47]. Although the carbon particles can be dispersed into the contaminated medium to adsorb target compounds, their recovery after the treatment is challenging. If iron oxide nanoparticles (e.g., Fe_2O_3 or Fe_3O_4) are placed into the pores and on the surface of carbon, their superparamagnetic ability will provide the adsorbent with a magnetic surface. This magnetization consequently increases the AC recovery and decreases the possibility of releasing the adsorbed PAHs back into the environment.

The current research project seeks to evaluate the magnetization of powder activated carbon (PAC) and granular activated carbon (GAC) and their application for the removal of LMW and HMW PAHs from aqueous solutions and aged contaminated soil samples. Various synthesis methods, including precipitation, hydrothermal, impregnation, ball milling, and microwave, have been applied by researchers to prepare iron oxide nanoparticles. Among these methods, precipitation, co-precipitation, and impregnation are known to be facile and effective methods, thus being considered for this study to fabricate the magnetite nanoparticles (Fe_3O_4) and attach them to the AC matrix.

To the author's knowledge, the present study is the first one that considers the application of MAC composites for the removal of PAHs in the adsorption and soil washing processes. Therefore, the objectives of this study are:

- To synthesize different MAC composites using PAC and GAC and three synthesis methods (six types of MAC in total) and evaluate them for PAHs adsorption from aqueous phase.
- To characterize the synthesized MACs using BET, XRD, SEM-EDS, and FTIR methods.
- To investigate desorption of the PAH analytes from the MAC particles and the possibility of the magnetic composites regeneration and reusability.
- To assess the adsorption uptake capacity of the MACs by different isotherm and kinetic models.
- To evaluate soil washing combined with adsorption using the MACs to remove PAHs from contaminated soil samples.
- To evaluate the effective parameters such as liquid/soil ratio, contact time, temperature, and adsorbent dosage to optimize the efficiency of the remediation process.
- To assess the performance of surfactant-enhanced soil washing (Tween 80) and its combination with adsorption using MAC in order to increase the removal efficiency of PAHs from the contaminated soil samples. The recycling and reuse of Tween 80 surfactant and MAC is assessed as well.

1.3 Importance and impact of the proposed research projects

The AC particles magnetized with nano-iron oxide combine the strong adsorption capacity of activated carbon and the superparamagnetic characteristic of the magnetic nanoparticles. MACs have recently been used to remove various types of organic and inorganic contaminants from the environment. However, there are still gaps in studying the application of these composites for the removal of PAHs from water and soil. The proposed research aims to address some of these knowledge gaps and existing challenges. This research will provide new findings on the application of MACs in PAHs removal processes. As such, the results of this research are expected to benefit the environment and be of great interest to environmental agencies, scientific community, decision-makers, consulting firms, and contractors looking for a reliable and effective treatment method to remove hazardous contaminants like PAHs from soil and natural resources.

1.4 Research hypothesises

Based on the literature review performed for this research (Chapter 2), the following hypotheses are made:

- AC has the potential to remove PAHs from contaminated soil and water; however, its adsorption capacity may be affected after magnetization.
- The synthesis method, the type of AC, and the size of MAC particles play an important role in the PAHs adsorption process.
- PAHs adsorption by MAC follows typical isotherm and kinetic models. Hence, its performance can be evaluated through adsorption isotherm experiments to determine the capacity of the magnetic adsorbent and the contact time required to remove the highest concentration of PAHs from contaminated media.
- It is expected that operational parameters such as pH and temperature influence PAHs removal efficiency from contaminated soil. The duration of the washing process (contact time), liquid to soil ratio, and dosage of MAC are other factors that might affect the removal of PAHs from soil.
- The use of surfactants in the soil washing process could offer the possibility of enhancing PAHs removal from the soil.

1.5 Research methodology

The flowchart in Figure 1.2 illustrates the four different experimental phases for this research project. The first phase contains the magnetization of PAC and GAC using three different synthesis methods. The characterization tests including BET, XRD, SEM-EDS, and FTIR will be performed on the synthesized MACs to evaluate their surface area, structure, morphology, and adsorption interactions, respectively. Afterward, PAHs uptake capacity of the MACs will be assessed through a series of batch adsorption experiments. In the second phase, the magnetic composite with the highest PAHs removal efficiency in phase one will be used in isotherms and kinetics experiments to determine its adsorption capacity and rate. The obtained results will then be evaluated by adsorption isotherm and kinetic models (e.g., Langmuir and Freundlich for adsorption isotherm data, and pseudo-first order and pseudo-second order models for kinetic experiments) to express and verify the type of PAHs adsorption mechanism by the MAC composite. In the next phase, the MAC particles will be employed in soil washing process to treat soil samples contaminated with PAHs. The effective parameters such as liquid/soil ratio (L:S), contact time, stirring speed, MAC dosage, temperature, and pH will be studied during the soil washing experiments. The combined

use of surfactant (Tween 80) and MAC will be considered for the soil washing process in the fourth phase to investigate the effect of the surfactant addition and the adsorbent for the removal of PAHs from soil and the soil washing effluent. The effective parameters of the surfactant-enhanced soil washing will also be optimized in this phase. In all four phases, the concentration of residual PAHs in the aqueous and soil samples will be analyzed by High Performance Liquid Chromatography (HPLC). The experimental setup for the assessment of PAHs removal from water and soil by powder and/or granular AC/Fe_3O_4 are schematically presented in Figure 1.3.

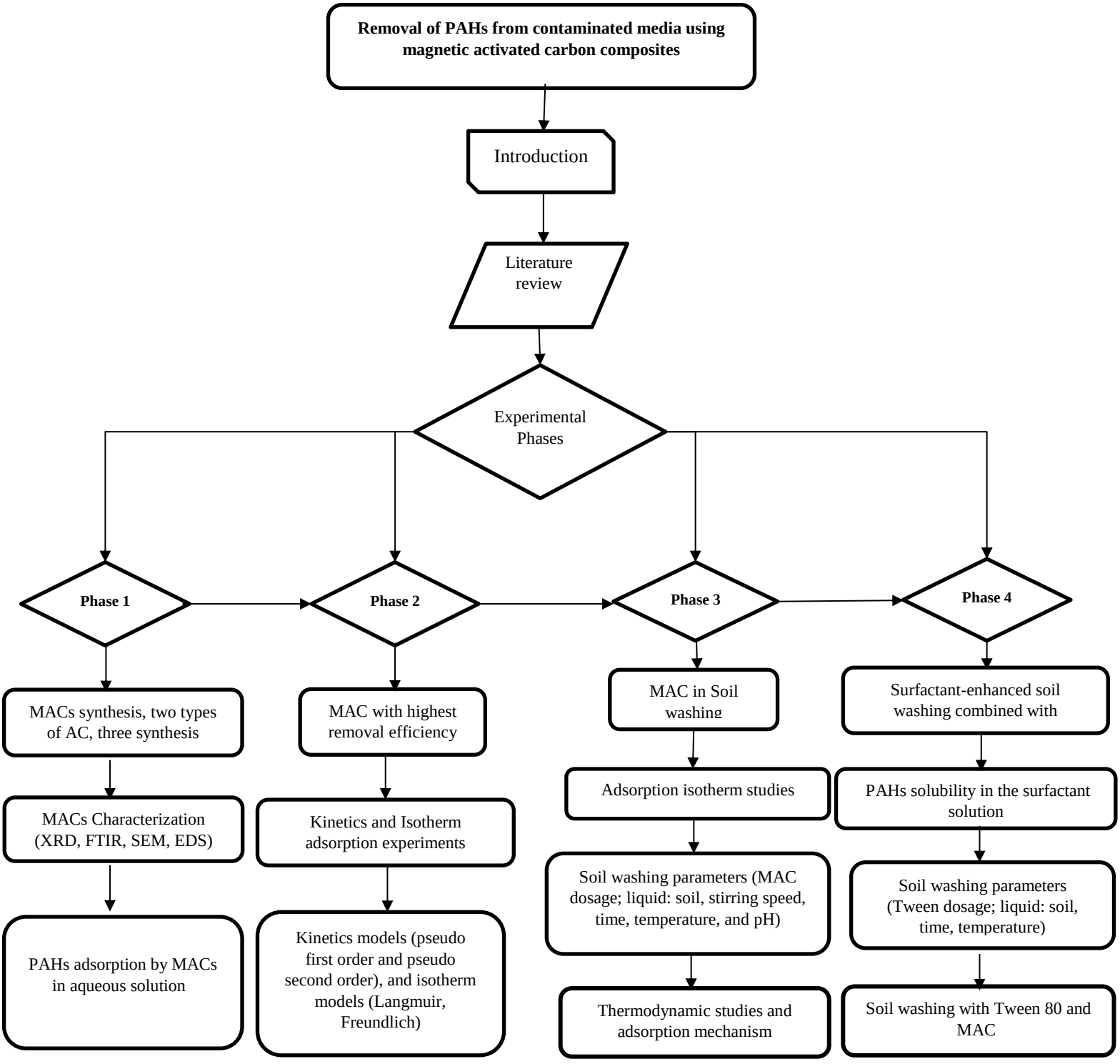

Figure 1.2. Research methodology and phases designed to evaluate the efficiency of MACs in removing PAHs from contaminated media

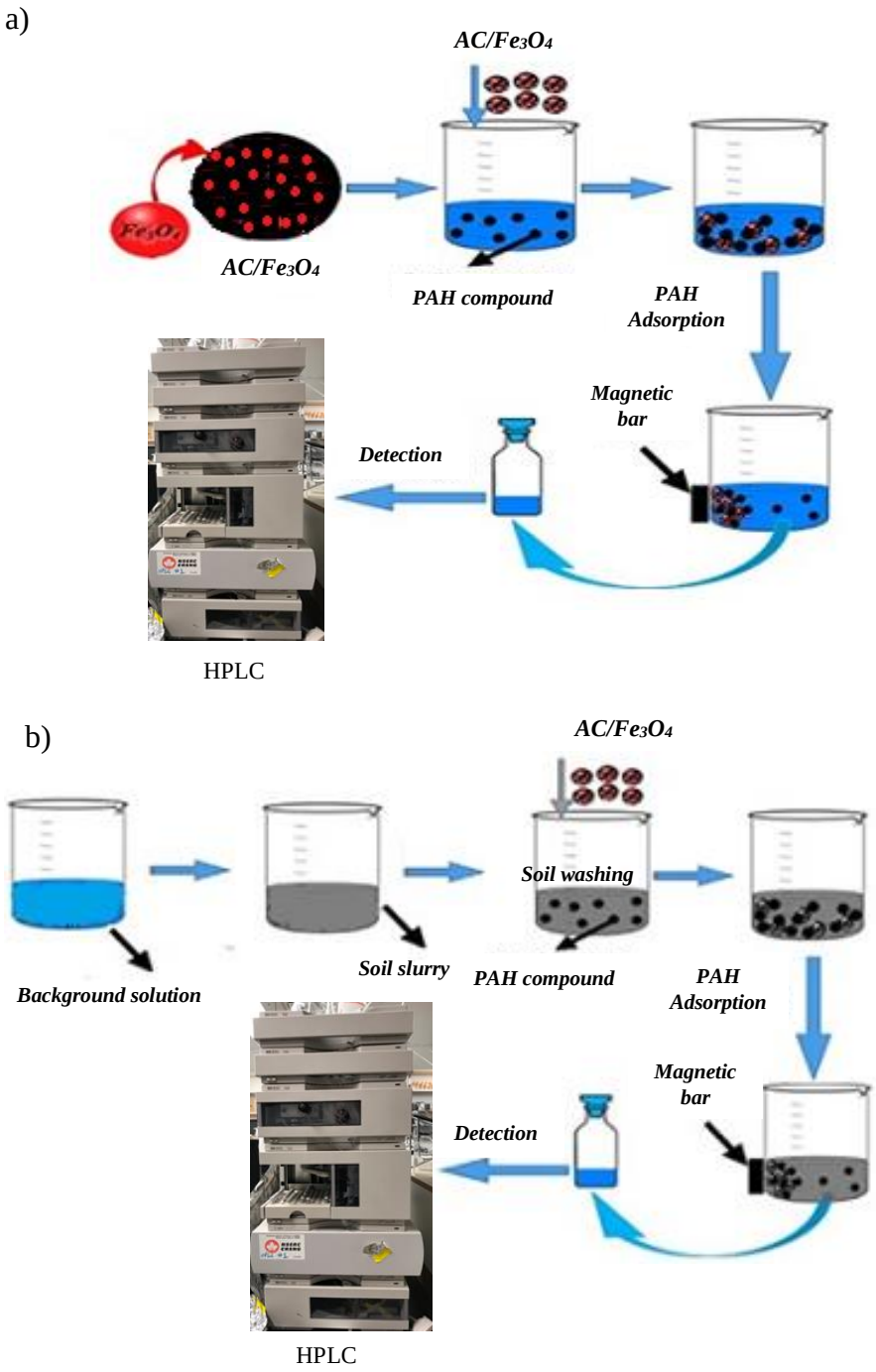

Figure 1.3. Application of AC/Fe_3O_4 composite for removal of PAHs from (a) water (b) soil

1.6 Thesis organization and outline

This thesis is organized into eight chapters to facilitate the presentation of the key findings. Chapter one offers a brief overview of the toxicity and carcinogenicity of PAHs and their adverse effects on humans and the environment. Besides, different technologies available for remediation of PAH-contaminated sites are introduced, and their advantages and drawbacks are discussed in this chapter. It also provides a general description, objectives, and the methodology used for this research. Chapter two contains a literature review about the theoretical and technical aspects of PAH adsorption by ACs and MACs used as treatment method for PAH-contaminated water and soil media. Apart from the fundamental background information on ACs and MACs, relevant previous studies on the application of these adsorbents for the removal of PAHs and other contaminants are presented. Chapters three through six contain the technical papers prepared based on the experimental results of the four phases presented in Figure 1.2. Chapter three (technical paper I) is intended to introduce three synthesis methods for the preparation of MPACs and MGACs, and presents results of the characterization tests conducted on the prepared composites. This chapter also evaluates the performance of the magnetic composites for PAH adsorption in aqueous solutions through a series of batch adsorption experiments. In addition, the desorption study on MPAC and MGAC composites is presented in this chapter to assess the possibility of MACs regeneration and reusability for the next experiments. In chapter four (technical paper II), the MAC with the highest PAHs removal efficiency is studied by conducting a series of adsorption isotherms and kinetics experiments. The experimental results are then evaluated using isotherm and kinetic models to determine the PAHs adsorption capacity and rate as well as the adsorption mechanism of the MACs.

In chapter 5 (technical paper 3), the application of MAC in soil washing for the removal of PAHs from contaminated soil samples is investigated. For this purpose, the isotherm studies of the employed MAC are conducted and optimal values of the effective washing parameters, including the MAC dose, liquid to soil ratio, washing time, stirring speed, pH, and temperature are determined. The thermodynamic study of the treatment process is the next step that is considered for this phase. In chapter 6 (technical paper 4), Tween 80 is used as surfactant in the soil washing process to improve the PAHs removal efficiency of the treatment process. Also, the effective parameters of the Tween 80-enhanced soil washing are assessed, and then, the application of MAC for sorbing the PAHs from the Tween 80 solution during the treatment process is examined.

Chapter 7 of the thesis includes the integration and general discussion of the research phases, and also, the main conclusions of the obtained findings. Lastly, in chapter 8, some recommendations for future work are provided. The organization of the thesis chapters is presented in Figure 1.4.

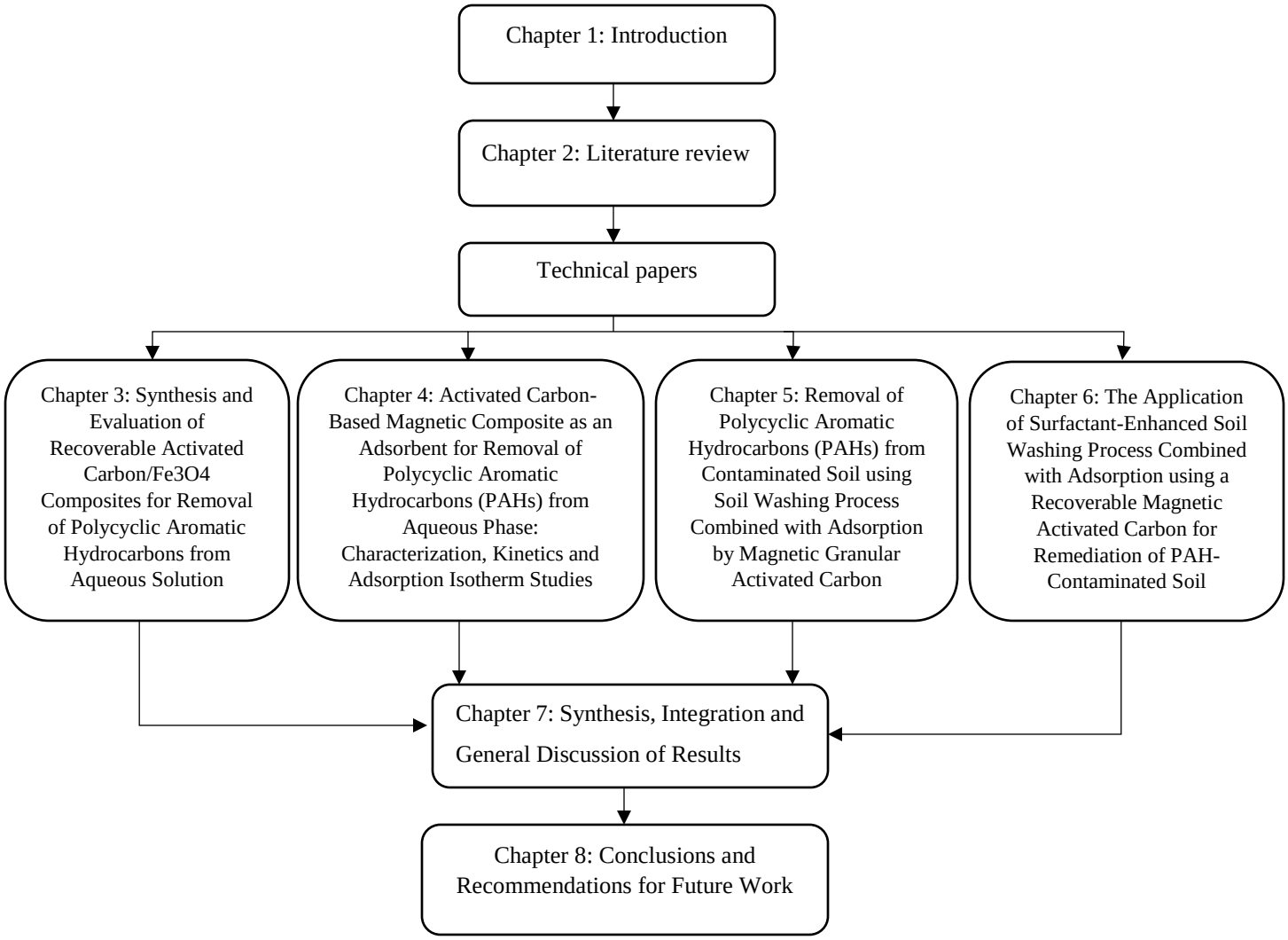

Figure 1.4. Thesis layout

1.7 References

This chapter's references are integrated with the references from the other chapters and provided at the end of the thesis.

2 Literature review

2.1 Polycyclic aromatic hydrocarbons (PAHs)

Over the last few decades, inefficient policies and regulations combined with the increased utilization of petrochemical products have resulted in an elevated number of sites contaminated with polycyclic aromatic hydrocarbons (PAHs). These organic contaminants are considered hydrophobic and persistent due to their aromatic structure, chemical stability, and biodegradation resistance. PAHs are released into soil or groundwater through different ways such as oil spillage and incomplete combustion of petrol, coal, oil, wood, and gas. Sixteen of these compounds are classified as priority pollutants by the European Union (EU), the US Environmental Protection Agency (USEPA), and the Canadian Council of Ministers of the Environment (CCME). The chemical structure of the 16 priority PAHs as well as some of their characteristics are presented in Chapter 1 (Table 1.1).

The number of benzene rings in the PAH structure affects its physical and chemical properties. Accordingly, PAHs are divided into two groups, low molecular weight (LMW) and high molecular weight (HMW) PAHs. LMW PAHs are composed of two or three benzene rings, which are less lipophilic but more water-soluble and volatile. They are also known to be more easily degraded through biological processes. On the other hand, HMW PAHs have more than three rings and tend to be more persistent with limited aqueous solubility. The HMW PAHs are considered highly toxic, hydrophobic, and resistant to microbial/biological degradation [14,48,49].

PAHs may reach the lower respiratory tract in the human body after being adsorbed by fine particles of soil (diameters< 2.5 μm), leading to adverse effects on human health [50,51]. In order to assess the health effects of exposure to PAHs, the International Agency for Research on Cancer (IARC), USEPA, and other regulatory agencies developed an estimation approach based on "potency equivalence factors" (PEFs). According to this approach, the PEFs are employed to relate the carcinogenic potential of LMW and HMW PAHs to that of benzo[a]pyrene, a known carcinogenic PAH [52,53]. As shown in Table 2.1, PAHs are classified into different groups, including probable human carcinogens (Group 2A) and possible human carcinogens (Group 2B) according to IARC carcinogenic classification system [53,54]. A similar classification system has been developed by USEPA, in which most of the HMW PAHs including benzo[b]fluoranthene, chrysene, benzo[k]fluoranthene, benzo[a]pyrene, benzo[a]anthracene, dibenz[a,h]anthracene and indeno[1,2,3-cd]pyrene are considered as potential carcinogen to humans [5,52].

Table 2.1. IARC and USEPA carcinogenicity classification systems for PAHs

	Carcinogenicity classification		
PAH compound	IARC	USEPA	PEF (Nisbet and LaGoy, 1992)
Naphthalene	2B[a]	C[b]	not available
Acenaphthene	3[c]	not available	0.001
Acenaphthylene	3	not available	0.001
Fluorene	3	D[d]	0.001
Phenanthrene	3	D	0.001
Anthracene	3	D	0.01
Fluoranthene	3	D	0.001
Pyrene	3	D	0.001
Benz[a]anthracene	3	B2[e]	0. 1
Chrysene	2B	B2	0.1
Benzo[b]fluoranthene	2B	B2	0.1
Benzo[k]fluoranthene	2B	B2	0.1
Benzo[a]pyrene	1[f]	B2	1
Benzo[ghi]perylene	3	D	0.01
Indeno[1,2,3-cd]pyrene	2B	B2	0.1
Dibenz[a,h]anthracene	2A[g]	B2	1

[a] Group 2B - possibly carcinogenic to human
[b] Group C: possible human carcinogen
[c] Group 3: unclassifiable as to carcinogenetic in humans
[d] Group D: not classifiable as to human carcinogenicity
[e] Group B2: probably carcinogenic to human
[f] Group 1: carcinogenic to human
[g] Group 2A - probably carcinogenic to humans (IARC, 1983; IARC, 2002; IARC, 2009a; USEPA, 1986).

2.2 Remediation technologies

Several remediation techniques have been employed to remove PAHs from contaminated soils, such as soil washing, soil vapour extraction, incineration, chemical oxidation, membrane, bioremediation, landfill, and solidification/stabilization. The main issue associated with the landfill technique is that the mass of the contaminated soil should be transferred to a landfill typically located far away from the contaminated area, which is an unsustainable and unsafe approach (e.g., potential spread of contaminated soil during the transportation). The other common method is surfactant enhanced soil washing, which is able to remove various types of pollutants

from soil (e.g., PAHs), while the required time for conducting the washing process is not very long. Despite the above advantage, this technique cannot be sustainable if the produced effluent is disposed of without treatment. On the other hand, the effluent treatment will increase the total cost and duration of the process [55]. Chemical oxidation is another cleanup method that provides rapid reactions to destroy PAH compounds at a much lower retention time compared to the other remediation methods. However, not only is this method expensive, but also a complete removal of the residual chemicals after treatment may be difficult and even impossible, negatively affecting the soil matrix and the neighbouring water resources [28]. Bioremediation is known as an environmentally friendly technique for the removal of PAHs from soil; nevertheless, its removal efficiency for some PAHs is not high due to their low biodegradability. Besides, PAH removal efficiency may be negatively affected by low temperature, suggesting that bioremediation is not appropriate for cold regions. The other associated issue is that the duration of the bioremediation process is much longer than other remediation techniques, making it less popular option for the environmental services to use it as the major cleanup process [55].

Figure 2.1 shows a comparison between the operational cost of different techniques employed to remediate soils contaminated with PAHs. As can be seen from this figure, incineration is the most expensive cleanup method and bioremediation is the least expensive one. Incineration is primarily used to remove organic pollutants and pathogens from soil. For this purpose, the contaminated soil is placed and heated under controlled conditions in an incinerator. The pollutants are collected and then destroyed inside the incinerator using the pyrolysis process. Although incineration is highly efficient and rapid, it consumes a lot of energy and costs a considerable amount of money, and its usage for PAH-contaminated soil could result in air pollution. Moreover, the residues generated during the incineration process should be disposed of, while they may contain some toxic pollutants [28].

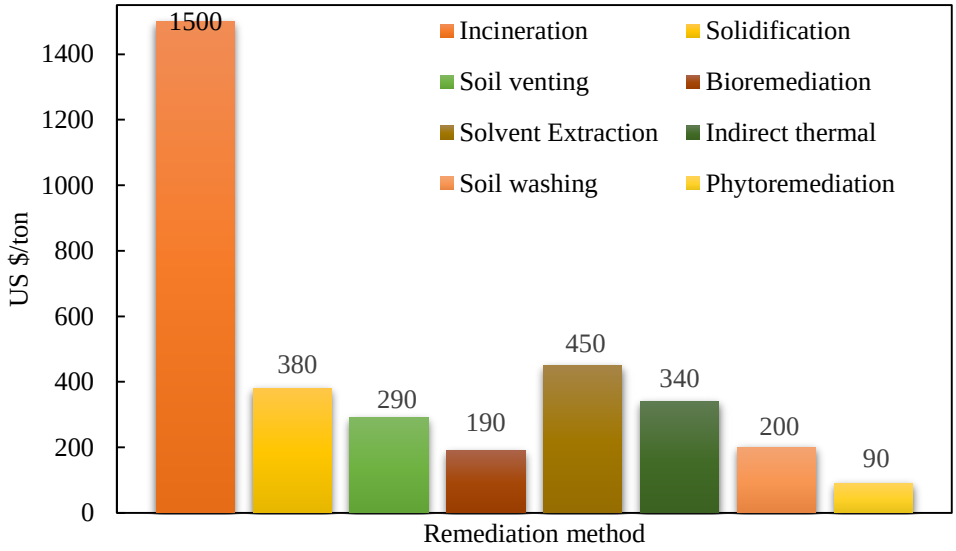

Figure 2.1. Cost comparison of remediation methods used for PAH-contaminated soils [56]

2.2.1 Soil washing

Soil washing is one of the technologies that has been widely employed to remediate PAH-contaminated soils [57–59]. To achieve greater pollutant removal efficiency from soil particles, a variety of non-ionic and ionic surfactants, such as Tween 80, Triton X100, and Sodium dodecyl sulphate have been utilized in the soil washing process [60,61]. This technology yields high removal efficiency of the contaminants while being cost-effective (Figure 2.1) and time saving. However, one drawback of using soil washing for the remediation of contaminated sites is that the generated washing solution may contain a high concentration of pollutants. Therefore, there is a need to conduct a follow-up treatment on the washing solution before it is discharged or reused [57]. Adsorption is one of the techniques that can be applied along with soil washing to remove the PAH compounds from the washing solution and provide a clean solution to be reused in further soil washing processes or discharged in the wastewater system [59].

2.2.2 Adsorption

Adsorption involves the transfer and accumulation of mass at the interface of two phases such as liquid-liquid and liquid-solid [62]. In other words, in the adsorption-based method, a molecule or ion called adsorbate present in a bulk of liquid is adsorbed on the surface of a solid or liquid adsorbent. Based on the nature of the interaction between adsorbent and adsorbed molecules, the adsorption process can be physisorption or chemisorption. In the first one, the mechanism of adsorption is physical and Van der Waals forces play the key role in the reactions, causing the

adsorbate to adhere to the adsorbent surface. In chemisorption, however, chemical bonding between adsorbed molecules and adsorbent surface proceeds the adsorption mechanism (the adsorbate is bonded chemically to the adsorbent surface) [23].

Adsorption is one of the most effective methods used to remove various groups of organic and inorganic contaminants from the environment. This method generates minimal chemical or biological waste, and under specific conditions, the adsorbent may be recycled and reused, providing a more cost-effective method for eliminating the contaminants [18,63]. There is no need to use large quantities of adsorbent or additional chemicals in adsorption and setting up a batch system for the removal of contaminants in this process is both easier and faster. The success of an adsorption-based process technically depends on the type of adsorbent used and the way it is in contact with the contaminant molecules [64]. The adsorption-based method is also less susceptible to shock loads, toxics, and low temperature.

One group of the adsorbents that has extensively been used for treatment purposes and is of scientific and technological interest is carbonaceous adsorbents. These products have shown excellent performance in the adsorption of many organic and inorganic contaminants, such as pesticides, polychlorinated biphenyls (PCBs), PAHs, atrazine, arsenic, and cadmium [18,36,40,65–70]. Activated carbon (AC) is one of these adsorbents that is chemically inert and thermally stable, being capable of sorbing contaminants in water, wastewater, and soil/sediment [33,47,71–75]. AC is well known for its large surface area, high porosity, non-toxicity, low price, and simplicity to be produced. It is primarily produced from coal, biochar, charcoal, and synthetic polymers, and its pore structure and chemical characteristics may be modified to improve its efficiency in removing various organic and inorganic contaminants from aqueous and soil environments [23,36,65,67,76,77].

2.3 PAHs adsorption by AC

Since PAHs have low aqueous solubility and strong sorption affinity to the adsorbent surface, adsorption is offered as a promising technique for their removal from contaminated media. However, the type of adsorbent and its characteristics may influence the PAHs removal efficiency to some extent [33,70]. Among the adsorbents, AC shows a high PAH adsorption capacity owing to its ability to facilitate the accommodation of different small or large size PAH molecules [75].

During the last two decades, a few studies have been conducted on the adsorption of PAHs with AC and other carbonaceous products like carbon nanotubes [4,18,32,33,78]. Eeshwarasinghe et al.

(2019) assessed the simultaneous removal of acenaphthylene and phenanthrene (two LMW PAHs) from water using granular AC (GAC). Their results illustrated 85% of acenaphthylene and 95% of phenanthrene removal after adding 0.7 g/L GAC to the solution. However, the GAC sorption ability decreased by 10% when PAHs and heavy metals were present together in the solutions compared to the situation that PAHs were the only existing contaminants. It was also shown that the PAH uptake by GAC was considerably higher than heavy metals due to the greater affinity of PAHs to GAC than heavy metals. The researchers proposed that the presence of GAC in PAH-contaminated water samples did not affect the zeta potential of the adsorbent since PAHs are almost neutral compounds. In contrast, when heavy metals were added to the suspension, they significantly changed the GAC zeta potential by reducing its negative surface potential [18]. The zeta potential is a measurement of electrical charge on a particle's surface (e.g., AC particles). Changes in the pH of the aqueous solution in which AC is utilized can affect the AC's zeta potential. The isoelectric point (IEP) is the pH value at which the zeta potential is zero, suggesting that no electric charge exists on the AC particle's surface. Determining the zeta potential and IEP of an AC (GAC/PAC) can be helpful to determine the adsorbent's stability/instability during the adsorption process [79]. In the above study, Eeshwarasinghe and colleagues indicated that a strong reduction in the negative zeta potential of GAC can lead to higher adsorption of the positively charged heavy metals reducing the adsorption capacity for PAHs. Consequently, the PAHs removal rates would face a reduction compared to the situation that there are no heavy metals in the suspension [18].

Gong et al. (2007) reported that GAC was able to adsorb almost 90% of PAHs from contaminated vegetable oil during batch adsorption and 68-93% of PAHs during column adsorption experiments. Adsorption equilibrium of PAHs on the applied GAC was modelled by the Langmuir and Freundlich isotherm models, and both the models confirmed the high affinity of the GAC for PAHs. The two isotherm models also showed that the PAH initial concentration and GAC dosage played a significant role in the efficiency of the adsorption process [78]. Brandli et al. (2008) reported that adding 2% powdered AC (PAC) to soil contaminated moderately with PAHs removed 100% of the freely dissolved aqueous concentration of the PAHs from the soil/water suspensions. In the case of GAC application, they reported that GAC amended to the soil could remove approximately 64% of the freely dissolved PAHs. They considered a treatment process of six weeks because they found that this period was sufficient for a PAC- sediment system to reach

equilibrium. The researchers also investigated the PAHs removal efficiency of PAC and GAC amended to a heavily contaminated creosote soil. Their results revealed that PAHs were removed from soil particles by 63% and 4% following the amendment period, respectively. The researchers concluded that a high concentration of PAHs could saturate AC sorption sites and block its pores, reducing its PAHs removal efficiency [66]. Hale et al. (2012) performed a field-scale amendment of either 2% PAC or GAC to PAH-contaminated soil in Norway. After adding the adsorbents to soil samples, they first measured the concentration of PAHs in drainage water of the soil. To assess the reduction of free aqueous PAHs concentration in the soil pore water, they used polyoxymethylene (POM) passive samplers placed directly in the AC amended and unamended soil. According to their analysis results, the total PAHs concentration in the drainage water was decreased by 14% for the PAC-amended soil and by 59% for the GAC-amended soil 12 months after amendment. On the other hand, POM extraction results demonstrated PAHs reduction of 93% and 56% in the pore water of the soil by PAC and GAC, respectively. They also showed that PAC had a higher impact on adsorption of freely dissolved PAHs than total dissolved PAHs compared to GAC, probably due to the leaching of microscopic AC particles from PAC [33]. Although these two studies demonstrated the high capacity of the ACs for removing PAHs from soil, they did not consider any method to separate the PAH-loaded ACs from the soil particles. Moreover, the time spent on adsorption of PAHs from the soil [33] was very long, showing that AC amendment is a very slow process. It can also be claimed that the PAHs removal efficiency obtained by soil amendment relies on many parameters such as weather conditions and change in soil characteristics (e.g., the change in soil pore water).

Kołtowski et al. (2017) employed a specific type of charcoal, namely biochar, to remove PAHs from contaminated soil samples. According to their results, the addition of activated biochar removed almost 86% of the freely dissolved PAHs in two collected soil samples and approximately 70% in the third sample. The researchers also reported almost 100% removal of bio-accessible PAHs from all three soil samples by the activated biochar. In order to clean up the soil samples, Kołtowski et al. added the biochar and water at 40% of water holding capacity of the soil to the samples, and then, the prepared soil slurries were mixed and rolled end over end at 10 rpm for 60 days [36], which was a very slow and long process. Besides, the technique they used for the biochar activation relied on specific equipment whose performance was energy-consuming and costly. The other point is that the biochar recovery from the soil slurries was performed by filtration after

centrifuging each sample. It means that some of the biochar particles might have remained in the samples after treatment, reducing the efficiency of the adsorption process. The presence of PAH-loaded activated biochar in soil can be more harmful to the environment if the biochar recovery is not performed completely [80].

2.4 AC magnetization

Despite the fact that AC amendment with soil reduces the contaminant accumulation, it may be partially aggressive to the ecosystem if the adsorbent particles remain in the soil for a long time or after treatment. The contaminant-loaded AC may change the physicochemical characteristics of the soil/sediment. Employing a high mass of AC in the cleanup process can lead to clogging the soil pores or changing their hydrophobicity. If AC particles remain in soil/sediment after use, it adversely affects water permeability, nutrient availability for plants, and the population of organisms [35]. The other drawback is dislocation or translocation of the AC particles in soil via precipitation or surface runoff which may spread the pollution to neighbouring soil [81]. Similar issues can occur in an aqueous medium if the AC particles are left or accumulated after use [35]. To promote a more sustainable approach, there is a need to separate AC from soil to reduce the environmental impacts and to recycle and reuse the AC particles. Some separation techniques, such as centrifugation and filtration, are used to recover the AC particles after the treatment process ends; however, these methods are costly and only applicable for liquid solutions with a high volume of water. If the surface of AC is given the required polarity or becomes magnetic, it can

Figure 2.2. Recoverable AC/F_3O_4 particles with high surface area and superparamagnetic characteristics (a) PAC/Fe_3O_4 (b) GAC/Fe_3O_4 (c) PAC/Fe_3O_4 recovery from aqueous solution with a magnetic bar

be trapped and recovered by an electric or external magnetic field without any difficulty (Figure 2.2). Therefore, some studies came up with the idea of combining AC and iron oxide particles to magnetize the sorbent and apply it in the adsorption process [80].

2.4.1 Magnetic ACs synthesis methods and applications

Magnetic AC (MAC) is known as a recoverable adsorbent with high surface area and superparamagnetic characteristics that contain the chemical binding of magnetic nanoparticles onto AC. There are different types of MAC synthesis methods that have been considered in the literature to produce highly active magnetic adsorbents. However, the type of synthesis procedure may affect the accessibility of the MAC adsorption sites to the contaminants, leading to lower removal efficiency and higher usage of MAC in the adsorption process [80]. For this reason, many studies attempted to find a proper and facile synthesis method to produce MAC particles with high surface area and adsorption capacity.

Iron oxide (e.g. magnetite, Fe_3O_4) nanoparticles is a popular magnetizing agent which has been proposed by different studies during the past years [40,74,80,82]. Inbaraj et al. (2021) magnetized PAC obtained from green tea waste biomass using ferric chloride and ferrous sulfate as the precursors of the Fe_3O_4 nanoparticles. The iron solution mixtures and PAC were mixed, followed by sonication, stirring, and heating to 80 ˚C for 1 h. The prepared magnetic adsorbent was employed in the isotherm adsorption experiments for removal of four PAH compounds (Benz[a]anthracene, Chrysene, Benzo[b]fluoranthene, and Benzo[a]pyrene) from aqueous solutions. Complete adsorption of the PAHs onto the magnetic PAC was gained, implying the high adsorption capacity of the prepared composite for the four PAH compounds. Cruz et al. (2020) synthesized magnetic PAC/Fe_3O_4 nanocomposite by vigourous mixing of a suspension containing $FeCl_3$ and $FeCl_2$ (as iron precursors) and PAC for 1 h. The suspension pH was raised to 11 by adding a 28 % NH_4OH solution dropwise to the suspension. The synthesized nanocomposite was able to remove 99.97% of promazine from wastewater in less than 10 min, which was an indication of its successful synthesis and high affinity for the contaminant [83]. In another study, Tu et al. (2021) prepared the magnetic GAC and PAC by mixing $FeSO_4$ solution and the adsorbents at pH 10 for 20 h and synthesizing the composite at 65 ˚C for 2 h. The prepared composites were applied to the adsorption experiments, and after 10 minutes, they could yield 97% removal of the contaminant (dibenzo-p-dioxin) from the solutions [84].

Cooper et al. (2010) applied the impregnation method to place iron oxide nanoparticles in the pores and on the surface of GAC. According to their method, the adsorbent is gently mixed with potassium permanganate for a few minutes on a rotating mixer. The prepared product is then mixed with Fe precursor ($FeSO_4 \cdot 7H_2O$) for a certain time, resulting in the formation of iron (hydr)oxide $Fe(OH)_2$ and the nanoparticles impregnation in the GAC porous structure. The Brunauer, Emmett, Teller (BET) characterization test conducted on the synthesized MAC composite revealed that the surface area of the GAC was reduced by 20% (from 696 to 572 m^2/g), while the iron content of the composite was determined to be 12% of the composite mass. The researchers were able to remove 190 µg/g trichloroethylene (TCE) and 120 µg/g arsenic from water using only 0.16g/L and 0.25 g/L of the synthesized MAC in the solutions, respectively [69].

In another synthesis method called Soak-calcination, the carbon precursor was soaked into a $FeCl_3$ aqueous solution at room temperature for a certain time. The prepared magnetic adsorbent particles were rinsed with de-ionized water and ethanol, and after being air-dried, they were calcined inside the furnace at 600 ˚C under nitrogen stream for 1 h. The morphology of the synthesized MAC showed that the size of magnetite nanoparticles (Fe_3O_4) ranged from 200 to 400 nm. The back scattered electron images taken from the magnetic composite confirmed that the distribution of iron oxide nanoparticles was homogenous within the carbon matrix. The synthesized MAC showed high adsorption capacity for methyl blue and chromium ions (Cr^{+6}) (>90%), while more than 85% of the magnetic adsorbent was successfully regenerated after treatment [77].

Ma et al. (2016) used the chemical co-precipitation method to fabricate the magnetic nanoparticles and attach them to the surface of PAC. The characteristics test results revealed that the surface area and total pore volume of PAC were reduced up to 67% and 70%, respectively, after being combined with the magnetic particles. Despite the fact that a considerable portion of the carbon surface area was occupied with the magnetic nanoparticles, only a few amounts of the prepared MAC (0.4 g/L) were sufficient to remove 98.9% of methylene blue from contaminated water samples after 5 h [85]. Juang et al. (2018) employed a polyol-mediated solvothermal reduction method to synthesize magnetite nanoparticles and attach them to the AC texture. For this purpose, $FeCl_3$ was used as the precursor of Fe_3O_4 nanoparticles and NaOH was applied to adjust the weight of Fe (Fe:N) in the prepared composite. This synthesis method helped the magnetite nanoparticles have a great distribution when they were combined with the AC particles. The scanning electron microscope (SEM) images taken from the prepared composite determined the size of the magnetite

nanoparticles ranging from 5 to 20 nm. The BET surface area measurement was conducted on the virgin AC and MAC accordingly, and the results showed that the AC surface area was reduced by 49%. The pore volume and porosity of the AC particles were also reduced by 50% after magnetization, which was due to the formation of the magnetite nanoparticles on the surface and in the pores of the adsorbent. However, regarding the experimental results, the adsorption capacity for methyl orange (MO) decreased by only 15% (from 384 mg/g on AC to 324 mg/g on MAC), indicating that the magnetization process had a negligible effect on the adsorption capacity of the MAC particles [80].

In another study conducted by Gu et al. (2005), GAC-Fe was selected as the adsorbent to remove arsenic from drinking water. They prepared the magnetic composite using the impregnation method, in which GAC, as a supporting base for iron particles, was impregnated by ferrous chloride treatment followed by chemical oxidation. The nitrogen adsorption/desorption analysis results illustrated a 30% decrease in BET specific surface area of the adsorbent (from 541 to 380 m^2/g). The characterization test also revealed a reduction in the total pore volume from 0.59 to 0.46 cm^3/g and the porosity from 0.37 to 0.14 nm, after iron was impregnated into the AC matrix. It was proposed by the researchers that GAC-Fe could remove arsenic most efficiently (80%) when the iron content of the composite was almost 6%, while any further increase of iron led to a decrease in the contaminant adsorption.

2.5 Interaction mechanisms

Gan et al. (2017) proposed that the carbon functional groups, including carboxyl and hydroxyl groups, play a significant role in the adsorption of PAHs by a carbonaceous product like graphene. The non-covalent interactions such as π-π and anion-π interactions are two mechanisms by which the carbonaceous adsorbent removes PAHs from a contaminated medium. A π-π interaction between a PAH molecule and an AC particle forms when π electron donors (the aromatic rings) in the PAH and π electron acceptors (the functional groups and carbon layers) in AC start interacting with each other (Figure 2.3). The soil washing by carbon particles provides the required condition for the removal of PAHs from soil and transferring them into the liquid phase [59]. Gan et al. (2017) claimed that they removed more than 80% of PAHs from contaminated soil using nano-sulfonated graphene in the soil washing process. However, since the employed nanoparticles did not have any magnetic ability, their separation from the treated samples was carried out by filtration and centrifugation. The use of these recovery methods can adversely affect the efficiency

of the remediation process and change the physical characteristics of soil by losing a portion of its fine particles.

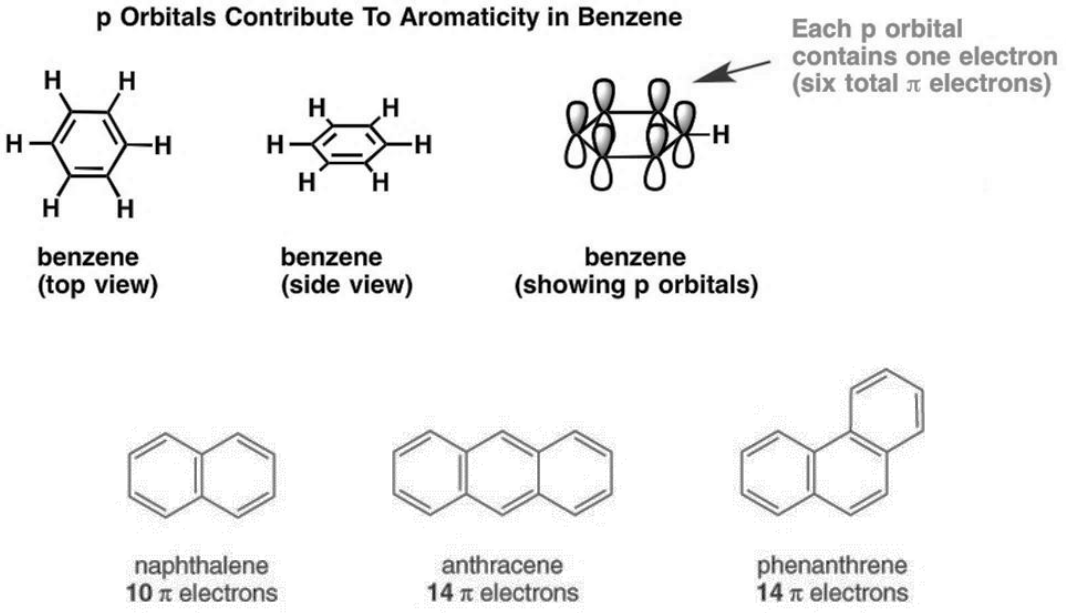

Figure 2.3. π–π electrons in structure of aromatic compounds [86]

Han et al. (2012) studied the interaction mechanism between magnetized graphene oxide (a carbonaceous product) and PAHs molecules in an aqueous solution. For this purpose, five PAHs (fluoranthene, pyrene, benzo[a]anthracene, benzo[b]fluoranthene, and benzo[a]pyrene) were selected as the model analytes to be used in the adsorption process. Based on the results, the researchers proposed that the magnetic graphene oxide had an excellent affinity for PAHs owing to the dominant roles of π–π stacking interactions and hydrophobic interactions between the adsorbent and the analytes. More adsorbent particles and the PAHs molecules could interact with each other by optimizing the adsorbent dosage and contact time, leading to the removal of 76.8 to 100.0% of the PAH compounds from the solutions [46]. However, one of the drawbacks of using graphene oxide for PAHs adsorption is its high cost, making it difficult to be used for large-scale treatment processes. Another drawback is the complicated synthesis method used for producing magnetic graphene oxide, in which the size of the synthesized composite particles is influenced by several variables such as temperature and time.

2.6 Factors affecting PAH removal from a contaminated medium

2.6.1 Properties of the contaminated medium

The adsorption capacity of adsorbents such as graphene and AC for PAHs is inversely proportional to the size of the medium particles on which the adsorption process takes place. For instance, the adsorption of PAHs (e.g., naphthalene and anthracene) in estuarine colloids is higher than their adsorption in soil and sediment. In the case of soils, the specific surface area of soil particles plays a very significant role in the adsorption mechanism, which is known as a surface phenomenon. In general, the smaller the particles of a contaminated medium and the higher their surface area, the harder the adsorption of contaminants is from the medium [23,70].

2.6.2 PAHs solubility

The other parameter affecting PAHs adsorption is the solubility of the PAH compounds in an aqueous solution, which has a significant impact on the adsorption capacity of the adsorbent. In fact, when the PAHs have low solubility, a higher amount of them are adsorbed by the adsorbent. Hu et al. (2009) observed that the PAH adsorption of sediments increased as the solubility of PAHs in the aqueous solution decreased [87]. A similar relationship exists between the PAHs solubility and their molecular weight. Balati et al. (2015) conducted some adsorption tests on naphthalene, acenaphthylene and phenanthrene. Their findings showed that the solubility of a higher molecular weight PAH like phenanthrene in the aqueous solution was lower than that of naphthalene [88].

2.6.3 Octanol-water partition coefficient

The sixteen USEPA PAHs are predominantly non-polar hydrocarbons with unique distribution patterns in contaminated media. The octanol-water partition coefficient (Log K_{ow}) is an essential parameter that is used to evaluate the distribution of PAHs in different media such as water, soil, air, biota. The PAH compounds with high Log K_{ow} values tend to remain insoluble in an aqueous solution and be adsorbed by organic matter in soils/sediments due to their low affinity for water. Besides, HMW PAHs with high Log K_{ow} values (>4.5) and low solubility have the potential to accumulate in the living organisms found in soil/sediment. K_{ow} is not only used to show the potential bio-concentration of PAHs in the environment, but it is considered as an important parameter to assess the toxicity of these contaminants for human and soil organisms by indicating their insolubility ranges in aqueous phase [89,90]. To calculate PAHs sorption onto soil/sediment particles, distribution coefficient (K_d) for the PAH compounds is used, which is related to the

fraction of organic carbon of soil/sediment (f_{oc}) and the octanol-water partition coefficient (K_{ow}) of the PAHs according to the Equation 2.1 [91]:

$$K_d = foc.Koc \qquad (2.1)$$

where Koc is soil organic carbon-water partition coefficient, and is calculated as:

log Koc = 0.00028 + (0.983 H log Kow) [92]

2.6.4 Initial PAH concentrations

Ping et al. (2007) conducted a study on the adsorption of phenanthrene using AC and observed that any increase in the initial concentration of the PAH would increase its uptake by AC [93]. Awoyemi (2011) performed a series of adsorption experiments using AC at different initial concentrations of naphthalene (1.6, 4.2, and 8.2 µg/mL) and found out that the PAH adsorption by AC is proportional to the initial contaminant concentration [52]. In another study, the researchers rose the initial concentration of acenaphthene from 0.376 to 1.795 µg/mL. They noticed that the adsorption of the PAH compound onto silica gel increased from 0.178 to 1.296 µg/mg during the extraction process [94]. Gupta (2015) considered adsorption of phenanthrene by AC and his findings revealed a rise in adsorption capacity of AC as the PAH concentration increased from 10 to 50 µg/mL [95]. Lamichhane et al. (2016) explained that the greater availability of the PAHs at their high concentrations would provide the active sites of AC with the opportunity to adsorb more PAH molecules from the medium [23].

2.6.5 AC size and dosage

The mass transfer of PAHs from soil to the AC particles in the treatment process is a three-step procedure. First, the contaminant is desorbed from the soil particle and transferred to the liquid phase (soil slurry), then the contaminant diffuses through the liquid to the AC particle, and finally, the contaminant is loaded on the AC surface [96]. McLeod et al. (2007) showed how smaller AC particles adsorbed a high number of PCBs compared to the larger AC particles. They reported that the use of AC particles with sizes ranging from 180 to 250 µm, 75 to 180 µm, and 25 to 75 µm led to a reduction in the concentration of PCB compounds in sediment by 41%, 73% and 89%, respectively. These results were obtained after the sediment was amended with 1.7% AC (w/w%) for 30 days [33,97]. In another study conducted by Zimmerman et al. (2005), the researchers reported that by reducing the AC particles size to 25-75 µm and adding them to contaminated sediment, the removal of aqueous PCB from the sediment increased from 82% to 97% [33,98].

Gan et al. (2017) stated that the rise in the adsorbent (e.g., nano-sulfonated graphene) dosage to its optimum could transfer many PAH compounds from soil into the liquid phase (slurry). However, any further increase beyond the optimal dosage resulted in a lower PAH removal since a portion of the adsorbent particles remained in the solid phase after the treated mixture was centrifuged. It negatively influenced the removal rate of PAHs in the treatment process [59].

2.6.6 Effect of magnetization on PAH adsorption capacity of AC

A detailed analysis of the AC surface area and pore size distribution is necessary to assess the impact of magnetization on the AC adsorption capacity. It will also help to determine the available AC pore volume after the iron oxide nanoparticles are placed onto AC. A tentative hypothesis is that attaching the magnetic nanoparticles to the AC surface decreases its micropore and mesopore volumes, potentially reducing the number of adsorption sites available for contaminants [64,68,69,99]. Castro et al. (2009) magnetized GAC at different mass ratios of the adsorbent to magnetite (5:1 and 1:1) for adsorption of atrazine in aqueous solutions. The BET tests of the prepared magnetic composite showed a reduction of 15% and 36% in the surface area due to magnetization, which consequently affected its adsorption capacity by 20% and 48%, respectively [72]. The magnetic GAC was also synthesized by Tu et al. (2021) for the removal of dibenzo-p-dioxin from water. After magnetization, the surface area and micropore volume of the magnetic adsorbent were reduced by 23 % and 33 %, respectively, according to the BET characterization test. Despite the reduction, the results of adsorption experiments showed only 3% drop in the contaminant adsorption capacity of magnetic GAC compared to the bare GAC [84]. Lompe et al. (2017) proposed that low w_t% of iron oxide nanoparticles to carbon did not have any significant effect on the magnetic PAC adsorption capacity. However, a high mass fraction of the magnetic nanoparticles onto PAC (e.g., more than 50%) would clog the mesopores in the structure of carbon particles and decrease their capacity for contaminant adsorption. Do et al. (2011) and Li et al. (2017) reported a reduction of 31% and 69% in the surface area of PAC particles after magnetization. The synthesized magnetic nanocomposites were used for removal of methyl orange (MO) and methylene blue (MB) from aqueous solutions, respectively. Despite the reduction in the surface area, both studies confirmed that the magnetized PAC could retain its adsorption capacity for removal of MO and MB [43,71].

2.6.7 Contact Time

Zeledon-Toruno et al. (2007) used leonardite, a type of immature coal, in aqueous solutions to adsorb five PAH compounds (pyrene, benzo[k]fluoranthene, benzo[a]pyrene, benzo[ghi]perylene, and fluorene) with an initial concentration of 100 mg/L. After 2 h of contact time, the adsorbent removed 70% of the PAHs from the solutions, while the adsorption equilibrium was achieved after 24 h with the removal of more than 78 % of the PAHs (Figure 2.4) [100]. AC was employed by Gupta (2015) in the batch adsorption experiments to eliminate phenanthrene from contaminated water. The findings of the investigation revealed that the PAH sorption process was rapid for the first 75 minutes and then it slowly reached equilibrium after 2.5 hours [95]. Hu et al. (2015) similarly obtained superior results in adsorption of phenanthrene by mesoporous molecular sieve MC-41 only after 20 min the experiment began. They did not observe any significant PAH removal after 2 h [101].

Gan et al. (2017) employed nano-sulfonated graphene (SGE) to remove PAHs from soil in the soil washing process. Based on their findings, the PAHs removal rate was elevated from 30.9% to 80.9% after the washing time was increased from 6 h to 24 h. One speculative explanation for the significant change in the adsorption rate was that the organically bound fractions of PAHs trapped in the soil pores needed more time to be removed by the adsorbent and transferred into the liquid phase. The 30.9% removal obtained during the 6 h washing time was mostly related to adsorption of a large portion of water-soluble and organic acid-soluble PAHs from soil by SGE [59].

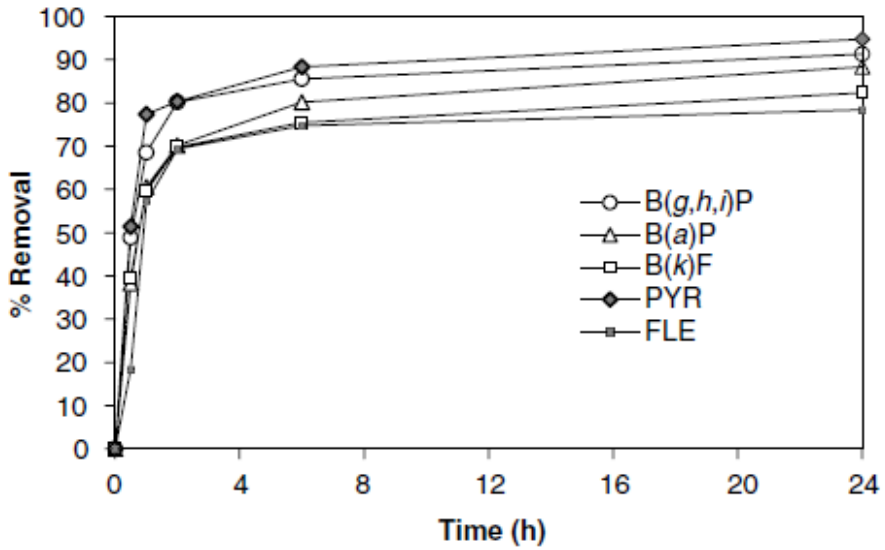

Figure 2.4. Effect of contact time on the adsorption of PAHs by leonardite [100]

2.6.8 Temperature

The influence of temperature on the adsorption of naphthalene, phenanthrene, and pyrene was investigated by Edgar et al. (2008). They discovered that increasing the temperature from 4 to 27 °C reduced PAH adsorption, with average values of 27.3, 17.0, and 27.4% for the three PAHs, respectively. The researchers claimed that the PAHs adsorption process was exothermic by use of the following equation (Van't Hoff equation), where the calculated enthalpies of sorption (ΔH˚) gave a negative value to the equation:

$$\ln Keq = \frac{\Delta H}{R} \times \frac{1}{T} + \frac{\Delta S}{TR} \qquad (2.2)$$

In this equation, ΔH˚ describes the change in enthalpy (KJ/mol), T is absolute temperature (K), ΔS˚ demonstrates the change in entropy KJ/mol/K, R is gas constant which equals 8.314×10^{-3} kJ/K/mol, and K_{ep} is equilibrium partition coefficient at a given temperature (cm^3/g) [23,102].

Podoll et al. (1989) observed a reduction in adsorption of naphthalene from the soil containing 1.6% of organic carbon by increasing the temperature from 15 to 35 ℃. In another study, He et al. (1995) reported that a rise at temperature from 5 to 25℃ would reduce adsorption of fluoranthene onto soil and lava by 1.6 times. Bekci et al. (2006) also discovered that PAHs sorption capacity of adsorbents in different media decreases when the temperature increases because the adsorption reactions are exothermic [23].

On the other hand, there are some studies that obtained opposite results. Balati et al. (2015) reported that the adsorption of three PAH compounds (naphthalene, acenaphthylene, and phenanthrene) from wastewater using NH_2-SBA-15 was improved when the temperature was raised. They highlighted the positive values of ΔH˚ (Eq. 2-2) determined from the adsorption experiments at various temperatures to show that the adsorption process was endothermic [88]. Lamichhane et al. (2016) proposed that the conduct of adsorption process at higher temperatures favours the sorption of compounds with lower solubility in aqueous solution. Compounds with high solubility are expected to follow the reverse trend, with any rise in temperature leading to a decrease in their sorption from the contaminated medium [23]. It means that the solubility of organic compounds (e.g., PAHs) and temperature have an inverse relationship with each other in the adsorption process when the temperature of media changes.

2.6.9 pH

Tran et al. (2017) reported that an increase in pH of the adsorption process can induce the density of π electrons in adsorbate and provide more π- π interaction between the adsorbate and adsorbent [103]. In contrast, there are some other studies stating that the adsorption process at neutral or acidic pH will yield better results than alkaline pH [39,63,73]. Balati et al. (2015) evaluated the effects of different pH values on naphthalene adsorption by silica-based organic-inorganic nan-hybrid material (NH_2-SBA-15). They observed that lowering pH from 8 to 2 caused a considerable increase in the PAH removal efficiency (79.3%) of the adsorbent. They attributed this high removal efficiency to the formation of NH_3^+ on NH_2-SBA-15 surface at very low pH, since such an acidic pH would elevate electrostatic interactions between the surface charges of NH_2-SBA-15 and the PAH molecule [23,88].

Gupta (2015) performed some batch experiments on the adsorption of phenanthrene by AC. Based on their results, the adsorption capacity of AC for the PAH reached its maximum (>90%) when pH of the solution was adjusted to 2.0, whereas the minimum sorption of PAH (<40%) was obtained when the solution was alkaline (pH 12.0). The researcher explained that an acidic pH increases the positive charge on the adsorbent surface, and it provides the adsorbent with the opportunity to interact with a higher concentration of PAHs. In contrast, when pH of the solution goes up, the positive charges on the adsorbent surface are reduced, leading to interactions between OH^- ions and PAH molecules to compete for adsorption onto the adsorbent. This would consequently reduce the PAH removal efficiency of the adsorbent [23,95].

However, there are some studies showing opposite results in terms of the pH role in the adsorption process. For example, Moradi Rad et al. (2014) reported that an acidic or alkaline organic solution (n-hexane) produces a high amount of hydroxide ions. Since organic compounds have bigger sizes when they are in their ionized form, a fewer number of them can occupy a greater number of the active sites of adsorbent (e.g., activated carbon), causing a reduction in the adsorption capacity of the adsorbent for contaminants. The researchers showed that maximum adsorption of phenanthrene onto AC happens when pH of the organic solution was set at 8 (close to neutral pH) with the lowest concentration of the ionized compounds [104]. There are also other studies, such as Mader et al. (1997), that have not considered the pH as a significant factor in the adsorption of PAHs (e.g., naphthalene, phenanthrene, anthracene, fluoranthene, and pyrene). The same theory was proposed by Zeledon-Toruno et al. (2007) after they conducted a series of adsorption

experiments on pyrene, benzo[k]fluoranthene, benzo[a]pyrene, and benzo[ghi]perylene using leonardite. The researchers observed that adjusting pH of the solutions at a range of 2.0-6.0 had no significant effect on the PAHs removal rate [23,100].

Adverse effects of very low or high pH values on the activity of magnetic adsorbents were shown by Andrade-Eiroa et al. (2016). The researchers claimed that the iron oxide (Fe_3O_4) particles in the structure of the composite adsorbent started degrading at pH<4, enforcing Fe (III) to form chelates with the target compounds (analytes). The same phenomenon happened when the pH value was higher than 9, where the electrostatic repulsion became prominent between the magnetic adsorbent and target anionic compound as a result of the negative charge of hydroxide groups formed by Fe_3O_4 particles. All of these reduced the adsorption rate of the compound by the magnetic adsorbents [4].

2.6.10 Soil characteristics

Soil organic matter (SOM) has a high tendency to absorb hydrophobic pollutants such as PAHs in soil, according to Delle Site (2001) and Ping et al. (2006). It is because PAHs have large K_{ow} values leading them to be insoluble in soil pore water and be adsorbed onto SOM. Furthermore, the larger the PAH molecules and the higher their $K_{ow,}$ the greater their adsorption rates are onto the organic matter of soil particles. Other soil parameters (e.g., surface area, total clay content, mineralogy) were also evaluated, and the results showed that these parameters could not compete with SOM for PAHs sorption in soil [91]. Ahangar (2010), Lamichhane et al. (2016), and Cao et al. (2008) confirmed that adsorption of PAH in soil is controlled by the SOM polarity and the carbon in the structure of the aromatic compound. In addition, it is believed that aliphatic groups found in the SOM matrix play a key role in the adsorption of non-ionic organic compounds such as PAHs [23,48,105]. Therefore, it can be claimed that PAH uptake by an adsorbent like AC in a soil-water system (e.g., the soil washing process) can be affected by the quantity of organic matter in the soil [105].

2.6.11 Liquid:soil ratio

The liquid to soil (L:S) ratio is one of the most important factors in the removal of PAHs by soil washing. The maximum solubilization of PAHs in soil washing process carried out by Peng et al. (2011) and Gan et al. (2017) was observed at L:S ratios of 10:1 for Tween 80 and 20:1 for nano-sulfonated graphene, respectively. However, it should be noted that a higher L:S ratio would result

in more wastewater output, and subsequently, more equipment and energy to deal with it. Besides, a higher L:S ratio may also have an adverse impact on the physicochemical properties of the treated soil [59,60].

2.7 Research gap

Previous studies conducted to remove PAHs from soils by the AC particles mostly focused on the amendment of bare PAC or GAC with the PAH-contaminated soils for different time periods, and were able to remove 40 to 60% of PAHs from the soils [33,36,48,66,106]. However, they did not perform any effective method for the recovery of ACs from the soil medium after use. If left in soil, AC could act as a secondary source of PAHs distribution in the environment, posing a threat to humans and soil organisms [41]. Another issue was that in some of these studies the AC amendment with soil lasted few weeks to several months [33,48,66,106], which is not only time-consuming but raises uncertainty about the role of AC as the only agent in the removal of contaminants. The addition of AC particles to the soil washing process to remediate the soil contaminated with PAHs is a viable remediation technique. However, the fate of the washing solution and the PAH-loaded AC particles after the cleanup process is of great concern due to associated health risks (the carcinogenic contaminants). This potential challenge motivates research into using adsorbents, such as magnetic activated carbon (MAC) composites, which can be recovered and are capable of removing PAHs from soil and washing effluent. The use of the recoverable MACs in soil washing can significantly provide high PAH removal efficiency and minimize the required time, energy, and operational costs for remediation of PAH-contaminated soils.

This research focuses on the synthesis and application of different recoverable magnetic powder and granular ACs (MPACs and MGACs) for the removal of PAHs from contaminated water and soil. The characterization and batch adsorption experiments will be conducted on the synthesized MACs to evaluate their morphology and performance for the adsorption of PAHs, respectively. Besides, the possibility of regenerating the magnetic composites will be investigated through a series of PAH desorption experiments. Using a series of adsorption isotherm and kinetic studies, the adsorption capacity of MAC with the highest PAH removal efficiency will be thoroughly assessed. The next phase involves remediation of an aged PAH-contaminated soil using soil washing combined with adsorption using MAC to explore the efficiency of the magnetic adsorbent for the removal of PAHs from the soil. Lastly, a proper surfactant will be utilized in soil washing

experiments to improve PAH removal from soil. The MAC composite will be added to the surfactant solution during the remediation process to contribute to the PAHs removal and recycle the surfactant solution for further washing cycles.

To the author's knowledge, this is the first study that considers the preparation of MAC particles with different affordable synthesis methods and evaluates the MAC applications in adsorption and soil washing processes to remove PAHs from water and soil.

2.8 References

This chapter's references are integrated with the references from the other chapters and provided at the end of the thesis.

3 Synthesis and Evaluation of Recoverable Activated Carbon/Fe_3O_4 Composites for Removal of Polycyclic Aromatic Hydrocarbons from Aqueous Solution[1]

3.1 Abstract

Three different synthesis methods were employed to prepare magnetic powder and granular activated carbons (MPAC and MGAC) as recoverable adsorbents to remove polycyclic aromatic hydrocarbons (PAHs) from aqueous solutions. The MPAC and MGAC composites were characterized by XRD, and the XRD patterns confirmed the presence of Fe_3O_4 particles with cubic crystal structure on the adsorbents surface. FE-SEM images showed that the magnetic composites had spherical morphologies, with clusters of iron oxide nanoparticles formed in the ACs pores and distributed evenly on their surface. FTIR spectra of the PAH-loaded adsorbents revealed that the analytes were attached to the surfaces of MPACs and MGACs by π-π and H-π interactions formed between PAHs and functional groups of the adsorbents. All the synthesized magnetic ACs were very effective in removing the PAH compounds from the aqueous solutions with removal percentages between 87.2% and 99.3%. The precipitation method of magnetization resulted in the highest PAHs removal efficiency (99.3%) using PAC as the base AC, while the co-precipitation method of magnetization provided the highest PAHs removal efficiency (98.3%) using GAC as the base AC. The PAHs desorption tests indicated that low molecular weight PAHs were more easily desorbed from MAC surface ranging from 38.1 to 60.1%, compared to high molecular PAHs ranging from 23.4 to 57.2%. This shows that the increase in the number of PAH rings would lead to the formation of more covalent bonds between the adsorbate and the adsorbent.

Keywords: Magnetic activated carbons, Polycyclic aromatic hydrocarbons (PAHs), Removal efficiency, π-π and H-π interactions, Desorption

[1] A version of this paper has been published in the Journal of Environmental Technology and Innovation. (https://doi.org/10.1016/j.eti.2021.102174)

3.2 Introduction

Polycyclic aromatic hydrocarbons (PAHs) are considered a group of ubiquitous contaminants in the environment containing two or more fused aromatic rings [107,108]. These persistent and hydrophobic compounds are mainly released into the environment through anthropogenic sources such as exhaust emissions, oil spills, industrial facilities processing petroleum and coal, and domestic/industrial heating systems [6,109]. PAHs are categorized as low molecular weight (LMW) with two- and three-aromatic ring structure and high molecular weight (HMW) with four to six aromatic rings in their structures [23]. It is reported that the combined toxicity of PAHs has more adverse effects on human health and the environment than a single PAH compound [110]. Due to their toxicity, carcinogenicity, and mutagenicity, 16 of the PAH compounds have been classified as priority pollutants by many regulatory bodies such as the US Environmental Protection Agency and Canadian Council of Ministers of the Environment [14,111].

Various treatment methods have been applied to remove these carcinogenic hydrocarbons from the environment, such as incineration, photolysis and thermal desorption [23], chemical oxidation [112], combined ultrasound and zero-valent iron/EDTA [113], zero-valent iron [6], biodegradation [107], and electrochemical techniques [114]. However, many of these methods are not practical on a large scale due to the need for a high dosage of reaction reagents, long treatment process, required acidic/alkaline condition, and high investment and maintenance costs [113]. Adsorption, however, is one of the popular techniques that can be considered for the removal of PAHs due to their low solubility and high sorptive ability [18,23]. This technique is fast and efficient, and produces a minimum waste compared to other treatment techniques [18,115,116]. Activated carbon (AC) is the most common adsorbent employed in many adsorption processes due to its high availability, low cost, large surface area, superior adsorption capacity, and reusability [117]. Examples of the AC application for removal of PAHs and the effect of adsorption process parameters were summarized by Laminchhane et al. (2016), which generally shows high PAH removal efficiencies (66-99%) for the adsorbent.

An important step in the application of AC as a sorbent is recovery, regeneration, and reuse in order to reduce the costs and complete the treatment cycle. After dispersing in an aqueous solution, the PAH-loaded AC particles can be separated using centrifugation and filtration techniques, which are not only expensive and time-consuming but also increase the operational complexity. If the adsorption of PAHs from aqueous phase is part of the remediation of contaminated soils, for

example using soil washing technology where adsorption follows a previous extraction or washing of PAHs from contaminated soils, this becomes more complex and challenging since AC is mixed with soil particles in a slurry. This makes the separation of AC from soil particles uneconomical and practically impossible. To overcome the difficulties in the recovery of the exhausted AC, the application of magnetic products has been considered by several literatures to modify AC in adsorption process [41,42,73,116,118,119]. Magnetic separation of AC/Fe_3O_4 composites could offer an alternative recovery method, which is facile, more convenient, economical, and efficient. Even though the application of magnetic AC (MAC) could be more advantageous than the bare one, the loss of pore space in the carbon matrix after magnetization can negatively affect the AC adsorption capacity for organic pollutants. Particularly, a reduction in the adsorption capacity could be a disadvantage if the magnetic nanoparticles themselves do not contribute to the adsorption of the pollutants. Therefore, a facile magnetization method for AC particles without adversely affecting their adsorption capacity needs to be considered [80]. Iron impregnation and co-precipitation are two of the methods that can uniformly distribute the magnetic nanoparticles on the surface and in the pores of AC, negligibly reducing the number of adsorption sites on AC surface [30,41,42].

A review of the previous studies conducted on the PAHs removal by ACs reveal that they have mainly focused on adsorption of a single PAH or LMW PAHs as the target compounds [18,120–122], and the more toxic and carcinogenic PAHs with four to six aromatic rings were less explored. Besides, the recovery of AC particles after PAH adsorption in aqueous media was not investigated in the aforementioned studies. Desorption of the PAH compounds from ACs is the other aspect that has not properly been studied by the literature. Therefore, the present research aims to investigate the feasibility of synthesis and application of six retrievable MACs (3MPACs and 3MGAC) for removal of the priority USEPA LMW and HMW PAHs from aqueous solutions. The synthesized MACs were characterized, and their performance were subsequently evaluated through a series of batch adsorption experiments. In addition, desorption tests were carried out on the PAH-loaded MPAC and MGAC to study the possibility of reusing the composites in the treatment process. The novelty of the research is to evaluate the feasibility of facile synthesis methods for MACs and the adsorbents performance on removal of PAHs from water and more complex aqueous phases such as contaminated soil slurries, which can then be recovered by a simple magnetic field. This research will also provide helpful information on how the magnetic

synthesis methods potentially affect the PAHs uptake by powder and granular ACs used for treatment purposes.

3.3 Materials and methods

3.3.1 Chemicals

Two types of AC, powder and granular, were employed to prepare the magnetic AC composites. The powder type (PAC) was produced from coconut shell, and the granular one (GAC) was Filtrasorb 400 made from bituminous coal with high activity and durability. Both the PAC and GAC were provided from CalgonCarbon Co. (Pennsylvania, USA). According to the data from the manufacturer, PAC was in size less than 45 µm, and GAC had a size ranging from 550 to 750 µm. The standard solutions of USEPA priority PAHs (500 mg/L and 10mg/L, each in acetonitrile) containing Acenaphthene (ACE), Anthracene (ANT), Fluoranthene (FLUO), Benzo[ghi]perylene (B[ghi]P), benzo[a]pyrene (B[a]P), chrysene (CHR), benz[a]anthracene (B[a]A), benzo[b]fluoranthene (B[a]F), benzo[k]fluoranthene (B[k]F), pyrene (PYR) , Phenanthrene (PHE), Indeno[1,2,3-cd]pyrene (IDP), Dibenz[a,h]anthracene (D[ah]A) (98%) were obtained from AccuStandard Co. (Connecticut, USA) and Sigma Aldrich Co. (St Louis, USA), respectively. The stock solutions of PAHs were prepared at a concentration of 50 mg/L in acetonitrile (HPLC grade, >99%). The working solutions were made through serial dilution of the stock solutions to provide the required PAHs concentrations in acetonitrile for the tests. Distilled deionized water used for preparing the aqueous solutions was obtained by a Millipore-Q purification system from Millipore Co. (Bedford, USA). The organic solvents, including acetone, hexane, acetonitrile, and methylene chloride (high-performance liquid chromatography (HPLC) grade), were purchased from VWR (Quebec, Canada). Iron (III) nitrate nonahydrate ($Fe(NO_3)_3 \cdot 9H_2O$) and Iron(II) sulfate heptahydrate ($FeSO_4 \cdot 7H_2O$) were acquired from Sigma-Aldrich Co. (St. Louis, USA). Potassium nitrate (KNO_3), sodium azide (NaN_3), nitric acid solution (20%), and sodium hydroxide were obtained from VWR Canada.

3.3.2 Preparation of AC/Fe_3O_4 composites

PAC and GAC were combined with iron oxide nanoparticles using three different synthesis methods. Therefore, there were a total of 6 magnetic AC composites, 3 MPACs and 3 MGACs. In all cases, the PAC and GAC particles were selected as the base material for the composites because they had an amorphous structure with high porosity. In the first method, which was a modified

form of an impregnation method (Imp.) reported by Do et al. (2011), 8 g Iron (III) nitrate nonahydrate ($Fe(NO_3)_3.9H_2O$) was dissolved in 40 mL nitric acid solution (20%). Then, 1g PAC or GAC was added to the solution with magnetic stirring and heating at 80℃ and for 1 h. The mixture was then dried and heated in a furnace at 600℃ for 2 h under nitrogen flow (thermal treatment) to form the high-quality magnetite nanoparticles (Figure 3.1a). The synthesized magnetic ACs (MPAC-Imp. and MGAC-Imp.) were then washed three times and placed in screw cap vials for later use in adsorption experiments. The percentage of iron oxide used in the synthesis procedure was 30% wt. of the carbon particles [41,42]. In the second synthesis method known as precipitation (Prec.), 2.78 g of ferrous sulfate ($FeSO_4.7H_2O$) was dissolved in 100 mL deionized water inside a 250 ml conical flask, and 0.5 g of PAC or GAC was added to the flask, subsequently [123]. The flask was then placed on a magnetic stirrer, and 10 mL sodium hydroxide (NaOH) solution (10%) was added dropwise to the flask for precipitation of the hydrated iron oxide particles. While mixing on the magnetic stirrer, the suspension was heated to 100 ℃ for 1 h (Figure 3.1b). The prepared composites were dried overnight and washed with deionized water three times to remove impurities and until their pH became neutral. The MPAC-Prec. and MGAC-Prec. particles were dried and separated by an external magnetic field and then stored in screw cap vials for next applications [123]. The MPAC and MGAC composites were also synthesized using a modified co-precipitation (CoPrec.) method [124]. As can be seen from Figure 3.1c, 50 mL $Fe(NO_3)_3 \cdot 9H_2O$ (1 M) and 25 mL $FeSO_4 \cdot 7H_2O$ (0.1 M) were prepared and added to 350 mL deionized water in a reaction vessel, followed by mixing on a magnetic stirrer. Then, 2 g PAC or GAC was brought in contact with the ferric ions in the solution and the mixture was stirred at 400 rpm in the presence of nitrogen gas. Simultaneously, 35 mL NaOH solution (1 M) was added dropwise for 10 min to increase pH of the solution to 10-11 and enable the precipitation of magnetic AC composite. The black precipitated product was then removed from the vessel using a simple magnet bar. The fabricated MPAC-CoPrec. and MGAC-CoPrec. particles were repeatedly rinsed with deionized water to remove the excess non-AC bound iron oxide nanoparticles. The composite was then dried in a vacuum oven overnight at 80 °C and stored in the screw cap vials prior to use in the PAHs adsorption experiments [124].

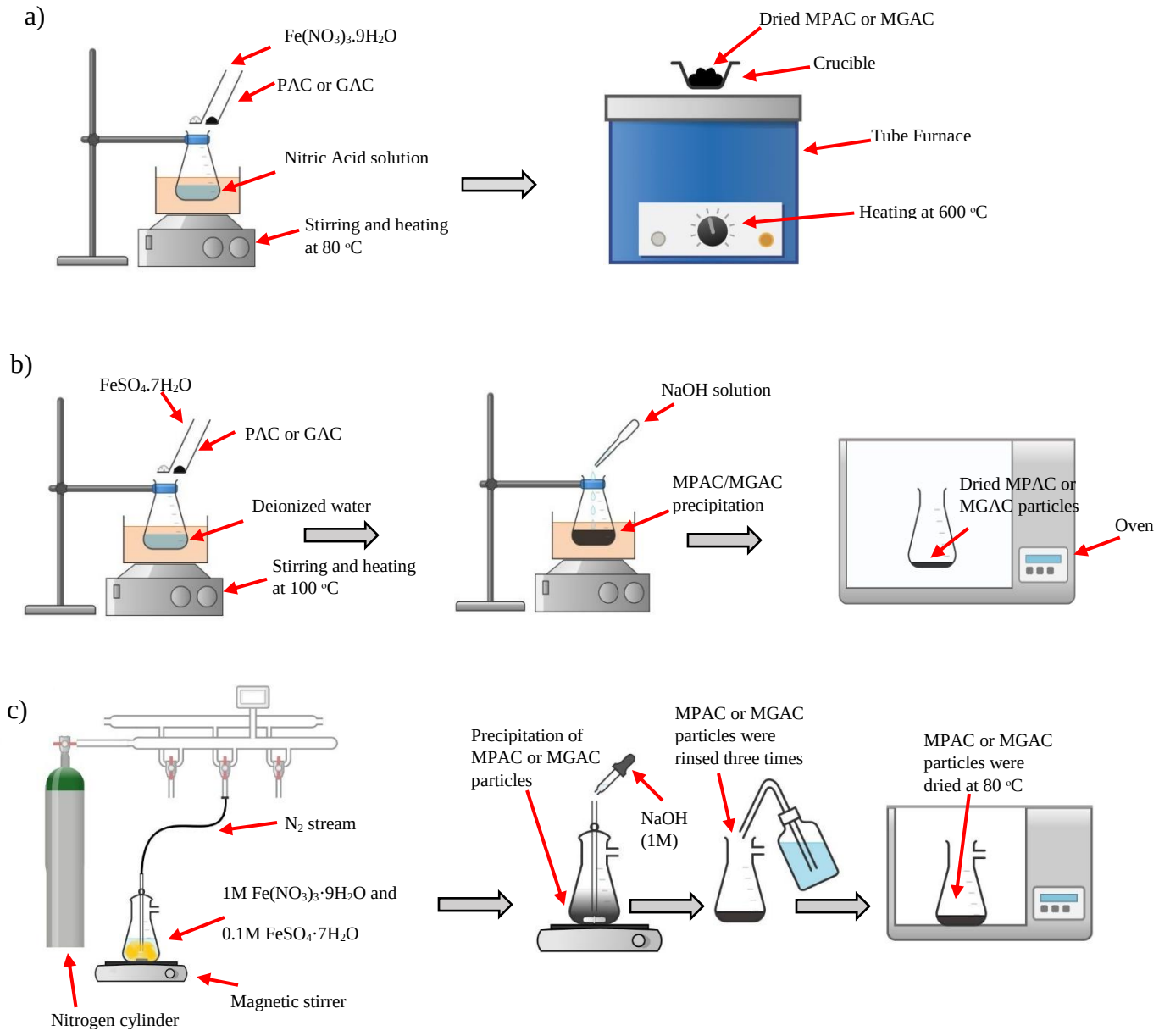

Figure 3.1. Three synthesis methods used for the preparation of MPAC and MGAC composites (a) Impregnation (b) Precipitation (c) Co-precipitation

Powder X-ray diffraction (XRD) patterns of the PAC, GAC, MPAC, and MGAC particles were analyzed on a Rigaku Ultima IV theta-theta X-ray diffractometer equipped with a Cu K_α radiation ($\lambda = 1.54185$ Å) sealed-tube source operating at 40 kV and 44 mA. The morphological analysis of the bare and magnetic ACs was carried out by a field emission scanning electron microscopy (SEM, JSM-7500F, and Oxford EDS system) equipped with an EDS Detector. Energy-dispersive spectroscopy (EDS) is a technique that applies X-ray to detect the composition of materials. Based

on the type of elements found in the material structure, EDS creates a spectrum with peaks of the elements. The ACs and the prepared magnetic composites were analyzed by EDS to identify the elements that were present in their structure. Fourier transform infrared spectroscopy (Nicolet 6700 FT-IR spectrometer, Thermo Fischer, USA) was used to analyze the MPAC and MGAC composites before and after PAHs adsorption. The FTIR spectra were determined in the region between 4500 and 400 cm^{-1} by applying 32 scans and a resolution of 4 cm^{-1} for each sample. Using the FTIR method, it became possible to evaluate the performance of surface functional groups of the composites involved in the PAHs adsorption. The specific surface area of PAC and GAC was determined using the nitrogen adsorption-desorption isotherm data measured at 77K from a relative pressure (P/P_0) of 10^{-5} to 0.99 by applying the Brunauer–Emmett–Teller (BET) equation.

3.3.4 Batch adsorption tests

Batch adsorption experiments were conducted in a series of 125 mL conical flasks to determine PAHs adsorption by the prepared MPAC and MGAC composites. To prepare the PAHs-contaminated samples, each flask was filled with 29.7 mL deionized water, and 200 mg/L sodium azide (NaN_3) and 0.01M potassium nitrate (KNO_3) were subsequently added to the flasks to inhibit microbial activity [59]. The samples were then spiked with 0.3 mL PAHs solution at an initial concentration of 50 mg/L and shaken at 50 rpm for 1 h to obtain homogenous solutions. The volume fraction of the solvent (acetonitrile) containing PAHs was adjusted to ≤ 1% to prevent the effect of the solvent on the adsorption process [125]. The solutions were then mixed with 30 mg of the adsorbent for each of the six synthesized magnetic AC composites and continuously agitated on the shaker at 100 rpm and 24±1 ℃ for 48 h. All the experiments were conducted in triplicate and the flasks were covered with aluminum foils to protect them against the light. The 48 h contact time was selected based on a set of preliminary tests to ensure that the solutions reach their adsorption equilibrium. At the end, each flask was taken out the shaker and the adsorbent was separated from the suspension by placing a simple magnetic bar at the bottom of the flask. After few seconds, the suspension became limpid and the liquid was decanted.

3.3.5 Desorption tests

For the PAHs desorption experiments, the PAH-loaded MAC was first dried under flowing nitrogen gas for approximately 15 min. The dried particles were then weighed to determine the

recovery (%) of the adsorbent mass separated using the magnetic bar. Subsequently, the target PAH analytes were eluted from the adsorbent particles with 10 mL of Hexane/Acetone (1:1 V:V) and after bath sonicating at 20–30 °C for 10 min (method 3550b, USEPA) [72,126]. The extraction of PAHs was repeated three times, and all the eluates were combined and then poured into Kuderna-Danish apparatus (K-D) (method 8310, USEPA) to be condensed to acetonitrile. Finally, an aliquot (25µL) of the acetonitrile solution was injected into the HPLC system for analysis purposes [46,127]. Thermal desorption was also tested for recovery of the PAHs from the MPAC and MGAC surfaces, however, high temperatures resulted in disintegration of the magnetic composites.

3.3.6 PAHs measurement

The PAHs in the solutions were first extracted by the liquid-liquid phase extraction (LLPE) method [45]. For this purpose, each solution was extracted with 8 mL organic solvent, methylene chloride, in a 50 mL centrifuge tube. The tubes were shaken by hand and then vortexed for about 1 min. The extract was separated from the liquid phase with centrifugation at 1500rpm for 2 min, and then, removed from the tubes using a pipette. The extraction process was conducted two more times and all the extracts were combined thoroughly. The K-D apparatus was used according to method 8310 [127] to condense the extract to 1 mL and exchange it for acetonitrile. 25µL of the acetonitrile solution was injected into HPLC to measure the residual PAHs concentration. The HPLC analysis of extracts was performed using a Hewlett–Packard 1100 chromatograph (Agilent Technologies, USA) equipped with a reverse phase HPLC column (ZORBAX Eclipse PAH, 95Å, 4.6 × 250 mm× 5 µm) and Multiple Wavelength Detector (MWD). 25 µL of the condensed extract was injected onto the column. Chromatography was conducted with acetonitrile/water (95/5, v/v) as the mobile phase at a flow rate of 1mL/min and 25 °C. The PAH compounds were detected at 210.8, 224.4, 230, 8, 254.4, and 270.9 nm using the MWD. The standard solutions were prepared and injected into HPLC to verify the extraction protocol of the PAH compounds [48].

3.4 Results and discussion

3.4.1 Characterization of bare and magnetic PACs/GACs

The specific surface area was 938.1 m^2/g for PAC and 822.8 m^2/g for GAC, respectively. The mineral composition of PAC, GAC, and their magnetic composites prepared by the precipitation and co-precipitation methods were characterized by the X-ray diffractometer (XRD). For this

purpose, the diffraction data were generated by exposing the adsorbents samples to Cu-Kα X-ray radiation (λ = 1.54185Å) operating at 40 kV and 44 mA. The XRD data were obtained at a diffraction region of 2θ from 10° to 80°. Figure 3.2a shows XRD patterns of the commercial PAC and GAC samples used as the base for the magnetic composites. As can be seen from this figure, both ACs have an amorphous structure. In their XRD pattern, there are one strong and one weak diffraction peak at 2θ = 23.4° and 2θ = 43.8°, respectively, indicating the presence of graphite crystallite in PAC and GAC. Xie et al. (2014) proposed that the entire wall of PAC particles is composed of graphite crystallite; however, the lower their crystallinity, the larger their specific surface area is for the adsorption of organic contaminants [128].

a)

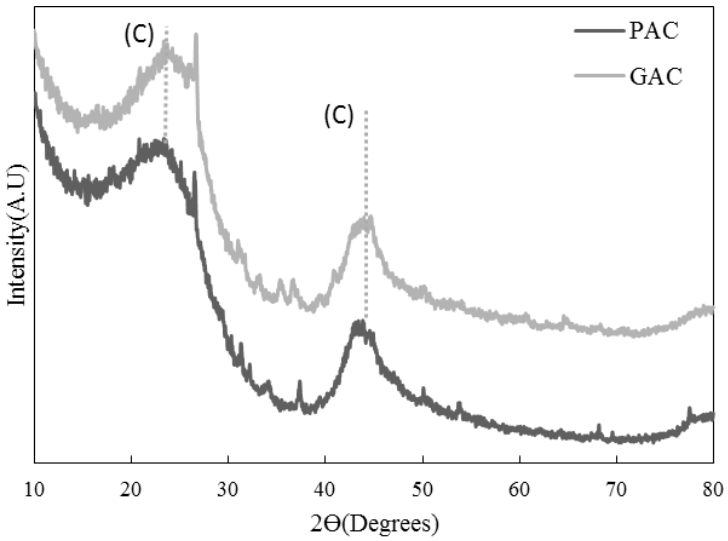

b)

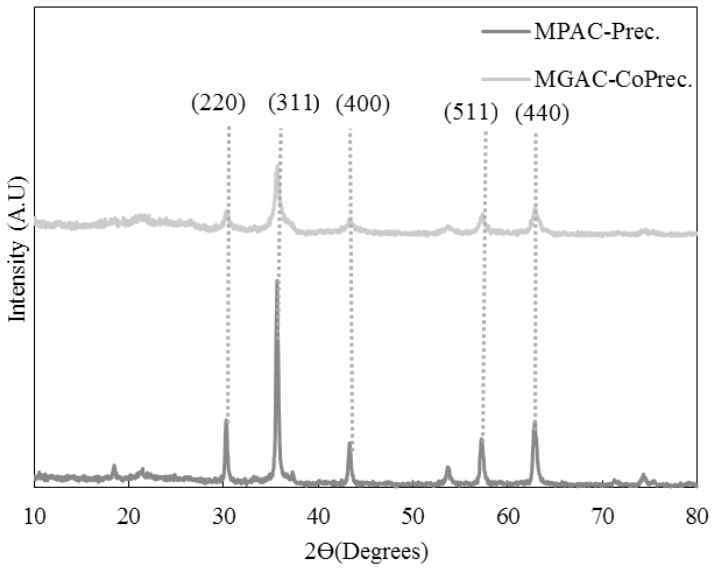

Figure 3.2. XRD patterns of (a) bare PAC and GAC (b) MPAC-Prec. and MGAC-CoPrec.

Figure 3.2b represents the XRD patterns of MPAC-Prec. and MGAC-CoPrec. According to the patterns obtained for MPAC-Prec., several characteristic peaks emerged at 21.9^0, 30.2^0, 35.6^0, 43.3^0, 53.8^0, 57.1^0, and 62.8. All the peaks except the one that emerged at $2\theta = 21.9^0$can be attributed to the cubic spinel structure of iron oxide particles (magnetite or maghemite). The peaks position and their intensity observed in the plane of the magnetic adsorbents ((220), (311), (400), (511) and (440) indices) matched well with the iron oxide standard data (Joint Committee for Powder Diffraction Studies, Card No. 19- 0629), which are direct evidence of the presence of the magnetic nanoparticles in the AC structure. The peak at $2\theta = 21.9^0$ shows the characteristic reflection of the AC particles. The diffraction peaks of MPAC-Prec. and MGAC-CoPrec. attributed to the iron oxide particles are very similar. This implies that the iron valence states are basically invariable after the iron oxide is placed into the amorphous structure of PAC and GAC [75,123].

The morphology and surface element distribution of PAC, GAC, MPAC-Prec., and MGAC-CoPrec. were determined by FE-SEM equipped with an Energy-dispersive X-ray spectroscopy detector (EDS). A few milligrams of each adsorbent were deposited on a conductive sticky pad to prepare the samples for the SEM-EDS analysis [38]. SEM images of the bare and magnetic ACs obtained at an accelerating voltage of 15.00 kV are illustrated in Figure 3.3. As presented in Figure 3.3a and b, both PAC and GAC are properly porous and bulky amorphous, and their pores are uniformly distributed throughout their matrix. Figure 3.3c and d indicate the formation of iron oxide particles in the texture of PAC and GAC. Comparing these images with those from the bare ACs, it is apparent that the synthesis methods utilized to attach the magnetic nanoparticles to PAC and GAC matrices were successful. According to the SEM images (Figure 3c and d), the magnetic nanoparticles were formed in a spongy crust shape. They were well-dispersed throughout the ACs texture and evenly covered the adsorbent surface with a thin layer, which is in agreement with the XRD results [68,99].

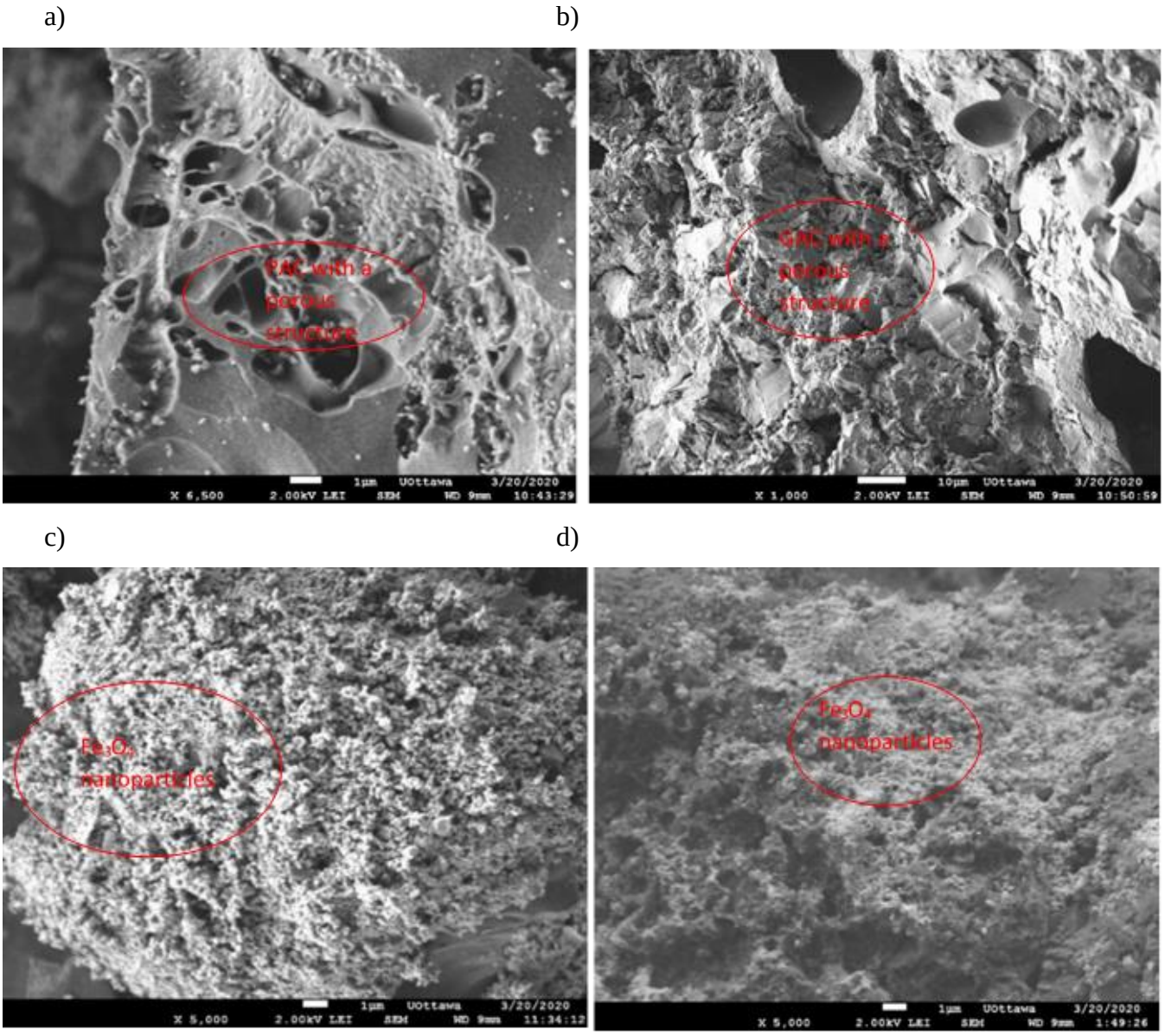

Figure 3.3. The SEM images of bare and magnetic activated carbons prepared with different synthesis methods (a) PAC (b) GAC (c) MPAC-Prec. nanocomposite (d) MGAC-CoPrec. Composite. The spinal core particles observed inside photos c and d present the clusters of Fe_3O_4 nanoparticles that were formed on the PAC and GAC surfaces, respectively.

EDS spectra of the PAC, GAC, and magnetic AC samples were presented in Figure 3.4. The spectra of PAC and GAC show that the texture of these adsorbents only contains carbon with a very narrow fraction of oxygen (Figure 3.4a, and b). However, as can be seen from Figure 3.4c and d, the elements of iron oxide (iron content and oxygen) in MPAC-Prec. and MGAC-CoPrec.

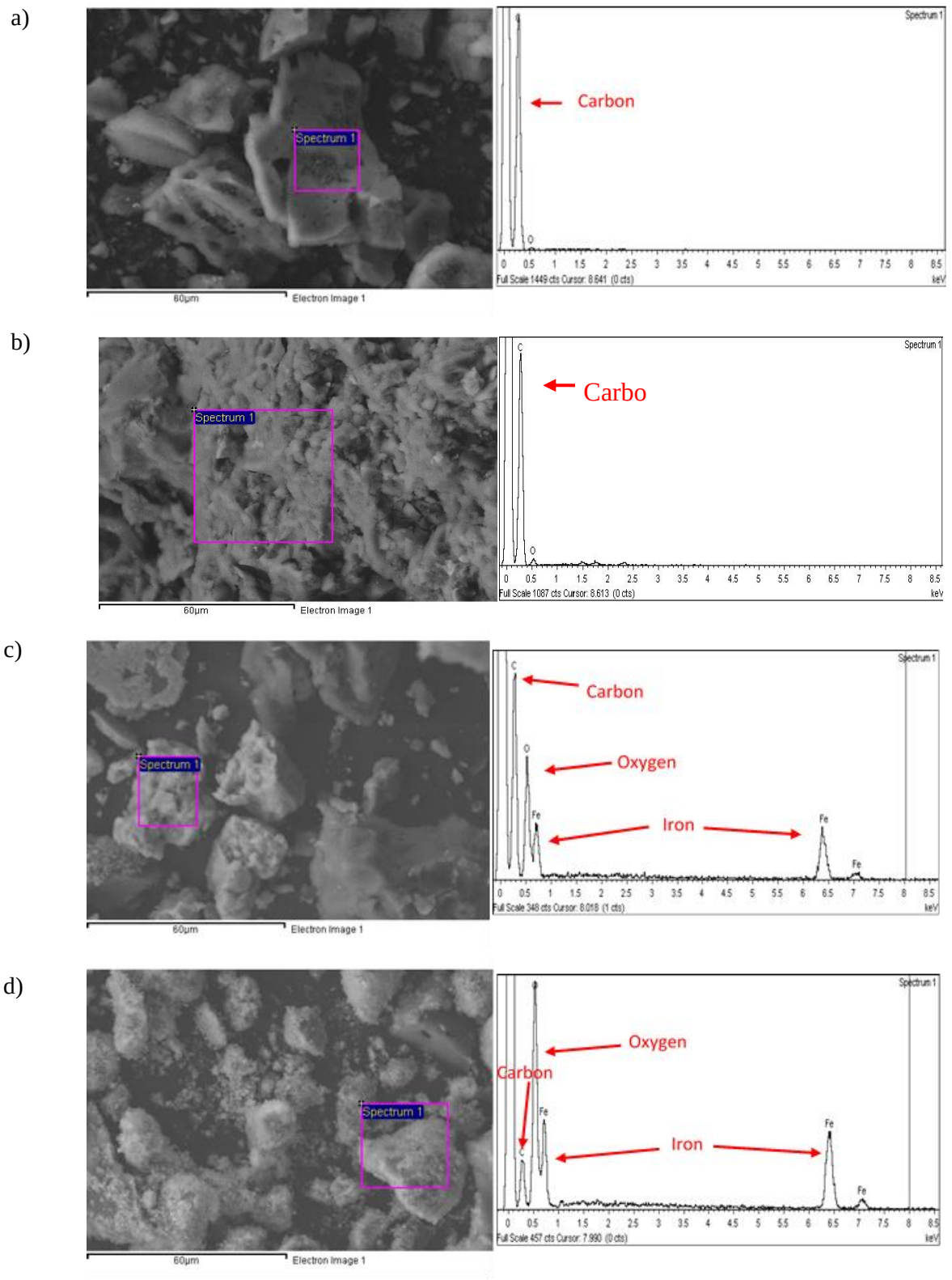

Figure 3.4. Energy-dispersive spectroscopy (EDS) spectra of (a) PAC, (b) GAC, (c) MPAC-Prec., (d) MGAC-CoPrec.

appeared in the spectra by sharp peaks of Fe and O, indicating that the magnetic nanoparticles were properly incorporated in the matrix of the PAC and GAC particles.

EDS spectrum of MPAC-Prec. (Figure 3.4c) display that the carbon content in this composite was significantly higher than the iron oxide nanoparticles, showing that the Fe_3O_4 aggregates bonded well with the PAC texture after the synthesis processes. A similar condition was observed for the MGAC composites (Figure 3.4d); however, the iron content in MGAC-CoPrec. seems to be slightly higher than the carbon one. A possible explanation for the observed difference is that the EDS spectrum was taken from a spot where the AC pores were filled with a high amount of Fe, and their outer side was covered with the iron oxide clusters. If it happens for the entire GAC media, the first phenomenon can reduce microporosity of the GAC, and the latter can partly block the mesopores of its matrix [73,99].

3.4.2 FTIR spectra analysis of magnetic ACs

The FT-IR spectra of MPAC-Prec. and MGAC-CoPrec. samples before and after PAHs adsorption were determined by Nicolet 6700 FT-IR spectrometer (Thermo Scientific, USA). According to Figure 3.5, the sharp peaks centered at 567 and 579 cm^{-1} in MGAC-CoPrec. and MPAC-Prec., and 532.19 and 609 cm^{-1} in PAH-loaded MPAC-Prec. and MGAC-CoPrec. represent the stretching band of Fe–O, which is due to the presence of Fe_3O_4 nanoparticles in the AC matrix [73]. The medium adsorption peaks at 785 and 789 cm^{-1} for MGAC-CoPrec. and MPAC-Prec. shifted to 804 and 785 cm^{-1} after the PAHs adsorption, which may be associated with C-H bending on the aromatic rings (angular deformation out of the plane of C-H bond in the aromatic analytes) [73,129]. The peaks located at 868 and 903 cm^{-1} in MPAC-Prec. and MGAC-CoPrec. shifted to 876 and 887 cm^{-1} after the PAH compounds were adsorbed on their surface. All these bands that appeared in the range of 850-1000 cm^{-1} may correspond to the hydroxyl groups attached by the hydrogen bonds in the adsorbents [73,130]. The peak centered at 1640 cm^{-1} in MGAC-CoPrec. can also be assigned to the stretching vibration of C=C bond. It means that π−π interactions between PAHs and the adsorbent were formed as a result of the existence of sp^2 hybridized structure on their surface [73,131].

The broad bands observed at 1310 and 1360 cm^{-1} in the spectra of PAH-loaded MPAC and MGAC correspond to the stretching vibration of carboxyl bond (O=C−O) after the PAHs adsorption. These differences observed in the FTIR spectra of the magnetic ACs before and after adsorption confirm the interactions between the PAH compounds and oxygen-containing functional groups of the

magnetic ACs (carboxyl functional group, −COOH) in the adsorption process. The broad bands identified at 3130 and 3320 cm^{-1} for MPAC-Prec. and MGAC-CoPrec. after PAHs adsorption can be due to the stretching vibration of the adsorbents hydroxyl groups (−OH) [30,132]. These changes in the FTIR spectra after PAHs adsorption indicate that the hydroxyl groups (hydrogen donor) of the ACs were involved in the adsorption of PAH molecules (hydrogen band acceptor) through H−π interaction [73].

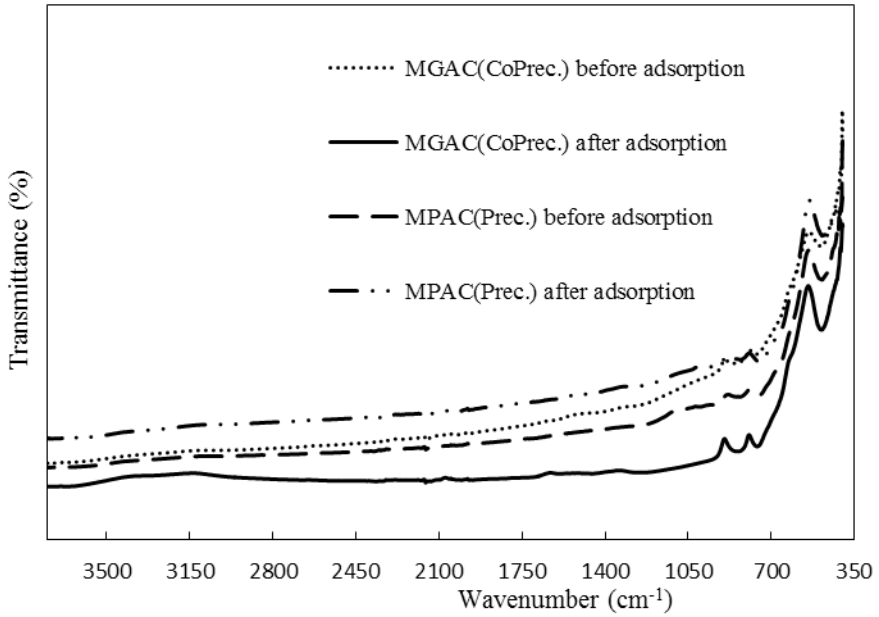

Figure 3.5. FTIR spectra of MPAC-Prec. and MGAC-CoPrec. before and after the PAHs adsorption

3.4.3 Adsorption tests

The initial and final PAHs concentrations measured for batch adsorption tests for all six AC/ Fe_3O_4 composites are presented in Table 3.1. The mean initial PAHs concentration in the control solutions determined by the ultrasonic extraction method was 0.425±0.027 with the highest concentration for IDP (0.542 ± 0.011 ppm) and the lowest one for ACE (0.274 ± 0.101ppm). The addition of MPACs and MGACs to the samples reduced these concentrations to varying degrees. Among the LMW PAHs, PHE was the only PAH compound that was completely removed by all the magnetic ACs. MGAC-Imp. and MPAC-Prec. were able to remove 100% of ACN from the solutions as well as the other adsorbents that achieved a high percentage of removal for this LMW PAH compound. Likewise, almost all the HMW PAHs, including PYR, B[a]A, CHR, IDP, and B[a]P were removed completely following the addition of MPAC-Imp., MPAC-Prec., and

MGAC-CoPrec. to the aqueous solutions. The other three magnetic composites (MGAC-Imp., MGAC-Prec., and MPAC-CoPrec.) also presented high adsorption capacity for the HMW PAHs, although these adsorbents acquired the lowest removal for IDP and B[a]P with the six and five benzene rings, respectively. As shown in Table 3.1, the more significant reductions of HMW PAHs were primarily achieved by the magnetic powder composites compared to the granular ones. The only exception was MGAC-CoPrec. which outperformed MPAC-CoPrec. and reduced the total concentration of PAHs more (average PAHs content of 0.005±0.002 ppm for MGAC-CoPrec. compared to the mean PAHs content of 0.054±0.015 ppm accounted for MPAC-CoPrec.). The reduction in PAHs concentrations attained by each of the magnetic ACs was fairly consistent for different-sized PAHs, except for the LMW PHE and HMW FLUO and B[a]A, which showed a higher affinity for the adsorbents.

Table 3.1. Total PAHs concentration in the solutions after the adsorption process

PAHs	PAHs initial conc. (ppm)	MGAC-Imp. (ppm)	MGAC-Prec. (ppm)	MGAC-CoPrec. (ppm)	MPAC-Imp. (ppm)	MPAC-Prec. (ppm)	MPAC-CoPrec. (ppm)
ACE	0.274±0.101	0.094±0.014	0.007±0.011	0.059±0.026	0.076±0.034	0.021±0.014	0.112±0.015
PHE	0.277±0.036	ND[a]	ND	ND	ND	ND	0.009±0.015
ANT	0.445±0.030	ND	0.071±0.080	0.003±0.003	0.012±0.020	ND	0.069±0.003
ΣLMW	**0.996±0.098**	**0.094±0.054**	**0.078±0.039**	**0.062±0.033**	**0.088±0.041**	**0.021±0.012**	**0.19±0.050**
FLUO	0.340±0.026	ND	ND	ND	ND	ND	ND
PYR	0.422±0.023	ND	0.017±0.030	ND	0.001±0.002	0.003±0.006	0.112±0.123
B[a]A	0.394±0.016	ND	0.011±0.019	ND	ND	ND	ND
CHR	0.460±0.018	0.050±0.007	0.031±0.054	ND	ND	ND	0.032±0.002
B[b]F	0.429±0.018	0.020±0.014	0.027±0.046	ND	ND	ND	0.007±0.009
B[k]F	0.480±0.015	0.074±0.023	0.043±0.063	ND	ND	ND	0.032±0.010
B[a]P	0.484±0.025	0.095±0.022	0.060±0.069	ND	ND	ND	0.069±0.004
B[ghi]P	0.500±0.001	0.106±0.031	0.055±0.060	ND	ND	ND	0.060±0.003
IDP	0.542±0.011	0.185±0.031	0.154±0.032	ND	ND	ND	0.152±0.009
D[a,h]A	0.475±0.025	0.083±0.025	0.048±0.047	ND	ND	ND	0.051±0.008
ΣHMW	**4.526+0.058**	**0.613±0.060**	**0.446±0.043**	**0.000±0.000**	**0.001±0.000**	**0.003±0.001**	**0.515+0.052**
Σ13PAHs	**5.522±0.083**	**0.707±0.057**	**0.524±0.041**	**0.062±0.016**	**0.089±0.021**	**0.024±0.006**	**0.705±0.048**

[a] Not detected

±: Standard deviation (n = 3).

Figure 3.6 shows the maximum PAHs removal efficiency for the treated samples after 48 h adsorption. A comparison of the PAHs removal obtained by the MPACs shows that MPAC-Prec. and MPAC-Imp. performed better than MPAC-CoPrec. and removed greater content of PAHs from the solutions, respectively. According to Figure 3.6a, the MPACs prepared by the precipitation and impregnation methods were able to remove almost all LMW and HMW PAHs. The ability of MPAC-CoPrec., however, for the removal of PAH compounds falls within the range of 58% to 96%, with the highest removal percentage for B[a]A and FLUO and the lowest for ACE. Among the magnetic GACs (Figure 3.6b), the adsorption uptake capacity of MGAC-CoPrec. for the PAHs appeared to be higher than the MGAC-Prec. and MGAC-Imp. adsorbents.

The MGAC-CoPrec. particles could reduce the concentration of most LMW and HMW PAHs to below detection limit, whereas the highest PAHs removal efficiency of MGAC-Imp. was obtained for the LMW PAHs plus FLUO, PYR, and B[a]A. In the case of MGAC-Prec., the PAHs removal percentages were mostly greater than 85% for the HMW PAHs, while this value for two of the three LMW PAHs, PHE and ACE, was almost 100% after adsorption. One speculative explanation for the lower adsorption capacity of MGAC-Imp. and MGAC-Prec. compared to MGAC-CoPrec. can be the higher accumulation of magnetic nanoparticles on the surface of the adsorbent or clog of the GACs pores by the nanoparticles during the synthesis process. These phenomena may cause a portion of the adsorption sites on the adsorbent surface to become inaccessible to the target compounds leading to a drop in the PAHs removal by the adsorbent [64,69,133]. The same explanation can be used for the MPACs, although MPAC-Imp. and MPAC-Prec. approximately had similar PAHs removal efficiency compared to the other MPAC.

Figure 3.6c represents the total PAHs removal efficiency of the six magnetic ACs used in the adsorption experiments. As shown in this figure, all the adsorbents successfully removed PAHs from the aqueous solutions with maximum removal efficiencies obtained for MPAC-Prec, MGAC-CoPrec., and MPAC-Imp. The total PAHs removal percentages of the MPACs produced using the impregnation, precipitation, and co-precipitation methods were 97.6, 99.3, and 87.2%, respectively, while the MGACs prepared by these methods could remove 87.9, 91.6, and 98.3% of the analytes, respectively. Comparison of the above results shows that the synthesis methods had a more significant effect than particle size, i.e., GAC vs. PAC, and type of original raw materials. For example, for the co-precipitation method, MGAC performed better than MPAC, while for precipitation and impregnation magnetization methods, the trend was reversed and the

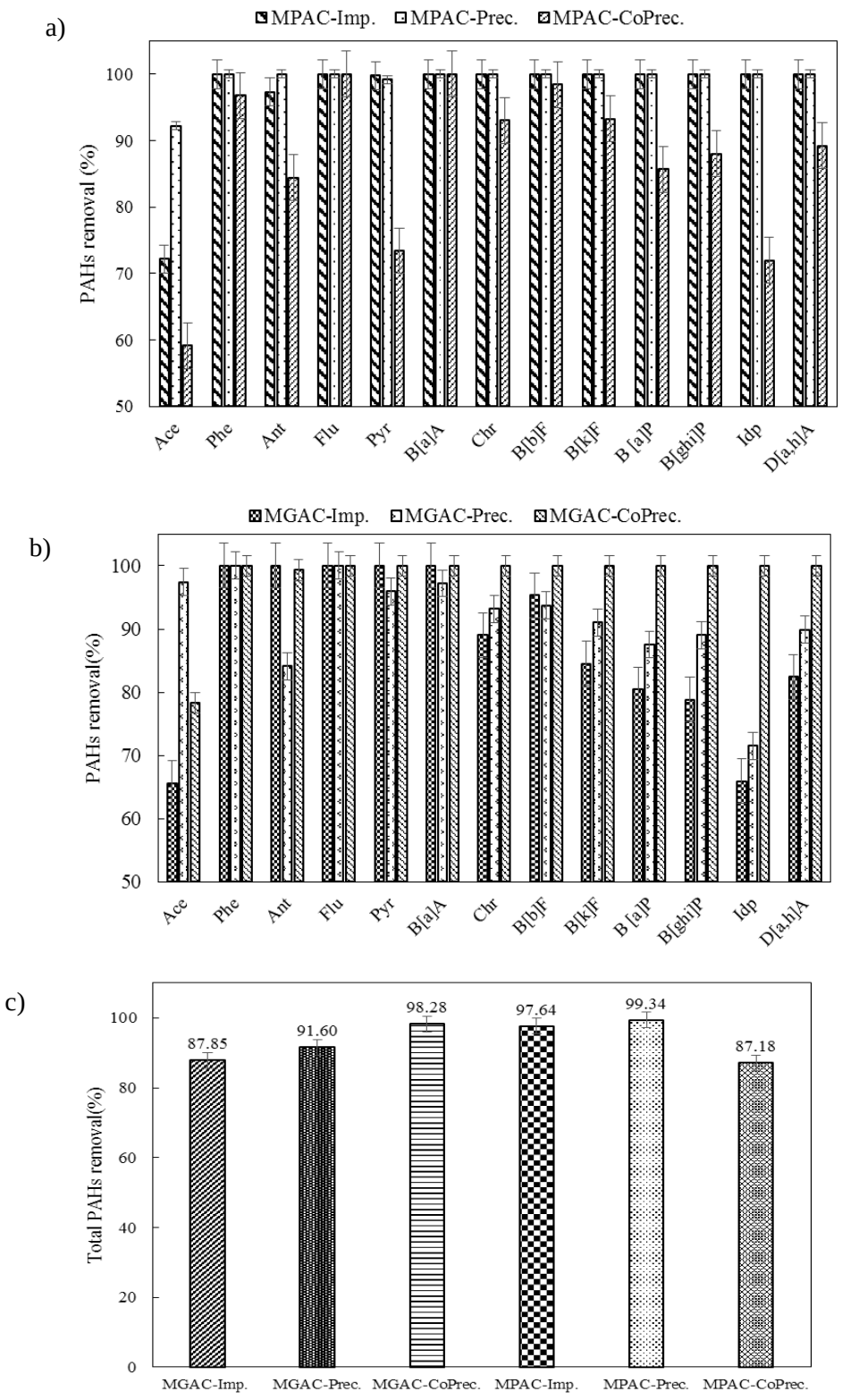

Figure 3.6. PAHs removal (%) in the aqueous solutions achieved by (a) MPACs and (b) MGACs (c) the six magnetic composites (total PAHs removal (%))

MPAC composite outperformed MGAC. Also, to compare the adsorption uptake capacity of MACs with the non-composite ACs, the adsorption uptake of bare PAC and GAC was explored. Both adsorbents showed a high affinity for all PAH compounds, similar to the results obtained by MPACs and MGACs (more than 97% of PAHs were removed by the bare ACs at PAHs concentration of 2.5 ppm).

The high adsorption uptake of PAH compounds by PAC is not uncommon since the use of powder type with smaller size in aqueous solution, compared to the granular AC, could provide a more significant number of AC particles per mL of water with a larger specific surface area and higher PAH adsorption capacity (PAC<45 μm and 550 μm <GAC<750 μm). The obtained results for MPAC-Imp. and MGAC-Imp. were exactly according to the expectation with higher PAHs removal for the MPAC than the granular type. A similar trend of PAHs adsorption was observed for the MPAC and MGAC fabricated using the precipitation method (99.3% for MPAC-Prec. vs. 91.6% for MGAC-Prec.). However, the magnetic ACs from the co-precipitation method showed different adsorption behavior, in which the MGAC-CoPrec. surpassed the MPAC-CoPrec. in the removal of the analytes from the solutions. A tentative explanation can be the availability of more strongly sorbing functional groups on MGAC-CoPrec. than MPAC-CoPrec. in the adsorption process. Also, the distribution of magnetic nanoparticles onto the granular type was likely more uniform than the small PAC particles as a result of their synthesis procedure.

Among all the six magnetic ACs, the lowest PAHs reduction was attained by MPAC-CoPrec. This indicates that the particle size and specific surface area are not the only parameters affecting the PAHs removal. The lower adsorption capacity of MPAC-CoPrec. may be due to the type of the synthesis process and the Fe to AC ratio (w%). Besides, when the distribution of iron oxide nanoparticles onto the adsorbent is uneven, the adsorption capacity would decrease, negatively affecting the uptake of PAH compounds by the adsorbent [64,68,69].

Table 3.2 summarizes some of the studies that used carbonaceous products for removal of PAH compounds from aqueous solutions. As it is evident from the Table 3.2, the carbonaceous products could adsorb a high portion of the PAHs from the contaminated solutions. However, none of these studies investigated the removal efficiency of the employed adsorbents for all the USEPA PAH compounds, while these contaminants are usually found together in the environment. Besides, the application of MAC for the PAHs removal was not explored that well by the literature. This study, however, was able to adsorb both LMW and HMW PAHs with removal percentages ranging from

87.2 to 99.3% by the use of different types of MPAC and MGAC composites. These results showed that the prepared magnetic adsorbents were highly efficient and affordable and may be considered for large-scale treatment processes while producing minimum waste and yielding maximum PAH uptake.

Table 3.2. Details of studies conducted on PAHs adsorption by carbonaceous products

Adsorbent	Description	PAHs removal (%)	Reference
Porous carbon	0.1 g porous carbon, 3.250-6.250 mg/mL PAHs 18 h contact time at 25 °C	NAP 94.0% PYR 78.4 % FLU 74.0% PHE 87.80% FLUO 88.20%	[121]
Magnetic graphene oxide	40 mg Fe_3O_4/GO 0.01 mg/L PAHs 10 min contact time	FlU 87.6% PYR 93.3% B[a]A 100.9% B[b]F 89.5% B[a]P 94.9%	[46]
Biochar	1-8 g/L biochar PHE (9.07 mg/L), FLU (10.05 mg/L), PYR (10.57 mg/L) 48h contact time at 25 °C	PHE 95.8% FLU 97.5% PYR 98.6%	[134]
Leonarditem	1g/L Leonarditem 5 to 100 mg/L PAHs 48h contact time at 25 °C	PYR 95% FLU 78% B[k]F 82% B[g,h,i]P 91% B[a]P 88%	[100]
Cork	300mg Cork o 1 to 50 mg/L PAHs 3 h contact time	PHE 95% FLU 90% ANT 96% ACE 80%	[135]

FTIR spectra of the magnetic ACs after PAHs adsorption (Figure 3.5) showed the molecular interaction of PAHs with the composite materials. For example, the peaks associated with

starching vibration of C=C bonds were observed at 1620 and 1640 cm^{-1} in PAH-loaded MPAC-Prec. and MGAC-CoPrec., which confirmed the formation of π-π interactions between the aromatic PAH molecules and the adsorbent surface. The broad bands centered at 1310, 1360, 3130, and 3320 cm^{-1} after the PAHs adsorption onto MPAC-Prec. and MGAC-CoPrec. correspond to the stretching vibration of carboxyl bonds and hydroxyl groups. All these changes in FTIR spectra of the PAH-loaded magnetic composites confirm the critical role of molecular interactions in PAHs adsorption by the composites [132].

There is a certain number of studies that have investigated the types of adsorption mechanisms performed by AC and other carbon based-adsorbents to sorb organic and inorganic compounds [23,36]. Wang et al. (2014) considered three mechanisms for adsorption of PAHs onto graphene and graphene oxide, including PAHs hydrophobic effects, molecular interactions (π electrons, Figure 3.7a) between the sorbent and PAHs, and change in the conformation of graphene which affects its adsorption sites during the PAHs uptake [132]. Yuan et al. (2010) proposed that a PAH compound is adsorbed onto carbon through the formation of H-bonding and the interactions between PAH molecule as electron donor and carbon molecule as electron acceptor (π-π interactions, Figure 3.7b). H-bonding interactions form between the hydrogen atoms of PAHs and oxygen atoms of carboxylic or hydroxyl groups in the carbon matrix. The electron donor-acceptor mechanism occurs when the adsorption sites of AC perform the role of electron acceptor and the PAH aromatic rings act as the electron donor. In other words, when carbon and PAH compound come into contact with each other, the π-π electron interactions form simultaneously between the PAH and layers of carbon due to the presence of π electrons in both carbon layers and non-polar and non-ionizable structure of the PAH (Figure 3.7b) [121]. According to a study conducted by Choi et al. (2016), there is a much greater adsorption affinity of AC surface than iron oxide surface to the aromatic pollutants, including PAHs. The researchers also indicated that iron oxide particles do not have any significant effect on PAH accessibility to the AC surface and pores structure as long as an appropriate synthesis method is applied for the preparation of the magnetic composite [72].

a)

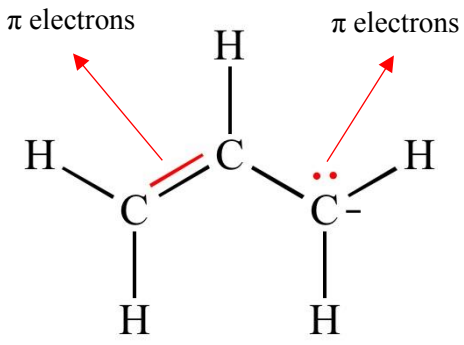

A three-ring PAH compound

b)

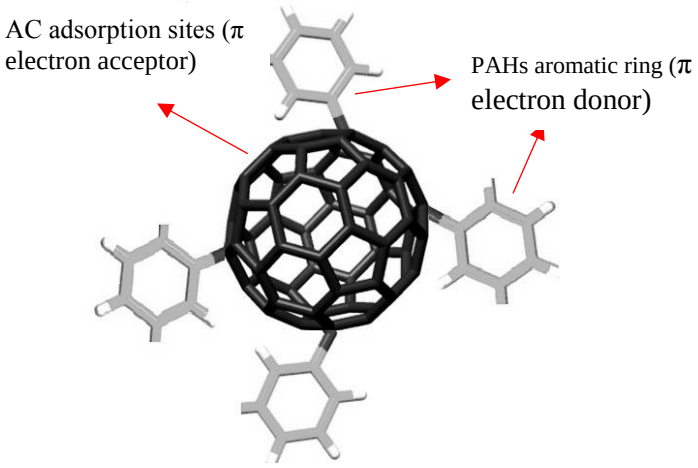

π-π interaction and H- bonding between aromatic ring of PAH compound and AC adsorption sites

Figure 3.7. (a) π electrons in the aromatic structure of a PAH compound, (b) molecular interactions between the aromatic ring of a PAH compound and carbon layers

3.4.4 Desorption experiments

The desorption experiments were conducted on the PAH-loaded MPAC-Prec. and MGAC-CoPrec. to evaluate the possibility of reusing the magnetic ACs in the adsorption process. For this purpose, samples with PAHs concentrations of 0.5 and 2 ppm were prepared from the working solutions, and the analytes were removed by the magnetic adsorbents according to the procedure discussed in this paper. The duplicate tests and control samples were also run in parallel. The recovered MPAC and MGAC particles were dried overnight and then weighed by a fine scale. Owing to the superparamagnetic characteristics of the magnetic nanoparticles, almost 100% adsorbent recovery was achieved with the magnetic bar. To determine the possibility of PAHs desorption from the used MPAC and MGAC particles, the adsorbents were subject to ultrasonic extraction using hexane/acetone as described in section 3.3.6 and the extracted analytes were subsequently analyzed by HPLC. According to the results presented in Table 3.3, the highest percentages of PAHs desorption from MPAC-Prec. and MGAC-CoPrec. were achieved for the PAHs with three and four aromatic rings. For example, for the solutions with an initial PAHs concentration of 2 ppm treated by MPAC-Prec., the desorption percentages of ACE, PHE, and FLUO were 44.1%, 57.2%, and 37.3%, respectively, whereas the desorption of the five- and six-ring PAHs was

significantly lower, with the highest desorption (8.5%) for B[a]P and the lowest (0.8%) for D[a, h]A. For the MPAC particles used in the 0.5 ppm PAHs solutions, the HMW PAH desorption percentages were below the detection limit, probably due to the low concentration of the analytes after desorption and difficulty in their detection by HPLC. The PAHs removal from the MGAC-CoPrec. surface showed a similar trend, with the highest desorption for the lighter PAHs (ACE, PHE, ANT, and FLUO) and the lowest for HMW ones. However, as shown in the Table 3.3, the PAHs removal from the used MGAC particles seems to be easier than the powder type. One possible reason for this behavior could be that the larger surface area and the stronger interactions between the PAH molecule and PAC surface make it more difficult for the extraction solvent to remove the analyte from the adsorbent efficiently [34].

The type of PAHs adsorption (i.e., physical vs. chemical) onto AC has been investigated by previous studies during the recent years with irreconcilable conclusions. Kumar et al. (2019) conducted a series of thermodynamic tests and reported that the adsorption of PAHs onto the AC particles was physical [136]. Based on pseudo-first order kinetic models, Eeshwarasinghe et al. (2018) also proposed that the adsorption of PAHs onto the GAC particles was a physical type [137]. However, Awoyemi (2011) observed that the kinetics of PAHs (Naphthalene (NAP) and FLU) adsorption were best fitted with the pseudo-second order model and concluded that it would validate the chemical adsorption of the PAHs by AC [52]. The fact that adsorption of PAHs is not fully reversible, and percent of the PAHs recovery is low (i.e. for MPAC, the PAHs recovery was between 0.8 and 57.2%, Table 3.3) could be an indication that PAHs adsorption was chemical type.

The results of PAHs desorption obtained for both MPAC and MGAC confirmed that the heavier PAH compounds are hardly eluted from the adsorbent because the non-covalent bonds and molecular interactions (π-π and H-π interactions) between the adsorbent and the analytes increase with the increase in the number of the PAH rings [46]. However, as can be seen from Table 3.3, no PAH analyte could be extracted completely from the adsorbents during the desorption experiments. Funada et al. (2018) studied PAHs recovery from Fe-AC-alginate with toluene and using ultrasonic irradiation. Their results showed that they could only remove a few PAH compounds (PYR, B[a]A, CHR, and B[b]F) with the desorption percentage ranging from 4 to 43%. The researchers concluded that most PAHs remained on the AC surface after the desorption process due to the strong interactions between the analytes molecules and the adsorbent [55].

However, more studies are needed to explore the recycling of the magnetic ACs, especially the most efficient extraction method and organic solvent to remove the PAH compounds from the adsorbents.

Table 3.3. Recovery (%) of PAHs from MPAC-Prec. and MGAC-Prec. after adsorption

	MPAC-Prec.		MGAC-CoPrec.	
PAHs	0.5ppm	2 ppm	0.5 ppm	2 ppm
ACE	78.03 ± 3.88	44.08 ± 12.94	44.11 ± 10.79	38.12 ± 2.72
PHE	18.42 ± 5.60	57.23 ± 5.81	28.41 ± 13.37	60.05 ± 6.60
ANT	9.70 ± 2.37	23.36 ± 10.02	25.24 ± 3.73	43.61 ± 7.31
FLU	60.13 ± 1.19	37.30 ± 14.76	26.37 ± 1.61	55.24 ± 11.40
PYR	9.01 ± 0.48	33.23 ± 36.38	22.98 ± 1.25	7.99 ± 5.06
B[a]A	30.57 ± 14.12	8.64 ± 10.37	7.55 ± 1.21	36.77 ± 2.76
CHR	11.35 ± 5.81	11.49 ± 8.99	20.22 ± 6.08	38.77 ± 5.93
B[b]F	< DL[a]	3.37 ± 4.47	8.26 ± 5.19	29.84 ± 7.09
B[k]F	< DL	3.01 ± 3.99	17.42 ± 6.49	30.22 ± 7.31
B[a]P	< DL	8.54 ± 5.31	19.41 ± 9.19	31.50 ± 9.33
B[ghi]P	< DL	1.06 ± 1.50	28.93 ± 7.76	21.61 ± 7.18
IDP	< DL	2.25 ± 3.18	42.31 ± 12.39	24.18 ± 7.82
D[a,h]A	< DL	0.82 ± 1.16	12.26± 4.45	17.811 ± 6.48

[a] Below detection limit

3.5 Conclusions

Three different magnetization methods were employed to prepare magnetic PAC and GAC composites. Under the conditions for this study, the results of the adsorption experiments, all the synthesized magnetic ACs (MACs) were effective in removing PAHs from the aqueous phase with removal efficiencies in the range 87.2–99.3%. Also, it was discovered that the type of magnetization method and AC particle size could affect the adsorption capacity of ACs and accessibility of their adsorption sites for the analytes. Magnetization using the precipitation method resulted in the highest PAHs removal efficiency (99.3%) with PAC as the base AC, while the co precipitation method could provide the highest PAHs removal efficiency (98.3%) using GAC as the base AC. The results of PAHs desorption tests indicated that full recovery of PAH compounds from the magnetic ACs is unlikely.

The XRD results confirmed the formation of iron oxide nanoparticles onto PAC and GAC with regard to the diffraction peaks that emerged at the MPAC and MGAC patterns. The SEM images

illustrated porous and bulky amorphous structures of PAC and GAC and spongy crust shape of the magnetite nanoparticles formed onto the ACs. The formation of Fe_3O_4 nanoparticles onto PAC and GAC was also confirmed by the EDS method. The FTIR spectra of MPAC-Prec. and MGAC-CoPrec. before and after PAHs adsorption revealed that the carboxyl and hydroxyl groups of the adsorbents were involved in the uptake of PAHs through π-π and H-π interactions and electron donor–acceptor mechanism.

3.6 References

This chapter's references are integrated with the references from the other chapters and provided at the end of the thesis.

4 Activated Carbon-Based Magnetic Composite as an Adsorbent for Removal of Polycyclic Aromatic Hydrocarbons (PAHs) from Aqueous Phase: Characterization, Kinetics and Adsorption Isotherm Studies[2]

4.1 Abstract

This study investigated the preparation, characterization, and capacity of a magnetic powder activated carbon (MPAC) composite to remove polycyclic aromatic hydrocarbons (PAHs) from aqueous solutions. The FTIR spectra of the PAH-loaded MPAC illustrated that the PAH compounds were adsorbed to the MPAC surface through π-π and H-π interactions formed between the adsorbate and adsorbent. The PAHs adsorption by MPAC was relatively fast and reached equilibrium in 6 h with the removal efficiency ranging from 95.6 to 100.0%. The pseudo-second order model exhibited the best fit for the kinetics data, suggesting that all the MPAC adsorption sites had an equal affinity for the PAHs molecules and the adsorption process was chemical. The results of the kinetics experiments also indicated the slower adsorption rate of the higher molecular weight PAHs due to the slower transfer of these analytes to the accessible adsorption sites of MPAC. The Langmuir model described the isotherm adsorption of both low molecular weight (LMW) and high molecular weight (HMW) PAHs well, with an R^2 in the range of 0.73-0.96. This model also showed that the MPAC particles had a maximum adsorption capacity ranging from 8.74 to 11.37 µg/mg for LMW PAHs and 8.43 to 20.21 µg/mg for HMW PAHs, respectively.

Keywords: Magnetic powder activated carbon, Polycyclic aromatic hydrocarbons, Adsorption, π-π interactions, Maximum adsorption capacity

[2] A version of this paper has been published in the Journal of Hazardous Materials Advances. (https://doi.org/10.1016/j.hazadv.2022.100083)

4.2 Introduction

Polycyclic aromatic hydrocarbons (PAHs) are a group of persistent and hydrophobic organic contaminants that can travel long distances and contaminate various environmental matrices such as air, water, and soil [107,138–140]. The main sources of PAHs discharge into the environment are anthropogenic activities such as the processing and handling petroleum products and incomplete combustion of organic material (e.g. coal, wood, and petrol) [138]. In many commercial and industrial sites in North America, the concentration of PAHs exceeded the regional and/or federal standards [12]. For example, in the United States, there are about 1300 abandoned contaminated sites where the soil has been highly contaminated with PAHs as a result of oil refinery activities [8]. Similar cases have been documented in Canada, with more than 6800 PAH-contaminated sites mostly located in the industrial areas [14].

Sixteen of the PAHs have been designated as priority pollutants by various environmental agencies, such as the U.S. Environmental Protection Agency (USEPA) and the Canadian Council of Ministers of the Environment [14,17]. These PAH compounds are toxic, thermodynamically stable, and resistant to biodegradation [4,14,107,111,129], and their release into the environment could have severe impacts on human health and living organism [134,141–143]. The USEPA priority PAHs are difficult to break down once dispersed into water or soil due to their low water solubility, high melting point, and other distinctive features [141,144,145].

In recent decades, various treatment techniques have been used to remove PAHs from aqueous solutions, including electrochemical techniques [146,147], biodegradation [47], chemical oxidation [112], solvent extraction, photolysis, and thermal desorption [148–150]. Adsorption using activated carbon (AC) is also one of the treatment techniques that has extensively been employed for the removal of PAHs due to its fast and easy implementation, high efficiency, low cost, and less or no harmful by-products [134,136,137,141,151]. However, the recovery of AC in the adsorption process could present major practical challenges if the contaminated aqueous phase contains other constituents and fine particles. A particular case is when soil is the contaminated medium and AC is used in washing solution to remove PAHs from the soil particles. In this case, separation of the AC particles from the soil slurry by the use of filtration or centrifugation is practically impossible. As a result, the PAH-loaded AC particles may remain in the soil after the treatment creating a secondary source of contamination for the soil organisms and plants.

The AC properties can be modified in order to make their recovery and recycling feasible [75,80,152]. Magnetization is one of the modification methods which is used to combine AC and iron oxide and synthesize a recoverable magnetic AC adsorbent for water/soil treatment purposes [80,99,152]. However, it has been reported that the type of magnetization can affect the composite characteristics such as specific surface area and pore volume, as well as adsorption capacity [74,77]. Mirzaee and Sartaj (2021) assessed the feasibility of preparing magnetic AC using both powder and granular AC and different synthesis methods, including precipitation, co-precipitation, and impregnation. Results indicated that the magnetic composite synthesized by the precipitation method and powder AC showed the greatest performance for removing PAHs from aqueous solutions [153]. To continue and advance the previous feasibility study, the authors conducted more detailed research to explore the affinity of a recoverable magnetic powder activated carbon (MPAC) composite, synthesized by the precipitation method, to both low molecular weight (LMW) and high molecular weight (HMW) PAHs in aqueous solutions. The objectives were to study adsorption isotherms and adsorption kinetics and to characterize MPAC using BET, XRD, FE-SEM, EDS, and FTIR. There is very limited information in the literature on the adsorption capacity of MPAC for PAHs. The previous studies either investigated other types of carbon-based materials such as graphene oxide [46] and carbon nanotubes [154] or granular AC (GAC) for removal of a limited number of PAH compounds [137,155]. To the best of the authors' knowledge, this is the first comprehensive study on the application of MPAC for adsorption of a broad range of USEPA priority PAHs from an aqueous medium.

4.3 Experimental

4.3.1 Materials

The powder AC (PAC) used as the base material was produced from coconut shell and was obtained from CalgonCarbon Co. (Pennsylvania, USA). The PAC particles were smaller than 45 μm in size with high activity and durability. Two PAH standard solutions (10 and 500 mg/L in acetonitrile) containing acenaphthene (ACE), chrysene (CHR), anthracene (ANT), benzo[ghi]perylene (B[ghi]P), benzo[a]pyrene (B[a]P), benz[a]anthracene (B[a]A), benzo[b]fluoranthene (B[b]F), benzo[k]fluoranthene (B[k]F), dibenz[a,h]anthracene (D[ah]A), and phenanthrene (PHE) were supplied by Sigma Aldrich Co. (St Louis, USA) and AccuStandard Co. (Connecticut, USA), respectively. Iron (II) sulfate heptahydrate ($FeSO_4 \cdot 7H_2O$) was purchased

from Sigma-Aldrich Co. (St. Louis, USA), and potassium nitrate (KNO_3), sodium azide (NaN_3), and acetonitrile and methylene chloride (HPLC grade, >99%) were obtained from VWR (Quebec, Canada). Distilled deionized water used in the batch adsorption experiments was sourced from a Millipore-Q purification system (Millipore Co., Bedford, USA).

4.3.2 Preparation of precipitated PAC/Fe_3O_4 composite

The MPAC (PAC/Fe_3O_4) composite was prepared using a modified precipitation method. PAC was selected as the inner core of the magnetic composite for two reasons: (1) it has an amorphous structure appropriate for impregnation of the magnetic nanoparticles, and (2) it is available at low cost. To prepare MPAC (PAC/Fe_3O_4) composite, 2.78 g ferrous sulphate ($FeSO_4.7H_2O$) was added to a 250 mL conical flask containing 100 mL deionized water. The solution was then mixed with 0.5 g of PAC, followed by agitation for 30 min using a magnetic stirrer. To precipitate the hydrated iron oxide particles, 10 mL NaOH solution (10%) was prepared and subsequently added dropwise to the flask. Afterward, the suspension was kept under stirring at 100 ℃ for 1 h to place the synthesized iron oxide particles onto PAC. The prepared composite particles were dried overnight and then repeatedly rinsed with deionized water to remove the excess non-PAC bound magnetic nanoprecipitate and until their pH became neutral. The MPAC particles <45 µm were finally separated by a magnetic bar and then placed in screw cap vials prior to use in the adsorption experiments [123].

4.3.3 Characterization of the prepared MPAC

The morphology of MPAC and the bare PAC particles was analyzed by a field emission scanning electron microscopy (FE-SEM, JSM-7500F, JEOL, USA) equipped with an EDS detector (Oxford EDS system). The energy-dispersive spectroscopy (EDS) technique was used to evaluate the distribution of magnetite nanoparticles (Fe_3O_4) in the matrix of the prepared composite. The EDS analysis was carried out by creating a spectrum of the elements found in the structure of the PAC and MPAC particles. The nature of the under-evaluation particles was also determined using a Rigaku Ultima IV X-ray apparatus (XRD). All XRD patterns obtained for the MPAC and bare PAC samples were determined in the range 10° to 80° with a scan speed of 4°/min. To evaluate the functional groups on the surface of MPAC particles before and after adsorption of the PAH compounds, Fourier transform infrared (FTIR) spectroscopy (Nicolet 6700 FTIR spectrometer, Thermo Fischer, USA) was employed. The FTIR spectra of the samples were examined in the

wavenumber range 400-4500 cm^{-1} by applying 32 scans and a resolution of 4 cm^{-1} for each sample. The Brunauer–Emmett–Teller (BET) surface area of PAC and MPAC were measured by conducting N_2 adsorption-desorption isotherms using an Accelerated Surface Area & Porosimetry System (ASAP) 2020 at 77 K (Micromeritics Instruments Inc., GA, USA). To perform the surface area measurement, the samples were loaded into a glass analysis tube and then heated at 100 °C under vacuum for 7 h followed by heating at 200 °C for 10 h. Afterward, the samples were backfilled with N_2 and then evacuated for a further 30 min at 200 °C before the analysis process. The porosity distribution of the adsorbents was determined by the Barrett-Joyner-Hanlenda (BJH) method.

4.3.4 Preparation of the mixed PAHs working solutions

1 mL of 500 mg/L standard solution of the mixed PAHs in acetonitrile was added to a 5 mL volumetric flask, and the volume was diluted with acetonitrile, providing a final concentration of 100 mg/L of each PAH compound. The prepared solution was then serially diluted to provide the PAHs concentrations ranging from 0.5 to 10 mg/L for the batch adsorption isotherm experiments. All the working solutions in the flasks were agitated at 50 rpm for 1 h in order to provide a homogeneous distribution of the PAH compounds in the solutions. Acetonitrile was used as the organic solvent to prepare the working solutions because it improves the solubilization of PAH compounds in the background solutions with regard to the applied PAHs concentration range [156,157].

4.3.5 Batch adsorption isotherms and kinetics experiments

To prepare the background solutions, 200 mg/L NaN_3 and 1 mmol KNO_3 were mixed with deionized water in a series of 125 mL conical flasks to inhibit any potential biological activities [59]. The mixtures were then homogenized on an orbital shaker device at 50rpm and 24 ± 1 °C for 0.5 h. The study of adsorption kinetics is essential for understanding the rate of reaction, reaction pathways, and efficiency of the adsorption process [23,129]. For the adsorption kinetics experiments, the PAHs working solution was added to each flask to adjust the PAHs concentration to 1 mg/L. The solutions were then mixed on the orbital shaker at 50 rpm and 24 ± 1 °C for 1 h to become homogeneous. Afterward, 30mg of MPAC was added to the flasks, and the suspensions were agitated at 100 rpm for preselected time intervals ranging from 2 min to 6 h. Finally, the used

MPAC particles were recovered from the suspensions by placing a magnetic bar at the bottom of the flasks and separating the aqueous solution.

For the adsorption isotherms experiments, samples with different initial concentrations of PAHs ranging from 0.5 to 10 mg/L were prepared. The samples were shaken for 1 h to spread the PAH compounds in the solutions uniformly and subsequently mixed with 30 mg of PAC or MPAC composite for the adsorption process. The samples were then continuously agitated on the orbital shaker at 100 rpm and 24±1 ℃ for 6 h determined based on the kinetic experiments. All the tests were conducted in duplicate, and the flasks were wrapped with aluminum foil to protect them against the potential effects of light. At the end, the MPAC particles were magnetically separated. In the case of PAC, the adsorbent particles were separated from the solutions using the centrifugation method. The control samples were run in parallel for both the adsorption isotherms and kinetics experiments. The preliminary tests conducted with the PAHs mixture alone indicated that the loss of PAHs due to flask wall adsorption was negligible. The residual concentration of PAHs in the samples was determined by the HPLC instrument, as explained in section 4.3.7.

The solid phase concentration of PAH compounds adsorbed onto PAC or MPAC at equilibrium can be calculated using the following equation:

$$q_e = \frac{(C_0 - C_e)V}{M} \qquad (4.1)$$

Where q_e (µg/mg) is the PAHs adsorption uptake of PAC or MPAC, C_0 and Ce represent the initial and equilibrium concentration of the PAH analytes in the solution (µg/mL), respectively. V is the volume of the background solution (mL), and M shows the mass of PAC or MPAC used in the adsorption process (mg) [158].

The Freundlich, Langmuir, and Temkin isotherm models were selected to evaluate the adsorption uptake capacity of PAHs on the PAC or MPAC and fit the obtained experimental data. According to the Freundlich model, an adsorbent surface contains numerous adsorption sites with varied potential sorption capacity, leading to multilayer and heterogeneous adsorption of contaminants onto the adsorbent. The other assumption considered by this model is that the stronger binding sites are occupied first with the adsorbate molecules, and as the degree of occupation increases, the binding strength decreases [73,157]. Freundlich model can be displayed as the following equation:

$$q_e = K_F C_e^{\frac{1}{n_f}} \qquad (4.2)$$

where K_F is the Freundlich constant known as the adsorption capacity parameter and n_f shows the adsorption intensity.

It has been reported that $1/n_f$ values in the range 0.1-1 are evidence of a favourable adsorption process, suggesting a stronger interaction between the adsorbent surface and the adsorbate molecules [137,157,158].

The Langmuir isotherm model describes an adsorbent with a certain number of homogeneous binding sites that all show the same affinity for the adsorbate molecules. This model also assumes that each binding site only adsorbs one molecule, leading to the formation of a single monolayer of the adsorbate on the adsorbent surface. The other assumption is that adsorption energy never changes and the adsorbate cannot be transmigrated on the adsorbent surface [73,159].

The Langmuir model plots the relationship between C_e and q_e in the adsorption process as follows:

$$q_e = q_m . \frac{K_L C_e}{1+K_L C_e} \qquad (4.3)$$

where K_L is the Langmuir affinity constant (mL/µg) and q_m (µg/mg) is the adsorption capacity of adsorbent, through which a certain number of the adsorbate molecules is sorbed by a unit mass of the adsorbent. Both K_L and q_m are considered as characteristics of the adsorbent and adsorbate pair.

Using the parameters from the Langmuir model, the separation factor, R_L, which is a dimensionless constant, can be obtained from the following equation:

$$R_L = \frac{1}{1+C_m K_L} \qquad (4.4)$$

where C_m represents the maximum initial concentration of the PAHs and K_L is the Langmuir constant. The separation factor is inversely related to the strength of binding [160]. An R_L value in the range of 0-1 indicates the favourable adsorption process. However, when the R_L approaches 0, the adsorption process becomes irreversible, and when R_L approaches 1.0, the adsorption will be linear [161].

The Temkin isotherm model considers indirect adsorbate/adsorbate interactions and their effects on the adsorption process. Another phenomenon considered by this model is the linear reduction in adsorption heat of all the adsorbate molecules due to the increase in coverage of the adsorbent surface. Besides, the characterization of the adsorption process is interpreted using a uniform distribution of binding energies, up to the highest binding energy in the adsorption [162,163]. The

following equilibrium equation is used for the Temkin model to plot PAHs adsorption isotherms of the MPAC composite:

$$q_e = \frac{RT}{B} (\ln K_T C_e) \quad (4.5)$$

Where R is the universal gas constant (8.314 J/mol/K); T is the constant parameter related to the heat of adsorption (J/mol); and B and K_T are the Temkin isotherm constant and equilibrium binding constant (mL/µg), respectively.

4.3.6 Kinetics modelling

Three kinetic models (pseudo-first order, pseudo-second order, and Intra-particle diffusion models) were employed to describe the adsorption kinetics of PAHs onto MPAC. The pseudo-first order (PFO) model evaluates the adsorption in the solid-liquid system using Lagergren's equation (Eq. 4.6):

$$\ln(q_e - q_t) = \ln q_e - K_1 . t \quad (4.6)$$

where q_t and q_e introduce the quantity of the PAH compounds (µg/mg) sorbed at time t and equilibrium, respectively, and k_1 (min^{-1}) is the rate constant parameter for PFO at equilibrium. The K_1 parameter can be obtained from the linear plot of ln (q_e-q_t) versus time (min) [73]. According to this model, one PAH compound is sorbed onto one adsorption site of the adsorbent surface. The pseudo-second order (PSO) model takes into account the chemisorption kinetics from liquid solutions. This model assumes that the type of adsorption process is chemical, and the adsorption rate relies on adsorption capacity, not on the concentration of the adsorbate [164]. The following equation is used to describe the PSO process:

$$\frac{t}{q_t} = \frac{1}{K_2 q_e^2} + \frac{1}{q_e} t \quad (4.7)$$

where k_2 is the rate constant parameter of PSO at equilibrium (g/µg.min) [4]. The values of $1/K_2.q_e$ and $1/q_e$, and subsequently, K_2 and q_e can be derived from the intercept and slope of the linear plot between t/q_t and time (min).

The intra-particle diffusion (IPD) model was the third kinetic model used to analyze the rate kinetics of PAHs adsorption onto MPAC. This model considers the importance of the diffusion phenomenon during the adsorption process and describes the movement of the analyte from the solution to the solid phase (adsorbent). According to this model, the PAHs adsorption on MPAC involves two steps: the first step represents the macropore diffusion of PAH compounds from the aqueous solution to the exterior surface of the MPAC composite (external diffusion), and the

second step shows micropore diffusion of PAHs into the composite pores. The following equation (Weber and Morris equation) was applied to explain the diffusion mechanism of PAHs in the adsorption process:

$$q_t = K_3 t^{0.5} + A \qquad (4.8)$$

where K_3 is the IPD rate constant (µg/g.min$^{0.5}$) and A displays the thickness of the boundary layer (ug/mg). The K_3 and A parameters can be calculated by plotting q_t versus $t^{0.5}$, where the slope of the linear plot reflects the value of K_3 and the intercept illustrates the A parameter or boundary layer effects [73,165].

Correlation coefficient (R^2) and residual root-mean-squared error (RMSE) were employed to evaluate the goodness of fitting of each model with the experimental data [166]. A higher R^2 (close to 1) and lower RMSE values (close to 0) propose a better-fitted model [167,168].

4.3.7 PAHs measurement

The PAHs concentrations in the samples were determined using High-Pressure Liquid Chromatography (HPLC, Hewlett–Packard 1100, Agilent Technologies, USA) equipped with a reverse phase HPLC column (ZORBAX Eclipse PAH, 95Å, 4.6×250mm×5µm) and multiple wavelength detector (MWD). For this purpose, calibration solutions were prepared by serial dilution of the 500 µg/mL stock solution in acetonitrile. An aliquot of the prepared solutions, with PAHs concentrations ranging from 0.05 to 100 µg/mL, was then injected into HPLC to provide six-point calibrations for the PAH compounds. To measure the PAHs residue after treatment, the solutions were added to a 50 mL centrifuge tube and extracted with methylene chloride (HPLC grade, >99%) using a vortex mixer (Cole-Parmer CO, QC, Canada). The mixture was then centrifuged at 1500rpm for 2 min and the solvent containing the analytes was removed from the tube by a pipette [45,169]. This process was repeated three times and all the extracts were combined before being concentrated by Kuderna-Danish (K-D) apparatus. The extracts were condensed to 1 mL and exchanged to the highly compatible solvent for HPLC, acetonitrile, using K-D according to method 8310, USEPA [17]. Finally, 25µL of the acetonitrile solution was injected onto the HPLC column to determine the concentration of the PAH analytes. The chromatography was conducted with acetonitrile and deionized water (95:5, v/v) as the mobile phase using a flow rate of 1 mL/min. The PAH compounds in the HPLC column were detected at 210.8, 224.4, 230, 8, 254.4, and 270.9 nm by use of the MWD [48,75].

4.4 Results and discussion

4.4.1 Characterization of unmodified and magnetic PAC

The XRD diffraction patterns of the unmodified PAC and MPAC samples are shown in Figure 4.1. According to this figure, the XRD pattern of the unmodified PAC has one strong and one weak diffraction peak at 2θ = 23.4° and 2θ = 43.8°, respectively, which reflect the amorphous structure of the PAC particles. The characteristic peaks in the MPAC sample were found at 21.9^0, 30.2^0, 35.6^0, 43.3^0, 53.8^0, 57.1^0, and 62.8^0, according to XRD analysis. All these peaks correspond to the cubic spinel structure of the magnetic nanoparticles (magnetite or maghemite) formed onto MPAC. The spinel reflection at (311), (400), and (440) showing the crystal structure of the iron oxide nanoparticles are in agreement with the iron oxide standard data (Joint Committee for Power Diffraction Studies, Card No. 40 -0748) [170]. The broad diffraction peak centered at $2\theta = 21.9^0$ of the PAC XRD pattern represents the characteristic reflection of the AC particles. This peak in the XRD pattern of MPAC, however, emerged as a very small characteristic peak, which was due to the formation of a layer of magnetite nanoparticles on the PAC surface after magnetization [75,123,170].

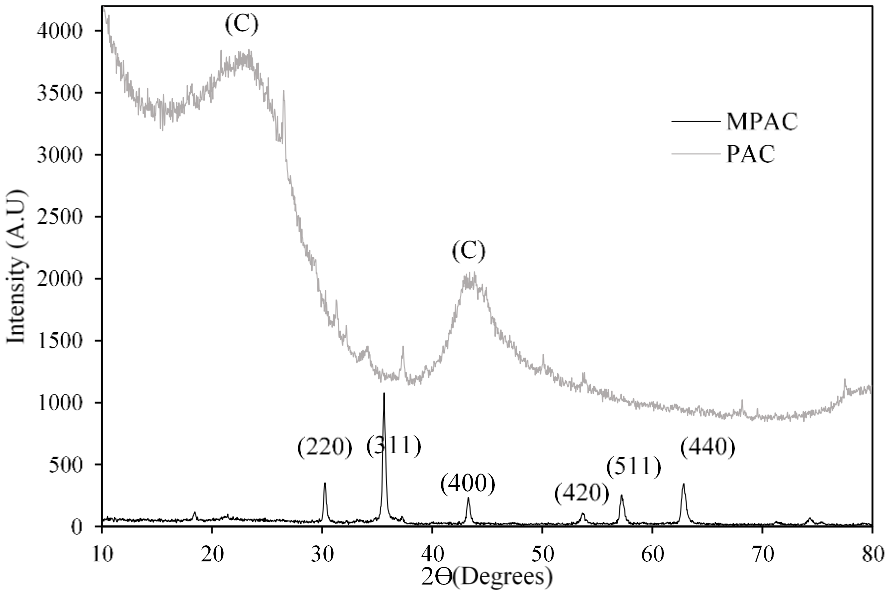

Figure 4.1. XRD patterns of bare PAC and MPAC composite

The size of the synthesized magnetic nanoparticles on MPAC can be determined by the use of the Scherrer equation as follows [170]:

$$D = \frac{K\lambda}{{}_{\beta}\cos\theta} \qquad (4.9)$$

where D is the size of the crystallites (nm), K is known as the Scherrer constant (K=0.9), λ is the X-ray wavelength equal to 1.5418, β is the full width at half maximum of the diffraction peak considered for (311), and (440) plane of the spinel reflections, and θ is the angle of X-ray diffraction. The Scherrer equation (Eq. 4.9) yielded values of 14.53 and 11.38 nm for the two spinel reflections, implying that the produced iron oxide particles maintained nano-size crystal structure in the composite matrix [170].

Figure 4.2 presents N_2 adsorption-desorption isotherms and pore size distribution of the unmodified PAC and MPAC particles. In

Figure 4.2a, the hysteresis loops for both samples show that their isotherms were of type I according to IUPAC classification; therefore, the solids had a mesoporous structure [76,80,171]. In addition, the hysteresis loop of the MPAC isotherm is smaller than the PAC, indicating that the formation of magnetite nanoparticles on the PAC surface reduced the total pore volume of the AC powders [80]. The pore size distribution (

Figure 4.2b) confirms this conclusion. As shown in

Figure 4.2b, the average pore size for PAC decreased after the magnetization process due to the occupation of the pores with the iron oxide nanoparticles. Consequently, the micropore volume of the prepared MPAC composite was lower than the bare PAC, which is in agreement with the results reported in the literature [30,41,68,80].

Table 4.1 shows that the deposit of magnetite nanoparticles on the surface and inside the pores of PAC reduced its pore properties, as expected. According to the Table 4.1, the values of the BET surface area, micro-pore volume, and total pore volume dropped from 920 to 324 m^2/g, 0.32 to 0.1 cm^3/g, and 0.41 to 0.14 cm^3/g, respectively, a reduction of nearly 65% for each parameter. The literature confirms that the reduction of the BET surface area for AC particles is usually more than 30% after magnetization, depending on the ratio of precursors used in the synthesis process [41,68,80,84].

a)

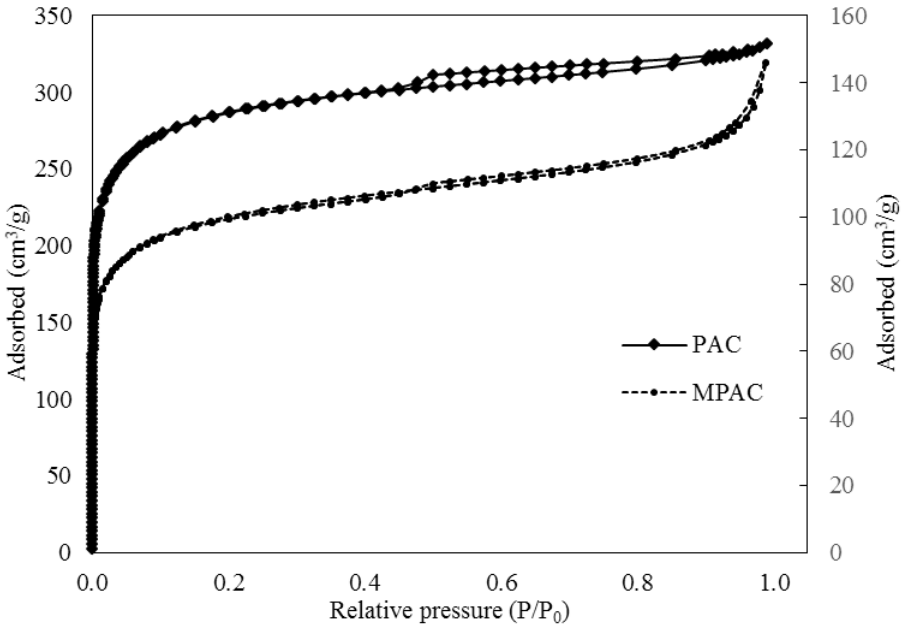

b)

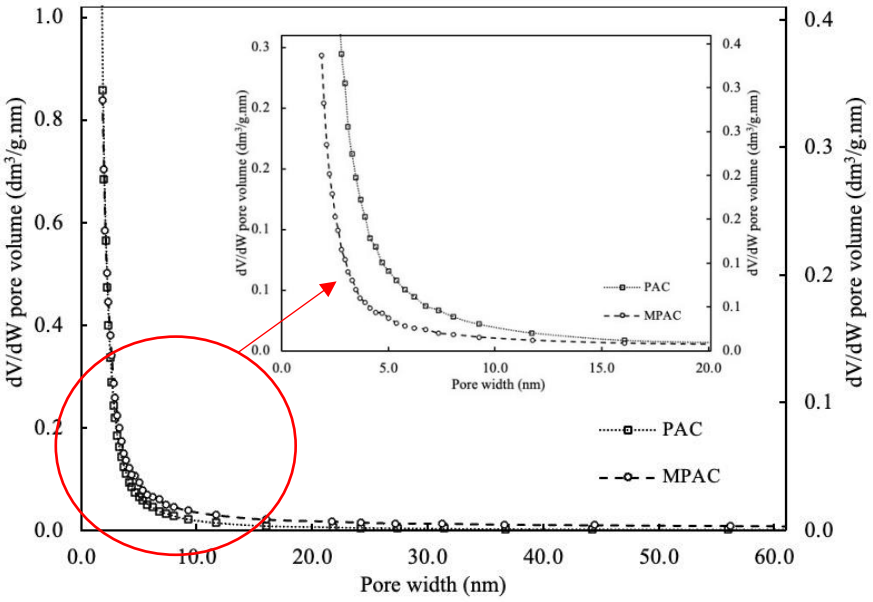

Figure 4.2. N_2 adsorption-desorption isotherms and pore size distribution of PAC and MPAC

Table 4.1. The pore characteristics of PAC and MPAC based on N_2 adsorption/desorption isotherms

Sample	BET surface area (m^2/g)	Micropore vol. (cm^3/g)	Total pore vol. (cm^3/g)
PAC	920.6	0.32	0.41
MPAC	324.7	0.10	0.14

Do et al. (2011) and Li et al. (2017) reported complete removal of methyl orange (MO) and methylene blue (MB) from the water solutions using MAC composites. The BET test results of these studies revealed a reduction of 31% and 69% in the surface area of the AC particles after magnetization, respectively. Despite the reduction in the surface area, both studies confirmed that the MAC composites could retain their adsorption capacities for removal of MO and MB, suggesting it as a promising adsorbent for organic contaminants in aqueous solutions [41,67]. Lompe et al. (2017) indicated that MPAC with different mass fractions of iron oxide nanoparticles had almost the same removal efficiency for dissolved organic carbon when it was normalized based on the available activated carbon content in the structure of MPAC. Park et al. (2015) also observed up to 10 times higher removal of natural organic matter (NOM) by MPAC prepared by the impregnation method, even though its surface area was estimated to be 50% lower than the surface area of the bare PAC. On the other hand, Kim et al. (2013) reported a reduction in adsorption of NOM by MPAC compared to the bare PAC. The researchers attributed this reduction to the lower micropore volume and surface area of MPAC than the bare PAC. Zahoor (2014) also reported that MPAC composite adsorbed 20% lower humic acid than the bare PAC and attributed this reduction to the lower available surface area of the composite [99]. However, with regard to the results of these two studies, the reduction in adsorption capacity could originate from the lower PAC mass fraction in the MPAC density. According to a study conducted by Lompe et al. (2017), it was proposed that the attachment of iron oxide nanoparticles onto PAC would increase the porosity of the MPAC composite [99]. For MPAC with an iron oxide mass fraction of 38% and mean size of 17 nm, the researchers estimated the specific pore volume per g of the adsorbent to be ranged from 0.15 - 0.39 mL/g, showing a significant increase compared to the bare PAC. Based on this estimate, they concluded that the presence of iron oxide nanoparticles in the matrix of PAC can compensate for the loss of pore volume in the micropores and mesopores of the adsorbent after the synthesis process and help it maintain its adsorption capacity for the analytes [99].

Figure 4.3 presents the SEM analysis of the PAC and MPAC samples. The bare PAC (Figure 4.3a) had a porous and bulky amorphous structure, with a smooth surface. In the MPAC matrix (Figure 4.3b), however, the surface was covered with the crystalline magnetic nanoparticles distributed uniformly onto PAC in the shape of spongy crust [68,73,99].

a) PAC

b) MPAC

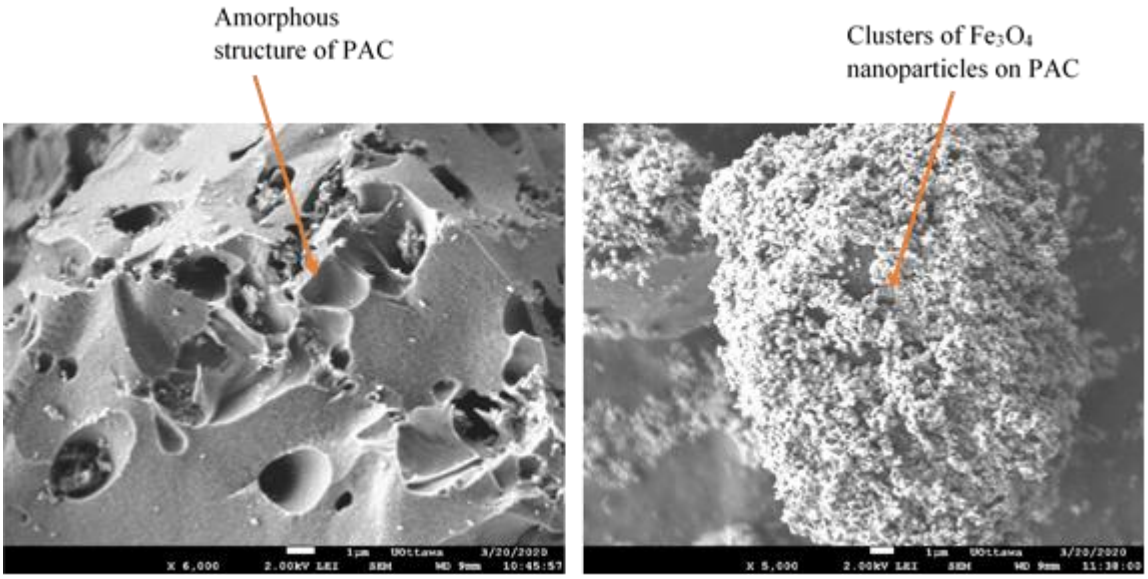

c) MPAC

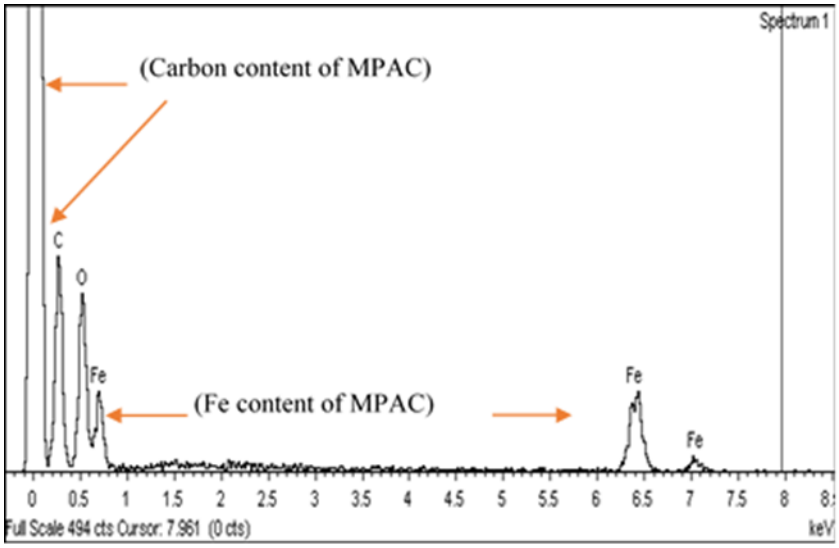

Figure 4.3. The SEM images of (a) PAC (b) MPAC (c) Energy-dispersive spectroscopy (EDS) spectra of MPAC

EDS analysis was used to gather information on the elemental distribution of magnetite nanoparticles on PAC. Figure 4.3c shows that the MPAC spectrum includes sharp peaks for Fe and O in addition to the peak for carbon content. This implies that during the synthesis process, the magnetite nanoparticles were appropriately produced and attached to the PAC matrix. Figure 4.3c further shows that the carbon content in the magnetic composite structure was

significantly higher than the iron content, implying the primary role of PAC as the adsorbent in the composite structure [73,99,172].

4.4.2 FTIR spectra analysis of MPAC

The FTIR analysis of MPAC before and after PAHs adsorption is shown in Figure 4.4. The sharp peaks in the spectrum of the unloaded MPAC were centred at 484 and 542 cm^{-1}, whereas the peaks in the spectrum of PAH-loaded MPAC were located at 509 cm^{-1} and 553 cm^{-1}, respectively. This can be due to the stretching vibration of Fe–O, which demonstrates the existence of Fe3O4 nanoparticles on PAC [73]. The medium peak at 793 cm^{-1} in the unloaded MPAC shifted to 789 cm^{-1} after the PAHs adsorption. This change is attributed to the deformation out of plane of the C-H bond in the PAHs aromatic rings [129]. The peak centred at 883 cm^{-1} in the spectrum of MPAC shifted to 879 cm^{-1} after the PAHs adsorption, which corresponds to the hydroxyl groups attached by the hydrogen bonds in the MPAC composite [52,70,73,130]. Furthermore, the weak signal observed at 1120 cm^{-1} in the spectrum of MPAC before the adsorption process shifted to 1131 cm−1 after the PAHs uptake, which can be attributed to the stretching vibration of C=C bonds in the carboxylic groups of the magnetic composite [130,155]. The broad bands located at 3103 cm^{-1} and 3398 cm^{-1} in the spectrum of the PAH-loaded MPAC can be associated with the stretching vibration of the hydroxyl groups (−OH) [30,70]. All these peak shifts observed in the spectrum of PAH-loaded MPAC confirm the formation of interactions between the hydroxyl and carboxyl groups of MPAC and the aromatic rings of PAH analytes during the adsorption process [155]. Furthermore, the broad peak that emerged at 1310 in PAH-loaded MPAC can be attributed to the vibration of carboxyl bond (O=C−O) following the PAHs adsorption. The other broad bands located at 3130 and 3420 cm^{-1} in the spectrum of the PAH-loaded MPAC can be associated with the stretching vibration of the hydroxyl groups (−OH) [30,70]. All these peak shifts observed in the spectrum of PAH-loaded MPAC confirm the formation of interactions between the hydroxyl and carboxyl groups of MPAC and the aromatic rings of PAH analytes during the adsorption process.

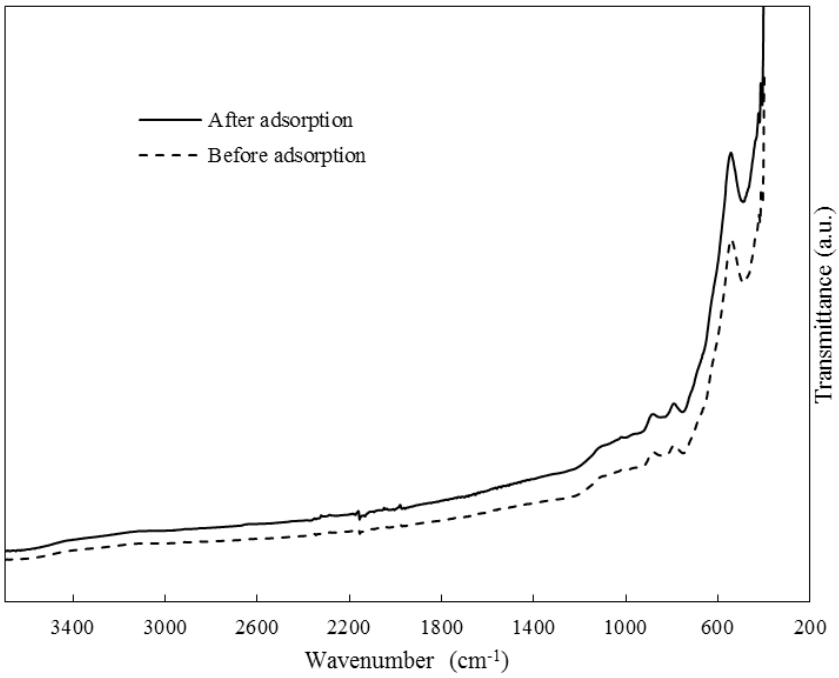

Figure 4.4. FTIR spectra of MPAC before and after PAHs adsorption

4.4.3 Batch adsorption results

4.4.3.1 Adsorption kinetics of PAHs onto MPAC

The adsorption kinetics of LMW and HMW PAHs onto MPAC were measured and interpreted by PFO, PSO, and IPD models. As shown in Table 4.2, all the three models satisfactorily described the kinetics data with R^2 values ranging from 0.83 to 0.95 for PFO, 0.90 to 0.99 for PSO, and 0.90 to 0.96 for IPD, respectively. However, with regards to the greater correlation coefficients and the predicted values of the adsorption uptake ($q_{e\,(cal)}$) being very close to the experimental values (q_{exp}), PSO model was considered as the best fit to the kinetics data. Besides, the RMSE values obtained for this model (Table 4.2) ranged from 0.04 to 0.10 µg/mg for the PAH compounds, which were lower than the values of RMSE for PFO (0.07 to 0.13 µg/mg) and IPD (0.06 to 0.11 µg/mg), suggesting that PSO could better describe the experimental kinetics data than the two other models.

Table 4.2. PFO, PSO, and IPD kinetics parameters for PAHs adsorption onto MPAC

	PFO				PSO				IPD			
PAH	q_e(cal)	K_1	R^2	RMSE	q_e(cal)	K_2	R^2	RMSE	A	K_3	R^2	RMSE
ACE	0.89	0.55	0.95	0.07	0.93	1.00	0.98	0.04	0.72	0.02	0.96	0.06
PHE	0.95	0.26	0.95	0.07	0.99	0.42	0.99	0.04	0.64	0.02	0.90	0.10
ANT	0.91	0.09	0.90	0.10	0.99	0.12	0.96	0.06	0.38	0.04	0.91	0.10
Σ3LMW	2.71	0.24	0.92	0.27	2.87	0.13	0.97	0.16	1.75	0.08	0.92	0.26
B[a]A	0.97	0.04	0.91	0.11	1.04	0.06	0.94	0.08	0.27	0.05	0.91	0.11
CHR	0.99	0.03	0.93	0.09	1.08	0.04	0.95	0.08	0.20	0.05	0.92	0.10
B[b]F	0.97	0.04	0.88	0.12	1.03	0.06	0.93	0.09	0.27	0.05	0.92	0.09
B[k]F	0.97	0.03	0.91	0.10	1.05	0.04	0.94	0.08	0.21	0.05	0.94	0.08
B[a]P	0.93	0.03	0.90	0.10	1.00	0.05	0.94	0.08	0.25	0.04	0.93	0.09
B[ghi]P	0.88	0.05	0.83	0.13	0.93	0.09	0.90	0.10	0.19	0.05	0.90	0.09
D[a,h]A	0.93	0.04	0.85	0.13	0.98	0.07	0.91	0.10	0.19	0.05	0.91	0.09
Σ7HMW	6.64	0.03	0.89	0.78	7.10	0.01	0.93	0.61	1.77	0.32	0.93	0.61
Σ10PAHs	8.79	0.08	0.85	1.26	9.58	0.01	0.92	0.88	3.52	0.40	0.93	0.83

The good fit of the PSO model to the experimental data is also illustrated in Figure 4.5 using a non-linear regression method. The kinetic curves in Figure 4.5a show the rapid adsorption of LMW PAHs within the first hour of contact time, proposing that this group of PAHs was primarily sorbed by the easily accessible adsorption sites on the external surface and in the larger-sized mesopores of MPAC. After the initial contact time, however, the PAHs adsorption rate was declined due to the slower transfer of the PAH compounds to less accessible sites of the MPAC micropores [121,137,175]. For HMW PAHs (Figure 4.5b), the adsorption rate was not that rapid within the first three hours, indicating slower uptake of these compounds by MPAC compared to the LMW PAHs. A possible explanation for this behaviour is that with an increase in the molecular weight and the number of aromatic rings, the PAHs show higher resistance against diffusion onto the magnetic adsorbent. As shown in Table 4.2, the rate constants of both PSO and PFO models were declined as the molecular weight of the PAH compounds increased, confirming a slower adsorption rate of HMW PAHs than LMW ones in the first hours of the experiments.

a)

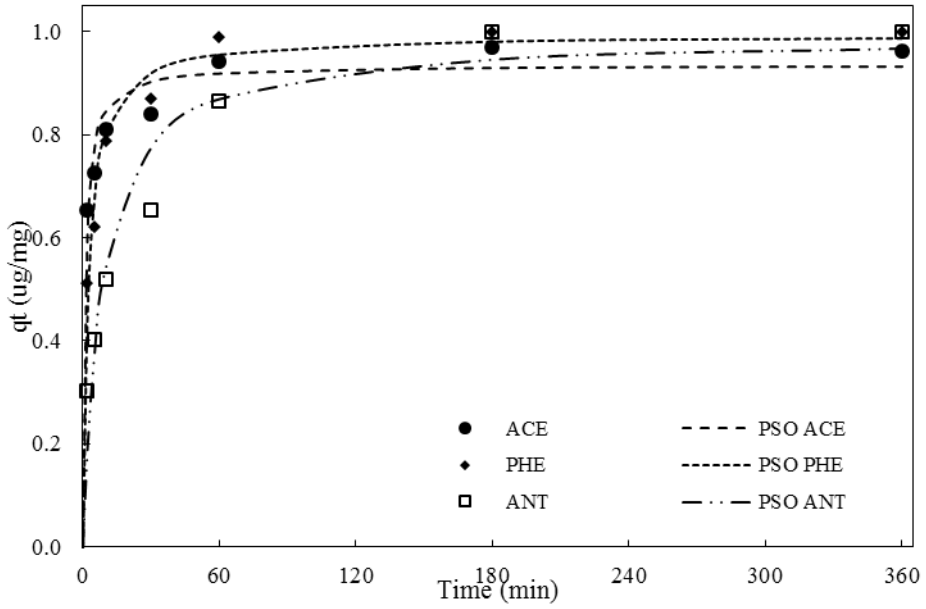

b)

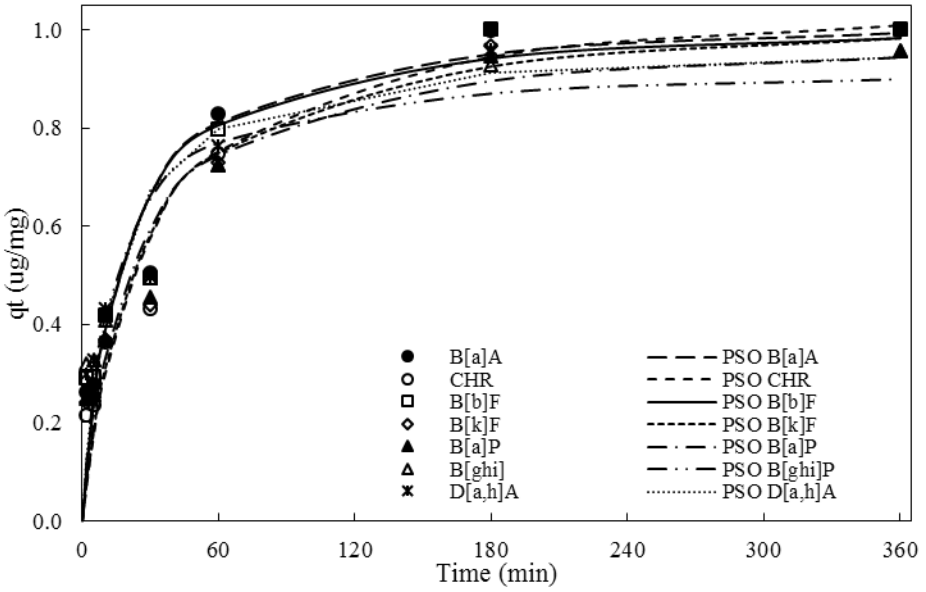

Figure 4.5. Adsorption kinetics of (a) LMW PAHs and (b) HMW PAHs onto MPAC, PSO model

The fitting of data to PSO suggests that the kinetics of the adsorption process are primarily controlled through the sharing or exchange of electrons between the adsorbent (MPAC) surface

and adsorbate (PAHs) molecules, leading to the formation of π-π and H- π interactions. Ho & McKay (1998) showed that PSO was a better predictor of the adsorption kinetics compared to PFO in terms of the PAHs uptake by AC and soil particles. The researchers proposed that the PFO model was only appropriate for interpreting the initial half an hour of the adsorption process [23]. According to Cheng et al. (2019), the adsorption kinetics of naphthalene (NAP), ACE, and PHE onto the porous carbon fitted most satisfactorily to the PSO model. The researchers came to this conclusion when they found a great agreement between the experimental and calculated adsorption capacities using this model. Long et al. (2008), however, demonstrated that the predicted adsorption capacity for NAP was close to the experimental values only for PFO, although both PFO and PSO models described the kinetics data very well (R^2>0.99).

The IPD model describes two diffusion rates of adsorption for the PAH compounds through the mesopores and micropores of MPAC. The diffusion rates have a reverse relationship with the molecular weight of PAHs so that LMW PAHs are able to diffuse faster than the HMW ones [137]. The R^2 values obtained by the IPD for the PAH compounds were lower than the PSO model (Table 4.2), which represented a poorer fit of this model to the kinetic data. According to Equation 8, the relationship between q_t and $t^{1/2}$ in IPD is linear and the intercept displays the boundary layer effects. If the intra-particle diffusion phenomenon occurs in the adsorption process, the plot of q_t vs. $t^{1/2}$ will pass through the origin. In this work, however, the line did not cut the origin due to the obtained values for A (intercept). It indicates that other process/processes might be involved in the adsorption of PAHs onto MPAC. Besides, the larger values of A exhibited the more significant effects of the boundary layer on the adsorption process [73].

According to the results of the adsorption kinetic experiments, the highest removal percentage for ACE, PHE, ANT in the first hour were 94.2%, 98.8%, and 86.4%, respectively, indicating that the LMW PAHs adsorption by MPAC composite rapidly reached equilibrium. The removal rate of the LMW PAH compounds did not have a remarkable change after 3 h, except for ANT which its removal rate reached 100%. In the first 3 h of the HMW PAHs sorption, the highest removal rate (100%) was achieved for B[a]A and B[b]F, whereas the adsorption of B[ghi]P from the solution reached 92.77% at the same contact time. The removal efficiency of the rest of HMW PAHs ranged from 94.57% to 99.87% after 3 h contact time, indicating a high affinity of MPAC for the adsorption of these insoluble and persistent PAH compounds in water. The high adsorption rates of the LMW and HMW PAHs after 3 h can be considered beneficial to large-scale applications as

it reduces the capital and operational costs of the treatment process [155]. Similar results were obtained by Awoyemi (2011) and Haro et al. (2011), where the researchers reported that the adsorption rate of NAP onto AC was considerably faster than fluorene (FLU). Both the studies attributed this difference in the kinetic behaviour of NAP and FLU to the lower molar volume and molecular dimensions of the former compound than the latter one [137]. Yuan et al. (2010) conducted a study on adsorption of NAP, PHE, FLU, PYR, and Fluoranthene (FLUO) using one type of coke-derived porous carbon. According to their results, NAP, which is known as the smallest and most water-soluble PAH compound, was adsorbed faster than the other PAHs with the same concentration. Besides, the adsorption rate obtained for this LMW compound was 94.0% only after 30 min contact time, while this rate for FLUO and PYR was 74.0% and 78.4%, respectively. The porous carbon particles were also able to adsorb 87.8% of PHE and 88.2% of FLU, which were higher than the rates obtained for FLUO and PYR, possibly due to the lower molecular weight and dimension of the two former compounds.

4.4.3.2 Adsorption isotherms of PAHs onto PAC and MPAC

The Langmuir, Freundlich, and Temkin isotherm models were employed to simulate the adsorption equilibrium data and interpret PAHs adsorption capacity of the MPAC composite. Table 4.3 presents the isotherm parameters obtained from non-linear regression analysis of these models and the experimental data. According to the R^2 values shown in the Table 4.3, the adsorption equilibrium data fitted well to the isotherm models in the order Langmuir> Temkin> Freundlich for LMW PAHs, and Langmuir> Freundlich> Temkin for the HMW PAHs. The relatively higher R^2 values of the Langmuir model (0.73-0.96) compared to the two other isotherm models indicated that Langmuir described the experimental data in a greater congruence. The RMSE values determined by Langmuir, Freundlich, and Temkin models for the individual PAH compounds ranged 0.51-1.73, 0.56-2.35, and 0.78-2.00 µg/mg, respectively (Table 4.3). These values for total LMW and HMW PAHs were 3.40 and 4.04 µg/mg for Langmuir, 5.40 and 4.54 µg/mg for Freundlich, and 3.90 and 5.595 µg/mg for the Temkin Model. The lower values of RMSE along with the greater correlation coefficients confirmed that the Langmuir model was the best fit to the experimental isotherm data, therefore verifying the monolayer adsorption of the PAH compounds onto MPAC [67,73]. It means that the adsorption sites of the adsorbent were homogeneously distributed on its surface and the adsorbed molecules do not interact with each other during the adsorption process [178]. According to the isotherm model, the main adsorption

mechanism of PAHs consists of rapid attraction of these compounds by the adsorption sites of MPAC, and consequently, formation of interactions between π electrons of the PAHs aromatic rings and carboxyl and hydroxyl functional groups of MPAC. The PAHs hydrophobicity in the aqueous solution, however, can affect the duration of the adsorption process. The more hydrophobic PAHs are surrounded by water molecules, forming stronger hydrophobic interactions and being stabilized in water. Therefore, for this group of PAHs, the speed of attraction by the MPAC functional groups may be slower compared to the less hydrophobic PAHs (e.g., ACE and PHE) (Costa et al., 2017).

In the Langmuir model, the q_{max} parameter indicates the maximum capacity of contaminant adsorption onto the adsorbent. As shown in Table 4.3, the q_{max} values for the adsorbed PAHs ranged from 8.74 to 11.37 µg/mg for LMW PAHs and 8.43 to 20.21 µg/mg for HMW PAHs. There exists only one study in the scientific literature investigating the adsorption capacity of MPAC for individual PAHs. Inbaraj et al. (2021) prepared a magnetic adsorbent through a series of carbonization, thermal activation, and magnetization procedures performed on powdered green tea waste biomass [155]. The prepared magnetic adsorbent was used in the isotherm adsorption experiments for removal of only four PAH compounds, i.e., B[b]F, B[a]P, CHR, and B[a]A, from aqueous solutions. After fitting the isotherm data with the Langmuir model, the maximum adsorption capacity of MPAC for the four PAH compounds was determined as 28.08, 22.75, 19.14, and 15.86 µg/mg, respectively, which are relatively higher than the ones obtained in this study. Zhang et al. (2019) used different types of magnetic carbon nanotubes to adsorb one PAH compound, PHE, from contaminated water solutions. The q_{max} parameter estimated for PHE adsorption of these adsorbents was in the range of 20.0 to 74.6 µg/mg [154]. Despite the high adsorption capacity of the magnetic carbon nanotubes for PHE, there was no information about their efficiency for the adsorption of heavier PAH compounds, which are considered more toxic and carcinogenic.

The R_L values obtained for adsorption of the PAH compounds onto MPAC are presented in Table 4.3. The separation factor R_L was found in the range of 0.01 (PHE) to 0.28 (B[a]P) ($0<R_L<1$), indicating that the adsorption process was favourable for all the PAHs [18,73,179]. In the case of the Langmuir affinity constant (K_L), its higher values for LMW PAHs were an indication of the higher rates of adsorption for these compounds compared to the HMW PAHs, which confirmed the results obtained by the kinetics experiments [180].

Table 4.3. Parameters of Langmuir, Freundlich and Temkin isotherm models obtained for the adsorption of PAH compounds onto MPAC and PAC

MPAC	Langmuir					Freundlich				Temkin			
PAH	K_L	q_{max}	R^2	RSME	R_L	K_f	$1/n_f$	R^2	RMSE	K_T	B	R^2	RMSE
ACE	5.74	9.51	0.73	1.73	0.02	6.68	0.30	0.51	2.35	50.64	1.27	0.64	2.00
PHE	10.14	8.74	0.90	0.99	0.01	6.68	0.28	0.72	1.69	49.98	1.29	0.75	1.60
ANT	1.72	11.37	0.90	1.02	0.05	6.36	0.50	0.81	1.45	15.73	0.95	0.91	0.98
Σ3LMW	1.37	29.03	0.88	3.40	0.07	13.38	0.36	0.70	5.40	11.75	0.39	0.84	3.90
B[a]A	1.05	8.43	0.95	0.59	0.09	3.81	0.46	0.93	0.65	48.31	2.11	0.84	1.01
CHR	0.65	9.36	0.95	0.55	0.13	3.31	0.55	0.94	0.64	13.76	1.56	0.91	0.78
B[b]F	0.87	9.01	0.96	0.53	0.10	3.69	0.51	0.94	0.64	20.24	1.65	0.90	0.80
B[k]F	0.38	13.20	0.95	0.59	0.21	3.39	0.67	0.95	0.64	10.07	1.30	0.89	0.90
B[a]P	0.25	20.21	0.93	0.81	0.28	3.91	0.78	0.92	0.85	8.38	1.06	0.87	1.07
B[ghi]P	0.31	14.13	0.96	0.51	0.24	3.14	0.70	0.96	0.56	7.96	1.23	0.91	0.80
D[a,h]A	0.43	13.18	0.95	0.60	0.19	3.68	0.66	0.94	0.66	10.82	1.26	0.90	0.90
Σ7HMW	0.07	78.94	0.95	4.04	0.57	7.57	0.61	0.94	4.54	1.74	0.20	0.90	5.95
Σ10PAHs	0.09	104.98	0.94	6.87	0.54	12.30	0.54	0.90	8.89	1.44	0.13	0.91	8.64
PAC	Langmuir					Freundlich				Temkin			
Σ3LMW	0.61	39.83	0.90	2.78	0.14	12.48	0.43	0.87	3.13	30.35	0.60	0.71	4.79
Σ7HMW	0.58	85.68	0.99	1.16	0.15	27.80	0.52	0.99	2.39	22.84	0.22	0.86	7.73
Σ10PAHs	0.21	152.60	0.99	2.23	0.33	25.31	0.65	0.98	4.18	3.78	0.10	0.96	6.04

The results of adsorption isotherm models for the bare (unmodified) PAC are also presented in Table 4.3 and Figure 4.6. All the three isotherm models fitted the adsorption data very well, with the most appropriate correlation and minimum deviation attained for the Langmuir model ($R^2 \geq 0.90$). The maximum PAC adsorption capacities for total LMW and HMW PAHs were 39.83 and 85.68 µg/mg, which compared with the values for MPAC (29.03 and 78.94 µg/mg) showed a reduction of nearly 27% and 9%, respectively. This could be attributed to the decrease of surface area due to magnetization, which was estimated to be 324.7 m^2/g (Table 4.1).

There are no detailed discussions in the literature on the adsorption of LMW and HMW PAHs by PAC. In the case of GAC, Eeshwarasinghe et al. (2019) reported a maximum adsorption capacity of 2.63 µg/mg for ACE and 7.36 µg/mg for PHE, both considered as LMW PAHs [18]. In another study, Valderrama et al. (2008) used GAC for the removal of a group of LMW and HMW PAHs, including NAP, ACE, FLU, ANT, PYR, and FLUO. According to the Langmuir isotherm model,

the maximum adsorption capacity of GAC for these PAHs was estimated: 0.14, 0.11, 0.15, 0.23, 0.11, and 0.09 µg/mg, respectively, with the highest for ANT [175]. The maximum PAH adsorption capacities obtained for both PAC and MPAC in this study were higher than the above two studies.

According to Table 4.3, the values of $1/n_f$ (the Freundlich model) for most of the PAHs were between 0.28 and 0.78, indicating that the adsorption process was favourable and there were strong interactions between the adsorption sites of the MPAC surface and the PAH compounds [39,73,137,179,181]. In the Temkin model, the adsorption of PAHs is attributed to the formation of uniform binding energies between the PAH compounds and the adsorbent functional groups. From Table 4.3, the values of the equilibrium binding energy constant (K_T) decrease with the increase in the number of PAH aromatic rings, suggesting that the heat of adsorption would linearly decrease when the MPAC surface is covered with the heavier PAH compounds [182].

Figure 4.6a and b demonstrate the isotherms data obtained for adsorption of LMW and HMW PAHs onto MPAC for a range of PAH concentrations from 0.5 to 10 µg/mL at room temperature (24 ˚C). The Langmuir model was used as the best model fit to the experimental data to describe the adsorption behaviour of the PAH compounds onto MPAC. As shown in Figure 4.6a, the amount of ACE and PHE adsorbed on MPAC particles sharply increased when their concentrations were raised from 0.5 to 2.5 mg/L. At the same concentration range, the adsorption uptake for ANT was slower than the two other LMW PAHs, possibly due to its higher molar weight and dimension and its slower transfer to the adsorption sites. From Figure 4.6b, all the HMW PAHs showed a similar adsorption behaviour, with lower adsorption equilibrium than LMW PAHs at the initial concentrations from 0.5 to 2.5 µg/mL. However, as it is evident from Figure 4.6 and Table 4.3, the maximum adsorption capacity of MPAC for the heavier PAHs, including B[k]F, B[a]P, B[ghi]P, and D[a,h]A, was higher than the LMW ones. It indicates that the adsorption of HMW PAHs by MPAC was a slower process compared to the LMW PAHs; however, they were able to form stronger bonds with the MPAC surface [175].

Figure 4.6c depicts the adsorption capacity of bare and magnetic PAC for the sum of 3 LMW PAHs, 7 HMW PAHs, and 10 PAHs fitted with the Langmuir model. Despite the lower adsorption capacity of the MPAC composite compared to the bare PAC, the magnetic adsorbent still showed a high affinity for the PAHs. Besides, the difficulty in recovering the PAC particles after use would

limit their application for the treatment of aqueous solutions, particularly for larger-scale projects [80].

a)

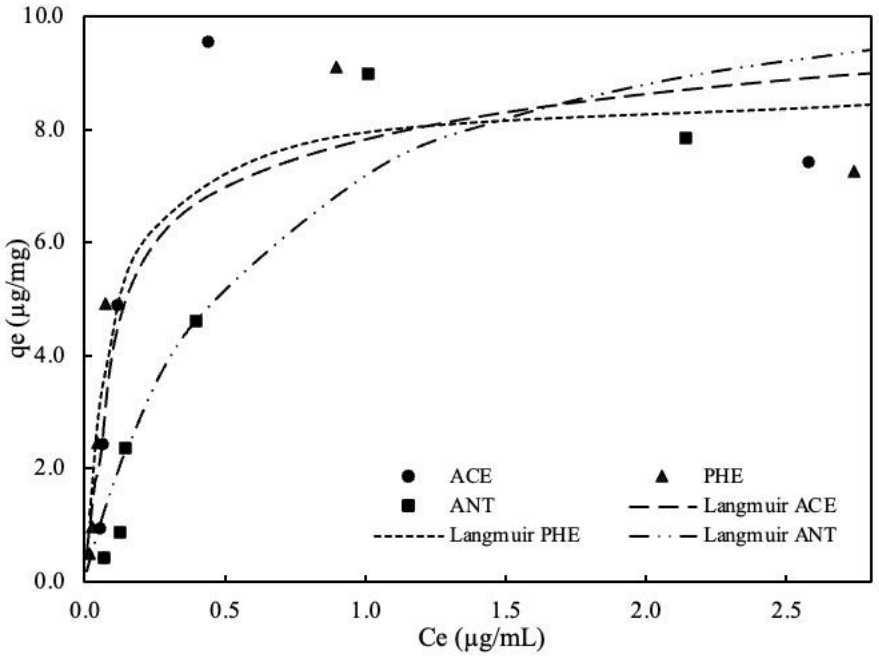

b)

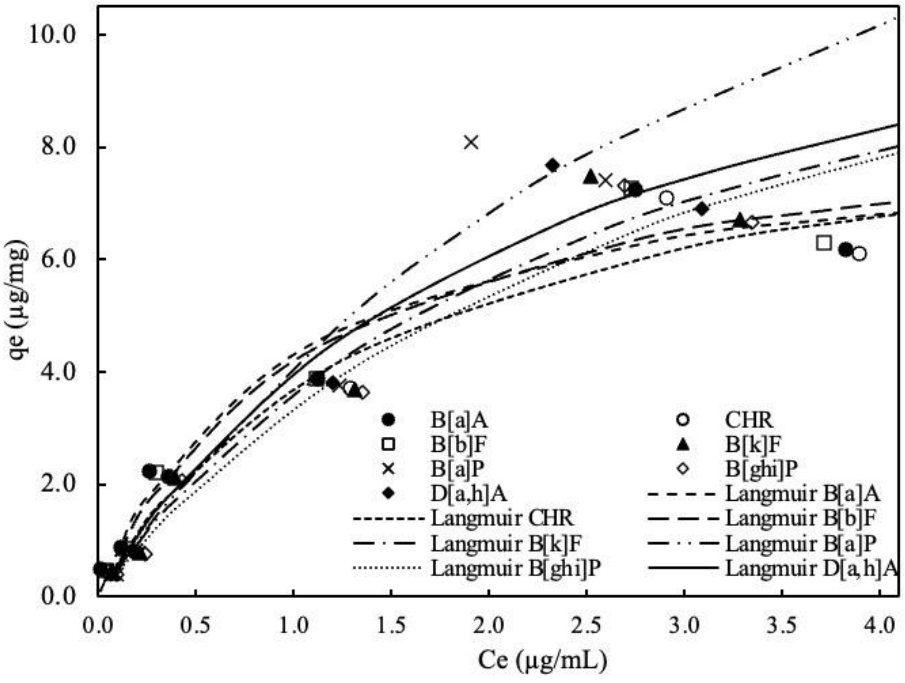

c)

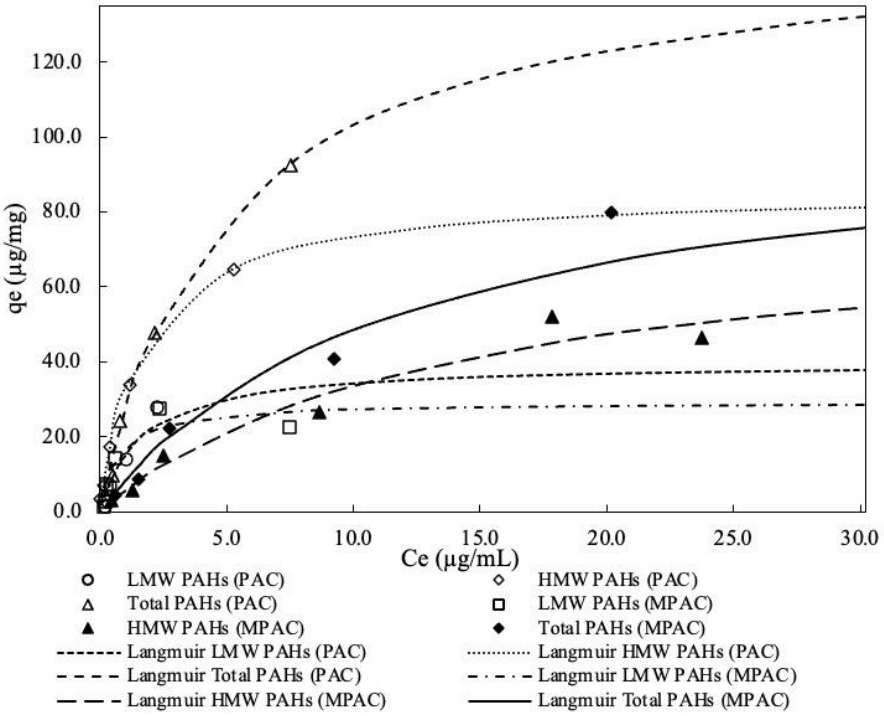

d)

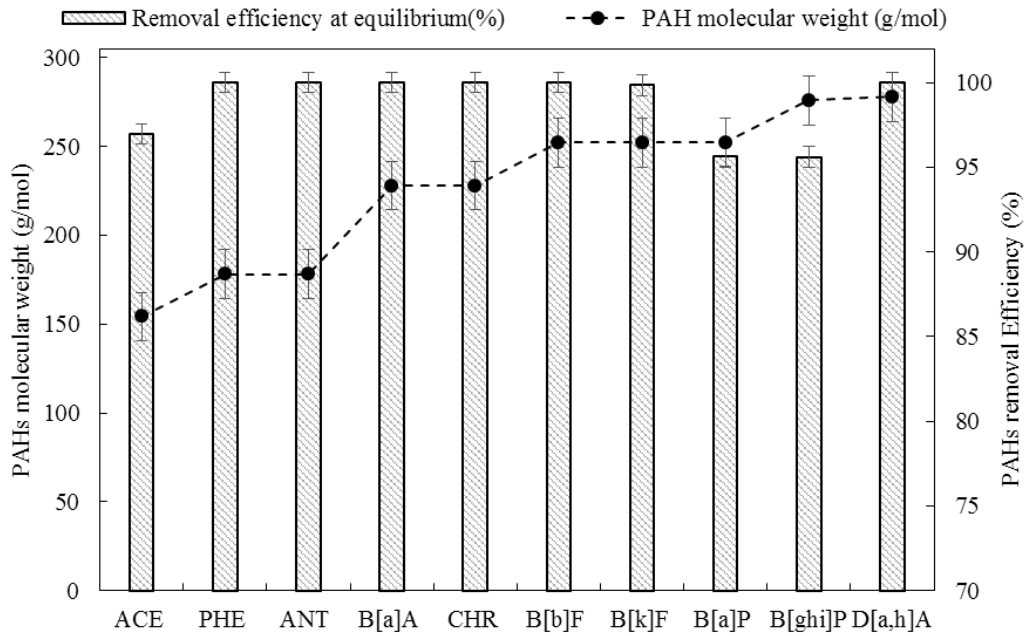

Figure 4.6. Adsorption isotherms of (a) LMW PAHs (b) HMW PAHs (c) Total LMW and HMW and PAHs, (d) Comparison of the PAHs molecular weight and their removal efficiency obtained at the equilibrium of adsorption using MPAC composite

In this work, the prepared MPAC composite showed a high affinity for all the PAHs. As shown in Figure 4.6d, after the equilibrium of adsorption was attained, almost all the LMW and HMW PAHs were completely removed by MPAC (except for B[a]P and B[ghi], which their removal rate was obtained 95.68 and 95.60%, respectively). It indicates that the magnetic adsorbent was able to adsorb all the PAH compounds with different molecular weights and numbers of aromatic rings. The higher PAH uptake by MPAC compared to the ranges of PAH adsorption reported in the literature for GAC is consistent with the pore adsorption mechanism. According to this mechanism, smaller adsorbents like PAC have a larger external surface area and shorter diffusion path length, enabling them to adsorb the PAH compounds at a faster and higher rate [183]. Besides, owing to their superparamagnetic properties, the MPAC particles used in this work had higher recovery rates, leading to the removal of all the PAH-loaded MPAC particles from the solutions after the adsorption process.

4.5 Conclusions

A magnetic powder activated carbon (MPAC) composite was synthesized using the precipitation method to remove PAHs from aqueous solutions. Although there was a decrease of 65% in the BET surface area of the AC particles after magnetization, the synthesized MPAC was effective in removing the PAHs from the aqueous phase with efficiency in the range of 95.6 to 100%. It exhibited a crystalline structure with a wide pore size distribution typical of the MAC family, as confirmed by the characterization tests. Owing to its high surface area, stability, and dispersibility, the magnetic composite showed an excellent adsorption capacity for PAHs in the aqueous solutions. The adsorption of LMW and HMW PAHs onto MPAC reached equilibrium in 6h with a complete removal obtained for most of the PAH compounds. The Langmuir model fitted the adsorption isotherm data the best with R^2 values greater than 0.9 for most PAHs. The maximum adsorption capacity was in the range of 8.74-11.37 µg/mg for LMW PAHs and 8.43-20.21 µg/mg for HMW PAHs according to the Langmuir model. The pseudo-second order model provided the best fit to the data, indicating that the adsorption of PAHs onto MPAC was dominated by the chemical adsorption, and the PAHs uptake rate was dependent on MPAC adsorption capacity, not on concentrations of PAHs. The electron-donor-acceptor interactions (π-π interactions) and pore-filling were also the main adsorption mechanisms formed between the analytes and MPAC. The results of this study showed that the MPAC composite is a promising adsorbent for the removal of PAHs from aqueous media.

4.6 References

This chapter's references are integrated with the references from the other chapters and provided at the end of the thesis.

5 Removal of Polycyclic Aromatic Hydrocarbons (PAHs) from Contaminated Soil using Soil Washing Process Combined with Adsorption by Magnetic Granular Activated Carbon

5.1 Abstract

This study investigated the application of magnetic granular activated carbon (MGAC) for the removal of polycyclic aromatic hydrocarbons (PAHs) from a real contaminated soil in soil washing process. The magnetic composite was prepared using a facile modified co-precipitation method. The presence of the synthesized magnetite (Fe_3O_4) nanoparticles on the composite surface was confirmed by the SEM and XRD characterization tests. The surface area and total pore volume of MGAC were determined to be 837.9 m^2/g and 0.5 cm^3/g, respectively, which were ≈ 10% smaller than those for the bare GAC. The Langmuir model fitted the adsorption isotherm data the best; therefore, monolayer adsorption was predominant in the treatment process with MGAC. The maximum PAH adsorption capacity of MGAC was obtained at 153.5 µg/mg for the total PAHs, which was nearly 20% lower than that of bare GAC (190.3 µg/mg). The soil washing parameters were optimized, and the results demonstrated that the total PAH removal reached a maximum of 47.4% at an MGAC dose of 2% (w/w), washing time of 24 h, liquid to soil ratio of 15:1, stirring speed of 100 rpm, pH of 8.3, and temperature of 25 ˚C. For low molecular weight (LMW) PAHs, the removal from soil ranged from 34.6% to 57.7%, whereas the removal of high molecular weight (HMW) PAHs was determined to be between 27.9 and 67.1 %. This indicated that the optimized soil washing with MGAC had a better efficiency for some HMW PAHs than the LMW PAHs. According to the thermodynamic studies, the adsorption of PAHs onto MGAC in the soil washing process was non-spontaneous ($\Delta G^\circ > 0$) and endothermic ($\Delta H^\circ > 0$) with increased randomness at the solid/solution interface of MGAC at the higher temperature.

Keywords: Magnetic granular activated carbon; Polycyclic aromatic hydrocarbons; Adsorption capacity, Soil washing; Thermodynamic parameters

5.2 Introduction

Polycyclic aromatic hydrocarbons (PAHs) pollution in the environment is mostly due to human activities. The combustion of carbon-containing fuels, inappropriate management during storage and transport, and accidental disposal of petroleum products release large amounts of PAHs into the environment [95,112,136,184]. Contamination of soil or water resources by PAH compounds could pose severe risks to human health and other organisms [109,112,185]. Among hundreds of PAHs, sixteen compounds are of particular importance and identified as U.S. Environmental Protection Agency (USEPA) 16 PAHs priority list. This group of PAHs comprises two or more aromatic rings, which are non-polar, stable, and hydrophobic. When these contaminants accumulate in soil or water, they have poor biodegradability, low volatility, and a high potential for toxicity [31,108,184,186]. Other organizations such as the International Agency for Research on Cancer and the Canadian Council of Ministers of the Environment (CCME) have adopted the same approach and use the same designation [14,17,54]. The high molecular weight (HMW) PAHs with four or more aromatic rings are prone to be more carcinogenic or mutagenic than the PAHs with fewer aromatic rings known as low-molecular-weight (LMW) PAHs [14,25,111,129].

Various physical, chemical, and biological remediation techniques have been employed to remove PAHs from contaminated soils, such as incineration, soil washing/flushing, soil vapour extraction, thermal desorption, advanced oxidation, and bioremediation [18,23–26,60,61,184]. Many of these techniques, however, are not applicable for field-scale projects due to high cost of the required facilities, high water and/or energy consumption, and slow operation [12,27]. Chemical techniques may produce some contaminant by-products during the remediation process that are toxic to soil species [4]. The biological technologies are less expensive and more environmentally friendly (e.g., microbial bioremediation and phytoremediation); however, they usually need a considerable amount of time to clean up the soil. Furthermore, compared to physical and chemical processes, they may yield low PAH removal efficiency depending on site conditions (e.g. soil pH, ambient temperature, nutrient element and dissolved oxygen levels of soil) [12,25,27,28]. In the case of soil-washing (physical technique), PAHs are transferred from soil to water, thus, necessitating the treatment of the PAH-contaminated water [187].

The use of activated carbon (AC) in the adsorption process for uptake of PAHs from aqueous solutions is one of the most frequent treatment approaches that has been reported in the literature [136,155]. Because of its unique features, including high porosity and hydrophobicity as well as

high specific surface area and adsorption capacity, AC shows a strong affinity for PAHs. Moreover, the AC surface has a variety of functional groups that help it form more interactions with PAHs during the adsorption process, providing it with great PAH removal efficiency in aqueous solutions [32,33,35,36]. Considering the AC high affinity for PAHs, its application in soil washing to adsorb PAHs from the soil slurry is a promising technique. However, one of the drawbacks of employing AC in soil washing is the difficulty to separate and retrieve it from the soil matrix after use [37], which undermines the application of this soil remediation technology. In addition, the application of AC in soil washing may lead to the loss of a fraction of PAH-loaded AC particles in the soil medium, which causes the contaminants to be released back into the environment. Furthermore, some delicate organisms may be harmed by the presence of AC particles in the soil [38]. To address these issues, AC particles can be modified with stable iron oxide nanoparticles (Fe_2O_3, Fe_3O_4, etc.) to prepare magnetic AC composites, which can be removed from the soil slurry using an external magnetic field after the remediation procedure [18,38–45].

In the previous work by the authors, six magnetic AC composites were prepared using different magnetization methods and either powder or granular AC. Magnetic granular activated carbon (MGAC) particles fabricated by the co-precipitation method showed high PAH removal efficiency from the aqueous phase [153]. Preliminary tests revealed that the efficiency of separation and recovery of MGAC particles from soil slurry using a basic magnetic field was significantly higher than those prepared by powder activated carbon as base material. Considering the above, the MGAC composite particles were utilized in soil washing experiments to remove PAHs from soil. Experiments were conducted in different phases. In phase one, a series of adsorption isotherm tests were carried out using MGAC to determine its efficiency and adsorption capacity for PAHs from aqueous solution. The adsorption behaviour of the MGAC composite was also modelled by Langmuir, Freundlich, and Temkin isotherm models. In phase two, MGAC was employed in the soil washing process to determine its capability of PAHs removal from real contaminated soil samples. To the best of the authors' knowledge, the use of MGAC in soil washing and its efficiency for removal of a wide range of PAHs, including both low molecular weight (LMW) and high molecular weight (HMW) PAHs, in the combined soil washing-adsorption process has not been reported yet. The application of MGAC in soil washing could offer a rapid and cost-effective method for the removal of PAHs from contaminated soil. Therefore, the specific goals of the

current work were to evaluate the PAH uptake capacity of the MGAC composite using the adsorption isotherms experiments and determine MGAC adsorption efficiency to clean up a real PAH-contaminated soil sample in the soil washing process.

5.3 Materials and methods

5.3.1 Chemicals

The GAC used as the base for the magnetic composite was supplied by CalgonCarbon Co. (Pennsylvania, USA). The GAC particles passed sieve # 16 (1.19mm) and were generally between 250 and 850 µm in size. Iron (III) nitrate nonahydrate ($Fe(NO_3)_3.9H_2O$) and Iron(II) sulphate heptahydrate ($FeSO_4.7H_2O$) were acquired from Sigma-Aldrich Co. as the magnetic nanoparticle precursors (St. Louis, USA). The standard solutions of the high priority USEPA PAHs including acenaphthene (ACE), fluorene (FLU), phenanthrene (PHE), anthracene (ANT), fluoranthene (FLUO), pyrene (PYR), benzo[a]anthracene (B[a]A), benzo[b]fluoranthene (B[b]F), benzo[k]fluoranthene (B[k]F), benzo[ghi]perylene (B[ghi]P), indeno[1,2,3-c,d]pyrene (IDP), and dibenz[a,h]anthracene (D[ah]A) were obtained from AccuStandard Chem. Co., USA (500 µg/mL PAHs, in acetonitrile with 99% purity). Other chemicals such as acetonitrile, methylene chloride, and hexane were obtained from VWR (Quebec, Canada).

5.3.2 Synthesis of GAC/Fe_3O_4 composite

The MGAC composite was prepared by a slight modification of a co-precipitation method reported by Yazdani and Seddigh (2016). Briefly, solutions of Iron (III) nitrate nonahydrate (1M) and Iron(II) sulphate heptahydrate (0.1M) were prepared and then mixed in a 500 mL reaction vessel containing 350 mL deionized water. The solution was vigorously stirred at 650 rpm using a magnetic stirrer and under nitrogen stream for 10 min [124]. Then, 2 g GAC was placed in the iron solution mixture, followed by adding 35 mL NaOH solution (1 M) dropwise into the solution for 5 min to enable the precipitation of the magnetic composite at pH of 10-11. The supernatant was discarded, and the black precipitated composite (MGAC) was washed with deionized water a few times to remove the excess non-GAC bound magnetite nanoparticles and neutralize pH of the prepared composite. The MGAC particles were vacuum dried overnight at 80 °C and then stored in the screw cap vials for further use.

5.3.3 Characterization of the synthesized MGAC

The Brunauer-Emmet-Teller (BET) surface area of the bare and magnetic GAC was determined from nitrogen adsorption-desorption isotherms using an Accelerated Surface Area and Porosimetry technique (ASAP, 2020, Micromeritics Instruments Inc., GA, USA). Before the BET measurement of GAC and MGAC samples, they were placed into glass analysis tubes and heated at 100-200 ˚C under vacuum for about 1 day to remove any potential contaminants and moisture from their surface. The porosity distribution of the bare and magnetic GAC was measured using the Barrett-Joyner-Hanlenda (BJH) technique in liquid N_2 at 77 K. The structures of GAC and MGAC were explored by obtaining their X-ray diffraction (XRD) patterns using a Rigaku Ultima IV X-ray diffractometer equipped with a Cu Kα radiation (λ = 1.54185 Å) at 40 kV and current at 44 mA, and an ASC-10 auto sample changer. The XRD patterns of the bare and magnetic GAC were obtained in the 2θ scanning range of 10° to 80° with a scan speed of 4°/min. The mean particle size of GAC and MGAC and their surface morphology were analyzed by field emission scanning electron microscopy (FE-SEM, JSM-7500F, JEOL, USA). The Energy-dispersive spectroscopy (EDS) technique was employed to determine the distribution of Fe_3O_4 nanoparticles in the matrix of the magnetic composite. The Fourier transform infrared (FTIR) spectra of MGAC composite, before and after use, were recorded on a Nicolet 6700 FT-IR spectrometer (Thermo Fischer, USA) in the wavenumber range of 4500–400 cm^{-1} by testing a small portion of each sample at a pressure of 150 kg/cm^2 and recording 32 scans at a resolution of 4 cm^{-1} for the samples.

5.3.4 Adsorption isotherm experiments

Adsorption isotherms study was conducted by preparing the PAHs concentration in the range 0.5 -10 ug/mL from dilution of the PAH standard solution in acetonitrile and then adding the diluted PAHs to conical flasks containing 30 mL deionized water. Afterward, the PAHs solutions were mixed with potassium nitrate (1 g/L) and sodium azide (0.2 g/L) to inhibit any potential biological activity during the test (Gan et al., 2017). The prepared samples were agitated at 50 rpm for 1 h to provide a uniform dispersion of the PAHs in the solutions. Subsequently, a fixed dose of MGAC (30mg) was added to each sample, and the solutions were then agitated on the horizontal shaker at 100 rpm and room temperature for 24 h. In the end, the samples were removed from the shaker, and the adsorbent particles were separated from the solutions using a magnet bar. The solutions were extracted and analyzed using HPLC to determine the residual PAHs concentration after adsorption. All the adsorption tests were performed in duplicate, and the flasks were covered with

aluminum foil to eliminate the potential effects of light. The control samples without the adsorbent were also run in parallel for the adsorption isotherm tests. The quantity of PAHs adsorbed onto MGAC at equilibrium (24h) can be calculated from the following equation:

$$q_e = \frac{(C_0 - C_e)V}{M} \quad (5.1)$$

Where q_e (µg/mg) represents the PAHs adsorption capacity of the magnetic adsorbent, C_0 and Ce are the initial and equilibrium concentration of the PAHs in the solution (µg/mL), respectively. V shows the solution volume (mL), and M is the mass of MGAC composite (mg) [80,188].

The adsorption capacity of the MGAC composite was investigated by fitting the Langmuir, Freundlich, and Temkin isotherm models to the obtained experimental data. The Langmuir model assumes that an adsorbent surface contains a finite number of homogeneous adsorption sites, which all have the same affinity for the adsorbate molecules. According to this concept, each adsorption site only adsorbs one molecule of the adsorbate, resulting in the formation of a single monolayer of adsorbate onto the adsorbent. This model also assumes that the adsorption energy is constant and that the adsorbate molecule cannot move on the adsorbent surface [73,159]. The Langmuir model presents the relationship between equilibrium concentration of adsorbate and adsorption capacity of adsorbent in the adsorption process as follows:

$$q_e = q_m . \frac{K_L C_e}{1 + K_L C_e} \quad (5.2)$$

where K_L is the Langmuir affinity constant (mL/µg) related to the adsorption energy and q_m shows the maximum amount of PAHs adsorbed per unit mass of MGAC (µg/mg) [136,188,189].

The separation factor could be used to determine the favourability of the adsorption process. This dimensionless constant is calculated using the following equation [137]:

$$R_L = \frac{1}{1 + C_m K_L} \quad (5.3)$$

where R_L represents the value of the separation factor and C_m is the maximum initial concentration of PAHs in aqueous solution. When the R_L value is between 0 and 1, the adsorption process is verified to be favourable. When R_L equals 0, the adsorption process is regarded irreversible, and for R_L=1.0, adsorption is linear [155,161,181].

According to the Freundlich isotherm model, the surface of an adsorbent with a large number of adsorption sites has a wide range of possible adsorption capacity for the contaminant molecules. This will result in a multilayer and heterogeneous adsorption of the contaminant on the adsorbent

surface during the adsorption process. The Freundlich model also assumes that the contaminant molecules occupy the stronger binding sites of the adsorbent first, and as the degree of occupation increases, the binding strength decreases [73,157].

The Freundlich model is expressed by the following equation:

$$q_e = K_F C_e^{\frac{1}{n_f}} \quad (5.4)$$

where K_F is the Freundlich constant (L/g), and the n_f parameter represents the adsorption intensity. When the value of $1/n_f$ is less than 1, the adsorption process is considered favourable, showing the formation of stronger interactions between the adsorbent and the contaminant molecules [137,157,158].

The Temkin isotherm model takes into account the effects of the interactions between adsorbate molecule and adsorbent surface on the adsorption process. This model also assumes that the heat of adsorption relies on the temperature of all the molecules existing in the adsorption layer, which decreases linearly as the adsorbent surface coverage increases by the number of the sorbed molecules. The derivation of adsorption in the Temkin model is characterized by a homogeneous distribution of binding energies up to maximum binding energy [190–192]:

The Temkin model is described using the following model:

$$q_e = \frac{RT}{B} (\ln K_T C_e) \quad (5.5)$$

where R is the universal gas constant (8.314 J/mol/K); B is the Temkin constant corresponding to the heat of adsorption (J/mol), T is the absolute temperature (K), and K_T is the Temkin isotherm constant related to the maximum binding energy (L/g) [190,192].

5.3.5 Soil washing combined with MGAC

The soil samples were collected from a depth of 10–40 cm beneath the ground surface at a contaminated industrial site in Ontario, Canada. The soil sample was air-dried for one week and then screened to pass sieve No. 40 (US Standard mesh) prior to use in the soil washing process. To investigate the impact of different washing parameters on the PAHs removal with soil washing-MGAC, a series of soil washing experiments were designed and carried out. The key parameters were tested in the following order: MGAC dose (0, 1, 2, and 5% w/w.), liquid to soil ratio (10:1, 15:1, and 20:1), shaker speed (75,100, 125, and 150 rpm), washing time (6, 24, 72, and 168 h), pH (7.0, 8.3, and 10.0), and temperature (5 and 25 ˚C). The best result obtained for each parameter was utilized to evaluate the next parameter in the subsequent test. All the experiments were

conducted in duplicate. For the first set of the tests, 30 mL deionized water was poured into conical flasks containing 3g of the PAH-contaminated soil. After being homogenized on a horizontal shaker for 0.5 h, the biological inhibitors NaN_3 (0.2 g/L) and KNO_3 (1 g/L) were added to the mixtures. The flasks were capped and covered with aluminum foils and subsequently agitated on the shaker at 100 rpm for 24 h. The samples were eventually removed from the shaker to settle the soil particles and centrifuge the liquid phase. The treated soil in the flasks and the soil residue in the centrifuge tubes were air-dried, followed by separating the PAH-loaded MGAC particles from the soils using a magnetic field. The soil samples were then extracted, and the PAHs concentrations were determined by HPLC.

5.3.6 Analytical method

High-Performance Liquid Chromatography (HPLC, Hewlett–Packard 1100, Agilent Technologies, USA) equipped with a reverse phase HPLC column (ZORBAX Eclipse PAH, 95Å, 4.6×250mm×5µm), was employed to measure the concentration of the PAHs in the samples. For the adsorption isotherms experiments, the treated solutions were extracted with methylene chloride (HPLC grade, >99%) through agitation on a vortex mixer for 2 min [193]. The mixture was then centrifuged and the methylene chloride containing the PAHs residue was separated from the solution. The extraction procedure was performed three times, after which all of the extracts were combined and the methylene chloride was exchanged to acetonitrile using the Kuderna-Danish (K-D) equipment [17].

The treated soil samples were extracted by mixing with acetone: hexane (1:1 V:V), followed by sonication in water bath for 10 min (USEPA 3045). The soil extraction procedure was repeated three times for each sample, and the extracts were combined and concentrated to acetonitrile by K-D for HPLC analysis [59,60]. Finally, 25µL of the concentrated acetonitrile was injected into HPLC to measure the residual PAHs concentration.

5.3.7 Thermodynamic studies

To understand the nature of PAHs adsorption onto the MGAC composite (physical/chemical adsorption), a thermodynamic examination of the treatment procedure was performed at temperatures of 5 ˚C and 25 ˚C [188,190]. For this purpose, the key thermodynamics parameters such as Gibbs free energy ($\Delta G°$), enthalpy ($\Delta H°$), and entropy ($\Delta S°$) were calculated using the following equations:

$$\Delta G^\circ = -RT\ln Kc \quad (5.6)$$

$$\Delta G^\circ = \Delta H^\circ - T\Delta S^\circ \quad (5.7)$$

$$\text{Ln } Kc = \left(\frac{\Delta S^\circ}{R} - \frac{\Delta H^\circ}{RT}\right) \quad (5.8)$$

where R is the universal gas constant (8.314 J/mol.K), T is the absolute temperature, and Kc is the distribution coefficient measured using the ratio of PAHs concentration on the adsorbent to the PAHs concentration in the solution under equilibrium conditions [136,158]. As can be seen from Eq. 5.7, the Gibbs free energy of a system is calculated from the difference between enthalpy and entropy of the reaction as well as the temperature at which the reaction occurs [190]. In fact, Gibbs free energy is an estimation of the amount of usable energy in a system. Any change in the quantity of this parameter during a reaction determines the reaction energetics and spontaneity (positive or negative ΔG°).

5.4 Results and discussion

5.4.1 Characterization of GAC and MGAC

The nitrogen adsorption-desorption measurements were performed to evaluate and compare the surface properties of the bare and magnetic GAC. As presented in Figure 5.1, the N_2 Isotherms of both GAC and MGAC can be classified as Type I (IUPAC classification system) with regard to the hysteresis loops formed on the isotherms. The type I isotherm indicates that the adsorbents possessed a mesoporous nature with a complex pore structure and a wide pore size distribution [76,83,155,194]. The pore size distribution (Figure 5.1b) shows that the total pore volume and micropore volume of the adsorbent slightly decreased after the iron oxide nanoparticles were deposited on the GAC surface. The measured values for these two parameters were 0.58 and 0.29 cm^3/g for GAC, while the total pore volume and micropore volume of MGAC were determined 0.53 and 0.26 cm^3/g, respectively. Using the BET technique, the surface areas of GAC and MGAC were obtained as 949.5 and 837.9 m^2/g, respectively. The difference in surface area between MGAC and GAC (12%) was due to the blocking of GAC pores by the iron and oxygen groups generated during the magnetization process [155].

a)

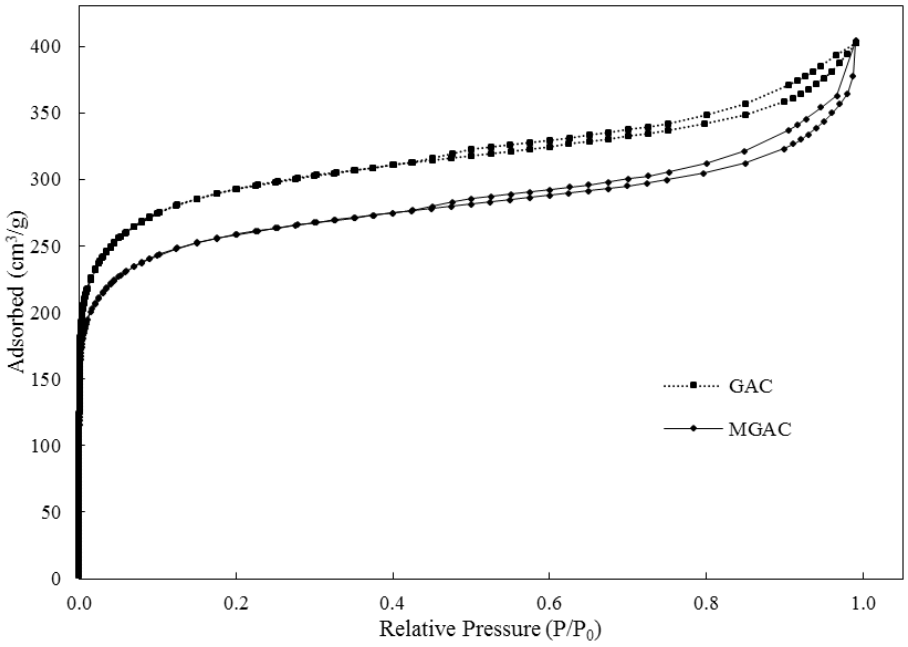

b)

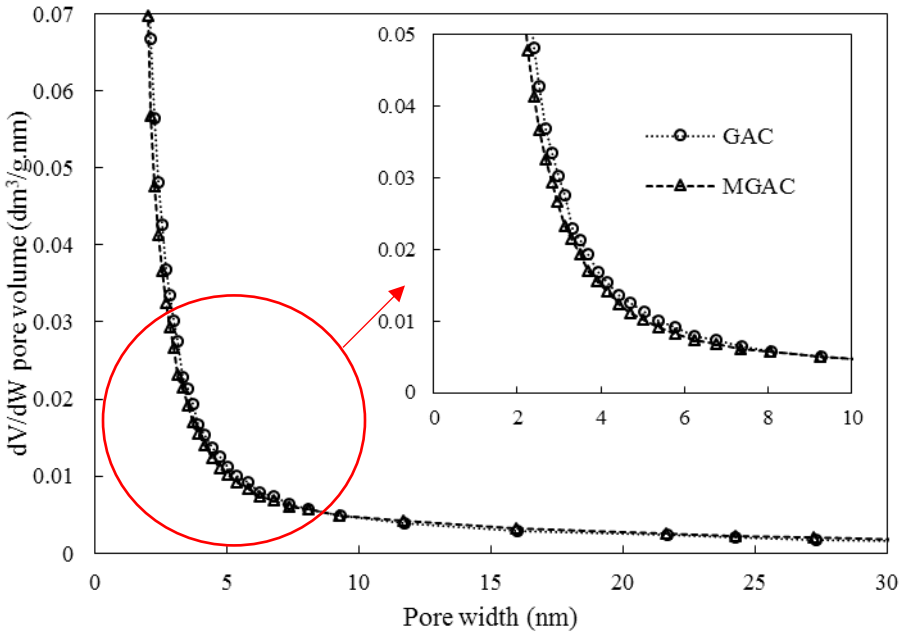

Figure 5.1. N_2 adsorption-desorption isotherms and pore size distribution of GAC and MGAC

The decrease in the surface area and pore volume of GAC after magnetization was also reported in the literature [39,68,84,155]. Inbaraj et al. (2021) fabricated a magnetic activated carbon from green tea waste biomass (GTAC) to use for removal of B[a]A, CHR, B[b]F, B[a]P from aqueous medium. The surface characterization of the GTAC and the magnetic GTAC was determined by

the BET method, and the results showed that the surface area decreased from 131.8 m^2/g to 118.8 m^2/g and the total pore volume was reduced from 0.065 g/cm^3 to 0.059 g/cm^3, a reduction of 10 % for each of them. Based on the results of the adsorption experiments, 100% of all the four PAH compounds were removed from the solutions containing 1 µg/mL PAHs by use of 50 mg/L magnetic GTAC and 0.1% sodium chloride and after 30 min. This demonstrated that the produced magnetic GTAC retained a significant adsorption ability for PAH compounds after magnetization [155]. Castro et al. (2009) magnetized commercial GAC at different mass ratios of GAC to Fe_3O_4 in order to remove atrazine from aqueous solutions. The BET tests of the prepared MGAC with mass ratios of 5:1 and 1:1 revealed a 15% and 36% reduction in the surface area due to magnetization, respectively. When compared to the bare AC, this reduction in the surface area reduced the maximum adsorption capacity of the magnetic composites by 20% and 48%, respectively [68]. In another study, Kalaruban et al. (2019) impregnated GAC with magnetite nanoparticles and then used the prepared composite in adsorption studies to remove arsenic from water. The surface area and micropore volume of the MGAC composite were reduced by 22% and 3%, respectively, after magnetization. Despite the reductions, the adsorption capacity of MGAC was increased for the inorganic contaminant. The researchers speculated that the enhanced affinity was due to the inter- and outer-sphere complexation of arsenic on iron oxide particles in the MGAC [39]. Tu et al. (2021) observed that, following magnetization of GAC, its surface area decreased from 822 m^2/g to 633 m^2/g, with a minor reduction in the micropore volume from 0.39 to 0.26 g/cm^3. The GAC and synthesized MGAC were used in the adsorption tests for removal of dibenzo-p-dioxin from aqueous solutions, and the analysis results showed no difference between the dioxin adsorption of GAC and MGAC (97% removal of dioxin after 1 h by each adsorbent). This confirmed that the changes in the morphology of GAC were minor after magnetization [84]. There are other studies that have reported similar results for the removal of inorganic and organic compounds using magnetic AC, with surface area reductions ranging from 10 to 70% following magnetization [38,41,67,123]. In this work, the 12% and 10% reduction in the surface area and pore volume of GAC after magnetization was not significant, suggesting that the MGAC composite could still have a high sorption affinity for the PAHs in the aqueous solutions.

The XRD patterns of the GAC and MGAC samples are shown in Figure 5.2. Two broad diffraction peaks for GAC were indexed at 23.7° and 44.7°, respectively, reflecting the amorphous nature of the GAC particles. The XRD spectrum of MGAC shows multiple intense diffraction peaks at 2Θ

of 30.4°, 35.7°, 44.4°, 53.8^0, 57.3°, and 62.8° for reflection planes of (220), (311), (400), (420), (511), and (440), respectively, indicating the formation of magnetite (Fe_3O_4) with cubic spinel structure onto GAC. The XRD results of the MGAC composite coincide with the iron oxide standard data published by Joint Committee for Powder Diffraction Studies (Card No.19-0629) [75]. The reflections of GAC in the MGAC XRD spectrum appeared as a very small distinctive peak, which is another evidence of formation of Fe_3O_4 on the GAC surface. The particle size of the synthesized magnetite can be calculated using the Scherrer equation, $D=k\lambda/\beta\cos\Theta$, where D represents the crystallite size of the particle (nm), K is the Scherrer constant (k=0.9), λ is the X-ray wavelength of 1.5418 Å, β is the full width at half maximum of the diffraction peak for the reflection planes of (311) and (440), and Θ is the diffraction angle (Bragg angle). According to the Scherrer equation, the size of magnetite particles was obtained 21.6 and 7.9 nm for the two spinel reflections (311) and (440), respectively, confirming that they possess nano-size crystal structure in the MGAC composite [29,83,155].

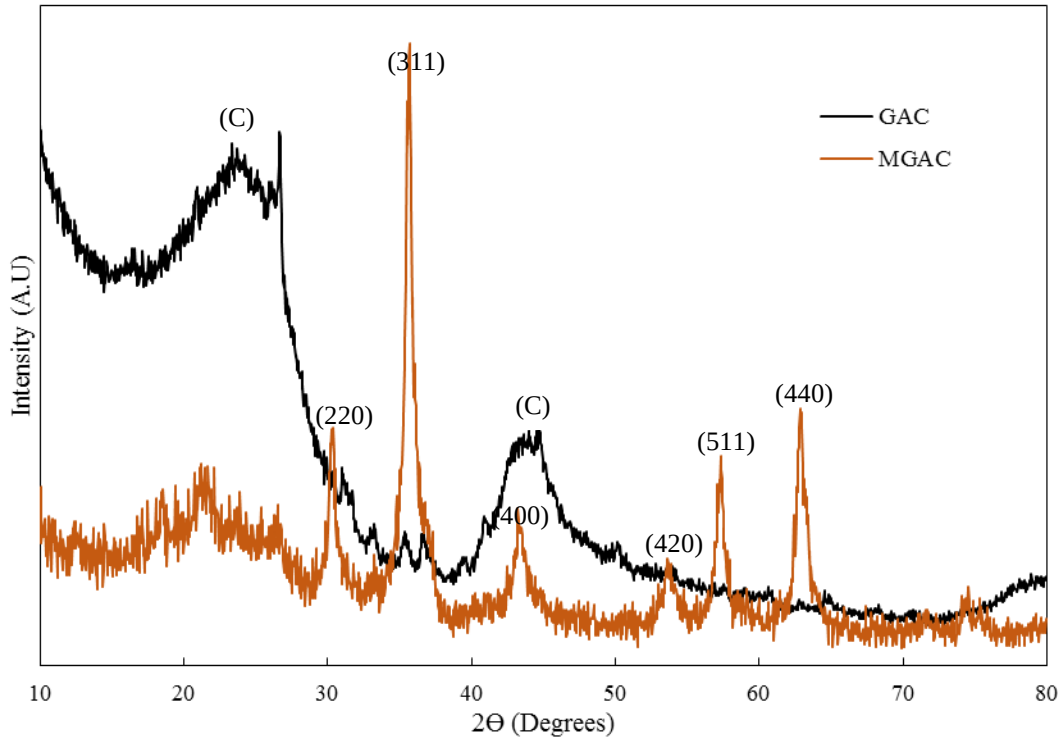

Figure 5.2. XRD patterns of the bare GAC and MGAC composite

The morphological properties of GAC and MGAC were determined using FE-SEM at 2 kV. As shown in Figure 5.3a, GAC possessed a broken surface with porous and rough structure, which is

in agreement with the XRD reflection planes showed for GAC (Figure 5.2). After the magnetization process, however, the surface of GAC became more spherical, with the magnetite nanoparticles in the shape of spongy crust covering it. The same observation was reported in the literature for AC-based magnetic composites [68,73,99,155].

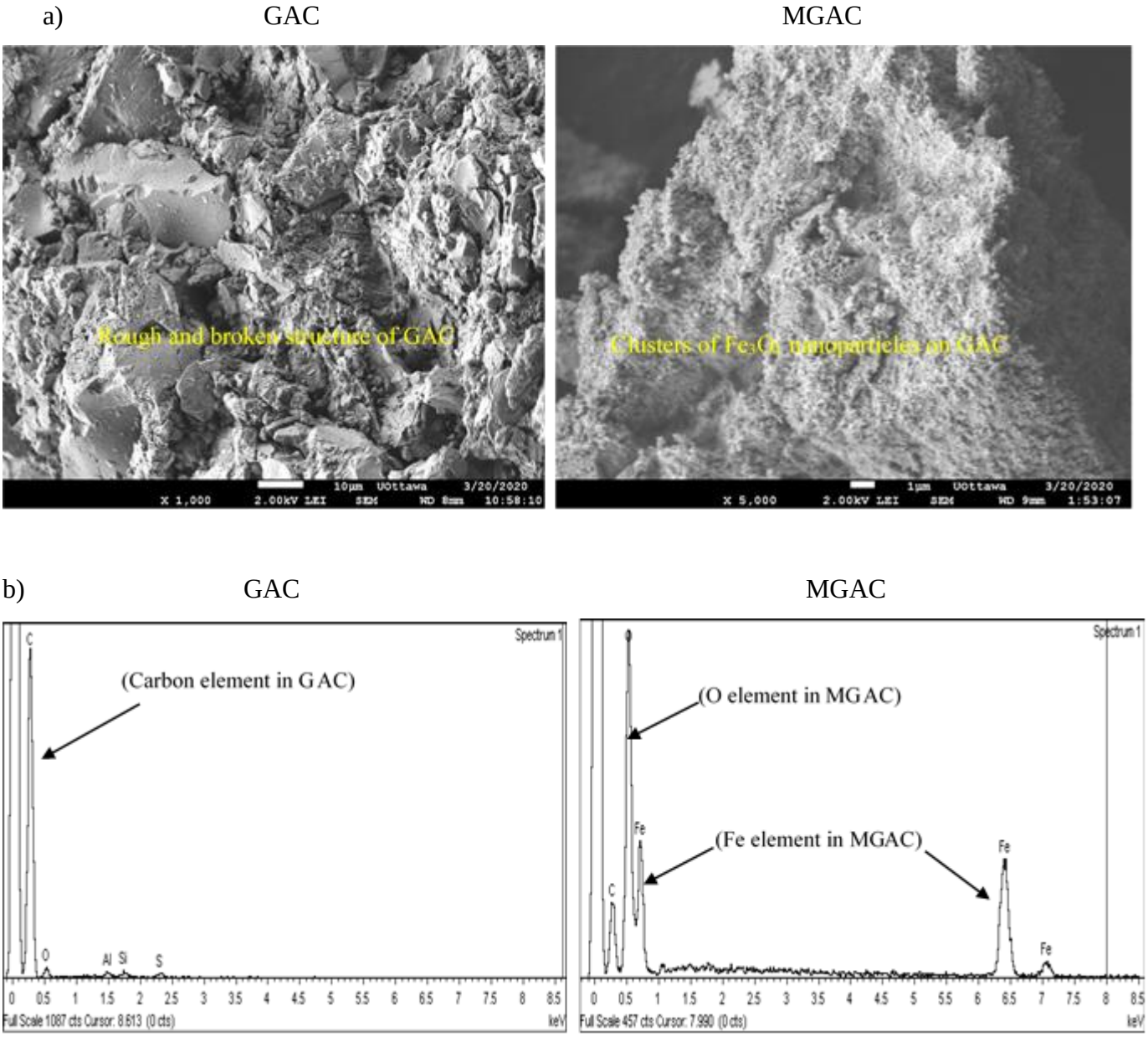

Figure 5.3. (a) The SEM images and (b) EDS spectra of GAC and MGAC

The elemental analysis of the GAC and MGAC surfaces obtained by the EDS technique is shown in Figure 5.3b. The predominant content of carbon and narrow fractions of oxygen, aluminum,

silicon, and sulfur can be observed in the GAC spectrum. In contrast, the MGAC spectrum shows intense peaks of iron and oxygen along with the peak of carbon. The carbon content of MGAC (Figure 5.3b) remained significantly higher than the iron and oxygen contents, implying that carbon was the principal element of the MGAC structure. The morphological analysis results confirmed that the synthesis process was successful, and Fe_3O_4 nanoparticles were distributed evenly over the GAC surface [172].

The interactions between PAHs and MGAC were investigated using the FTIR analysis method performed on the MGAC samples before and after adsorption. From Figure 5.4, the major peaks at 492 and 525 cm^{-1} in the spectrum of pure MGAC and the sharp peaks centered at 482 cm^{-1} and 536 cm^{-1} in the spectrum of PAH-loaded MGAC can be attributed to stretching vibration of the iron oxide ions. These changes confirmed presence of the Fe-O band, and therefore, the formation of a chemical bond between the magnetite nanoparticles and the GAC matrix [29]. The medium peak centered at 785 cm^{-1} in the pure MGAC shifted to 804 cm^{-1} after PAHs adsorption, which is correspondent to the deformation out of the plane of C-H bond in the MGAC composite. The peak at 903 cm^{-1} shifted to 887 cm^{-1} after PAHs adsorption, which may be attributed to the formations of bonds between the hydroxyl groups of MGAC and hydrogen components of PAH molecule [52,70,73,130]. Besides, the weak peaks that appeared at 1360 and 1640 cm^{-1} in PAH-loaded MGAC can be associated with the stretching vibration of C=C and C=O bonds in the carboxylic groups (O=C−O) after the PAHs adsorption. Finally, the broad band emerged at 3340 cm^{-1} in the spectrum of PAH-loaded MGAC belonged to the stretching vibration of hydroxyl–OH groups [30,132]. All these changes imply the formation of interactions between the hydroxyl and carboxyl groups of MGAC and PAH molecules during the adsorption process.

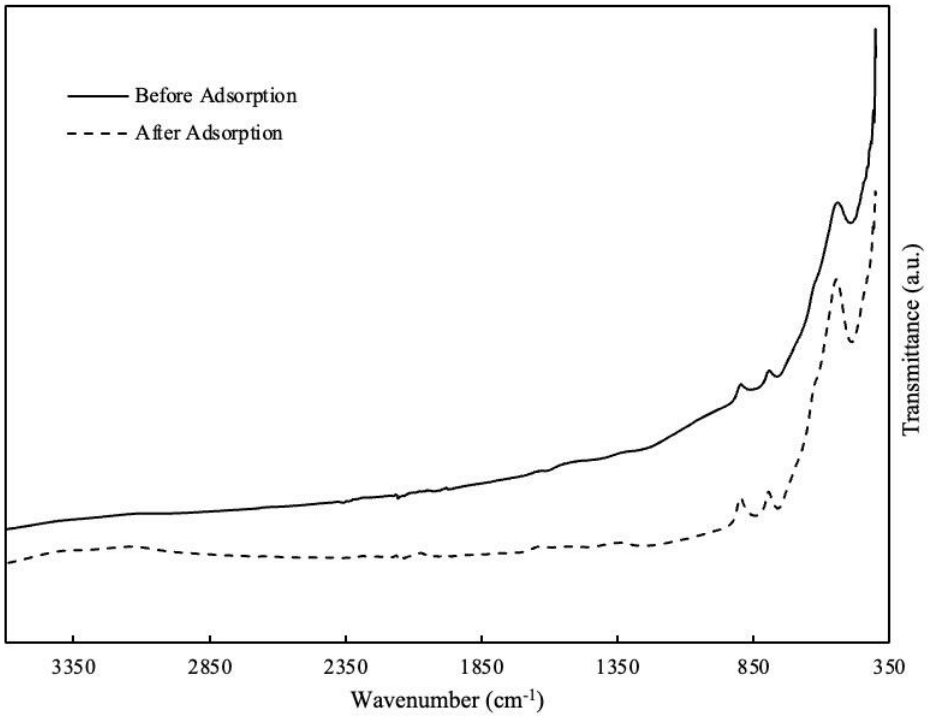

Figure 5.4. FTIR spectra of MGAC before and after PAHs adsorption

5.4.2 Adsorption isotherms

The adsorption affinity of MGAC for PAHs was described using Langmuir, Freundlich, and Temkin. The non-linear regression analysis method (SOLVER) was utilized to fit these models to the experimental data and estimate their isotherm variables as well as correlation coefficient (R^2) and error parameter (RMSE). As shown in Table 5.1, the R^2 values for the Langmuir model were in the range 0.82 – 1.0. The R^2 values for the two other isotherm models were lower than Langmuir ranging from 0.80 to 0.98 for the Freundlich and 0.72 to 0.99 for the Temkin models. In addition, Langmuir exhibited lower RMSE values (0.12-0.92), implying that this model is the best fit to the experimental isotherm data. As a result, the adsorption of both LMW and HMW PAHs onto MGAC can be considered as monolayer adsorption, in which the MGAC adsorption sites were homogeneously distributed on its surface and the PAH molecules did not interact during the adsorption process [67,73,178].

The values of the separation factor (R_L) were between 0.01 (ACE and FLU) and 0.44 (B[ghi]P) (Table 5.1), confirming the favourability of the PAHs adsorption ($0<R_L<1$) by the magnetic composite [73,179]. The rate of PAHs adsorption by MGAC is represented by the Langmuir

affinity constant (K_L). As seen in Table 5.1, the 3-ring ACE, FLU, and PHE have greater K_L values than the heavier PAHs (except for FLUO), with values of 21.89, 57.47, and 2.94 mL/ug, respectively, indicating that the LMW PAHs were adsorbed onto the magnetic adsorbent more quickly [180]. The Langmuir model was also used to attain the maximum adsorption capacity (q_{max}) of the MGAC composite for PAHs. The q_{max} values for the LMW PAHs varied from 7.93 to 9.89 µg/mg, whereas these values for the HMW PAHs were obtained in the range 6.22-12.42 µg/mg for the 4-ring PAHs, 14.18-18.41 µg/mg for the 5-and 6-ring PAHs. These findings imply that the MGAC affinity for the PAH compounds increased with the rise in the PAH aromatic ring, although PAHs with more rings (≥4) showed slower sorption onto MGAC than LMW PAHs.

Table 5.1. The parameters of Langmuir, Freundlich and Temkin isotherm models for the adsorption of PAHs onto MGAC

		Langmuir					Freundlich				Temkin			
	PAH	q_{max} (µg/mg)	K_L (mL/µg)	R^2	R_L	RMSE µg/mg	$1/n_f$	K_F (µg/mL)	R^2	RMSE µg/mg	B J/mol	K_T (L/mg)	R^2	RMSE µg/mg
3-ring PAHs	ACE	9.89	21.89	0.92	0.01	0.92	0.33	10.44	0.87	1.20	1.38	268.88	0.92	0.90
	FLU	8.82	57.47	0.92	0.01	0.87	0.23	9.02	0.93	0.84	1.68	496.57	0.76	1.55
	PHE	7.93	2.94	0.98	0.03	0.33	0.37	4.87	0.89	0.83	1.53	30.62	0.98	0.35
	ANT	9.18	1.65	0.99	0.06	0.31	0.47	4.93	0.96	0.53	1.34	20.79	0.99	0.17
4-ring PAHs	FLUO	6.22	7.60	0.82	0.01	0.81	0.38	3.55	0.80	0.84	3.07	182.23	0.72	1.00
	PYR	8.36	1.00	0.96	0.09	0.47	0.49	3.56	0.89	0.76	1.28	8.67	0.98	0.31
	B[a]A	9.65	0.31	1.00	0.24	0.12	0.63	2.23	0.98	0.25	1.73	7.57	0.92	0.55
	CHR	12.42	0.18	0.94	0.36	0.52	0.83	1.71	0.93	0.53	1.30	3.33	0.87	0.73
5-ring PAHs	B[b]F	16.13	0.13	0.93	0.43	0.55	0.84	1.76	0.93	0.58	1.23	3.20	0.87	0.76
	B[k]F	15.05	0.19	0.98	0.35	0.31	0.70	2.43	0.97	0.36	1.57	7.82	0.86	0.80
	B[a]P	15.65	0.26	0.95	0.28	0.48	0.74	2.98	0.94	0.56	2.08	38.39	0.88	0.80
	D[a,h]A	14.18	0.22	0.98	0.31	0.31	0.73	2.50	0.97	0.38	1.44	6.85	0.87	0.80
6-ring PAHs	B[ghi]P	18.41	0.13	0.88	0.44	0.80	0.96	1.78	0.89	0.77	1.04	2.75	0.83	0.96
	IDP	17.69	0.18	0.98	0.35	0.30	0.74	2.75	0.98	0.36	1.36	7.21	0.88	0.82

The adsorption of LMW and HMW PAHs by MAC composites has not been thoroughly explored in the literature. Inbaraj et al. (2021) studied the adsorption capability of magnetic PAC obtained from the powdering and activation of green tea waste for the removal of four HMW PAHs, B[b]F, B[a]P, CHR, and B[a]A, from aqueous solutions. For the PAH compounds, the maximum adsorption capacity of the magnetic PAC was estimated 28.08, 22.75, 19.14, and 15.86 µg/mg, respectively, which were greater than the results attained in this work [155]. The researchers,

however, did not determine the adsorption uptake of the synthesized composite for LMW PAHs and other toxic HMW PAHs such as D[a,h]A and IDP. Eeshwarasinghe et al. (2019) utilized GAC to adsorb LMW ACE and PHE from water samples. The isotherm modelling of their experimental data showed a maximum adsorption capacity of 2.63 µg/mg for ACE and 7.36 µg/mg for PHE [18]. GAC was also employed by Valderrama et al. (2008) for the removal of NAP, ACE, FLU, ANT, PYR, and FLUO from water. The maximum adsorption capacity of the adsorbent for the six PAH compounds was estimated by the Langmuir model to be 0.14, 0.11, 0.15, 0.23, 0.11, and 0.09 µg/mg, respectively [175]. The results of the two aforementioned studies showed a lower maximum adsorption capacity of GAC for the LMW PAHs compared to those achieved by MGAC in this work (Table 5.1). Furthermore, neither of the two studies assessed the efficiency of GAC for adsorption of the heavier PAHs such as B[a]P, B[ghi], D[a,h]A, and IDP.

For comparison purposes, the bare GAC was used in the adsorption isotherm experiments to determine its adsorption capacity for the PAH compounds. The experimental data were fitted to the Langmuir model, and the isotherm parameters were presented in Table 5.2. GAC had a higher maximum adsorption capacity than MGAC for both groups of PAHs (53.93 µg/mL for LMW PAHs and 154.45 µg/mL for HMW PAHs). The maximum adsorption capacity of GAC for the total PAHs was determined to be 190.30 µg/mL showing a difference of 20% with that of MGAC (153.50 µg/mL).

Table 5.2. Estimated variables of the Langmuir model for adsorption of PAHs by GAC and MGAC

		Langmuir				
AC	PAHs	q_{max}	K_L	R^2	R_L	RMSE
GAC	LMW	53.93	0.20	0.80	0.33	5.18
	HMW	154.45	0.01	0.98	0.88	2.60
	Total	190.30	0.02	0.98	0.85	4.55
MGAC	LMW	37.52	0.94	0.99	0.10	0.98
	HMW	109.52	0.03	0.98	0.75	2.86
	Total	153.50	0.03	0.99	0.74	3.22

These findings indicate that the magnetization procedure reduced the MGAC adsorption capacity; however, the magnetic adsorbent still retained a high affinity for the PAHs. Furthermore, the difficulty of retrieving the bare GAC would limit their employment in the treatment of aqueous solutions, especially in larger-scale projects [80]. Hence, the MGAC composite could be

considered a more practical choice for adsorption of PAHs from aqueous solutions than the bare GAC.

Figure 5.5 shows the adsorption isotherms data for the 14 PAH compounds adsorbed onto MGAC for a range of PAH concentrations from 0.5 to 10 µg/mL. The Langmuir model was used as the best model fit to the experimental data (Table 5.1 and Table 5.2) to describe the adsorption behaviour of PAHs onto MGAC. According to Figure 5.5a, the amounts of three-ring PAHs, ACE and FLU, adsorbed by the magnetic composite significantly increased when the PAH concentration was increased to 1 µg/mL. However, as it is evident, the adsorption capacity of MGAC for these two compounds reached a plateau (9.8 and 8.8 µg/mL) after rising the initial PAH concentration to 10 µg/mL. The adsorption uptake of MGAC for PHE and ANT appeared to be lower at the same concentration range, probably due to their higher molecular weight than ACE and FLU. For the 4-ring PAHs (Figure 5.5b), the highest uptake by MGAC was obtained for PYR and FLUO at the initial PAH concentration of 0.5 -10 µg/mL. As illustrated in Figure 5.5b, the FLUO isotherm pattern was similar to that of LMW PAHs, which was likely due to its molecular structure being close to that of LMW PAHs. The MGAC adsorption uptake for PYR, B[a]A, and CHR was not significant at their lower initial concentrations (Figure 5.5b), however, when the PAH concentration was raised to 10 µg/mL, greater amounts of these three compounds were sorbed onto MGAC, with CHR showing the highest sorption affinity to the adsorbent (q_{max} =12.4 µg/mg).

The adsorption capacity of MGAC for the 5-ring and 6-ring PAHs (Figure 5.5c and d) followed a similar pattern, showing the lowest sorption affinity to MGAC at the PAH initial concentrations of 0 to 1 µg/mL and the highest affinity at the PAH concentration of 10 µg/mL compared with the lighter PAH compounds. According to the Langmuir affinity constant (KL) (Table 5.1 and Table 5.2), the LMW PAHs were rapidly attracted by the adsorption sites of MGAC, and subsequently, connected with the adsorbent carboxyl and hydroxyl functional groups via the π-π and H-π interactions. The hydrophobicity of HMW PAHs in aqueous solution, however, could have an effect on how rapidly they are adsorbed on the adsorbent surface. In fact, water molecules surround the HMW PAHs in aqueous solution and form stronger hydrophobic interactions with them, causing this group of PAHs to be stabilized in water. As a result, the MGAC functional groups adsorb HMW PAHs slower than the less hydrophobic PAHs such as LMW FLU and PHE [129]. However, as it is evident from the isotherm patterns of Figure 5.5, the MGAC composite

had the highest adsorption capacity for the 5-ring and 6-ring PAHs. One possible explanation is that the increased number of aromatic rings in HMW PAHs provided them with the opportunity to establish more π- π interactions and stronger bonds with the MGAC surface than LMW PAHs.

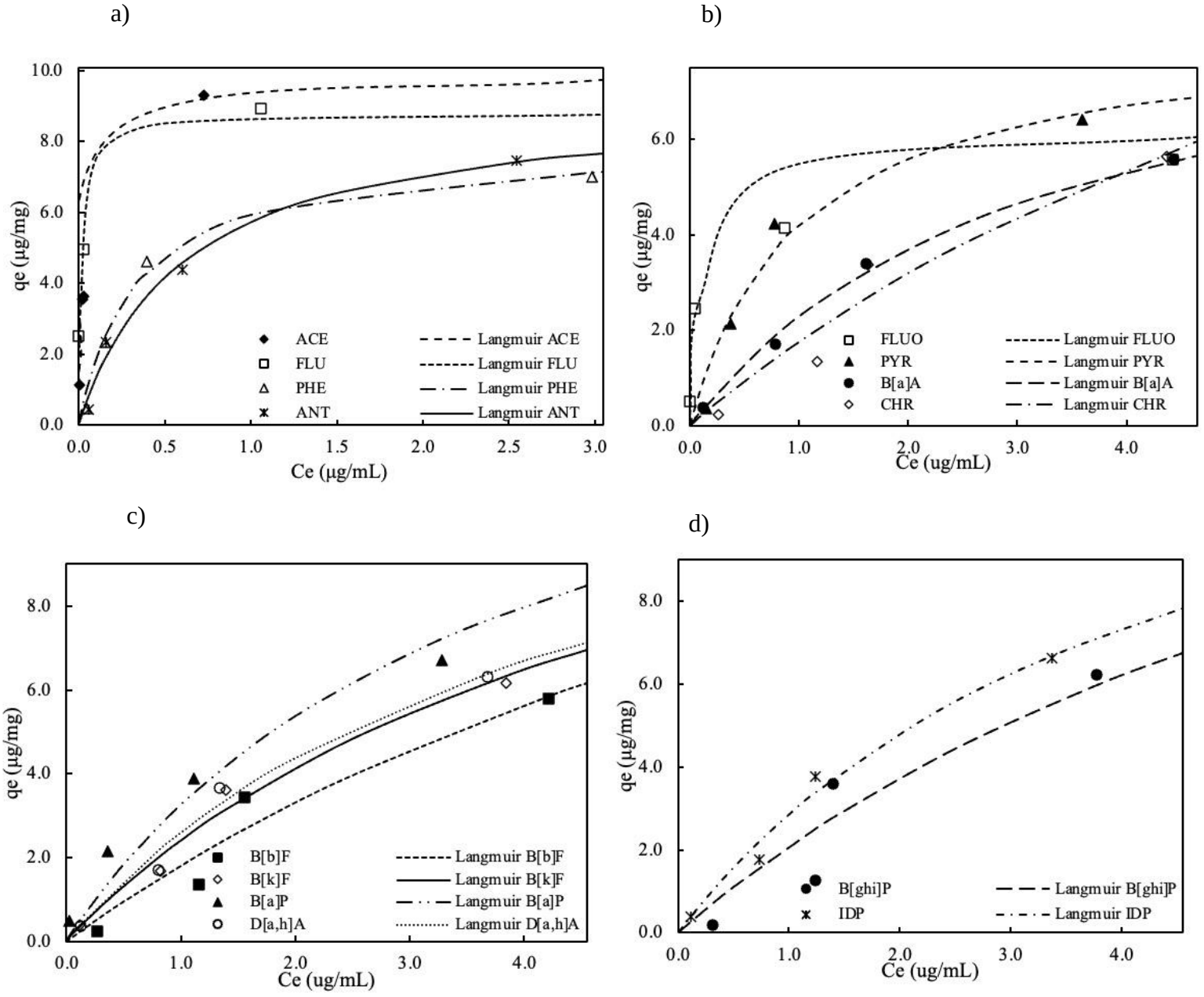

Figure 5.5. The experimental data fitted to the Langmuir model for (a) 3-ring LMW PAHs (b) 4-ring HMW PAHs (c) 5-ring HMW PAHs (d) 6-ring HMW PAHs adsorption onto MGAC

5.4.3 Combined soil washing and adsorption with MGAC

The soil samples were characterized as a well-graded sand with silt (SW-SM), containing 36.7% gravel, 58.0% sand, 4.0% silt, and 1.3% clay. The pH of the soil was 8.3 at 20% (W/V) soil in deionized water, indicating that it was alkaline soil. The soil organic matter level was determined 4.14%, which was not significant. For the soil washing experiments with MGAC, the soil sample was stored in the refrigerator to prevent any potential loss of the analytes.

The effects of various washing factors on PAHs removal with MGAC were investigated in a series of soil washing experiments. For this purpose, the critical factors were assessed in the following sequence: MGAC dose (0, 1, 2, and 5% (w/w)); liquid to soil ratio (L:S) (10:1, 15:1 and 20:1); Shaker speed (75, 100, 125, and 150 rpm); washing time (6, 24, 72, and 168 h), pH (7.0, 8.3, and 10), and Temperature (5 and 25 ˚C). For each set of the tests, one factor was examined at different values, while the others remained constant. The most efficient value was then employed in the following set of experiments to examine the next factor.

5.4.3.1 MGAC dose

The first set of the soil washing tests was conducted at different doses of MGAC, constant L/S ratio of 10:1 (30 mL DI water: 3g soil), washing time of 24 h, pH of 8.3 (the pH of the contaminated soil), and temperature of 25 ˚C. As shown in Figure 5.6a, the total removal of the LMW and HMW PAHs with the addition of only water (0% MGAC) was ≈10%, indicating that the soil washing process without the addition of removal agents such as adsorbents or surfactants would be ineffective in removing PAHs from soil. The removal percentage of LMW PAHs increased significantly by increasing the MGAC dose up to 5% w/w (150 mg). One possible reason is that by increasing the dose of MGAC, the physical contact between the magnetic adsorbent and soil particles increases, causing PAHs to segregate from soil particles and be removed by MGAC. Also, in comparison with the LMW PAHs (Figure 5.6a), the uptake of the HMW PAHs was higher at low dosages of the MGAC composite, which can be attributed to the higher affinity of MGAC for these compounds [59]. Regarding the PAHs removal percentages shown in Figure 5.6a, the 5% MGAC achieved the maximum total PAHs removal (29.5%), which was slightly higher than the 26.5% total PAHs removal by 2% MGAC. From the practical point of view, the difference between the PAHs removal efficiencies of 2% and 5% MGAC in soil washing was negligible. Therefore, the 2% dosage was selected for the next soil washing experiments to reduce the quantity of MGAC in the remediation process and lower the associated cost.

5.4.3.2 Liquid:soil ratio

Different washing water to soil (L:S) ratios ranging from 10:1 to 20:1 were assessed for the PAHs removal with MGAC in the second set of the experiments, while the other effective parameters of soil washing were kept constant. After the 24 h soil washing with MGAC (Figure 5.6b), the L:S ratios of 20:1 and 15:1 could remove 47.5% and 46.5% of the total PAHs from the soil, respectively. According to Figure 5.6b, the removal patterns for LMW and HMW PAHs were similar, suggesting that the increase in the liquid phase could facilitate the separation of all the PAHs from the soil and their uptake by MGAC [59–61].

The effect of higher L:S ratios on PAH removal in the soil washing process has also been reported in the literature. Peng et al. (2011) stated that raising the L:S to 20:1 enhanced the efficacy of soil washing for PHE removal in a nonlinear pattern (Peng et al., 2011). Gan Xinhong et al. (2017) reported the same L:S leading to the maximum PAH removal from soil using nano-sulfonated graphene, although they ultimately selected the L:S of 10:1 as the optimal L:S due to the similar PAHs removal efficiency [59]. Considering the slight difference in PAHs removal efficiency between the L:S of 20:1 and 15:1, the L:S of 15:1 was taken as the optimal ratio to avoid using more water. A higher L:S means that there will be more wastewater discharge and that more energy will be required to handle it [195]. A smaller L:S ratio also has a less adverse impact on the physicochemical characteristics of soil [59].

5.4.3.3 Stirring speed

The influence of shaker speed on PAH removal from soil was explored in the third set of soil washing studies. The samples were washed at a shaker speed of 75-150 rpm, MGAC dose of 2%, and L/S ratio of 15:1 for this purpose, with the rest of the soil washing parameters remaining the same as set 1. According to Figure 5.6c, the removal of LMW PAHs was close to zero at 75 rpm and then it sharply increased when the stirring speed was raised, with the maximum removal efficiency achieved at 125 rpm (53.5%). The removal percentages of HMW PAHs also increased from 28.2 to 48.0% by increasing the stirring speed to 100 rpm; however, the pattern fluctuated when the stirring speed was adjusted to 125 and 150 rpm. The removal percentages of total PAHs followed the same pattern as HMW PAHs, peaking at the 100 rpm stirring speed with 47.5% removal. Peng et al. (2011) discovered that increasing the stirring speed leads to more collision between soil particles, which can result in more adsorbed or crusted contaminants being stripped

away. They also proposed that further increase in the stirring speed may cause the soil slurry to move in bulk formation with less relative movement, leading to fewer soil collisions and lower adsorbate removal from the soil [60].

5.4.3.4 Washing time

The optimal values of the soil washing parameters determined in the previous sets of tests were used in set 4 with a washing time ranging from 6 to 168 h. Figure 5.6d shows that the patterns of LMW, HMW, and total PAHs removal followed a similar trend for the varied washing time periods. The PAHs removal significantly increased after changing the washing time to 24 h, with the highest removal percentages of 45.8, 48.0, and 47.4% for the LMW, HMW, and total PAHs, respectively. However, increasing the washing period to 72 h resulted in a 5% reduction in the removal of all the PAHs from the soil, and an additional slight reduction of 2% in the total PAHs removal with further increase of time to 168 h (Figure 5.6d). One possible reason is the difficulty in recovering some small MGAC particles trapped in the soil after the long washing period. As a result, a portion of PAHs sorbed onto these MGAC particles was extracted along with the soil during the analysis phase, raising the residual PAHs concentration for the treated soil.

PAHs can form incrustation on the soil surface, with some of them being water-soluble. They could also be trapped in soil pores or absorbed by soil organic matter and fine soil particles [60]. The enhanced removal of PAHs during the 24 h washing time could be explained by uptake of water-soluble PAHs and a fraction of PAHs that were weakly attached to soil particles [196,197]. The fraction of PAHs trapped in the pores of soil particles and some organically bound fraction of PAHs can also be removed from the soil within the first hours of the washing process [59,195]. As a result, the most potentially accessible PAHs were eliminated during the 24 h soil washing process. However, further increase in the washing period would negatively affect the PAHs removal, either due to the precipitation of a portion of the PAH-loaded MGAC in the soil or re-sorption of some fractions of the dissolved PAHs by soil particles [59,60].

5.4.3.5 pH

The influence of pH on removing the LMW, HMW, and total PAHs is illustrated in Figure 5.6e. When the pH was reduced from 8.3 to 7.0, the removal efficiency significantly decreased from 45.8 to 29.3 % for LMW PAHs, 48.0 to 26.3% for HMW PAHs, and 47.4 to 27.1% for the total PAHs. The same tendency was observed when the pH was elevated to 10.0, with the reduction in

the PAH removal from 45.8% to 27.2% for LMW PAHs, 48.0% to 28.7% for HMW PAHs, and 47.4% to 28.3% for total PAHs. These results demonstrated that soil washing with MGAC performed in the original soil condition yielded better PAHs removal. A possible reason is that the magnetite particles might hydrolyze to form iron (II) hydroxide ($Fe(OH)_2$) precipitate under neutral (pH 7) or alkaline (pH 10) conditions, which negatively affected the performance of the MGAC composite in soil washing [29]. These findings were in line with those of Egbosiuba et al. (2020) and Hung et al. (2020), who discovered that acidic and alkaline conditions negatively affected the adsorbent capacity to extract methylene blue and PAHs from aqueous solutions, respectively [29,198]. Therefore, the MGAC/soil washing system was pH-dependent, and the PAH removal was most efficient at the original pH of the soil samples.

5.4.3.6 Temperature

Figure 5.6f shows the effect of temperature on the PAHs removal during the soil washing process with MGAC. The test was carried out at temperatures of 5 and 25˚ C, with the optimal values of the influencing parameters remaining constant. Evidently, lowering the temperature from 25 to 5˚ C had an adverse impact on the treatment process, reducing the PAHs removal efficiency from 45.8 to 37.9% for LMW PAHs, 48.0 to 32.3% for HMW PAHs, and 47.4 to 33.8% for the total PAHs. These significant reductions indicate that the PAH adsorption via MGAC in the soil washing process was temperature-dependent and endothermic. Barman et al. (2021) achieved similar results when they used modified biochar to remove two LMW PAHs, naphthalene (NAP) and ACE, from aqueous solutions. According to their findings, the increase in temperature to 35˚C could assist the adsorbent in removing 94.0 and 92.5% of the two PAHs from solutions, respectively, implying that PAH adsorption was endothermic [188]. Awoyemi (2011) proposed that water molecules form hydrogen bonds with the oxygen groups of the AC surface at lower temperatures, resulting in a steric impediment to the PAH adsorption. However, when the temperature rises, the steric impediment is reduced, which consequently leads to an increase in the AC adsorption capacity [52,121]. From these findings, it can be inferred that the efficiency of the MGAC-based soil washing for the removal of PAHs from soil may be affected in cold climates.

a)

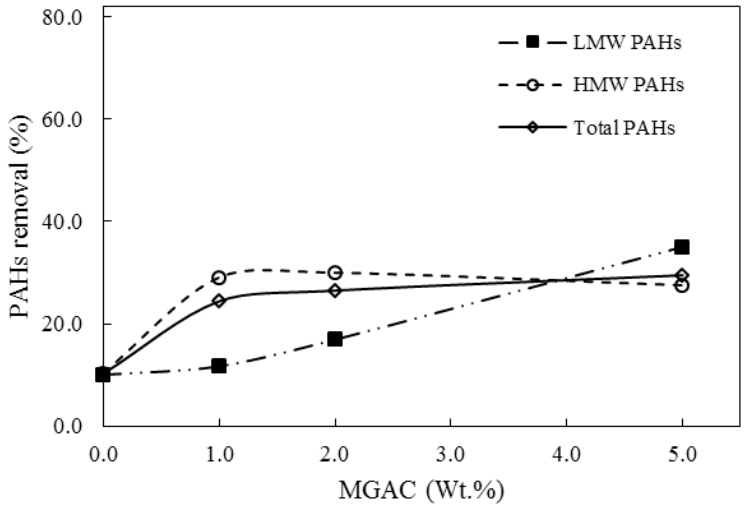
80.0
60.0
40.0
20.0
0.0
PAHs removal (%)
LMW PAHs
HMW PAHs
Total PAHs
0.0
1.0
2.0
3.0
4.0
5.0
MGAC (Wt.%)

b)

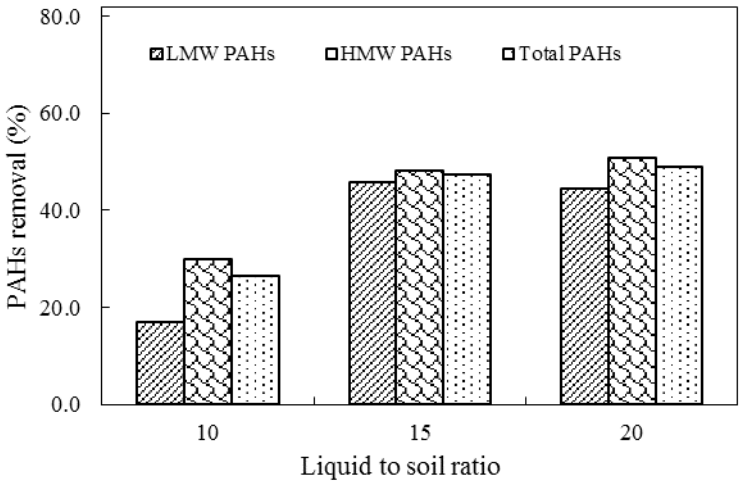
80.0
60.0
40.0
20.0
0.0
PAHs removal (%)
LMW PAHs
HMW PAHs
Total PAHs
10
15
20
Liquid to soil ratio

c)

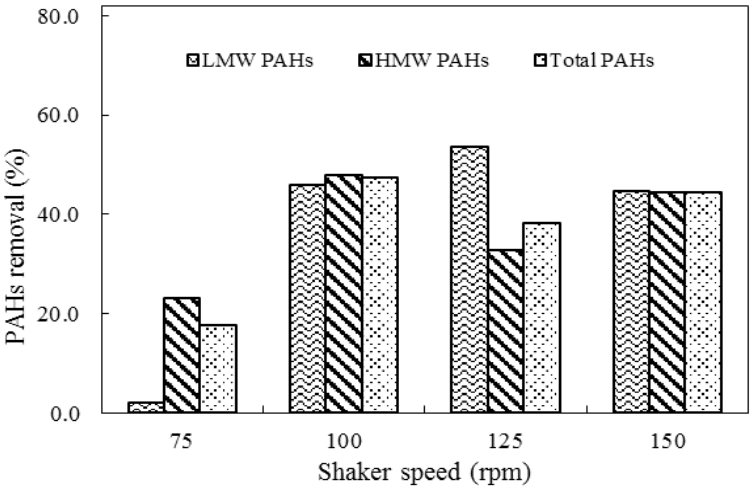
80.0
60.0
40.0
20.0
0.0
PAHs removal (%)
LMW PAHs
HMW PAHs
Total PAHs
75
100
125
150
Shaker speed (rpm)

d)

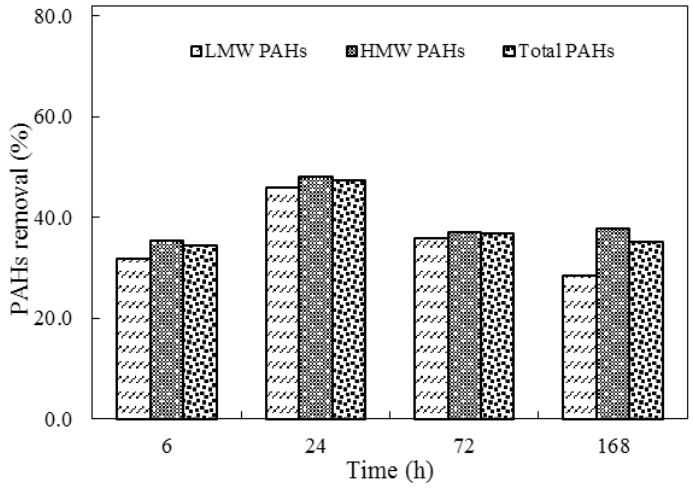

e)

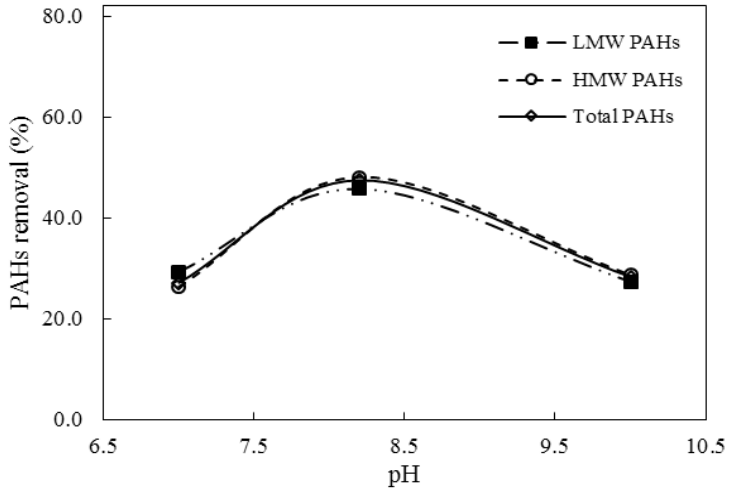

f)

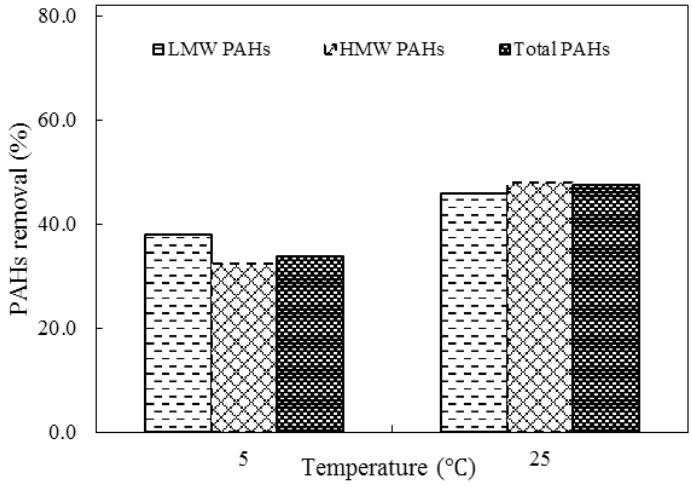

Figure 5.6. Removal of PAHs from soil with MGAC in soil washing at different washing parameters (a) MGAC dose, (b) Liquid/ soil ratio, (c) stirring speed, (d) washing time, (e) pH, (f) temperature

The soil washing process was optimized at MGAC dose of 2% (w/w), L:S ratio of 15:1, stirring speed of 100 rpm, washing period of 24 h, natural pH of the soil, and temperature of 25 °C, removing 47.4% of the total PAHs from the soil. The employed remediation method had the benefit of using an adsorbent with high PAH uptake capacity which removed PAHs from a real contaminated soil within a short time. Furthermore, in this method, the PAH-loaded MGAC particles were easily retrieved from the soil using a magnetic field, suggesting that no secondary source of pollution would be left in the soil after treatment.

5.4.4 Thermodynamic study

The difference in bond energies between adsorbate and the adsorbent is denoted by the enthalpy parameter (ΔH°). A negative ΔH° indicates that the heat is released from the reactions, while a positive ΔH° means that the heat is absorbed in the adsorption process. The affinity of the MGAC towards the PAHs can be reflected by a positive value of the entropy parameter (ΔS°), implying that the PAHs adsorption becomes more disordered (randomness) during the treatment process. On the other hand, when ΔS° is negative, the system is more ordered [188,190]. Spontaneous reactions have a negative Gibb's free energy (ΔG°), which implies they release energy during the adsorption process and can proceed without energy input. On the other hand, reactions with a positive ΔG° (non-spontaneous reactions) require energy input to proceed. Table 5.3 shows the thermodynamic parameters for the LMW, HMW, and total PAHs adsorption onto MGAC in the soil washing process. The quantities of enthalpy (ΔH°) and entropy (ΔS°) were obtained by plotting LnKc versus 1/T (Eq. 5.6), where the slope represented enthalpy and the intercept was entropy. Positive ΔG° values of 1.14, 1.71, and 1.55 kJ/mol at 5 ˚C and 0.41, 0.19, and 0.25 kJ/mol at 25 ˚C suggested that the reactions between the PAHs and MGAC during the soil washing process required energy/heat, and therefore, were endothermic [88]. The increase in ΔG° values as the temperature was reduced to 5˚ C and the positive values of ΔH° (11-23 KJ/mol) were other evidence indicating the process favoured heat to progress [136,188]. Besides, as shown in Table 5.3, the ΔH° values for the LWM, HMW, and total PAHs fell in the range of 1-40 kJ/mol, which implies that adsorption of the PAHs onto the magnetic adsorbent was physical (Cheng et al., 2021; Egbosiuba et al., 2020). The positive values of ΔS°: 36.29, 75.82, and 65.11 for the LMW, HMW, and total PAHs, respectively, confirmed that MGAC had a high affinity for all the PAHs and that the randomness at the MGAC/soil slurry interface increased after PAH adsorption [158,199].

Table 5.3. Thermodynamic parameters for LMW, HMW, total PAHs adsorption onto MGAC

	ΔH° (kJ/mol)	ΔS° (J/mol.K)	ΔG°(kJ/mol)	
Temperature			5˚ C	25˚ C
LMW PAHs	11.23	36.29	1.14	0.41
HMW PAHs	22.80	75.82	1.71	0.19
Total PAHs	19.67	65.11	1.55	0.25

5.4.5 Adsorption mechanism

In a well-stirred soil–liquid mixture (soil slurry), PAH uptake by adsorbents such as MGAC takes place in four steps: (1) desorption of PAH from soil particles using the washing solution (2) diffusive transport of the PAH molecule to the exterior surface of MGAC via a boundary layer; (3) PAH intra-particle diffusion over the interior pores of MGAC; and (4) PAH adsorption on MGAC adsorption sites [121]. The mechanisms of PAH adsorption on the GAC/PAC surface has been investigated by several studies [59,73,121,153]. These mechanisms involve π- π stacking interactions and H-bonding. The π- π interaction is a type of dispersion force derived from van der Waals forces that occurs between the PAH molecule and the carbon surface. Since PAHs and carbonaceous products, such as GAC/PAC and graphene, have the same hexatomic rings of a carbon atom, they can stack with each other by stabilizing the π- π interactions [73]. H-bonding is another electrostatic force that can be formed between a PAH molecule and a GAC/PAC surface, in which the hydrogen atom of the PAH is covalently bonded to oxygen on the carbon surface. . In this study, the interactions formed between the LMW and HMW PAHs and the carbon layer and functional groups of MGAC, as stated in section 5.4.1 (FTIR analysis), played the main role in adsorbing the PAH analytes during the soil washing process.

The concentrations of PAHs in the soil before and after the treatment process are presented in Table 5.4. For LMW PAHs, the removal % was in the range 34.6-57.7%, with the highest being recorded for ANT. The removal efficiency for the HMW PAHs ranged from 27.9% (B[a]A) to 67.1% (FLUO), indicating that the MGAC composite was also capable of adsorbing this group of PAHs from the soil. Furthermore, these findings (Table 5.4) revealed that the adsorption efficiency of MGAC for most of the LMW and HMW PAHs was almost in the same range, although the removal % was slightly higher for the total HMW PAHs (45.8% LMW PAHs vs. 48.0% HMW PAHs). The adsorption capacity of the MGAC for each PAH compound was also presented in

Table 5.4. The PAH uptake of the magnetic adsorbent from the soil slurry was determined to be 38.1, 110.5, and 148.6 µg/mg for the LMW, HMW, and total PAHs, respectively, which was in agreement with the range of maximum adsorption capacities obtained using the Langmuir isotherm model for the PAHs (Table 5.1 and Table 5.2).

Table 5.4. PAHs removal by soil washing combined with adsorption (MGAC)

PAH Component	Initial PAH concentration in soil (µg/g)	Final PAH concertation (µg/g)	PAHs Removal (%)	MGAC q_e (µg/mg)	No. of aromatic rings	Molecular weight ($g.mol^{-1}$)
ACE	3.9	2.4	37.3	1.1	3	154
FLU	1.4	0.7	46.3	0.5	3	166
PHE	52.9	34.6	34.6	13.7	3	178
ANT	52.8	22.3	57.7	22.8	3	178
Σ4LMW	110.9	60.1	45.8	38.1	-	-
FLUO	131.3	43.2	67.1	66.1	4	202
PYR	77.0	51.1	33.6	19.4	4	202
B[a]A	26.5	19.1	27.9	5.6	4	228
CHR	14.6	10.0	31.4	3.4	4	228
B[b]F	12.5	8.7	29.9	2.8	5	252
B[k]F	6.6	4.1	38.4	1.9	5	252
B[a]P	16.7	10.1	39.3	4.9	5	252
B[ghi]P	4.8	2.7	43.7	1.6	6	276
IDP	7.7	4.6	40.2	2.3	6	276
D[a,h]A	9.0	5.7	35.9	2.4	5	278
Σ10HMW	306.7	159.4	48.0	110.5	-	-
Σ14PAHs	417.6	219.5	47.4	148.6	-	-

There are some previous studies on the bare (unmodified) activated carbon for treatment of the PAH-contaminated soil; however, very limited information exists on the application of magnetized activated carbon. Hale et al. (2012) applied a GAC amendment method to a PAH-contaminated soil in a field-scale study. According to their findings, the adsorbent reduced the concentration of the total PAHs in the soil by 56% 12 months after amendment [33]. Despite the relatively successful PAH removal by the bare GAC, the researchers did not report any method for the adsorbent recovery from the soil. Besides, a twelve-month treatment process was very long and expensive as it could demand significant energy consumption and system maintenance. In another

study, Jakob et al. (2012) investigated the amendment of GAC to PAH-contaminated soil samples for 28 days. Their results showed that the amendment of 2% GAC (w/w) decreased the PAHs concentration in the soil by nearly 47 % after the treatment period. The researchers used an excavator to mix GAC with soil; however, they did not determine how the PAH-loaded GAC particles were retrieved from the soil after treatment [34]. The GAC amendment method discussed in both studies was time-consuming with higher operational costs and unclear retrieval of the GAC after use. In this study, however, the results obtained for removing PAHs by the magnetized GAC (Table 5.4) are comparable to those reported above. Aside from the shorter remediation time, another advantage of utilizing MGAC in the soil washing process was its high recovery percentage after adsorption (more than 95%), suggesting that the magnetic susceptibility of the MGAC particles was at an optimal level.

5.5 Conclusions

This study examined the performance of soil washing in combination with adsorption by magnetized granular activated carbon (MGAC) to remove PAHs from a real contaminated soil sample. The presence of magnetite nanoparticles on the MGAC surface was confirmed by XRD, FTIR, and EDS techniques used to characterize the synthesized adsorbent. The BET test results revealed that the specific surface area and total pore volume of GAC were reduced by 12% and 10%, respectively, after the magnetization procedure. The Langmuir isotherm model was found to fit the experimental data the best, demonstrating monolayer adsorption of PAHs onto MGAC. The maximum PAH adsorption capacity of MGAC was estimated in the range 7.9-9.9 µg/mg for the LMW PAHs, 6.2-18.4 µg/mg for the HMW PAHs, which showed a higher affinity of the magnetic adsorbent for the HMW PAHs than LMW PAHs.

For the contaminated soil sample used in this research, the optimum soil washing parameters were determined as: 2% MGAC (w/w), L:S of 15:1, stirring speed of 100 rpm, washing time of 24 h, pH of 8.3 (original soil pH), and temperature of 25°C. The performance of soil washing under the optimal conditions resulted in the highest removal efficiency of 45.8, 48.0%, and 47.4% for the LMW, HMW, and total PAHs, respectively. After treatment, 95% of the MGAC particles were recovered from the soil, indicating that only a small amount of the PAH-loaded MGAC remained in the soil, which would not constitute a significant source of pollution. Considering the adsorption affinity of MGAC for PAHs and the proportion of MGAC particles recovered from the treated soil, it can be concluded that the optimized soil washing using MGAC as the adsorbent was

relatively efficient in removing PAHs from the soil. According to the thermodynamic study, the PAH adsorption onto MGAC was endothermic and non-spontaneous. The thermodynamic results also indicated the physical adsorption of LMW and HMW PAHs onto MGAC through the formation of the π- π interactions and H-bonding between PAHs and the magnetic adsorbent.

5.6 References

This chapter's references are integrated with the references from the other chapters and provided at the end of the thesis.

6 The Application of Surfactant-Enhanced Soil Washing Process Combined with Adsorption using a Recoverable Magnetic Granular Activated Carbon for Remediation of PAH-Contaminated Soil

6.1 Abstract

The efficiency of surfactant-enhanced soil washing combined with adsorption for PAHs removal from a real contaminated soil and the feasibility of surfactant recycling were investigated in this study. A synthesized magnetic granular activated carbon (MGAC) was used as the adsorbent and Tween 80 was the surfactant employed in this research. The experimental data for the adsorption of PAHs from aqueous phase by the MGAC composite were fitted the best with the Dubinin–Radushkevich isotherm model ($0.66<R^2<0.91$), with the maximum adsorption capacity of MGAC for the PAHs being in the range 6.2-10.9 µg/mL. According to the PAH solubilization tests, the increase in the Tween 80 dose from 1% to 5% (v/v) resulted in an increase in the total PAHs solubility up to ≈ 40%. The optimum range of the operational parameters of Tween 80 enhanced soil washing were determined as 5% Tween 80, a liquid to soil ratio of 10:1, and a 72h washing time at 20°C. Under these conditions, the average PAHs percent removal from soil was 67.6 %. The remediation of contaminated soil samples using recycled 5% Tween 80 and 2% (w/w) MGAC (with no regeneration) was assessed in 7 successive cycles. The results indicated that removal efficiencies were 68.6, 70.7, 70.3, 61.6, 55.5, 50.2, and 39.4% for the repeated washing cycles, respectively. Tween 80 and the non-regenerated MGAC did not produce any waste or effluent after six times reuse in the treatment. The surfactant adsorption tests showed that only 5 to 10% of Tween 80 would be adsorbed to the soil particles, suggesting the high recovery of the surfactant solution from the soil.

Keywords: Polycyclic aromatic hydrocarbons; Surfactant (Tween 80); Magnetic granular activated carbon; Soil washing; Adsorption

6.2 Introduction

Polycyclic aromatic hydrocarbons (PAHs) have been designated as hazardous pollutants by several environmental bodies, including the US Environmental Protection Agency and the Canadian Council of Ministers of the Environment [14,127,200]. The majority of these persistent hydrocarbons originate from human-made sources such as coal combustion, vehicle emissions, and leakage from storage tanks and transport pipes [31,155,184,186]. They may then accumulate in soil or leak into water resources, therefore, contaminating the food chain and water supplies, and posing a risk to human health [59,155].

PAH-contaminated soil has been found in a vast number of industrial sites (e.g., coking factories) and transportation infrastructure (e.g., gas stations) around the world, threatening human health and the environment. These contaminated sites, designated as superfund sites in US or brownfields in Canada, require cleanup to meet existing regulations and policies. In addition, with the expansion of metropolitan areas over the last few decades, many of these sites are now located within urban areas and are being considered for redevelopment. Thus, there is a need for the implementation of rapid and cost-effective remediation strategies [8,59,201–203]. Solidification/stabilization, soil vapour extraction, vitrification, supercritical fluid extraction, bioremediation, soil washing, and soil replacement are some of the technologies utilized to remediate PAH-contaminated soils [12,55,204]. Bioremediation, which is known to be affordable, may not be effective in areas with cold climatic conditions as it takes a long time (i.e., several months) to remove the contaminants from soil [55]. Although most of the above-mentioned remediation techniques have been reported to remove significant amounts of PAHs from contaminated soil, they can be expensive due to the required treatment facilities and maintenance services or severely impacted by cold climatic conditions [55,204].

Soil washing with surfactant is one of the potential remediation techniques that can effectively remove contaminants from soil in a relatively short time duration [60,61]. This remediation process has been implemented in the USA, Canada, and many European countries in accordance with regulatory standards and best management practices in recent years [59]. A major step in successful soil washing process is identifying and utilizing a proper surfactant for the soil and the type of target contaminants (e.g., PAHs as organic and heavy metals as inorganic contaminants). In the case of PAH-contaminated soils, the efficiency of surfactants such as Triton X-100 (TX100), Polysorbate 80 (Tween 80), and Sodium dodecyl sulfate (SDS) has been reported in literature [59–

61]. However, one major drawback of surfactant-enhanced soil washing is that it generates polluted washing effluent, which could be subject to discharge standards and needs to be treated before final disposal or recycle [55,61]. Therefore, it is essential to treat the contaminated washing effluent.

Adsorption using activated carbon (AC) is a potential method to remove PAHs from washing effluent due to its high efficiency, easy implementation, and low cost [33,66]. However, the recovery of AC from soil slurries after the treatment is a very challenging task, and the separation methods such as filtration or centrifugation are ineffective or impractical for this purpose. As a result, the PAH-loaded AC particles may remain in the soil after treatment, forming a secondary source of contamination that is toxic to soil organisms and plants. The use of a magnetized AC (MAC) in the combined soil washing and adsorption process can address this issue and be more practical since the MAC particles can be readily separated from soil using an external magnetic field.

Considering the above, the primary goal of this study was to employ a surfactant-enhanced soil washing process combined with adsorption by MAC composite to remove PAHs from contaminated soil. Also, the feasibility of recycling and reuse of surfactant was investigated, which could result in decreasing the washing effluent volume and operating costs. Mirzaee and Sartaj (2021) demonstrated the use of magnetic powder and granular activated carbons (MPACs and MGACs) for the removal of PAHs from aqueous solutions [153]. The PAH removal efficiency of MGAC synthesized by co-precipitation (MGAC-Cop) was obtained at 98.3%, and this MGAC was selected for the current research to be used in conjunction with the surfactant-enhanced soil washing process. Although MPAC synthesized by the precipitation method also showed high removal percentage (99.3%), the findings from preliminary tests indicated much greater recovery of MGAC particles from the soil washing stage compared with MPAC particles (95% vs 67%). Moreover, the ionic and non-ionic surfactants, SDS and Tween 80, were used in the soil washing preliminary tests, and Tween 80 showed better performance in removing PAHs from soil. This surfactant has also been reported to be more environmentally friendly and cost-effective than SDS [61,205,206]. Hence, Tween 80 was selected for remediation of a real PAH-contaminated soil. The recovery and reuse of MGAC by a regeneration method or just simple washing was another objective of this work. To the best of the authors' knowledge, there is no similar study employing a combined surfactant-magnetic adsorbent system for remediation of PAH-contaminated soil.

6.3 Experimental

6.3.1 Materials

The Tween 80 surfactant (density: 1.064 g/cm^3; critical micelle concentration (CMC): 0.012 mM) was purchased from VWR (Radnor, PA, USA). Granular activated carbon with particle sizes mostly in the range of 250-850 µm was supplied by Calgon Carbon (Pittsburgh, PA, USA). The iron precursors, Iron (II) Sulfate Heptahydrate ($FeSO_4 \cdot 7H_2O$) and Iron (III) nitrate nonahydrate ($Fe(NO_3)_3 \cdot 9H_2O$), used for the synthesis of the MGAC composite were obtained from Sigma-Aldrich (St. Louis, USA). The PAH standard solutions containing LMW PAHs: phenanthrene (PHE), acenaphthene (ACE), anthracene (ANT), and fluorine (FLU), and HMW PAHs: pyrene (PYR), benzo(a)pyrene (B[a]P), benzo[a]anthracene (B[a]A), benzo[ghi]perylene (B[ghi]P), fluoranthene (FLUO), benzo[b]fluoranthene (B[b]F), chrysene (CHR), benzo[k]fluoranthene (B[k]F), dibenz[a,h]anthracene (D[a,h]A), and indeno[1,2,3-c,d]pyrene (IDP) were purchased from AccuStandard (New Haven, CT, USA). HPLC-grade solvents such as acetonitrile, hexane, and acetone were provided from VWR (Radnor, PA, USA) for PAH analysis and soil extraction purposes. Sodium azide (NaN_3) and Potassium nitrate (KNO_3) used as the biological inhibitors were purchased from Sigma Aldrich (St. Louis, MO, USA).

6.3.2 MGAC synthesis

The MGAC (GAC/Fe_3O_4) composite was synthesized using a modified co-precipitation method [124]. Briefly, solutions of 1 M $Fe(NO_3)_3 \cdot 9H_2O$ and 0.1 M $FeSO_4 \cdot 7H_2O$ were prepared separately, and then, mixed with 350 mL deionized water inside a 500mL reaction vessel. On a magnetic stirrer, the mixture was aggressively stirred at 650 rpm for 10 min, and the agitation was supplemented with nitrogen bubbling to prevent ferrous ion oxidation. After that, 2 g GAC was added to the mixture as the magnetic composite base, and the agitation was continued for another 10 min. Finally, 35 mL of 1M NaOH solution was added dropwise to the reaction vessel to enable the magnetic composite to precipitate. The reaction vessel was then taken from the stirrer and the black precipitated particles were separated from the supernatant. To eliminate impurities and neutralize the pH of the prepared magnetic composite, the MGAC particles were rinsed three times

6.3.3 MGAC characterization

The surface area of GAC and the synthesized MGAC was determined by Brunauer-Emmet-Teller (BET)-N_2 adsorption using the Micromeritics Accelerated Surface Area & Porosimetry technique

(2020) (GA, USA). The pore size distribution of GAC and MGAC was measured using the Barrett-Joyner-Hanlenda (BJH) technique at 77.3 K. To characterize the surface morphology of the bare and magnetic adsorbents, a small amount of each sample (<10 mg) was placed on a carbon-coated grid, and then, analyzed by a field emission scanning electron microscope (FE-SEM, JSM-7500F, JEOL, USA) [155]. A Nicolet 6700 Fourier transform infrared (FTIR) spectrometer (Thermo Fischer, USA) was used to collect the MGAC FTIR spectra before and after PAHs adsorption. The FTIR spectra were recorded at a pressure of 150 kg/cm^2 and in the wavenumber range of 4500–400 cm^{-1}, with 32 scans per spectrum at a resolution of 4 cm^{-1}.

6.3.4 Preparation of the mixed PAHs working solutions

In order to evaluate the PAH adsorption capacity of MGAC using the adsorption isotherms experiments, a series of PAH working solutions were prepared according to method TO-13A [207]. For this purpose, a 500 µg/mL PAH standard solution (1mL) was diluted in a 5 mL volumetric flask using acetonitrile to obtain a final PAH concentration of 100 µg/mL. The diluted solution was then serially diluted with acetonitrile in separate volumetric flasks and used to provide the PAH working solutions with concentrations ranging from 0.5 to 10 µg/mL. Before the adsorption isotherm tests, all of the PAH solutions were agitated on an orbital shaker for 1 h to ensure that they were sufficiently homogenized.

6.3.5 PAHs adsorption experiments

The adsorption isotherms experiments were carried out by loading 125 mL conical flasks with 30 mL deionized water and different amounts of PAHs to obtain final PAH concentrations of 0.5-10 µg/mL. Potassium nitrate (1 g/L) and sodium azide (0.2 g/L) were added to the flasks to prevent the potential growth of microorganisms, followed by homogenizing the solutions on the orbital shaker at 50 rpm for 0.5 h. Then, 30 mg of the magnetic composite (MGAC-CoP) was applied to each sample, and the solutions were shaken at 100 rpm and 20°C until the PAH adsorption reached equilibrium (24 h) [137,141,153,157]. Prior to analysis, the MGAC particles were separated from the flasks using a magnetic bar. The solutions were extracted with methylene chloride by hand shaking and stirring on a vortex mixer for 2 min [193]. The methylene chloride containing residual PAHs were then separated from the solution by centrifugation at 7000 rpm for 3 min and using a pipette. The extraction process was repeated three times and all the extracts were combined, and subsequently, concentrated into 2-4 mL in acetonitrile for HPLC analysis [127]. The adsorption

tests were conducted in duplicate, and control samples without the addition of MGAC were run in parallel to estimate the recoveries of PAH compounds from the solutions [141].

The following equation was used to calculate the amounts of PAHs sorbed onto the magnetic composite at equilibrium:

$$q_e = \frac{(C_0 - C_e)V}{M} \quad (6.1)$$

Where q_e (µg/mg) represents the PAHs adsorption capacity of MGAC-CoP, and C_0 and Ce (µg/mL) are the initial and final concentrations of PAHs in the solutions, respectively. V describes the solution quantity (mL) and M is the mass of the magnetic composite (mg) added to each solution [137,158].

The PAHs adsorption isotherms of MGAC-CoP were investigated by fitting the Dubinin–Radushkevich and Redlich-Peterson isotherm models to the experimental adsorption data. The Dubinin–Radushkevich (D-R) isotherm model was employed to determine the type of adsorption mechanism that occurred during the treatment process [208]. The D–R model takes into account the impact of the porous structure of the adsorbent on the adsorption process and correlates the contaminant adsorption to pore volume filling rather than layer-by-layer adsorption on the pore wall [209]. This model describes the characteristic porosity and mean free energy of adsorption using the following equations:

$$q_e = q_m . \exp(-K_{ad}(RT . \ln\left(1 + \frac{1}{C_e}\right))^2 \quad (6.2)$$

$$E = \sqrt{(\frac{1}{-2K_{ad}})} \quad (6.3)$$

where qe shows the adsorption capacity of MGAC-CoP at equilibrium, q_m is the theoretical maximum adsorption capacity of the MGAC composite (µg/mg); K_{ad} is the D-R constant associated with the mean adsorption energy (kJ/mol); R is the universal gas constant (J/mol.K), T is the temperature (K), and E represents the mean adsorption energy (kJ/mol) [208].

Equation 6.3 is used to assess the type of adsorption process, which can be physical or chemical. To do this, the model determines the mean free energy of adsorption per molecule of adsorbate in solution as it is transferred from infinity to the adsorbent surface. When the E value lies between 1 and 8 kJ/mol, the adsorption behaviour is physical, and when E is over this value, it means that the adsorption is chemical [158].

Redlich-Peterson (R-P) is an empirical isotherm model consisting of three parameters that incorporates the features of the Langmuir and Freundlich isotherm models into a single model.

The R-P model represents the adsorption equilibrium over a wide concentration range and can be utilized for both homogeneous and heterogeneous adsorption surfaces[157]. This isotherm model is expressed using the following equation:

$$q_e = \frac{K_{RP} C_e}{1 + \propto_{RP} C_e^{\beta}} \qquad (6.4)$$

where K_{RP} and α_{RP} are the adsorption capacity and isotherm constants of the R-P model, and β is the exponent factor which ranges from 0 and 1. When β=1, the R-P model equation changes to the Langmuir equation, and when this parameter equals 0, the R-P equation becomes Henry's Law equation [157,210–212]. A value of β between 0 and 1 indicates that the adsorption process is favorable. In the case of K_{RP} and α_{RP}, they suggest an approximation of the Freundlich model when their values are far above 1 [157,211].

6.3.6 PAHs solubilization

Batch solubilization experiments with solutions containing 1 µg/mL PAHs and various doses of Tween 80 (0.5-5% v/v) were conducted to determine the maximum solubility of PAHs in the surfactant solution [60,208]. The quantity of the solutions and doses of Tween 80 were the same as in the soil washing tests for the sake of comparison. After adding potassium nitrate and sodium azide to the samples, they were sealed and mixed on the orbital shaker at 150 rpm for 24 h. The solutions were then extracted by methylene chloride on the vortex mixer [193], and the solvent was condensed to a more compatible HPLC solvent, acetonitrile. 25 µL of the extracts were injected into HPLC to measure the concentration of residual PAHs in the solutions. The solubilization rate was obtained by plotting the PAH solubility (%) versus the surfactant doses [61].

6.3.7 Surfactant (Tween 80)-enhanced soil washing combined with adsorption by MGAC

As the first phase, a series of soil washing experiments were performed to investigate the effects of different parameters on the removal of PAHs using Tween 80-enhanced soil washing. The soil samples were collected from an abandoned industrial site in Canada containing residues of coal and ash. The soil samples were air-dried, and then, passed through a 0.425 mm sieve to remove coarse particles and debris [120]. The pH of the soil samples was found to be 8.3 due to the industrial activities in the contaminated site. The soil contained 36.7% gravel, 58% sand, 4% silt, and 1.3% clay, and 4% soil organic matter (ASTM D2487-06), indicating a sandy soil with silt and low organic matter content. The critical washing parameters were examined in the following

order: washing time (3, 10, 24, and 72 h), liquid to soil ratio (5:1, 10:1, and 15:1), temperature (4 °C and 20 °C), and Tween 80 dose (0, 1, 2, and 5% v/v). For each set of tests, one parameter was examined at different values, while the others were maintained constant. The optimal value achieved was used in subsequent tests to optimize the remaining parameters. The first set of tests was carried out with different time periods, a Tween 80 dose of 2% (v/v), an L/S ratio of 10:1, and a temperature of 20 °C. In 125 mL conical flasks, the 2% Tween 80 was added to 30 mL deionized water and the solution was homogenized for half an hour. The biological inhibitors were added to the solutions, followed by placing 3g of the contaminated soil in each flask. The flasks were covered with aluminum foils, and subsequently, agitated at 150 rpm on the shaker for certain time periods.

To evaluate the feasibility of the surfactant solution recycling, the MGAC composite (2%, w/w) was added to the samples after 24 h, and the agitation was continued for another 48 h. After shaking, the flasks were set aside for a few minutes to allow the soil particles to settle. Then, the surfactant solutions were separated from the treated soils and poured into centrifuge tubes, followed by centrifuging at 7000 rpm for 8 min. The soil residue in the centrifuge tubes and the soil in the flasks were air-dried and then combined. The MGAC particles were separated from the dried soils using a magnetic bar and rinsed with distilled water to remove the fine soil particles. The treated soil was extracted using 1/1 (v/v) acetone/hexane in an ultrasonic bath for 10 min according to method 3045, USEPA [127]. The soil extraction procedure was repeated three times for each sample, and the extracts were then mixed and concentrated into acetonitrile for analysis purposes [59,60,72]. All the soil washing experiments were performed in triplicate and the parallel control samples were also tested without the addition of Tween 80 and MGAC.

The adsorption of Tween 80 onto soil particles was measured using DR6000 UV-VIS Laboratory Spectrophotometer (HACH, Canada). For this reason, 10 mL of the Tween 80 solution was tested in the spectrophotometer at a wavelength of 282 nm after each washing cycle. The adsorbed portion of the surfactant solution was determined based on the difference between the acquired concentration and the concentration of the solution in the previous washing cycle.

6.3.8 PAH measurement

The supernatants extract containing PAHs in methylene chloride or acetone/hexane (1/1 v/v) were exchanged to acetonitrile according to method 8310 [127]. After filtration with 0.45 µm PTFE filter, 25 µL of the PAH extracts were injected into the High-Pressure Liquid Chromatography

(HPLC, Hewlett–Packard 1100, Agilent Technologies, USA) instrument equipped with a reverse phase HPLC column (ZORBAX Eclipse PAH, 95Å, 4.6×250mm×5µm). The calibration samples for the HPLC analysis were prepared at concentrations ranging from 0.5 to 100 µg/mL. The mobile phase for the HPLC chromatography column was determined as 95/5 (v/v) acetonitrile and deionized water with a flow rate of 0.6 mL/min. The PAHs in the HPLC column were detected using a multiple wavelength detector (MWD, Agilent Technologies, USA) at the wavelengths of 210.8, 224.4, 230, 8, 254.4, and 270.9 nm.

6.4 Results and discussion

6.4.1 Characterization of GAC and MGAC-CoP

According to the BET technique, the surface area of the MGAC-CoP composite was measured at 837.9 m^2/g, which was nearly 12% less than the GAC surface area (949.5 m^2/g). The total pore volume and micropore volume of MGAC were obtained as 0.53 and 0.26 cm^3/g, respectively, whereas these were 0.58 and 0.29 cm^3/g for the bare GAC. The difference in surface area and total pore volume between MGAC and GAC was due to the blocking of the GAC pores by iron and oxygen groups due to the magnetization process [141,155]. However, with regard to the results obtained in similar studies for GAC magnetization [39,68,84,155], these reductions (≈10%) would not negatively impact the MGAC adsorption capacity for the PAH compounds.

The nitrogen adsorption-desorption isotherm of the MGAC composite is illustrated in Figure 6.1a. The isotherm has the shape of a type I isotherm with an H4 hysteresis loop that appeared at the relative pressure (P/P0) of 0.4–1.0. This type of isotherm is regarded by the IUPAC classification for adsorbents with a significant number of mesopores, micropores, and macropores in their matrices [141,190]. The pore-filling phenomenon occurs without capillary condensation in the low relative pressure region (Figure 6.1a). After filling the micropores, adsorption continues on the external surface of the adsorbent. However, at the high relative pressures, the majority of the adsorption sites are occupied, lowering the sorption capacity of the adsorbent [213,214]. The type H4 hysteresis loop is tied to the type I isotherm, as shown in Figure 6.1a, indicating the presence of micropores in the MGAC matrix [171,213,215].

The pore size distribution of the prepared MGAC composite was presented in Figure 6.1b. The shape of the graph reflects the fraction of the total pore volume in MGAC that is accessible to the PAHs molecules. MGAC has an average pore size of approximately 5.5 nm, with some micropores

and the greatest peaks falling between 0.4 and 3 nm in the pore size distribution (Figure 6.1b). The average diameter of a Tween 80 micelle, on the other hand, was estimated to be around 7 nm [216], and the average width and length of the PAH compounds were in the range 0.85-1.05 nm and 0.92-1.18 nm, respectively [217,218]. It means that the Tween 80 micelles were unable to penetrate the MGAC micropores, whereas the majority of the PAHs could be adsorbed by the MGAC micropores during the treatment process [208].

a)

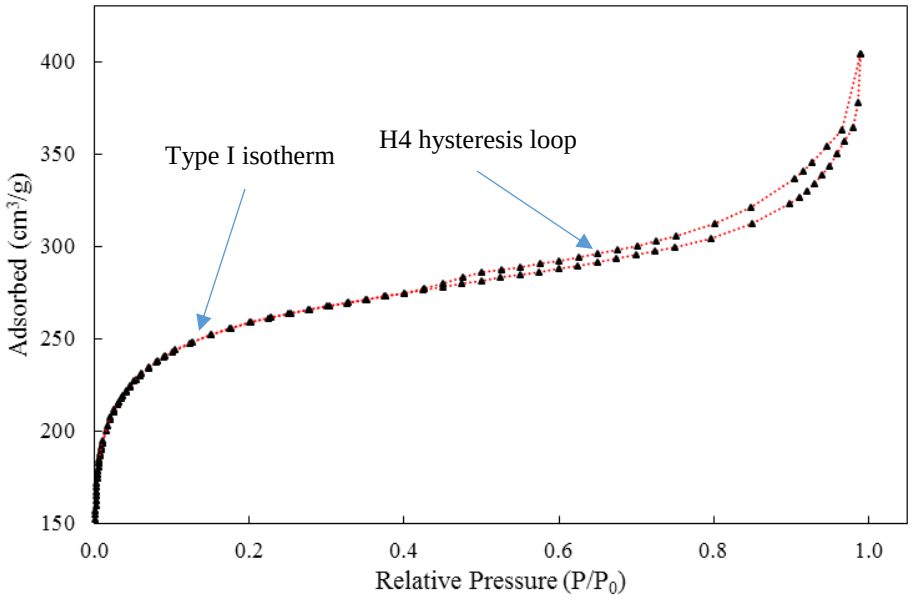

b)

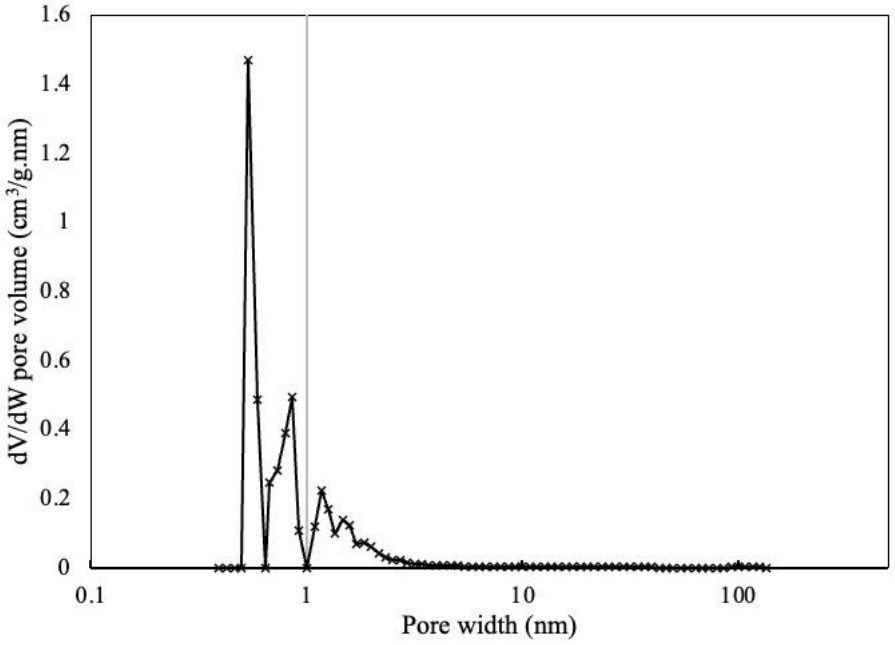

c) GAC MGAC-CoP

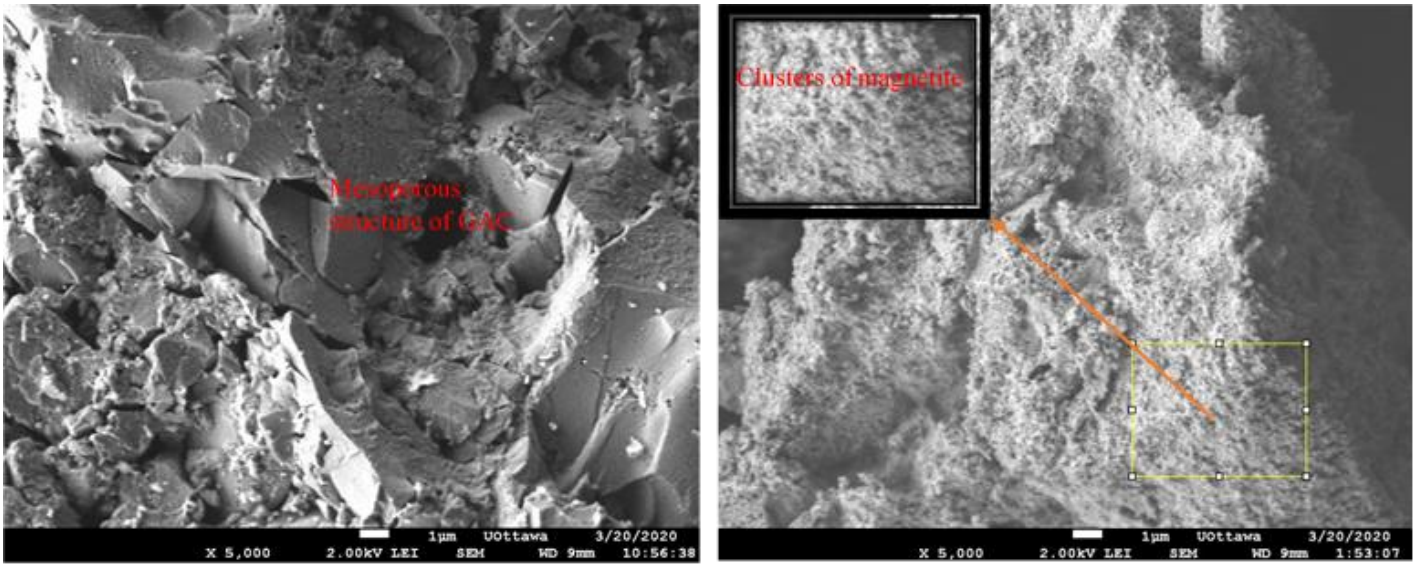

d)

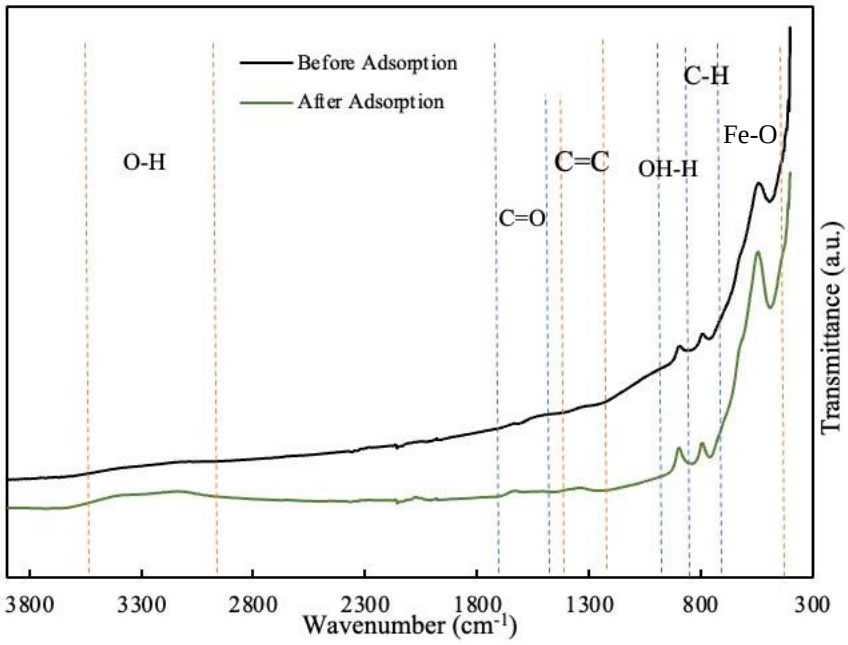

Figure 6.1. (a) N_2 adsorption-desorption isotherm (b) pore size distribution (c) and FE-SEM images of MGAC-CoP (d) FTIR spectra of MGAC-CoP before and after PAHs adsorption

Figure 6.1c illustrates the morphological properties of GAC and MGAC obtained using the FE-SEM instrument. The SEM image of GAC indicates that it was a porous adsorbent with an irregular shape, while the image for MGAC clearly shows that the clusters of iron oxide particles covered

the porous surface of AC. The Fe_3O_4 nanoparticles were evenly dispersed in a form of spongy crust across the GAC matrix, providing the adsorbent with appropriate superparamagnetic properties [99,219]. The SEM image of the MGAC composite was also analyzed using the ImageJ software, of which the length of the nanoparticles we found to be in the range 5-25 nm.

Figure 6.1d presents the FTIR analysis results for the MGAC composite before and after the PAHs adsorption. The sharp peaks emerged at 492 and 525 cm^{-1} in the MGAC spectrum before adsorption as well as the peaks centered at 482 cm^{-1} and 536 cm^{-1} in the PAH-loaded MGAC spectrum are correspondent to stretching vibration of Fe-O band in the magnetite nanoparticles of MGAC [29]. The medium peak centered at 785 cm^{-1} in the spectrum of the pure MGAC shifted to 804 cm^{-1} after the PAHs adsorption, which is attributed to the deformation out of plane of the C-H bond in the PAHs molecules. The other medium peak located at 903 cm^{-1} in the spectrum of the pure MGAC shifted to 887 cm^{-1} after PAHs adsorption, which can be associated with the stretching vibration of bonding of the MGAC hydroxyl groups and PAHs hydrogen [52,70,130,153]. The spectrum of MGAC after the PAHs adsorption shows some weak signals emerged at 1360 and 1640 cm^{-1}, which can be assigned to the stretching vibration of C=C and C=O bonds in the carboxylic groups (O=C−O) of MGAC. Also, the two broad bands that appeared at 3160 and 3340 cm^{-1} in the spectrum of PAH-loaded MGAC may be related to the stretching vibration of hydroxyl–OH groups of MGAC after PAHs adsorption [132,153]. All of these changes observed in the spectrum of MGAC after the adsorption tests are evidence of the formation of physical bonds (van der Waals forces) between PAHs and MGAC.

6.4.2 PAHs adsorption isotherms

The experimental data obtained from the PAHs adsorption tests were fitted with the R-P and D-R isotherm models using a non-linear regression method (SOLVER, Microsoft Excel). As can be seen from Table 6.1, the range of correlation coefficient (R^2) of the D-R model for most of the PAHs were relatively higher than those calculated by the R-P model, except for ACE, FLU, and PHE. The same condition has been observed for the calculated root mean square error (RMSE), with lower values for D-R model compared with R-P (Table 6.1), indicating that D-R fits the experimental data better than the R-P model.

According to the D-R model, the maximum adsorption capacity of MGAC for the LMW PAHs (ACE, FLU, PHE, and ANT) was greater than the HMW PAHs. It implies that the MGAC had a stronger affinity for the LMW PAHs. The maximum PAHs adsorption capacity values obtained

for MGAC were lower than those reported by Inbaraj et al. (2021) for B[b]F, B[a]P, CHR, and B[a]A (28.08, 22.75, 19.14, and 15.86 µg/mg) using magnetic AC, and Zhang et al. (2019) for PHE (74.6 µg/mg) using carbon nanotubes. Despite the higher adsorption capacity of the carbonaceous adsorbents, the researchers did not provide any information on the efficiency of the employed adsorbents for other USEPA priority PAHs. Eeshwarasinghe et al. (2019) reported a maximum adsorption capacity of 2.63 µg/mg for ACE and 7.36 µg/mg for PHE using GAC. Valderrama et al. (2008) used GAC to remove NAP, ACE, FLU, ANT, PYR, and FLUO from aqueous solutions. According to their isotherm modeling results, the maximum adsorption capacities of GAC for the six PAHs were as 0.14, 0.11, 0.15, 0.23, 0.11, and 0.09 µg/mg, respectively. Although the two latter studies used the bare GAC, which has a larger adsorption capacity than MGAC, their estimated maximum adsorption capacities of GAC for PAHs were significantly lower than those determined in this study (Table 6.1).

Table 6.1. Evaluation of the PAHs adsorption isotherms using the D-R and R-P isotherm models

	Dubinin–Radushkevich (D-R)					Redlich-Peterson (R-P)				
PAH	q_{max} (µg/mg)	Kad (mol^2/kJ^2)	E (kJ/mol)	R^2	RMSE	K_{RP} (L/mg)	α_{RP} (L/mg)	β	R^2	RMSE
ACE	10.87	0.01	6.98	0.66	2.15	0.26	0.026	1.19	0.80	1.64
FLU	10.11	0.01	8.98	0.81	1.58	0.58	0.062	1.06	0.85	1.40
PHE	8.54	0.05	3.30	0.83	1.30	0.02	0.002	1.24	0.86	1.20
ANT	8.29	0.06	2.80	0.91	0.93	0.02	0.002	0.94	0.90	0.98
FLUO	6.19	0.02	5.47	0.77	1.28	0.34	0.064	0.84	0.76	1.31
PYR	7.96	0.12	2.04	0.87	1.05	0.03	0.004	0.64	0.68	1.65
B[a]A	7.15	0.36	1.19	0.84	1.02	0.79	0.272	0.43	0.73	1.33
CHR	7.94	0.56	0.95	0.82	1.14	0.44	0.178	0.30	0.67	1.53
B[b]F	8.16	0.54	0.96	0.82	1.14	0.46	0.181	0.29	0.68	1.55
B[k]F	8.15	0.37	1.16	0.87	0.99	0.36	0.113	0.38	0.75	1.37
B[a]P	7.65	0.15	1.85	0.87	1.01	0.04	0.009	0.54	0.85	1.09
B[ghi]P	8.93	0.54	0.96	0.78	1.35	0.11	0.039	0.22	0.65	1.71
IDP	8.74	0.32	1.24	0.89	0.96	0.02	0.005	0.37	0.78	1.34
D[a,h]A	8.40	0.36	1.18	0.87	1.00	0.23	0.069	0.36	0.75	1.39

Table 6.1 also shows that the mean energy sorption (E) of PAHs calculated using Equation 6.3 fell in the range of 1 kJ/mol and 8 kJ/mol, suggesting that the adsorption of PAHs was physical adsorption [158]. Besides, the majority of the PAHs had a β value between 0 and 1 according to

the R-P isotherm model, which indicates that the adsorption process was favourable. For all HMW PAHs, the β values ranged from 0.22 to 0.84, while these values for LMW PAHs were estimated to be nearly 1 (0.94-1.24), showing that the R-P model was approaching the ideal Langmuir model [209,212]. Furthermore, K_{RP} and α_{RP} values were found to be lower than 1, implying that the adsorption process did not exhibit the characteristics of the Freundlich model. As a result, the MGAC surface could be considered homogeneous, and the adsorption sites were distributed uniformly on the adsorbent surface[190,211].

6.4.3 PAHs solubilization

The relationship between PAHs solubility and Tween 80 dosage is shown in Figure 6.2. The initial concentration of each PAH compound in the solution was set at 1 µg/mL. As it is apparent from the figure, increasing the surfactant dose resulted in an increase in the solubility of both LMW and HMW PAHs and hence the total PAHs in a nonlinear pattern. The total solubility of the LMW PAHs (ACE, FLU, PHE, and ACN) was raised from 0.05 to 1.14 µg/mL after the Tween 80 dose was increased from 1% to 5% (v/v). The solubility of the HMW PAHs, likewise, increased from 1.38 µg/mL to 4.85 µg/mL. Ahn et al. (2008) investigated the efficiency of soil washing using four different surfactants (Tween 40, Tween 80, Brij 30, and Brij 35) for removal of PHE from the soil, as well as the PHE adsorption by GAC during the surfactant recovery process. According to their findings, Brij 30 (2 g/L) had the highest PHE solubilizing capacity (84.1%) and the lowest adsorption to the soil particles (11%) compared to the other surfactants. However, the PHE adsorption onto GAC in the Brij 30 recovery process was only 33.9%, while the highest efficiency for GAC was obtained during the Tween 80 recovery with 56.4% PHE uptake (Ahn et al., 2008). Surfactant recycling is only considered successful if the adsorbent eliminates a significant amount of contaminants from the surfactant solution; otherwise, the solution is processed as wastewater [61]. In the present work, the MGAC-CoP composite was employed in soil washing to remove the PAHs from the surfactant solutions and clean them up before they were reused.

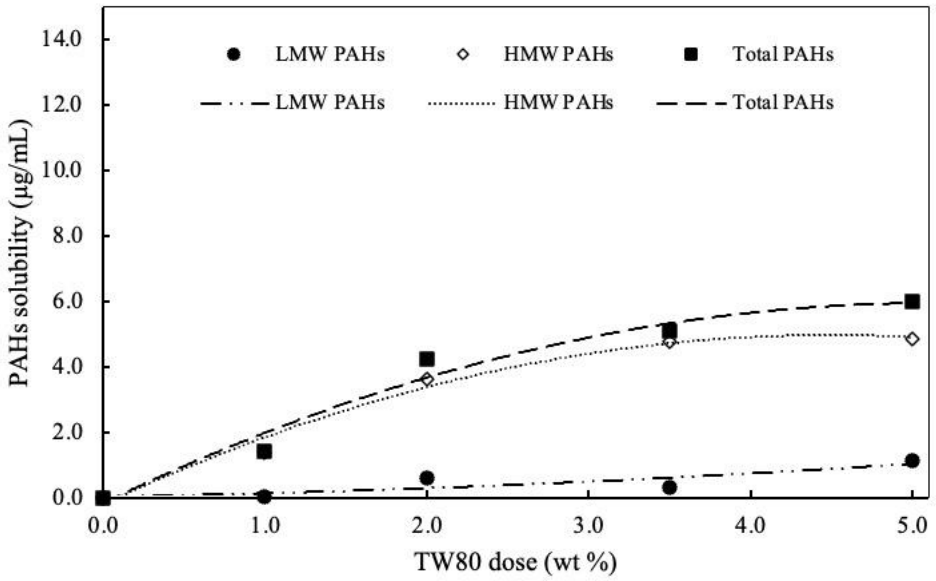

Figure 6.2. Solubility of the LMW, HMW, and total PAHs in surfactant solution at different doses of Tween 80

6.5 Soil washing tests with Tween 80

6.5.1 Washing time

A series of soil washing tests were performed at different washing periods (6-72 h), 2 % (v/v) Tween 80, stirring speed of 150 rpm, and temperature of 20 ˚C. Figure 6.3a demonstrates that the PAHs removal rate rapidly increased from 13.1% to 42.9% when the soil washing time was increased from 6 h and 24 h. The maximum PAHs removal rate was obtained 56.6% after the 72h washing period, which was relatively higher than the result of the first 24 h. One speculative explanation for the faster PAH removal during the first 24 h of washing can be faster desorption of PAHs from the coarse soil particles and uptake of residual fractions of PAHs trapped in the soil pores [59,60]. Furthermore, as shown in Figure 6.3b, c, and d, the 3-ring PAHs (LMW PAHs) were removed from the soil more quickly than the higher molecular weight PAHs, with removal percentages ranging from 55.4% (PHE) to 83.6% (FLU). According to Figure 6.3c, the removal efficiencies for the 4-ring HMW PAHs fell in the range 47.9-70.4% after 72 h, with FLUO having the greatest rate. In the case of the 5- and 6-ring PAHs, however, the PAH removal efficiency was attained between 36.6% (b[B]f) and 53.5% (B[k]F) for the same washing period (Figure 6.3d), indicating that the HMW PAHs were more strongly bonded to soil particles, and therefore, they

might need more time to desorb. Based on the above findings, the 72 h washing period was taken as the optimum for the next soil washing tests.

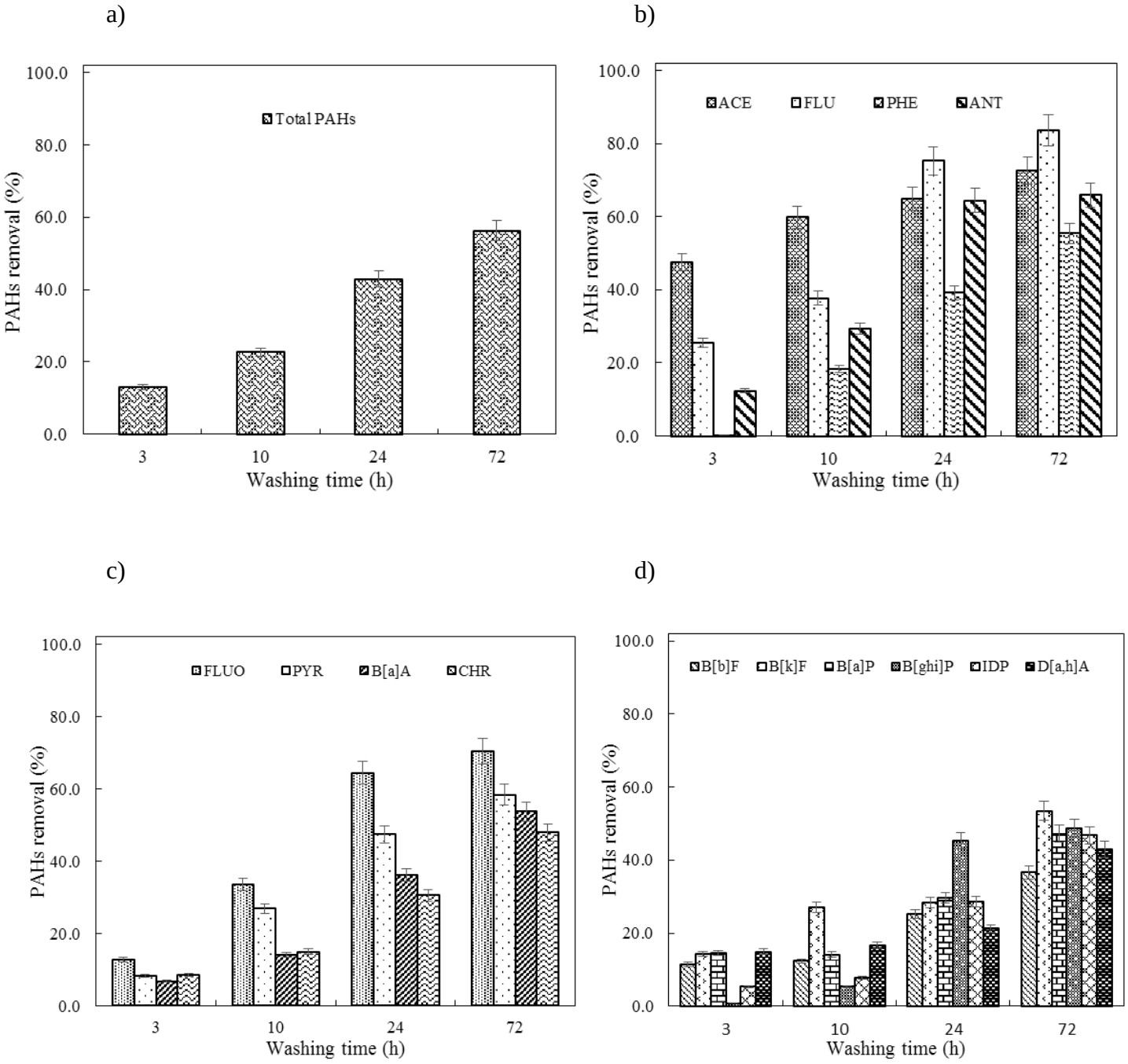

Figure 6.3. PAHs removal rates at different washing periods; (a) total PAHs, (b) 3-ring LMW PAHs, (c) 4-ring HMW PAHs, (d) and 5-and 6-ring HMW PAHs

6.5.2 Liquid:soil ratio

The surfactant solution to soil ratio (L:S) is another key element in the soil washing process. To study the effect of surfactant solution volume on PAHs removal, different ratios of liquid to soil were examined in the soil washing tests for 72 h. As shown in Figure 6.4a, the shift in L:S from 5:1 to 10:1 resulted in a significant increase in the total PAHs removal from 39.9% to 55.4%. However, further increase in the L:S from 10:1 to 15:1 led to a minor decline in the surfactant solution ability to remove the total PAHs. One possible reason is that the number of micelles generated in the surfactant solution with L:S of 15:1 was lower than the effective critical micelle concentration (CMC) required for PAH removal from the soil [220]. The formation of a sufficient amount of micelles in the surfactant solution would solubilize higher amounts of PAH compounds and increase their removal from the soil particles [205,221]. In this study, the effective CMC was formed in the L:S of 10:1, resulting in the greatest removal of total PAHs from the soil using 2% Tween 80 (Figure 6.4a). This trend can also be seen in Figure 6.4c and d, where the largest quantities of 4- ring PAHs and 5- and 6-ring PAHs were desorbed from the soil at the L:S of 10:1. For LMW PAHs (Figure 6.4b), the trend was different (except for FLU), as the greatest removal efficiency was gained at L:S of 15:1, with the lowest removal for PHE (66.7%) and the highest removal for ACE (100 %). However, because of the priority of HMW PAHs, the L:S of 10:1 was selected as the optimal value for the soil washing experiments. Furthermore, greater L/S ratios necessitate more water use in a large-scale project, resulting in higher expenditures for providing required equipment and energy as well as more effluents for post-treatment. As a result, the L:S of 10:1 appeared to be the best option in this case [60].

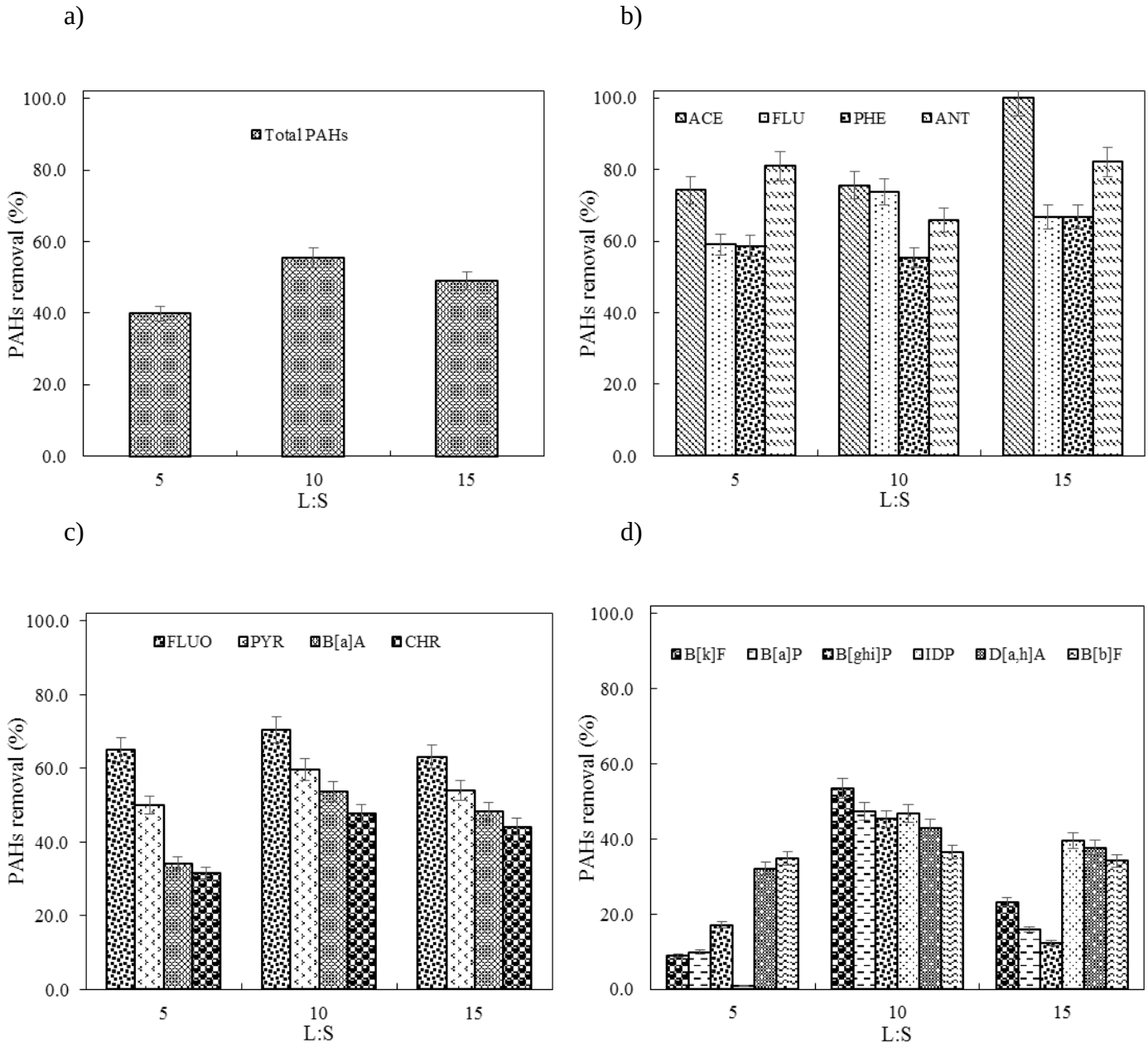

Figure 6.4. PAHs removal efficiencies at the different liquid to soil ratios; (a) total PAHs, (b) 3-ring LMW PAHs, (c) 4-ring HMW PAHs, (d) and 5-and 6-ring HMW PAHs

6.5.3 Temperature

The influence of temperature on PAH removal performance of Tween 80 was investigated by running tests at 4 and 20˚ C with 2% Tween 80, L:S of 10:1, stirring speed of 150 rpm, and washing time of 72 h. As presented in Figure 6.5a, the total PAHs removal efficiency decreased significantly from 55.3% to 35.7% after the temperature was reduced to 4 ˚C. The observation of

Figure 6.5b, c, and d reveal how the low temperature had an adverse effect on the removal of the LMW, 4-ring HMW, and 5- and 6-ring HMW PAHs throughout the 72h soil washing procedure. Among the LMW PAHs (Figure 6.5b), the removal of ANT fell dramatically from 65.9% to 25.6% after the temperature reduction. In contrast, the ACE removal efficiency was only reduced by 3.5% at 4˚ C, indicating that the removal of the lightest PAH component was less sensitive to the temperature change. According to Figure 6.5c, all the 4-ring HMW PAHs showed a similar trend, with an average reduction of about 20% after the temperature reached 4˚ C. The PAHs removal efficiency of soil washing decreased the most at the cold temperature for 5- and 6-ring PAHs as demonstrated in Figure 6.5d. At 20 ˚C, the removal percentages for B[b]F, B[k]F, B[a]P, B[ghi]P, IDP, and D[a,h]A were 36.6, 53.5, 47.2, 45.3, 46.8, and 43.0%, respectively. These values plummeted to 27.1, 25.8, 23.9, 18.8, 18.5, and 23.7%, respectively, after the temperature was reduced to 4 ˚C, showing a 22.4% decline in Tween 80 removal performance for these compounds. The remarkable changes in the PAHs removal as a function of temperature indicated that the desorption and dissolution of PAHs in Tween 80-enhanced soil washing were temperature-dependent, and hence the treatment process was endothermic [60]. The effect of temperature on removal of organic contaminants from soil using soil washing has also been reported in the literature [205,222,223]. Kuyukina et al. (2005) indicated that the efficiency of Tween 60 in soil washing for removal of crude oil was 40% lower at 15 ˚C than it was at 28 ˚C [205,223]. In another study, Urum et al. (2004) employed sodium dodecyl sulfate (SDS) surfactant in the soil washing process to clean-up soil contaminated with crude oil. Their findings demonstrated that crude oil removal from soil at temperatures over 20 ˚C was significantly higher than at 5 ˚C. The researchers concluded that raising the temperature will decrease crude oil viscosity, and increase the oil mobility and interaction with the surfactant micelles [222].

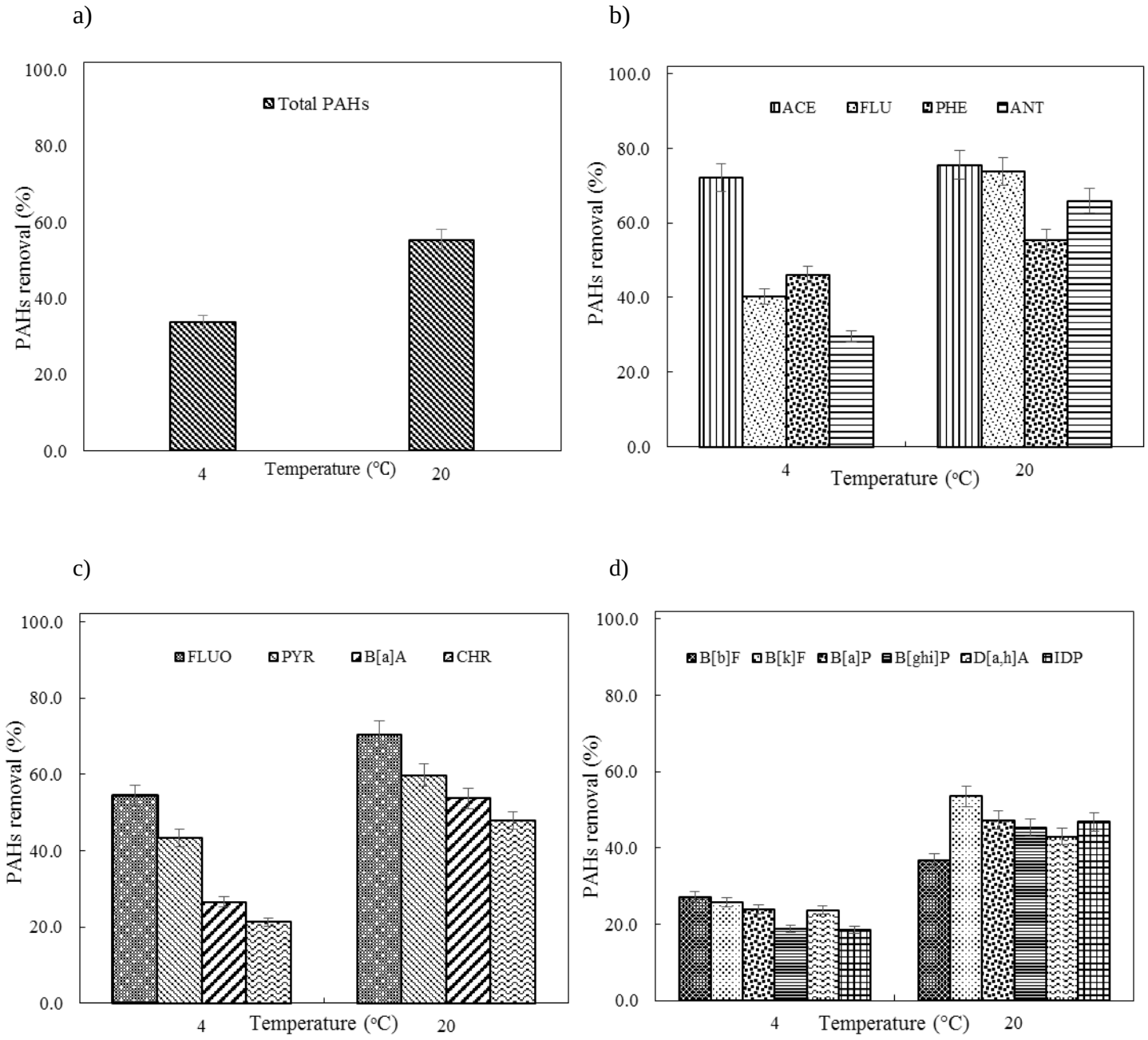

Figure 6.5. PAHs removal efficiencies of soil washing at different temperatures; (a) total PAHs, (b) 3-ring LMW PAHs, (c) 4-ring HMW PAHs, (d) and 5-and 6-ring HMW PAHs

6.5.4 Surfactant dosage

In the following set of tests, varying surfactant doses (0.5 to 5%, v/v) were utilized in soil washing, while other parameters with optimal values remained constant. The results showed that the rise in the Tween 80 dosage had a significant impact on the PAHs removal from the soil. As shown in Figure 6.6a, the total PAHs removal rose dramatically from 20.3 to 67.6% after increasing the dose

of Tween 80 to 5%. The detailed results obtained for the LMW and HMW PAHs were presented in Figure 6.6b, c, and d. Among the LMW PAHs (Figure 6.6b), FLU showed the highest affinity to the Tween 80 with 100% desorption from the soil at the surfactant dose of 5%. More than 80% of ANT and ACE were also removed from the soil when the Tween 80 dose was risen to 5%. PHE was the only LWM PAH that did not demonstrate significant desorption from the soil at high Tween 80 doses (59.8% removal at 5% Tween 80). The amounts of 4-ring PAHs (including FLUO,

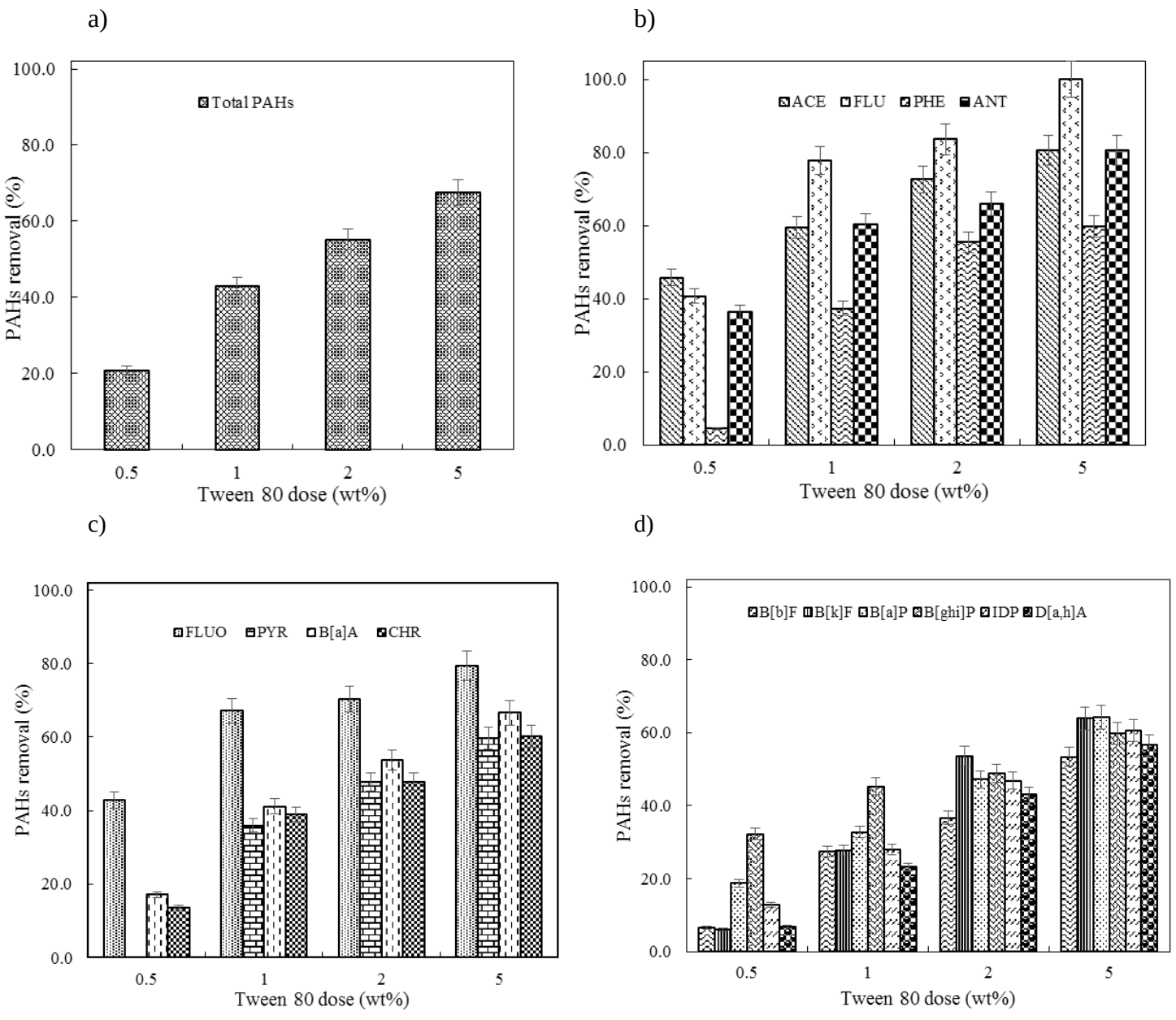

Figure 6.6. The effect of the Tween dose on the removal of (a) total PAHs, (b) 3-ring LMW PAHs, (c) 4-ring HMW PAHs, (d) and 5-and 6-ring HMW PAHs

PYR, B[a]A, and CHR) removed from soil at 5% surfactant were slightly lower than the LMW PAHs (Figure 6.6c), with PYR having the lowest removal (59.8%) and FLUO having the highest removal (79.3%). As can be observed from Figure 6.6c and d, the increase in the number of aromatic rings resulted in a decrease in the PAH removal efficiency of the surfactant. For the 5- and 6-ring PAH compounds, the removal percentages varied from 53.4% for B[b]F to 64.2% for B[a]P, which could be explained by the distribution coefficient equation as follows [91]:

$$K_d = F_{oc} \times K_{oc} \quad (6.6)$$

where K_d describes the amount of sorbed PAH in its aqueous phase equilibrium, F_{oc} is the organic carbon fraction of soil, and K_{oc} is the soil organic carbon-water partition coefficient. HMW PAHs have a larger K_{oc} value than LMW PAHs indicating a greater affinity to soil particles [91]. In other words, the values of K_{oc} and K_d go up with the increase in the number of aromatic rings, signifying the formation of stronger bonds between the PAH molecule and soil particles. As a result, extraction of the HMW PAHs from soil would be more difficult for the surfactant solution compared to the LMW PAHs [59,91,197].

6.6 Soil washing with Tween 80 and MGAC

To investigate the possibility of recycling the Tween 80 solution, MGAC composite was employed in the soil washing process to extract PAHs from the solution and clean it up for more soil washing cycles. For this purpose, a series of soil washing experiments were carried out according to the washing procedure discussed in section 6.3.7, and the 2% (w/w) MGAC composite was added to each sample after 24 h to remove the desorbed PAHs from the washing solutions. The reason for incorporating the magnetic adsorbents into the samples after 24 h was to provide the surfactant solution with sufficient time to separate PAHs from the soil. To control the residual PAHs concentration in the Tween 80 solution after treatment, one sample of the solution was extracted (section 6.3.8) and the extracts were analyzed using HPLC. The analysis result revealed that 86.3% LMW PAHs and 94.7% HMW PAHs (accounting for 92.3% of the total PAHs) were eliminated from the surfactant solution either by dissolution or adsorption.

With regard to the PAHs solubilization and PAHs adsorption isotherms results, the magnetic adsorbent was shown to be capable of adsorbing the majority of residual PAHs from the surfactant solution during soil washing, indicating that the solution could be used for additional washing procedures. To reuse the MGAC composite, it was regenerated with acetone: hexane (1:1 v/v) [127] or just rinsed with deionized water (no-regeneration). The regenerated/non-regenerated

MGAC was then dried overnight (80 ˚C) and stored in sealed vials before being used in subsequent washing processes. As presented in Figure 6.7a, Tween 80 treated with regenerated MGAC during the process removed 53.7, 52.8, 51.1, 46.8, and 43.4% of the PAHs from the soils in the five consecutive washing cycles. The results for soil washing cycles with the Tween80 and non-regenerated MGAC were determined as 54.4, 53.9, 55.6, 49.0, and 45.8%, which were totally 2.5% higher than those with the recycled Tween80 and regenerated MGAC. One tentative explanation for this difference is the adverse impact of regenerating the MGAC particles with the solvents, which could reduce the number of active adsorption sites onto MGAC due to saturation with the solvent molecules.

Besides the better results obtained with the non-regenerated MGAC, the solvents used in the regeneration process would produce waste, which was another reason for selecting the non-regenerated MGAC as the ideal adsorbent for Tween 80 cleanup in soil washing. In addition, as the tests results for optimal values of the soil washing parameters showed, the use of 5% (v/v) Tween 80 in the treatment procedure yielded the highest PAH removal from the soil. Hence, this dose of Tween 80 along with 2% (w/w) MGAC, being added after 24 h, were employed in the soil washing process and could remove 68.6% of the total PAHs from soil, as shown in Figure 6.7b. The reuse of the surfactant solution (5%) and non-regenerated magnetic adsorbent (2%) were examined in 6 consecutive cycles, leading to the elimination of 70.7, 70.3, 61.6, 55.5, 50.2, and 39.4% of PAHs from the soil samples, respectively (Figure 6.7b). The decrease in PAH removal efficiency after the third washing cycle could be due to the PAH uptake by MGAC approaching the saturation level. These results were significantly greater than the PAHs removal efficiencies obtained by 2% Tween 80 and non-regenerated/regenerated MGAC (Figure 6.7a). Furthermore, after five times reuse in the soil washing process, the recycled 5% Tween 80 and non-regenerated MGAC were able to remove more than 50% PAHs from soils without producing any waste or effluent. This implies that soil washing with Tween 80 and MGAC is a very affordable, efficient, and practical method for PAH-contaminated soil remediation.

The constant partitioning between soil particles and the Tween 80 solution appears to be the primary strategy for desorption of PAHs from soil [60]. The MGAC composite did not contribute significantly to the PAH removal from soil particles due to the difficulty in adsorption of the PAHs which were strongly bonded to the soil. Moreover, since the surfactant was able to desorb and mobilize the majority of PAHs during the first 24 hours (Figure 6.7), the addition of MGAC had

no specific effect on the separation of these PAHs from the soil particles. However, the magnetic composite successfully adsorbed most of PAHs from the Tween 80 solution during the washing process, resulting in a clean solution that could be used in subsequent washing cycles.

a)

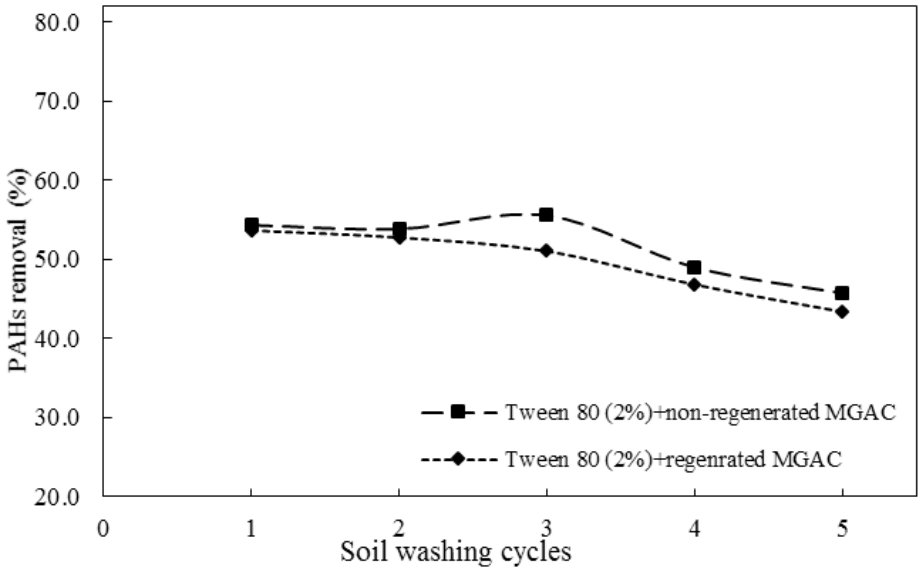

b)

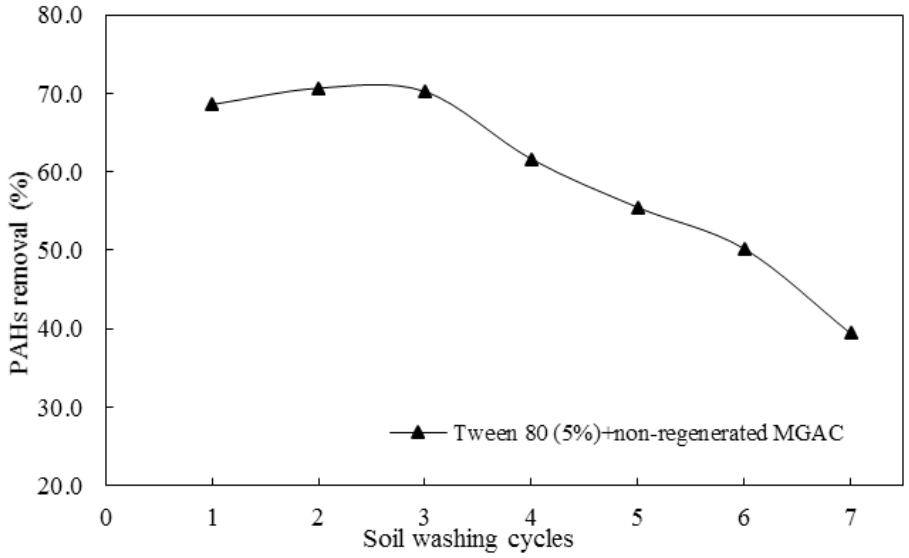

Figure 6.7. (a) The use of Tween 80 (2% v/v) in combination with regenerated/non-regenerated MGAC (2% w/w) in five successive soil washing cycles, (b) the use of Tween 80 (5% v/v) with non-regenerated MGAC (2% w/w) in seven successive soil washing cycles

The Tween 80 adsorption onto the soil was measured at the end of each cycle according to the procedure described in section 6.3.7 (Spectrophotometer), and the results indicated a reduction in the concentration of the surfactant solution ranging from 5% to 10%. An equivalent dose of Tween 80 was added to the solution before the next washing cycle to compensate for the reduced concentration.

A separate surfactant recovery process requires additional equipment and facilities, and their relevant costs could be a potential issue for large-scale projects. Besides, a surfactant recovery is operationally successful only if the adsorbent removes the majority of the contaminants from the surfactant, otherwise, the recovery process will be ineffective, and the amount of effluent to be treated will increase [61,208]. In this study, almost 70% of the LMW and HMW PAHs were successfully removed from the soil using the Tween 80-enhanced soil washing combined with adsorption by MGAC. The amount of soil organic matter in the examined soil of this study was low (4%), and therefore, its adverse impact on the Tween 80 efficiency and PAHs adsorption by MGAC was not significant [224,225]. Another factor that could affect the performance of MGAC in the soil slurry is a reduction in the number of the MGAC adsorption sites due to the pore-clogging by fine soil particles. The more the amount of clay particles in soil, the lower the adsorbent capacity is for removal of contaminant from the solution [61]. The percentage of fine particles in the soil studied was 5%, indicating that the soil is mostly comprised of coarse particles. As a result, the effect of soil particle size on PAH adsorption was minor.

6.7 Conclusions

The performance of surfactant enhanced-soil washing combined with adsorption was investigated using Tween 80 and a recoverable magnetic granular activated carbon (MGAC-CoP) to clean up a real PAH-contaminated soil. The Dubinin–Radushkevich isotherm model revealed that the MGAC composite had a high affinity for PAHs, with maximum adsorption capacities ranging from 8.3 to 10.9 µg/mL for LMW PAHs and 6.2 to 8.9 µg/mL for HMW PAHs. According to the PAHs solubilization results, the solubility of the analytes increased as the dosage of Tween 80 solution increased. The Tween 80 surfactant showed high efficiency to transfer PAHs from soil to liquid phase, while its adsorption onto the soil particles was not significant.

The soil washing experiments using Tween 80 indicated that 67.6% of the total PAHs were removed from the contaminated soil investigated in this research and under the optimal conditions (washing time of 72 h, L:S of 10:1, Tween dose of 5% (w/w), and temperature of 20˚C). The

possibility of recycling the Tween 80 solution was assessed by adding the MGAC composite to the soil washing process. Because the non-regenerated MGAC sorbed PAHs more efficiently than the regenerated MGAC, it was selected for the successive washing cycles with 5% Tween 80. The 5% Tween 80 solution, recycled with MGAC, was able to remove almost 70% of the PAHs in the first three washing cycles, and more than 50% of PAHs in the next three washing cycles. The number of PAH rings, the age of the contaminated soil, and the bonding of PAHs with fine soil particles and organic matter could all influence the PAH removal efficacy of Tween 80 in the soil washing process. The findings of this study suggest that soil washing with tween-80 and MGAC is an efficient method for the removal of PAHs from soils with a high portion of coarse particles. However, further studies are needed to explore the efficiency of this technique for the contaminated soils which mostly consist of fine particles.

6.8 References

This chapter's references are integrated with the references from the other chapters and provided at the end of the thesis.

7 Synthesis, Integration and General Discussion of Results

The USEPA, CCME, and other environmental protection agencies and organization have categorized polycyclic aromatic hydrocarbons (PAHs) as one of the most hazardous groups of petroleum hydrocarbons released into the environment. In the present work, the removal of PAHs from contaminated water and soil was investigated using magnetic powder activated carbon (MPAC) and magnetic granular activated carbon (MGAC) as recoverable adsorbents. The magnetic adsorbents were prepared via the precipitation, co-precipitation, and impregnation methods in the first phase of the work, and then characterized and evaluated (Chapter 3). A series of adsorption experiments was subsequently conducted in the second phase (Chapter 4) to investigate the PAH removal efficiency of the prepared magnetic activated carbons (MACs) in more details through comprehensive adsorption kinetics and isotherm studies of the MAC with the highest PAHs removal efficiency (MPAC). In the third phase (Chapter 5), the application of MGAC in a series of soil washing tests was investigated. The major goal of this phase was to determine the role of effective washing parameters in the remediation of a PAH-contaminated soil. These included the adsorbent dosage, liquid to soil ratio, stirring speed, washing time, pH, and temperature. In the fourth and last phase, the MGAC composite was used in conjunction with a surfactant (Tween 80) to enhance the soil washing performance for PAH removal from soil (Chapter 6). The feasibility of recycling the surfactant and recovery and reuse of MGAC composite was assessed as well. The main findings of this work are integrated and presented below.

7.1 The effect of synthesis methods on PAH adsorption capacity of MACs

The MPAC and MGAC composites were synthesized and then characterized by BET, XRD, FE-SEM, and FTIR methods. According to the BET data, the surface area of MPAC and MGAC was reduced by 65% and 12%, respectively, after magnetization. The XRD patterns confirmed the presence of Fe_3O_4 nanoparticles on surface of the magnetic adsorbents. The SEM images showed that the magnetic composites had spherical morphologies, with clusters of iron oxide nanoparticles dispersed throughout the PAC/GAC pores and surface. As seen in the FTIR spectra, the PAH analytes were sorbed onto MACs via π-π and H-π interactions formed between PAHs and the magnetic adsorbents. The six synthesized MACs were then used in a series of adsorption tests, and the results showed that all the magnetic composites were very effective in removing PAHs from aqueous phase with removal percentages ranging from 87.2% and 99.3%. Among them, the

MPAC prepared by the precipitation method and using powder AC as the supporting base showed the greatest PAHs removal efficiency (99.3%) in the aqueous solutions. Besides, the MGAC synthesized by the co-precipitation method and using granular AC as the base obtained the next highest PAHs removal (98.3%) efficiency.

The PAHs desorption tests indicated that the low molecular weight (LMW) PAHs were more easily desorbed from the magnetic composite surface (38.1-60.1%) compared with the high molecular weight (HMW) PAHs (23.4-57.2%). This indicated that the increase in the number of PAH rings would lead to the formation of stronger bonds between the adsorbate and the adsorbent, making desorption of these PAHs from the MAC surface more challenging.

7.2 Kinetics and adsorption isotherm studies of MPAC synthesized by the precipitation method for PAHs adsorption in aqueous solutions

The adsorption kinetics and isotherms of MPAC with the highest PAHs removal efficiency were thoroughly studied using a series of adsorption experiments. According to the kinetics data, the PAHs adsorption onto MPAC was relatively fast, reaching equilibrium in 6 h with adsorption rates ranging from 95.6 to 100.0 %. The pseudo-second order model was the best fit for the kinetics data ($0.83 \leq R^2 \leq 0.95$), suggesting that the adsorption rate relies on adsorption capacity, not on the concentration of the adsorbate and that the adsorption process was chemical. The results of the kinetic experiments also revealed that higher molecular weight PAHs had lower adsorption rates in the first hours of the experiments due to a slower transfer of these analytes to the accessible adsorption sites of MPAC. The Langmuir model described the experimental adsorption data well with an R^2 in the range of 0.73-0.96, therefore, implying the monolayer adsorption of PAHs onto the magnetic adsorbent. This model also showed that the MPAC particles had a maximum adsorption capacity ranging from 8.74 to 11.37 µg/mg for LMW PAHs, and 8.43 to 20.21 µg/mg for HMW PAHs, respectively.

7.3 The use of MGAC synthesized by the co-precipitation method in soil washing for the removal of PAHs from contaminated Soils

The application of soil washing combined with adsorption using MGAC (synthesized by the co-precipitation method) was studied for removal of PAHs from a real contaminated soil. According to the BET test results, the surface area and total pore volume of MGAC were determined to be 837.9 m^2/g and 0.5 cm^3/g, respectively, approximately 10% smaller than those for the bare GAC.

Modelling of the experimental data using different isotherm models indicated that Langmuir provided the best fit. Therefore, the monolayer adsorption was regarded to be predominant in the treatment process with MGAC. The maximum PAH adsorption capacity of MGAC in liquid phase was estimated to be 157.0 µg/mg for the total PAHs, which was nearly 18% lower than that of GAC (190.3 µg/mg), confirming the minor impact of the magnetization process on the MGAC adsorption capacity. For the soil washing tests, the PAH-contaminated soil sample was characterized as well-graded sand with silt (SW-SM) containing 4.14% soil organic matter content. The effects of various soil washing factors on PAHs removal with MGAC were investigated in a series of soil washing experiments and summarized below.

7.3.1 MGAC dose

The first set of soil washing tests was conducted at different doses of MGAC (0 to 5% w/w). Raising MGAC dose to 5% w/w resulted in a considerable increase in the percentage of LMW PAHs removed from soil. The total PAH adsorption by 2% and 5% (w/w) MGAC in the soil washing process was determined to be 26.5% and 29.5%, respectively. With regard to the small difference in the PAHs removal efficiency, the 2% MGAC was selected as the optimal MGAC dose for the next experiments.

7.3.2 Liquid:soil ratio

Different liquid to soil ratios (L:S) from 5:1 to 20:1 was assessed for the PAHs removal with MGAC (2% w/w) in the second set of the experiments. The results showed that the increase in the liquid volume could facilitate the removal of PAHs from the soil using MGAC by providing greater accessibility of the MGAC particles to the analytes. The L/S ratio of 15:1 and 20:1 could remove 46.5% and 47.5% of the total PAHs from the soil, respectively. To avoid producing more effluent and since there is a slight difference in PAHs removal efficiency of L:S of 20:1 and 15:1, the L:S of 15:1 was taken as the optimal ratio for the next soil washing experiments.

7.3.3 Stirring speed

The soil samples were washed at shaker speeds of 75, 100, 125, and 150 rpm, with the 100 rpm speed showing the highest PAH removal (47.5%). The further increase in the stirring speed caused the soil slurry to move in bulk formation with limited movement (due to the disintegration of soil clumps) and consequently lower PAHs removal from the soil.

7.3.4 Washing time

The assessment of the soil washing period (6-168 h) showed an upward pattern for removal of PAHs by MGAC as the time increased from 6 to 24 h. However, further increase in the washing period to 72 h resulted in a 5% reduction in the PAHs removal, which was followed by a steady rate until 168 h. Based on this finding, it was concluded that the 24 h washing period was more practical, and therefore, was selected as the optimal time for the next experiments.

7.3.5 pH

The natural pH of the soil was determined to be 8.3, which could be attributed to the industrial activities in the contaminated site. When the pH was reduced to 7.0, the PAHs removal efficiency significantly dropped from 47.4 to 27.1% for the soil washing with MGAC. The same tendency was observed when the pH was raised to 10.0, with the reduction in the PAHs removal from 47.4% to 28.3%. These reductions were probably due to the hydrolysis of the magnetite nanoparticles under neutral (pH 7) or alkaline (pH 10) conditions, leading to the formation of iron (II) hydroxide ($Fe(OH)_2$) precipitate on the surface, and therefore, the adsorption sites of MGAC.

7.3.6. Temperature

Lowering the temperature from 25 ˚C to 5 ˚C reduced the PAHs removal efficiency from 47.4% to 33.8%. As a result, the removal efficiency of the treatment procedure may be affected to some extent if it is applied to the PAH-contaminated soils in cold weather. Thermodynamic studies confirmed that the adsorption of PAHs onto MGAC was non-spontaneous ($\Delta G^{\circ}>0$) and endothermic ($\Delta H^{\circ}>0$).

The six key soil washing parameters were optimized as an MGAC dose of 2% (w/w), washing time of 24 h, liquid to soil ratio of 15:1, stirring speed of 100 rpm, pH of 8.3, and temperature of 25 ˚C, removing 47.4% of PAHs from the soil. Among the PAHs, the LMW ANT and HMW FLUO showed the greatest affinity to MGAC during the treatment process, with 57.7% and 67.1% removal from the soil, respectively.

7.4 The application of surfactant-enhanced soil washing for remediation of PAH-contaminated soil and the role of MGAC in the surfactant solution recycling

A surfactant-enhanced soil washing process combined with adsorption using the MGAC composite was employed to remove PAHs from a real contaminated soil sample. Also, the

feasibility of recycling the surfactant (Tween 80) was explored to reduce volume of the soil washing effluent and operational costs. The PAHs solubility in the Tween 80 solution was examined at different doses of the surfactant (1- 5% v/v), and the results indicated that the LMW and HMW PAHs were more soluble at higher doses of the Tween 80 solution. The total PAHs solubility at 5% Tween 80 was measured at nearly 40%, with the majority of PAHs remaining non-dissolved in the surfactant solution. This confirmed the need for treatment of the solution before reuse.

According to the surfactant adsorption tests, up to 19% of the Tween 80 concentration could be sorbed onto the soil particles during the remediation process, implying that most portion of the surfactant is retrievable from the soil. The effective parameters of soil washing with Tween 80 were also evaluated, including washing period, liquid/soil ratio, temperature, and Tween 80 dosage.

7.4.1 Washing period

Different soil washing periods (6-72 h) were examined in the soil washing tests using 2 % (v/v) Tween 80 at stirring speed of 150 rpm and temperature of 20 ˚C. It was observed that the increase in the washing time from 6 h and 24 h elevated the PAHs removal rate from 13.1% to 42.9%. The maximum efficiency for the remediation process was determined to be 56.6% after the 72h washing period. Thus, this period was selected as the optimum to allow the surfactant solution to remove more strongly bound PAHs from the soil.

7.4.2 Liquid: soil

Changing L:S from 5:1 to 10:1 led to a significant increase in the total PAHs removal from 39.9% to 55.4%. However, a further increase in L:S from 10:1 to 15:1 slightly declined the surfactant ability to remove the total PAHs from the soil. The formation of an insufficient amounts of micelles in the surfactant solution with L:S of 15:1 was the main reason for its lower PAHs removal efficiency than the L:S of 10:1.

7.4.3 Temperature

The removal of total PAHs from soil was reduced from 55.3 % to 35.7 % after lowering the temperature from 20 to 4 ° C. The reduction in PAHs removal efficiency was greater for the 5- and 6-ring HMW PAHs (22.4%) than the 3- ring LMW PAHs (20.7%). These findings implied that

the desorption of PAHs from soil in the Tween 80-enhanced soil washing was temperature-dependent.

7.4.4 Tween 80 dosage

Increasing the Tween 80 dose from 0.5% to 5% significantly improved the PAHs removal from soil by 47.3% (from 20.3 to 67.6%). It was also observed that the increase in the number of aromatic rings resulted in a decrease in the PAH removal efficiency of the surfactant due to the formation of stronger bonds between the PAH molecule and soil particles. Therefore, extraction of the HMW PAHs from soil was more difficult for the surfactant solution compared to the LMW PAHs.

7.4.5 Soil washing with TW80 and MGAC

To investigate the possibility of recycling Tween 80, MGAC was employed in the surfactant-enhanced soil washing process (after 24 h) to extract PAHs from the Tween 80 solution. The MGAC composite was either regenerated with solvents (acetone: hexane) or simply rinsed with deionized water (no-regeneration) to be reused in the next washing cycles. According to the results, the soil washing with 2% (v/v) Tween 80 and 2% (w/w) MGAC was able to remove 54.4% of PAHs from the solutions. In the next four washing cycles, the recycled Tween 80 with the non-regenerated MGAC eliminated 53.9, 55.6, 49.0, and 45.8% PAHs from the soil, which were totally 8.5% higher than those with the recycled Tween80 and regenerated MGAC.

The no-regeneration method was therefore selected to clean up MGAC before it was utilised in the successive washing cycles with the optimal 5% Tween 80. The surfactant solution could remove nearly 70% of PAHs from the soil samples in each of the first three cycles and more than 50% of PAHs in the next three successive washing cycles, respectively, without producing any waste or effluent. This indicated that the Tween 80 solution had been successfully recycled in soil washing with non-regenerated MGAC, and the magnetic composite successfully extracted most of the PAHs from the Tween 80 solution. The MGAC composite, however, did not contribute significantly to the PAH removal from soil due to the difficulty in adsorption of the PAHs, which were strongly bonded to the soil.

8 Conclusions and Recommendations for Future Work

8.1 Conclusions

In this research, six different magnetic granular and powder activate carbons (MPAC and MGAC) were synthesized to assess their affinity for USEPA priority polycyclic aromatic hydrocarbons (PAHs) in aqueous solutions and in a combined soil washing process. Two of the magnetised ACs (MPAC-Prec. and MGAC-CoPrec.) outperformed the others in removing PAHs from the aqueous phase, and therefore, were selected for removal of PAHs from aqueous phase and soil washing experiments, respectively. Tween 80 surfactant was used in the last phase in conjunction with MGAC in soil washing process to enhance PAHs removal from a real contaminated soil. Under the conditions tested and the type of soil used in this study, the following conclusions can be drawn from this research:

- The presence of magnetite nanoparticles on the MACs surface was confirmed by XRD, SEM, and EDS.
- BET N_2-adsorption tests indicated that the surface area of the synthesized MPAC and MGAC composites decreased 65% and 12%, respectively, compared with bare AC.
- The electron-donor and electron-acceptor interactions (π-π interactions) were the main adsorption mechanism formed between the PAHs molecules and MPAC adsorption sites, according to the FTIR test results.
- All the prepared MACs could effectively remove the PAH compounds from water with an efficiency ranging from 87.2% to 99.3%. The obtained PAH removal efficiency was a function of PAH concentration and mass of the magnetic adsorbent in in the samples.
- The MPAC composite synthesized by the precipitation method showed the highest PAH-removal efficiency from the aqueous solutions.
- Among the adsorption isotherm models, the Langmuir model fitted the experimental isotherm data the best, suggesting the monolayer adsorption of PAHs onto MPAC and MGAC.
- The pseudo-second order model showed the best fit to the kinetics data, implying that all the MPAC adsorption sites had an equal affinity for the PAHs molecules.
- The results of PAHs desorption tests indicated that full recovery of the PAH compounds from the MACs is unlikely.

- The optimized scenario for the soil washing with MGAC was: 2% MGAC (w/w), L:S of 15:1, stirring speed of 100 rpm, washing time of 24 h, pH of 8.3 and temperature of 25 ˚C, resulting in the removal of 47.4% total PAHs from a real contaminated soil sample.
- According to the thermodynamic studies, the PAH adsorption onto MGAC was endothermic and non-spontaneous. The type of PAHs adsorption by MGAC in the soil washing process was also determined to be physical adsorption.
- The Tween 80 surfactant was found to have a high efficiency in transferring PAHs from the soil to the liquid phase, while its adsorption to the soil particles was not significant.
- Nearly 70% of the total PAHs were removed from soil under the optimal condition, which included a washing time of 72 h, an L:S of 10:1, a Tween dose of 5% (w/w), and a temperature of 20˚C.
- In the soil washing cycles with 2% Tween 80, the non-regenerated MGAC sorbed PAHs from the surfactant solution more efficiently compared with the regenerated MGAC, probably due to saturation of some of the regenerated MGAC adsorption sites with the solvent molecules.
- The 5% Tween 80 solution, recycled with the non-regenerated MGAC, removed 70% of the PAHs in the first three washing cycles and more than 50% PAHs in the six consecutive washing cycles.

8.2 Recommendations for future work

The future works may involve investigation of the following topics:

- The assessment of other synthesis methods and their effects on the PAH removal efficiency of MACs
- The use of other characterization methods such as XPS for better understanding the mechanism of PAHs adsorption by MACs in water and soil.
- The exploration of effective regeneration techniques for MACs in order to recycle them for more treatment processes.
- The efficiency of MPAC/MGAC for remediation of soil with high proportion of fine particles.
- The effect of soil organic matter content on the PAHs removal efficiency of MACs. It is hypothesized that PAHs have high affinity to sorb to organic content of the soil, and thus, adversely affect the efficiency of soil washing solution during remediation.

- The impact of soil organic matter (SOM) content and its effect on the desorption of PAHs and their removal in soil washing and MAC combined process.
- The use of other types of or combination of surfactants (ionic or nonionic) with MACs in soil washing.
- The application of surfactant-enhanced soil washing combined with adsorption for removal of other types of organic contaminants from soil.

References

[1] C. Moeckel, K. Breivik, T.H. Nøst, A. Sankoh, K.C. Jones, A. Sweetman, Soil pollution at a major West African E-waste recycling site: Contamination pathways and implications for potential mitigation strategies, Environ. Int. 137 (2020). https://doi.org/10.1016/j.envint.2020.105563.

[2] F. Topuz, T. Uyar, Cyclodextrin-functionalized mesostructured silica nanoparticles for removal of polycyclic aromatic hydrocarbons, J. Colloid Interface Sci. 497 (2017) 233–241. https://doi.org/10.1016/j.jcis.2017.03.015.

[3] Y. Song, G. Fang, C. Zhu, F. Zhu, S. Wu, N. Chen, T. Wu, Y. Wang, J. Gao, D. Zhou, Zero-valent iron activated persulfate remediation of polycyclic aromatic hydrocarbon-contaminated soils: An in situ pilot-scale study, Chem. Eng. J. 355 (2019) 65–75. https://doi.org/10.1016/j.cej.2018.08.126.

[4] A.A. Akinpelu, M.E. Ali, M.R. Johan, R. Saidur, M.A. Qurban, T.A. Saleh, Polycyclic aromatic hydrocarbons extraction and removal from wastewater by carbon nanotubes: A review of the current technologies, challenges and prospects, Process Saf. Environ. Prot. 122 (2019) 68–82. https://doi.org/10.1016/j.psep.2018.11.006.

[5] K. Sayed, L. Baloo, N.K. Sharma, Bioremediation of total petroleum hydrocarbons (Tph) by bioaugmentation and biostimulation in water with floating oil spill containment booms as bioreactor basin, Int. J. Environ. Res. Public Health. 18 (2021) 1–27. https://doi.org/10.3390/ijerph18052226.

[6] M.C. Chang, H.Y. Shu, W.P. Hsieh, M.C. Wang, Using nanoscale zero-valent iron for the remediation of polycyclic aromatic hydrocarbons contaminated soil, J. Air Waste Manag. Assoc. 55 (2005) 1200–1207. https://doi.org/10.1080/10473289.2005.10464703.

[7] M. Meskar, Treatment of Petroleum Contaminated Soil Using Supercritical Fluid Extraction (SFE) Technology, (2017) 1–80.

[8] USEPA, National Priorities List (NPL) Sites - by State, Superfund, (2021). https://www.epa.gov/superfund/national-priorities-list-npl-sites-state.

[9] K.H. Tiedemann, Brownfield site rehabilitation: A Canadian perspective, WIT Trans. Ecol. Environ. 107 (2008) 15–23. https://doi.org/10.2495/BF080021.

[10] C. Di Dong, C.W. Chen, C.M. Hung, Synthesis of magnetic biochar from bamboo

biomass to activate persulfate for the removal of polycyclic aromatic hydrocarbons in marine sediments, Bioresour. Technol. 245 (2017) 188–195. https://doi.org/10.1016/j.biortech.2017.08.204.

[11] B. Desalegn, M. Megharaj, Z. Chen, R. Naidu, Green mango peel-nanozerovalent iron activated persulfate oxidation of petroleum hydrocarbons in oil sludge contaminated soil, Environ. Technol. Innov. 11 (2018) 142–152. https://doi.org/10.1016/j.eti.2018.05.007.

[12] M. Meskar, M. Sartaj, J.A.I. Sedano, Optimization of operational parameters of supercritical fluid extraction for PHCs removal from a contaminated sand using response surface methodology, J. Environ. Chem. Eng. 6 (2018) 3083–3094. https://doi.org/10.1016/j.jece.2018.04.048.

[13] I.C. Ossai, A. Ahmed, A. Hassan, F.S. Hamid, Remediation of soil and water contaminated with petroleum hydrocarbon: A review, Environ. Technol. Innov. 17 (2020) 100526. https://doi.org/10.1016/j.eti.2019.100526.

[14] CCME, Canadian soil quality guidelines for the protection of environmental and human health: Polycyclic aromatic hydrocarbons, Can. Environ. Qual. Guidel. (2010) 19.

[15] Treasury Board of Canada Secretariat, Contaminants and Media in Canada, (2018). https://www.tbs-sct.gc.ca/fcsi-rscf/cm-eng.aspx (accessed May 15, 2020).

[16] C.M.A. Iwegbue, G.O. Irerhievwie, G.O. Tesi, C. Olisah, G.E. Nwajei, B.S. Martincigh, Polycyclic aromatic hydrocarbons (PAHs) in surficial sediments from selected rivers in the western Niger Delta of Nigeria: Spatial distribution, sources, and ecological and human health risks, Mar. Pollut. Bull. 167 (2021) 112351. https://doi.org/10.1016/j.marpolbul.2021.112351.

[17] USEPA, Polycyclic Aromatic Hydrocarbons, 1986.

[18] D. Eeshwarasinghe, P. Loganathan, S. Vigneswaran, Simultaneous removal of polycyclic aromatic hydrocarbons and heavy metals from water using granular activated carbon, Chemosphere. 223 (2019) 616–627. https://doi.org/10.1016/j.chemosphere.2019.02.033.

[19] B. Han, A. Liu, J. Gong, Q. Li, X. He, J. Zhao, L. Zheng, Spatial distribution , source analysis , and ecological risk assessment of polycyclic aromatic hydrocarbons (PAHs) in the sediments from rivers emptying into Jiaozhou Bay , China, Mar. Pollut. Bull. 168 (2021) 112394. https://doi.org/10.1016/j.marpolbul.2021.112394.

[20] Z. Košnář, F. Mercl, P. Tlustoš, Ability of natural attenuation and phytoremediation using

maize (Zea mays L.) to decrease soil contents of polycyclic aromatic hydrocarbons (PAHs) derived from biomass fly ash in comparison with PAHs–spiked soil, Ecotoxicol. Environ. Saf. 153 (2018) 16–22. https://doi.org/10.1016/j.ecoenv.2018.01.049.

[21] O. Zitka, P. Babula, J. Sochor, M. Kummerova, O. Krystofova, V. Adam, L. Havel, M. Beklova, J. Hubalek, R. Kizek, Determination of eight polycyclic aromatic hydrocarbons and in pea plants (Pisum sativum L.) Extracts by high performance liquid chromatography with electrochemical detection, Int. J. Electrochem. Sci. 7 (2012) 908–927.

[22] E. Manoli, C. Samara, Polycyclic aromatic hydrocarbons in natural waters: Sources, occurrence and analysis, TrAC - Trends Anal. Chem. 18 (1999) 417–428. https://doi.org/10.1016/S0165-9936(99)00111-9.

[23] S. Lamichhane, K.C. Bal Krishna, R. Sarukkalige, Polycyclic aromatic hydrocarbons (PAHs) removal by sorption: A review, Chemosphere. 148 (2016) 336–353. https://doi.org/10.1016/j.chemosphere.2016.01.036.

[24] S.M. Yakout, A.A.M. Daifullah, S.A. El-Reefy, Adsorption of naphthalene, phenanthrene and pyrene from aqueous solution using low-cost activated carbon derived from agricultural wastes, Adsorpt. Sci. Technol. 31 (2013) 293–302. https://doi.org/10.1260/0263-6174.31.4.293.

[25] W. Shi, Y. Guo, G. Ning, C. Li, Y. Li, Y. Ren, O. Zhao, Z. Yang, Remediation of soil polluted with HMW-PAHs by alfalfa or brome in combination with fungi and starch, J. Hazard. Mater. 360 (2018) 115–121. https://doi.org/10.1016/j.jhazmat.2018.07.076.

[26] S. Alagić, B.S. Maluckov, V.B. Radojičić, How can plants manage polycyclic aromatic hydrocarbons? May these effects represent a useful tool for an effective soil remediation? A review, Clean Technol. Environ. Policy. 17 (2015) 597–614. https://doi.org/10.1007/s10098-014-0840-6.

[27] G. Anitescu, L.L. Tavlarides, Supercritical extraction of contaminants from soils and sediments, J. Supercrit. Fluids. 38 (2006) 167–180. https://doi.org/10.1016/j.supflu.2006.03.024.

[28] E. Lombi, R.E. Hamon, Remediation of Polluted Soils, Encycl. Soils Environ. 4 (2004) 379–385. https://doi.org/10.1016/B0-12-348530-4/00087-4.

[29] C.M. Hung, C.P. Huang, S.S. Lam, C.W. Chen, C. Di Dong, The removal of polycyclic aromatic hydrocarbons (PAHs) from marine sediments using persulfate over a nano-sized

iron composite of magnetite and carbon black activator, J. Environ. Chem. Eng. 8 (2020) 104440. https://doi.org/10.1016/j.jece.2020.104440.

[30] L.A. da Silva, S.M.S. Borges, P.N. Paulino, M.A. Fraga, S.T. de Oliva, S.G. Marchetti, M. do C. Rangel, Methylene blue oxidation over iron oxide supported on activated carbon derived from peanut hulls, Catal. Today. 289 (2017) 237–248. https://doi.org/10.1016/j.cattod.2016.11.036.

[31] G.L. Sullivan, R.M. Prigmore, P. Knight, A.R. Godfrey, Activated carbon biochar from municipal waste as a sorptive agent for the removal of polyaromatic hydrocarbons (PAHs), phenols and petroleum based compounds in contaminated liquids, J. Environ. Manage. 251 (2019) 109551. https://doi.org/10.1016/j.jenvman.2019.109551.

[32] K. Amstaetter, E. Eek, G. Cornelissen, Sorption of PAHs and PCBs to activated carbon: Coal versus biomass-based quality, Chemosphere. 87 (2012) 573–578. https://doi.org/10.1016/j.chemosphere.2012.01.007.

[33] S.E. Hale, M. Elmquist, R. Brändli, T. Hartnik, L. Jakob, T. Henriksen, D. Werner, G. Cornelissen, Activated carbon amendment to sequester PAHs in contaminated soil: A lysimeter field trial, Chemosphere. 87 (2012) 177–184. https://doi.org/10.1016/j.chemosphere.2011.12.015.

[34] L. Jakob, T. Hartnik, T. Henriksen, M. Elmquist, R.C. Brändli, S.E. Hale, G. Cornelissen, PAH-sequestration capacity of granular and powder activated carbon amendments in soil, and their effects on earthworms and plants, Chemosphere. 88 (2012) 699–705. https://doi.org/10.1016/j.chemosphere.2012.03.080.

[35] I. Hilber, T.D. Bucheli, Activated carbon amendment to remediate contaminated sediments and soils: A review, Glob. Nest J. 12 (2010) 305–317. https://doi.org/10.30955/gnj.000723.

[36] M. Kołtowski, I. Hilber, T.D. Bucheli, B. Charmas, J. Skubiszewska-Zięba, P. Oleszczuk, Activated biochars reduce the exposure of polycyclic aromatic hydrocarbons in industrially contaminated soils, Chem. Eng. J. 310 (2017) 33–40. https://doi.org/10.1016/j.cej.2016.10.065.

[37] E.M.L. Janssen, B.A. Beckingham, Biological Responses to Activated Carbon Amendments in SedimentRemediation.pdf, (2013). https://doi.org/10.1021/es401142e.

[38] Z. Han, B. Sani, J. Akkanen, S. Abel, I. Nybom, H.K. Karapanagioti, D. Werner, A

critical evaluation of magnetic activated carbon's potential for the remediation of sediment impacted by polycyclic aromatic hydrocarbons, J. Hazard. Mater. 286 (2015) 41–47. https://doi.org/10.1016/j.jhazmat.2014.12.030.

[39] M. Kalaruban, P. Loganathan, T.V. Nguyen, T. Nur, M.A. Hasan Johir, T.H. Nguyen, M.V. Trinh, S. Vigneswaran, Iron-impregnated granular activated carbon for arsenic removal: Application to practical column filters, J. Environ. Manage. 239 (2019) 235–243. https://doi.org/10.1016/j.jenvman.2019.03.053.

[40] E. Deliyanni, T.J. Bandosz, Importance of carbon surface chemistry in development of iron-carbon composite adsorbents for arsenate removal, J. Hazard. Mater. 186 (2011) 667–674. https://doi.org/10.1016/j.jhazmat.2010.11.055.

[41] M.H. Do, N.H. Phan, T.D. Nguyen, T.T.S. Pham, V.K. Nguyen, T.T.T. Vu, T.K.P. Nguyen, Activated carbon/Fe3O4 nanoparticle composite: Fabrication, methyl orange removal and regeneration by hydrogen peroxide, Chemosphere. 85 (2011) 1269–1276. https://doi.org/10.1016/j.chemosphere.2011.07.023.

[42] N. Yang, S. Zhu, D. Zhang, S. Xu, Synthesis and properties of magnetic Fe3O4-activated carbon nanocomposite particles for dye removal, Mater. Lett. 62 (2008) 645–647. https://doi.org/10.1016/j.matlet.2007.06.049.

[43] B. Kakavandi, A.J. Jafari, R.R. Kalantary, S. Nasseri, A. Ameri, A. Esrafily, Synthesis and properties of Fe3O4-activated carbon magnetic nanoparticles for removal of aniline from aqueous solution: Equilibrium, kinetic and thermodynamic studies, J. Environ. Heal. Sci. Eng. 10 (2013) 2–10.

[44] N. Jaafarzadeh, B. Kakavandi, A. Takdastan, R.R. Kalantary, M. Azizi, S. Jorfi, Powder activated carbon/Fe3O4 hybrid composite as a highly efficient heterogeneous catalyst for Fenton oxidation of tetracycline: Degradation mechanism and kinetic, RSC Adv. 5 (2015) 84718–84728. https://doi.org/10.1039/c5ra17953j.

[45] S. Zhang, H. Niu, Z. Hu, Y. Cai, Y. Shi, Preparation of carbon coated Fe3O4 nanoparticles and their application for solid-phase extraction of polycyclic aromatic hydrocarbons from environmental water samples, J. Chromatogr. A. 1217 (2010) 4757–4764. https://doi.org/10.1016/j.chroma.2010.05.035.

[46] Q. Han, Z. Wang, J. Xia, S. Chen, X. Zhang, M. Ding, Facile and tunable fabrication of Fe3O4/graphene oxide nanocomposites and their application in the magnetic solid-phase

extraction of polycyclic aromatic hydrocarbons from environmental water samples, Talanta. 101 (2012) 388–395. https://doi.org/10.1016/j.talanta.2012.09.046.

[47] S.S.M. Hassan, H.I. Abdel-Shafy, M.S.M. Mansour, Removal of pyrene and benzo(a)pyrene micropollutant from water via adsorption by green synthesized iron oxide nanoparticles, Adv. Nat. Sci. Nanosci. Nanotechnol. 9 (2018). https://doi.org/10.1088/2043-6254/aaa6f0.

[48] Y. Cao, B. Yang, Z. Song, H. Wang, F. He, X. Han, Wheat straw biochar amendments on the removal of polycyclic aromatic hydrocarbons (PAHs) in contaminated soil, Ecotoxicol. Environ. Saf. 130 (2016) 248–255. https://doi.org/10.1016/j.ecoenv.2016.04.033.

[49] H. Yi, D.E. Crowley, Biostimulation of PAH degradation with plants containing high concentrations of linoleic acid, Environ. Sci. Technol. 41 (2007) 4382–4388. https://doi.org/10.1021/es062397y.

[50] K. Kume, T. Ohura, T. Noda, T. Amagai, M. Fusaya, Seasonal and spatial trends of suspended-particle associated polycyclic aromatic hydrocarbons in urban Shizuoka, Japan, J. Hazard. Mater. 144 (2007) 513–521. https://doi.org/10.1016/j.jhazmat.2006.10.079.

[51] M. Koyano, S. Mineki, Y. Tsunoda, O. Endo, S. Goto, T. Ishii, Effects of fish (mackerel pike) broiling on polycyclic aromatic hydrocarbon contamination of suspended particulate matter in indoor air, J. Heal. Sci. 47 (2001) 452–459. https://doi.org/10.1248/jhs.47.452.

[52] A. Awoyemi, Understanding the Adsorption of Polycyclic Aromatic Hydrocarbons From Aqueous phase onto Activated Carbon, Master's Thesis, Dep. Chem. Eng. Appl. Chem. Univ. Toronto. (2011) 1–146. https://tspace.library.utoronto.ca/bitstream/1807/30169/6/Awoyemi_Ayodeji_O_201111_MASc_thesis.pdf.

[53] A.M. El-Mekawy, A.M.F. Mohammed, S.K.M. Hassan, A review of airborne polycyclic aromatic hydrocarbons (PAHs) and their, Egypt. J. Environ. Res. 25 (2016) 107–123.

[54] IARC, Polynuclear Aromatic Compounds, Part 1: Chemical, Environmental and Experimental Data., 1983.

[55] M. Funada, T. Nakano, H. Moriwaki, Removal of polycyclic aromatic hydrocarbons from soil using a composite material containing iron and activated carbon in the freeze-dried calcium alginate matrix: Novel soil cleanup technique, J. Hazard. Mater. 351 (2018) 232–

239. https://doi.org/10.1016/j.jhazmat.2018.02.054.

[56] L.D.C. Stamets, Best Mycorestoration Practices for Habitat Restoration of Small Land Parcels, Evergreen State College, 2013.

[57] W. Chen, H. Zhang, M. Zhang, X. Shen, X. Zhang, F. Wu, J. Hu, B. Wang, X. Wang, Removal of PAHs at high concentrations in a soil washing solution containing TX-100 via simultaneous sorption and biodegradation processes by immobilized degrading bacteria in PVA-SA hydrogel beads, J. Hazard. Mater. 410 (2021) 124533. https://doi.org/10.1016/j.jhazmat.2020.124533.

[58] S. Pourfadakari, M. Ahmadi, N. Jaafarzadeh, A. Takdastan, A.A. Neisi, S. Ghafari, S. Jorfi, Remediation of PAHs contaminated soil using a sequence of soil washing with biosurfactant produced by Pseudomonas aeruginosa strain PF2 and electrokinetic oxidation of desorbed solution, effect of electrode modification with Fe3O4 nanoparticles, J. Hazard. Mater. 379 (2019) 120839. https://doi.org/10.1016/j.jhazmat.2019.120839.

[59] X. Gan, Y. TENG, W. REN, J. MA, P. CHRISTIE, Y. LUO, Optimization of Ex-Situ Washing Removal of Polycyclic Aromatic Hydrocarbons from a Contaminated Soil Using Nano-Sulfonated Graphene, Pedosphere. 27 (2017) 527–536. https://doi.org/10.1016/S1002-0160(17)60348-5.

[60] S. Peng, W. Wu, J. Chen, Removal of PAHs with surfactant-enhanced soil washing: Influencing factors and removal effectiveness, Chemosphere. 82 (2011) 1173–1177. https://doi.org/10.1016/j.chemosphere.2010.11.076.

[61] C.K. Ahn, Y.M. Kim, S.H. Woo, J.M. Park, Soil washing using various nonionic surfactants and their recovery by selective adsorption with activated carbon, J. Hazard. Mater. 154 (2008) 153–160. https://doi.org/10.1016/j.jhazmat.2007.10.006.

[62] S.D. Khattri, M.K. Singh, Removal of malachite green from dye wastewater using neem sawdust by adsorption, J. Hazard. Mater. 167 (2009) 1089–1094. https://doi.org/10.1016/j.jhazmat.2009.01.101.

[63] A.V. Vitela-Rodriguez, J.R. Rangel-Mendez, Arsenic removal by modified activated carbons with iron hydro(oxide) nanoparticles, J. Environ. Manage. 114 (2013) 225–231. https://doi.org/10.1016/j.jenvman.2012.10.004.

[64] Z. Gu, J. Fang, B. Deng, Preparation and evaluation of GAC-based iron-containing adsorbents for arsenic removal, Environ. Sci. Technol. 39 (2005) 3833–3843.

https://doi.org/10.1021/es048179r.

[65] C.O. Ania, B. Cabal, C. Pevida, A. Arenillas, J.B. Parra, F. Rubiera, J.J. Pis, Effects of activated carbon properties on the adsorption of naphthalene from aqueous solutions, Appl. Surf. Sci. 253 (2007) 5741–5746. https://doi.org/10.1016/j.apsusc.2006.12.036.

[66] R.C. Brändli, T. Hartnik, T. Henriksen, G. Cornelissen, Sorption of native polyaromatic hydrocarbons (PAH) to black carbon and amended activated carbon in soil, Chemosphere. 73 (2008) 1805–1810. https://doi.org/10.1016/j.chemosphere.2008.08.034.

[67] C. Li, J. Lu, S. Li, Y. Tong, B. Ye, Synthesis of magnetic microspheres with sodium alginate and activated carbon for removal of methylene blue, Materials (Basel). 10 (2017). https://doi.org/10.3390/ma10010084.

[68] C.S. Castro, M.C. Guerreiro, M. Gonçalves, L.C.A. Oliveira, A.S. Anastácio, Activated carbon/iron oxide composites for the removal of atrazine from aqueous medium, J. Hazard. Mater. 164 (2009) 609–614. https://doi.org/10.1016/j.jhazmat.2008.08.066.

[69] A.M. Cooper, K.D. Hristovski, T. Möller, P. Westerhoff, P. Sylvester, The effect of carbon type on arsenic and trichloroethylene removal capabilities of iron (hydr)oxide nanoparticle-impregnated granulated activated carbons, J. Hazard. Mater. 183 (2010) 381–388. https://doi.org/10.1016/j.jhazmat.2010.07.036.

[70] J. Wang, Z. Chen, B. Chen, Adsorption of polycyclic aromatic hydrocarbons by graphene and graphene oxide nanosheets, Environ. Sci. Technol. 48 (2014) 4817–4825. https://doi.org/10.1021/es405227u.

[71] I. Šafařík, K. Nymburská, M. Šafaříková, Adsorption of water-soluble organic dyes on magnetic charcoal, J. Chem. Technol. Biotechnol. 69 (1997) 1–4. https://doi.org/10.1002/(SICI)1097-4660(199705)69:1<1::AID-JCTB653>3.0.CO;2-H.

[72] Y. Choi, Y. Wu, B. Sani, R.G. Luthy, D. Werner, E. Kim, Performance of retrievable activated carbons to treat sediment contaminated with polycyclic aromatic hydrocarbons, J. Hazard. Mater. 320 (2016) 359–367. https://doi.org/10.1016/j.jhazmat.2016.08.047.

[73] M. Jain, M. Yadav, T. Kohout, M. Lahtinen, V.K. Garg, M. Sillanpää, Development of iron oxide/activated carbon nanoparticle composite for the removal of Cr(VI), Cu(II) and Cd(II) ions from aqueous solution, Water Resour. Ind. 20 (2018) 54–74. https://doi.org/10.1016/j.wri.2018.10.001.

[74] L.C.A. Oliveira, R.V.R.A. Rios, J.D. Fabris, V. Garg, K. Sapag, R.M. Lago, Activated

carbon/iron oxide magnetic composites for the adsorption of contaminants in water, Carbon N. Y. 40 (2002) 2177–2183. https://doi.org/10.1016/S0008-6223(02)00076-3.

[75] X. Bao, Z. Qiang, J.H. Chang, W. Ben, J. Qu, Synthesis of carbon-coated magnetic nanocomposite (Fe3O4 at C) and its application for sulfonamide antibiotics removal from water, J. Environ. Sci. (China). 26 (2014) 962–969. https://doi.org/10.1016/S1001-0742(13)60485-4.

[76] X. Ge, Z. Wu, Z. Wu, Y. Yan, G. Cravotto, B.C. Ye, Enhanced PAHs adsorption using iron-modified coal-based activated carbon via microwave radiation, J. Taiwan Inst. Chem. Eng. 64 (2016) 235–243. https://doi.org/10.1016/j.jtice.2016.03.050.

[77] J. Ma, S. Sun, K. Chen, Facile and scalable synthesis of magnetite/carbon adsorbents by recycling discarded fruit peels and their potential usage in water treatment, Bioresour. Technol. 233 (2017) 110–115. https://doi.org/10.1016/j.biortech.2017.02.075.

[78] Z. Gong, K. Alef, B.M. Wilke, P. Li, Activated carbon adsorption of PAHs from vegetable oil used in soil remediation, J. Hazard. Mater. 143 (2007) 372–378. https://doi.org/10.1016/j.jhazmat.2006.09.037.

[79] Entegris, Isoelectric Point (IEP) Determination, 2018. (n.d.) 1–3.

[80] R.S. Juang, Y.C. Yei, C.S. Liao, K.S. Lin, H.C. Lu, S.F. Wang, A.C. Sun, Synthesis of magnetic Fe3O4/activated carbon nanocomposites with high surface area as recoverable adsorbents, J. Taiwan Inst. Chem. Eng. 90 (2018) 51–60. https://doi.org/10.1016/j.jtice.2017.12.005.

[81] J.R. Zimmerman, J.D. Bricker, C. Jones, P.J. Dacunto, R.L. Street, R.G. Luthy, The stability of marine sediments at a tidal basin in San Francisco Bay amended with activated carbon for sequestration of organic contaminants, Water Res. 42 (2008) 4133–4145. https://doi.org/10.1016/j.watres.2008.05.023.

[82] M.T.H. Siddiqui, S. Nizamuddin, H.A. Baloch, N.M. Mubarak, D.K. Dumbre, Inamuddin, A.M. Asiri, A.W. Bhutto, M. Srinivasan, G.J. Griffin, Synthesis of magnetic carbon nanocomposites by hydrothermal carbonization and pyrolysis, Environ. Chem. Lett. 16 (2018) 821–844. https://doi.org/10.1007/s10311-018-0724-9.

[83] B. D'Cruz, M. Madkour, M.O. Amin, E. Al-Hetlani, Efficient and recoverable magnetic AC-Fe3O4 nanocomposite for rapid removal of promazine from wastewater, Mater. Chem. Phys. 240 (2020). https://doi.org/10.1016/j.matchemphys.2019.122109.

[84] Y.J. Tu, G.S. Premachandra, S.A. Boyd, J.B. Sallach, H. Li, B.J. Teppen, C.T. Johnston, Synthesis and evaluation of Fe3O4-impregnated activated carbon for dioxin removal, Chemosphere. 263 (2021). https://doi.org/10.1016/j.chemosphere.2020.128263.

[85] L. Ma, Fang; Zhou, Jiahui; Guo, Haijuan; Yang, Study on preparation and adsorption properties of magnetic activated carbon, J. Harbin Inst. Technol. 48 (2016) 50–56.

[86] E.M. Pérez, N. Martín, π-π Interactions in carbon nanostructures, Chem. Soc. Rev. 44 (2015) 6425–6433. https://doi.org/10.1039/c5cs00578g.

[87] Q. Hu, J.J. Li, Z.P. Hao, L.D. Li, S.Z. Qiao, Dynamic adsorption of volatile organic compounds on organofunctionalized SBA-15 materials, Chem. Eng. J. 149 (2009) 281–288. https://doi.org/10.1016/j.cej.2008.11.003.

[88] A. Balati, A. Shahbazi, M.M. Amini, S.H. Hashemi, Adsorption of polycyclic aromatic hydrocarbons from wastewater by using silica-based organic–inorganic nanohybrid material, J. Water Reuse Desalin. 5 (2015) 50–63. https://doi.org/10.2166/wrd.2014.013.

[89] Chemsafetypro, Polycyclic-aromatic hydrocarbons (PAHs), (2016). https://www.chemsafetypro.com/Topics/EU/Polycyclic-aromatic_hydrocarbons_(PAHs)_and_REACH.html (accessed May 16, 2020).

[90] S.K. Sahu, G.G. Pandit, Estimation of octanol-water partition coefficients for polycylic aromatic hydrocarbons using reverse-phase HPLC, J. Liq. Chromatogr. Relat. Technol. 26 (2003) 135–146. https://doi.org/10.1081/JLC-120017158.

[91] M. Saeedi, Role of heavy metals and organic matter on sorption and mobility of polycyclic aromatic hydrocarbons in soil : implications for remediation, 2019.

[92] USEPA, Superfund Soil Screening Guidance - Part 5, Chemical Specific Parameters, in: Soil Screen. Guid. Tech. Backgr. Doc., 1996: pp. 133–160. https://semspub.epa.gov/work/HQ/175235.pdf.

[93] L.F. Ping, Y.M. Luo, H.B. Zhang, Q.B. Li, L.H. Wu, Distribution of polycyclic aromatic hydrocarbons in thirty typical soil profiles in the Yangtze River Delta region, east China, Environ. Pollut. 147 (2007) 358–365. https://doi.org/10.1016/j.envpol.2006.05.027.

[94] S. Hall, R. Tang, J. Baeyens, R. Dewil, Removing polycyclic aromatic hydrocarbons from water by adsorption on silicagel, Polycycl. Aromat. Compd. 29 (2009) 160–183. https://doi.org/10.1080/10406630903017534.

[95] H. Gupta, Removal of Phenanthrene from Water Using Activated Carbon Developed from

Orange Rind, Int. J. Sci. Res. Environ. Sci. 3 (2015) 248–255. https://doi.org/10.12983/ijsres-2015-p0248-0255.

[96] D. Werner, U. Ghosh, R.G. Luthy, Modeling polychlorinated biphenyl mass transfer after amendment of contaminated sediment with activated carbon, Environ. Sci. Technol. 40 (2006) 4211–4218. https://doi.org/10.1021/es052215k.

[97] P.B. McLeod, M.J. Van Den Heuvel-Greve, S.N. Luoma, R.G. Luthy, Biological uptake of polychlorinated biphenyls by Macoma balthica from sediment amended with activated carbon, Environ. Toxicol. Chem. 26 (2007) 980–987. https://doi.org/10.1897/06-278R1.1.

[98] J.R. Zimmerman, D. Werner, U. Ghosh, R.N. Millward, T.S. Bridges, R.G. Luthy, Effects of dose and particle size on activated carbon treatment to sequester polychlorinated biphenyls and polycyclic aromatic hydrocarbons in marine sediments, Environ. Toxicol. Chem. 24 (2005) 1594–1601. https://doi.org/10.1897/04-368R.1.

[99] K.M. Lompe, D. Menard, B. Barbeau, The influence of iron oxide nanoparticles upon the adsorption of organic matter on magnetic powdered activated carbon, Water Res. 123 (2017) 30–39. https://doi.org/10.1016/j.watres.2017.06.045.

[100] Z.C. Zeledón-Toruño, C. Lao-Luque, F.X.C. de las Heras, M. Sole-Sardans, Removal of PAHs from water using an immature coal (leonardite), Chemosphere. 67 (2007) 505–512. https://doi.org/10.1016/j.chemosphere.2006.09.047.

[101] G. Hu, S. Chen, W. Shi, B. Zhang, Y. Zhang, J. Huang, J. Chen, J.P. Giesy, H. Yu, Identification of polycyclic aromatic hydrocarbons in soils in Taizhou, East China, Environ. Geochem. Health. 37 (2015) 429–439. https://doi.org/10.1007/s10653-014-9656-x.

[102] E. Hiller, L. Jurkovič, M. Bartal, Effect of temperature on the distribution of polycyclic aromatic hydrocarbons in soil and sediment, Soil Water Res. 3 (2008) 231–240. https://doi.org/10.17221/28/2008-swr.

[103] H.N. Tran, Y.F. Wang, S.J. You, H.P. Chao, Insights into the mechanism of cationic dye adsorption on activated charcoal: The importance of Π–Π interactions, Process Saf. Environ. Prot. 107 (2017) 168–180. https://doi.org/10.1016/j.psep.2017.02.010.

[104] R.M. Rad, L. Omidi, H. Kakooei, F. Golbabaei, H. Hassani, R.A. Loo, K. Azam, Adsorption of Polycyclic Aromatic Hydrocarbons on Activated Carbons: Kinetic and Isotherm Curve Modeling, Int. J. Occup. Hyg. 6 (2014) 43–49.

http://ijoh.tums.ac.ir/index.php/ijoh/article/view/188.

[105] A.G. Ahangar, Sorption of PAHs in the Soil Environment with Emphasis on the Role of Soil Organic Matter: A Review, World Appl. Sci. J. 11 (2010) 759–765.

[106] Y. Wu, Y.M. Cho, R.G. Luthy, K. Kim, J. Jung, W.R. Gala, Y. Choi, Assessment of hydrophobic organic contaminant availability in sediments after sorbent amendment and its complete removal, Environ. Pollut. 231 (2017) 1380–1387. https://doi.org/10.1016/j.envpol.2017.08.117.

[107] H.I. Abdel-Shafy, M.S.M. Mansour, A review on polycyclic aromatic hydrocarbons: Source, environmental impact, effect on human health and remediation, Egypt. J. Pet. 25 (2016) 107–123. https://doi.org/10.1016/j.ejpe.2015.03.011.

[108] A.O. Adeola, P.B.C. Forbes, Influence of natural organic matter fractions on PAH sorption by stream sediments and a synthetic graphene wool adsorbent, Environ. Technol. Innov. 21 (2021) 101202. https://doi.org/10.1016/j.eti.2020.101202.

[109] N.H. AL Sbani, S.R.S. Abdullah, M. Idris, H.A. Hasan, I.A. Al-Baldawi, O.H. Jehawi, N. ‘Izzati Ismail, Remediation of PAHs-contaminated water and sand by tropical plant (Eleocharis ochrostachys) through sub-surface flow system, Environ. Technol. Innov. 20 (2020) 101044. https://doi.org/10.1016/j.eti.2020.101044.

[110] P. Wang, L. Luo, L. Ke, T. Luan, N.F.Y. Tam, Combined toxicity of polycyclic aromatic hydrocarbons and heavy metals to biochemical and antioxidant responses of free and immobilized Selenastrum capricornutum, Environ. Toxicol. Chem. 32 (2013) 673–683. https://doi.org/10.1002/etc.2090.

[111] USEPA, Deposition of Air Pollutants to the Great Waters, 2000. https://www3.epa.gov/air/oaqps/gr8water/3rdrpt/index.html.

[112] X. Liao, Z. Wu, Y. Li, J. Luo, C. Su, Enhanced degradation of polycyclic aromatic hydrocarbons by indigenous microbes combined with chemical oxidation, Chemosphere. 213 (2018) 551–558. https://doi.org/10.1016/j.chemosphere.2018.09.092.

[113] X. Man, X. an Ning, H. Zou, J. Liang, J. Sun, X. Lu, J. Sun, Removal of polycyclic aromatic hydrocarbons (PAHs) from textile dyeing sludge by ultrasound combined zero-valent iron/EDTA/Air system, Chemosphere. 191 (2018) 839–847. https://doi.org/10.1016/j.chemosphere.2017.10.043.

[114] J. Muff, E.G. Søgaard, Electrochemical degradation of PAH compounds in process water:

A kinetic study on model solutions and a proof of concept study on runoff water from harbour sediment purification, Water Sci. Technol. 61 (2010) 2043–2051. https://doi.org/10.2166/wst.2010.129.

[115] M.H. Mahmoudian, M. Fazlzadeh, M.H. Niari, A. Azari, E.C. Lima, A novel silica supported chitosan/glutaraldehyde as an efficient sorbent in solid phase extraction coupling with HPLC for the determination of Penicillin G from water and wastewater samples, Arab. J. Chem. 13 (2020) 7147–7159. https://doi.org/10.1016/j.arabjc.2020.07.020.

[116] A. Azari, M. Yeganeh, M. Gholami, M. Salari, The superior adsorption capacity of 2,4-Dinitrophenol under ultrasound-assisted magnetic adsorption system: Modeling and process optimization by central composite design, J. Hazard. Mater. 418 (2021) 126348. https://doi.org/10.1016/j.jhazmat.2021.126348.

[117] Y. Rashtbari, S. Hazrati, A. Azari, S. Afshin, M. Fazlzadeh, M. Vosoughi, A novel, eco-friendly and green synthesis of PPAC-ZnO and PPAC-nZVI nanocomposite using pomegranate peel: Cephalexin adsorption experiments, mechanisms, isotherms and kinetics, Adv. Powder Technol. 31 (2020) 1612–1623. https://doi.org/10.1016/j.apt.2020.02.001.

[118] M. Yegane Badi, A. Azari, H. Pasalari, A. Esrafili, M. Farzadkia, Modification of activated carbon with magnetic Fe3O4 nanoparticle composite for removal of ceftriaxone from aquatic solutions, J. Mol. Liq. 261 (2018) 146–154. https://doi.org/10.1016/j.molliq.2018.04.019.

[119] A. Azari, R. Nabizadeh, A.H. Mahvi, S. Nasseri, Magnetic multi-walled carbon nanotubes-loaded alginate for treatment of industrial dye manufacturing effluent: adsorption modelling and process optimisation by central composite face-central design, Int. J. Environ. Anal. Chem. 00 (2021) 1–21. https://doi.org/10.1080/03067319.2021.1877279.

[120] S. Li, U. Turaga, B. Shrestha, T.A. Anderson, S.S. Ramkumar, M.J. Green, S. Das, J.E. Cañas-Carrell, Mobility of polyaromatic hydrocarbons (PAHs) in soil in the presence of carbon nanotubes, Ecotoxicol. Environ. Saf. 96 (2013) 168–174. https://doi.org/10.1016/j.ecoenv.2013.07.005.

[121] M. Yuan, S. Tong, S. Zhao, C.Q. Jia, Adsorption of polycyclic aromatic hydrocarbons

from water using petroleum coke-derived porous carbon, J. Hazard. Mater. 181 (2010) 1115–1120. https://doi.org/10.1016/j.jhazmat.2010.05.130.

[122] X. Xiao, D. Liu, Y. Yan, Z. Wu, Z. Wu, G. Cravotto, Preparation of activated carbon from Xinjiang region coal by microwave activation and its application in naphthalene, phenanthrene, and pyrene adsorption, J. Taiwan Inst. Chem. Eng. 53 (2015) 160–167. https://doi.org/10.1016/j.jtice.2015.02.031.

[123] S. Nethaji, A. Sivasamy, A.B. Mandal, Preparation and characterization of corn cob activated carbon coated with nano-sized magnetite particles for the removal of Cr(VI), Bioresour. Technol. 134 (2013) 94–100. https://doi.org/10.1016/j.biortech.2013.02.012.

[124] F. Yazdani, M. Seddigh, Magnetite nanoparticles synthesized by co-precipitation method: The effects of various iron anions on specifications, Mater. Chem. Phys. 184 (2016) 318–323. https://doi.org/10.1016/j.matchemphys.2016.09.058.

[125] W.P. Ball, P. V. Roberts, Long-Term Sorption of Halogenated Organic Chemicals by Aquifer Material. 1. Equilibrium, Environ. Sci. Technol. 25 (1991) 1223–1237. https://doi.org/10.1021/es00019a002.

[126] USEPA, Ultrasonic Extraction, in: Method 3550b, 1996: pp. 1–14.

[127] USEPA, Solid Phase Extraction of Polynuclear Aromatic Hydrocarbons (PAHs) in Water, in: Clim. Change, 1986: pp. 123–128.

[128] Z. Xie, W. Guan, F. Ji, Z. Song, Y. Zhao, Production of biologically activated carbon from orange peel and landfill leachate subsequent treatment technology, J. Chem. 2014 (2014). https://doi.org/10.1155/2014/491912.

[129] J.A.S. Costa, R.A. de Jesus, C.M.P. da Silva, L.P.C. Romão, Efficient adsorption of a mixture of polycyclic aromatic hydrocarbons (PAHs) by Si–MCM–41 mesoporous molecular sieve, Powder Technol. 308 (2017) 434–441. https://doi.org/10.1016/j.powtec.2016.12.035.

[130] C. Di Dong, C.W. Chen, C.M. Kao, C.C. Chien, C.M. Hung, Wood-biochar-supported magnetite nanoparticles for remediation of PAH-contaminated estuary sediment, Catalysts. 8 (2018) 1–13. https://doi.org/10.3390/catal8020073.

[131] H. Yu, H. Xiao, D. Wang, Effects of soil properties and biosurfactant on the behavior of PAHs in soil-water systems, Environ. Syst. Res. 3 (2014) 6. https://doi.org/10.1186/2193-2697-3-6.

[132] F. Wang, J.J.H. Haftka, T.L. Sinnige, J.L.M. Hermens, W. Chen, Adsorption of polar, nonpolar, and substituted aromatics to colloidal graphene oxide nanoparticles, Environ. Pollut. 186 (2014) 226–233. https://doi.org/10.1016/j.envpol.2013.12.010.

[133] K.D. Hristovski, P.K. Westerhoff, T. Möller, P. Sylvester, Effect of synthesis conditions on nano-iron (hydr)oxide impregnated granulated activated carbon, Chem. Eng. J. 146 (2009) 237–243. https://doi.org/10.1016/j.cej.2008.05.040.

[134] H. Li, R. Qu, C. Li, W. Guo, X. Han, F. He, Y. Ma, B. Xing, Selective removal of polycyclic aromatic hydrocarbons (PAHs) from soil washing effluents using biochars produced at different pyrolytic temperatures, Bioresour. Technol. 163 (2014) 193–198. https://doi.org/10.1016/j.biortech.2014.04.042.

[135] M.À. Olivella, P. Jové, A. Oliveras, The use of cork waste as a biosorbent for persistent organic pollutants-Study of adsorption/desorption of polycyclic aromatic hydrocarbons, J. Environ. Sci. Heal. - Part A Toxic/Hazardous Subst. Environ. Eng. 46 (2011) 824–832. https://doi.org/10.1080/10934529.2011.579845.

[136] J.A. Kumar, D.J. Amarnath, S. Sathish, S.A. Jabasingh, A. Saravanan, R. V. Hemavathy, K.V. Anand, P.R. Yaashikaa, Enhanced PAHs removal using pyrolysis-assisted potassium hydroxide induced palm shell activated carbon: Batch and column investigation, J. Mol. Liq. 279 (2019) 77–87. https://doi.org/10.1016/j.molliq.2019.01.121.

[137] D. Eeshwarasinghe, P. Loganathan, M. Kalaruban, D.P. Sounthararajah, J. Kandasamy, S. Vigneswaran, Removing polycyclic aromatic hydrocarbons from water using granular activated carbon: kinetic and equilibrium adsorption studies, Environ. Sci. Pollut. Res. 25 (2018) 13511–13524. https://doi.org/10.1007/s11356-018-1518-0.

[138] Q. Wang, H. Li, K. Feng, Effect of honeycomb, granular, and powder activated carbon additives on continuous lactic acid fermentation of complex food waste with mixed inoculation, J. Biosci. Bioeng. xxx (2021). https://doi.org/10.1016/j.jbiosc.2021.02.009.

[139] M. Izawa, M. Sakai, J.F. Mori, R.A. Kanaly, Cometabolic benzo[a]pyrene biotransformation by Sphingobium barthaii KK22 proceeds through the kata-annelated ring and 1-pyrenecarboxylic acid to downstream products., J. Hazard. Mater. Adv. 4 (2021) 100018. https://doi.org/10.1016/j.hazadv.2021.100018.

[140] J. Zhai, I.T. Burke, D.I. Stewart, Potential reuse options for biomass combustion ash as affected by the persistent organic pollutants (POPs) content, J. Hazard. Mater. Adv. 5

(2022) 100038. https://doi.org/10.1016/j.hazadv.2021.100038.

[141] H. Cheng, Y. Bian, F. Wang, X. Jiang, R. Ji, C. Gu, X. Yang, Y. Song, Green conversion of crop residues into porous carbons and their application to efficiently remove polycyclic aromatic hydrocarbons from water: Sorption kinetics, isotherms and mechanism, Bioresour. Technol. 284 (2019) 1–8. https://doi.org/10.1016/j.biortech.2019.03.104.

[142] C.G. Okoli, D.H. Ogbuagu, C.L. Gilbert, S. Madu, R.F. Njoku-Tony, Proximal Input of Polynuclear Aromatic Hydrocarbons (PAHs) in Groundwater Sources of Okrika Mainland, Nigeria, J. Environ. Prot. (Irvine,. Calif). 02 (2011) 848–854. https://doi.org/10.4236/jep.2011.26096.

[143] D.L. Diggs, A.C. Huderson, K.L. Harris, J.N. Myers, L.D. Banks, P. V. Rekhadevi, M.S. Niaz, A. Ramesh, Polycyclic aromatic hydrocarbons and digestive tract cancers: A perspective, J. Environ. Sci. Heal. - Part C Environ. Carcinog. Ecotoxicol. Rev. 29 (2011) 324–357. https://doi.org/10.1080/10590501.2011.629974.

[144] Y. Meng, X. Liu, S. Lu, T. Zhang, B. Jin, Q. Wang, Z. Tang, Y. Liu, X. Guo, J. Zhou, B. Xi, A review on occurrence and risk of polycyclic aromatic hydrocarbons (PAHs) in lakes of China, Sci. Total Environ. 651 (2019) 2497–2506. https://doi.org/10.1016/j.scitotenv.2018.10.162.

[145] J. Wang, J. Wang, Z. Zhao, J. Chen, H. Lu, G. Liu, J. Zhou, X. Guan, PAHs accelerate the propagation of antibiotic resistance genes in coastal water microbial community, Environ. Pollut. 231 (2017) 1145–1152. https://doi.org/10.1016/j.envpol.2017.07.067.

[146] P.P. Falciglia, G. De Guidi, A. Catalfo, F.G.A. Vagliasindi, Remediation of soils contaminated with PAHs and nitro-PAHs using microwave irradiation, Chem. Eng. J. 296 (2016) 162–172. https://doi.org/10.1016/j.cej.2016.03.099.

[147] H. Ajab, M.H. Isa, A. Yaqub, Electrochemical oxidation using Ti/RuO2 anode for COD and PAHs removal from aqueous solution, Sustain. Mater. Technol. 26 (2020) e00225. https://doi.org/10.1016/j.susmat.2020.e00225.

[148] E. Hamann, P.J. Stuyfzand, J. Greskowiak, H. Timmer, G. Massmann, The fate of organic micropollutants during long-term/long-distance river bank filtration, Sci. Total Environ. 545–546 (2016) 629–640. https://doi.org/10.1016/j.scitotenv.2015.12.057.

[149] S.S. Lam, R.K. Liew, Y.M. Wong, P.N.Y. Yek, N.L. Ma, C.L. Lee, H.A. Chase, Microwave-assisted pyrolysis with chemical activation, an innovative method to convert

orange peel into activated carbon with improved properties as dye adsorbent, J. Clean. Prod. 162 (2017) 1376–1387. https://doi.org/10.1016/j.jclepro.2017.06.131.

[150] M.B. Ahmed, J.L. Zhou, H.H. Ngo, W. Guo, N.S. Thomaidis, J. Xu, Progress in the biological and chemical treatment technologies for emerging contaminant removal from wastewater: A critical review, J. Hazard. Mater. 323 (2017) 274–298. https://doi.org/10.1016/j.jhazmat.2016.04.045.

[151] R.A. Solano, L.D. De León, G. De Ávila, A.P. Herrera, Polycyclic aromatic hydrocarbons (PAHs) adsorption from aqueous solution using chitosan beads modified with thiourea, TiO2 and Fe3O4 nanoparticles, Environ. Technol. Innov. 21 (2021) 101378. https://doi.org/10.1016/j.eti.2021.101378.

[152] L. Ai, Y. Zhou, J. Jiang, Removal of methylene blue from aqueous solution by montmorillonite/CoFe2O4 composite with magnetic separation performance, Desalination. 266 (2011) 72–77. https://doi.org/10.1016/j.desal.2010.08.004.

[153] E. Mirzaee, M. Sartaj, Synthesis and evaluation of recoverable activated carbon/Fe3O4 composites for removal of polycyclic aromatic hydrocarbons from aqueous solution, Environ. Technol. Innov. 25 (2021) 102174. https://doi.org/10.1016/j.eti.2021.102174.

[154] J. Zhang, R. Li, G. Ding, Y. Wang, C. Wang, Sorptive removal of phenanthrene from water by magnetic carbon nanomaterials, J. Mol. Liq. 293 (2019) 111540. https://doi.org/10.1016/j.molliq.2019.111540.

[155] B.S. Inbaraj, K. Sridhar, B.H. Chen, Removal of polycyclic aromatic hydrocarbons from water by magnetic activated carbon nanocomposite from green tea waste, J. Hazard. Mater. 415 (2021) 125701. https://doi.org/10.1016/j.jhazmat.2021.125701.

[156] R. Crisafully, M.A.L. Milhome, R.M. Cavalcante, E.R. Silveira, D. De Keukeleire, R.F. Nascimento, Removal of some polycyclic aromatic hydrocarbons from petrochemical wastewater using low-cost adsorbents of natural origin, Bioresour. Technol. 99 (2008) 4515–4519. https://doi.org/10.1016/j.biortech.2007.08.041.

[157] C.B. Vidal, A.L. Barros, C.P. Moura, A.C.A. de Lima, F.S. Dias, L.C.G. Vasconcellos, P.B.A. Fechine, R.F. Nascimento, Adsorption of polycyclic aromatic hydrocarbons from aqueous solutions by modified periodic mesoporous organosilica, J. Colloid Interface Sci. 357 (2011) 466–473. https://doi.org/10.1016/j.jcis.2011.02.013.

[158] A. Babakhani, M. Sartaj, Removal of Cadmium (II) from aqueous solution using

tripolyphosphate cross-linked chitosan, J. Environ. Chem. Eng. 8 (2020) 103842. https://doi.org/10.1016/j.jece.2020.103842.

[159] T.A. Khan, S.A. Chaudhry, I. Ali, Equilibrium uptake, isotherm and kinetic studies of Cd(II) adsorption onto iron oxide activated red mud from aqueous solution, J. Mol. Liq. 202 (2015) 165–175. https://doi.org/10.1016/j.molliq.2014.12.021.

[160] R. Black, M. Sartaj, A. Mohammadian, H.A.M. Qiblawey, Biosorption of Pb and Cu using fixed and suspended bacteria, J. Environ. Chem. Eng. 2 (2014) 1663–1671. https://doi.org/10.1016/j.jece.2014.05.023.

[161] A. Mirahsani, J.B. Giorgi, M. Sartaj, Ammonia removal from aqueous solution by sodium functionalized graphene oxide: Isotherm, kinetics, and thermodynamics, Desalin. Water Treat. 178 (2020) 143–154. https://doi.org/10.5004/dwt.2020.24961.

[162] N. Ayawei, A.N. Ebelegi, D. Wankasi, Modelling and Interpretation of Adsorption Isotherms, J. Chem. 2017 (2017). https://doi.org/10.1155/2017/3039817.

[163] J.S. Piccin, G.L. Dotto, M.L.G. Vieira, L.A.A. Pinto, Kinetics and mechanism of the food dye FD&C Red 40 adsorption onto chitosan, J. Chem. Eng. Data. 56 (2011) 3759–3765. https://doi.org/10.1021/je200388s.

[164] T.R. Sahoo, B. Prelot, Adsorption processes for the removal of contaminants from wastewater, Elsevier Inc., 2020. https://doi.org/10.1016/b978-0-12-818489-9.00007-4.

[165] P. SenthilKumar, S. Ramalingam, V. Sathyaselvabala, S.D. Kirupha, S. Sivanesan, Removal of copper(II) ions from aqueous solution by adsorption using cashew nut shell, Desalination. 266 (2011) 63–71. https://doi.org/10.1016/j.desal.2010.08.003.

[166] K. Yang, L. Zhu, B. Xing, Adsorption of polycyclic aromatic hydrocarbons by carbon nanomaterials, Environ. Sci. Technol. 40 (2006) 1855–1861. https://doi.org/10.1021/es052208w.

[167] Z. Wu, Z. Sun, P. Liu, Q. Li, R. Yang, X. Yang, Competitive adsorption of naphthalene and phenanthrene on walnut shell based activated carbon and the verification: Via theoretical calculation, RSC Adv. 10 (2020) 10703–10714. https://doi.org/10.1039/c9ra09447d.

[168] J. Wang, Q. Zhang, H. Yang, C. Qiao, Adsorptive Desulfurization of Organic Sulfur from Model Fuels by Active Carbon Supported Mn (II): Equilibrium, Kinetics, and Thermodynamics, Int. J. Chem. Eng. 2020 (2020). https://doi.org/10.1155/2020/2813946.

[169] H.A. Mahgoub, Extraction Techniques for Determination of Polycyclic Aromatic Hydrocarbons in Water Samples, Int. J. Sci. Res. 5 (2016) 268–272. https://doi.org/10.21275/v5i1.nov152648.

[170] Y. Ao, J. Xu, D. Fu, C. Yuan, A simple route for the preparation of anatase titania-coated magnetic porous carbons with enhanced photocatalytic activity, Carbon N. Y. 46 (2008) 596–603. https://doi.org/10.1016/j.carbon.2008.01.009.

[171] M. Thommes, K. Kaneko, A. V. Neimark, J.P. Olivier, F. Rodriguez-Reinoso, J. Rouquerol, K.S.W. Sing, Physisorption of gases, with special reference to the evaluation of surface area and pore size distribution (IUPAC Technical Report), Pure Appl. Chem. 87 (2015) 1051–1069. https://doi.org/10.1515/pac-2014-1117.

[172] H.S. Park, J.R. Koduru, K.H. Choo, B. Lee, Activated carbons impregnated with iron oxide nanoparticles for enhanced removal of bisphenol A and natural organic matter, J. Hazard. Mater. 286 (2015) 315–324. https://doi.org/10.1016/j.jhazmat.2014.11.012.

[173] S. Kim, J. Kim, G. Seo, Iron oxide nanoparticle-impregnated powder-activated carbon (IPAC) for NOM removal in MF membrane water treatment system, Desalin. Water Treat. 51 (2013) 6392–6400. https://www.tandfonline.com/doi/full/10.1080/19443994.2013.781000?scroll=top&needAccess=true.

[174] M. Zahoor, No Title, Desalin. Water Treat. 52 (2014) 7983–7992. https://www.tandfonline.com/doi/abs/10.1080/19443994.2013.855885.

[175] C. Valderrama, X. Gamisans, X. de las Heras, A. Farrán, J.L. Cortina, Sorption kinetics of polycyclic aromatic hydrocarbons removal using granular activated carbon: Intraparticle diffusion coefficients, J. Hazard. Mater. 157 (2008) 386–396. https://doi.org/10.1016/j.jhazmat.2007.12.119.

[176] Y.S. Ho, G. McKay, Sorption of dye from aqueous solution by peat, Chem. Eng. J. 70 (1998) 115–124. https://doi.org/10.1016/S1385-8947(98)00076-X.

[177] M. Haro, B. Cabal, J.B. Parra, C.O. Ania, On the adsorption kinetics and equilibrium of polyaromatic hydrocarbons from aqueous solution, Adsorpt. Sci. Technol. 29 (2011) 467–478. https://doi.org/10.1260/0263-6174.29.5.467.

[178] M. El Khames Saad, R. Khiari, E. Elaloui, Y. Moussaoui, Adsorption of anthracene using activated carbon and Posidonia oceanica, Arab. J. Chem. 7 (2014) 109–113.

https://doi.org/10.1016/j.arabjc.2013.11.002.

[179] S.M. Yakout, A.A.M. Daifullah, S.A. El-Reefy, Adsorption of naphthalene, phenanthrene and pyrene from aqueous solution using low-cost activated carbon derived from agricultural wastes, Adsorpt. Sci. Technol. 31 (2013) 293–302. https://doi.org/10.1260/0263-6174.31.4.293.

[180] L. Anah, N. Astrini, Isotherm adsorption studies of Ni(II) ion removal from aqueous solutions by modified carboxymethyl cellulose hydrogel, IOP Conf. Ser. Earth Environ. Sci. 160 (2018). https://doi.org/10.1088/1755-1315/160/1/012017.

[181] R. Rusmin, B. Sarkar, Y. Liu, S. McClure, R. Naidu, Structural evolution of chitosan-palygorskite composites and removal of aqueous lead by composite beads, Appl. Surf. Sci. 353 (2015) 363–375. https://doi.org/10.1016/j.apsusc.2015.06.124.

[182] S.A. Younis, N.S. El-Gendy, W.I. El-Azab, Y.M. Moustafa, Kinetic, isotherm, and thermodynamic studies of polycyclic aromatic hydrocarbons biosorption from petroleum refinery wastewater using spent waste biomass, Desalin. Water Treat. 56 (2015) 3013–3023. https://doi.org/10.1080/19443994.2014.964331.

[183] M.I. Rakowska, D. Kupryianchyk, T. Grotenhuis, H.H.M. Rijnaarts, A.A. Koelmans, Extraction of sediment-associated polycyclic aromatic hydrocarbons with granular activated carbon, Environ. Toxicol. Chem. 32 (2013) 304–311. https://doi.org/10.1002/etc.2066.

[184] J. Lemaire, V. Mora, P. Faure, K. Hanna, M. Buès, M.O. Simonnot, Chemical oxidation efficiency for aged, PAH-contaminated sites: An investigation of limiting factors, J. Environ. Chem. Eng. 7 (2019). https://doi.org/10.1016/j.jece.2019.103061.

[185] R. Wang, Q. Huang, J. Cai, J. Wang, Seasonal variations of atmospheric polycyclic aromatic hydrocarbons (PAHs) surrounding Chaohu Lake, China: Source, partitioning behavior, and lung cancer risk, Atmos. Pollut. Res. 12 (2021) 101056. https://doi.org/10.1016/j.apr.2021.101056.

[186] P.A. Alaba, N.A. Oladoja, Y.M. Sani, O.B. Ayodele, I.Y. Mohammed, S.F. Olupinla, W.M.W. Daud, Insight into wastewater decontamination using polymeric adsorbents, J. Environ. Chem. Eng. 6 (2018) 1651–1672. https://doi.org/10.1016/j.jece.2018.02.019.

[187] A.B. Patel, S. Shaikh, K.R. Jain, C. Desai, D. Madamwar, Polycyclic Aromatic Hydrocarbons: Sources, Toxicity, and Remediation Approaches, Front. Microbiol. 11

(2020). https://doi.org/10.3389/fmicb.2020.562813.

[188] S.R. Barman, P. Das, A. Mukhopadhayay, Biochar from waste Sterculia foetida and its application as adsorbent for the treatment of PAH compounds: Batch and optimization, Fuel. 306 (2021) 121623. https://doi.org/10.1016/j.fuel.2021.121623.

[189] J.J. Liu, X.C. Wang, B. Fan, Characteristics of PAHs adsorption on inorganic particles and activated sludge in domestic wastewater treatment, Bioresour. Technol. 102 (2011) 5305–5311. https://doi.org/10.1016/j.biortech.2010.12.063.

[190] M.A. Al-Ghouti, D.A. Da'ana, Guidelines for the use and interpretation of adsorption isotherm models: A review, J. Hazard. Mater. 393 (2020) 122383. https://doi.org/10.1016/j.jhazmat.2020.122383.

[191] D. A.O, Langmuir, Freundlich, Temkin and Dubinin–Radushkevich Isotherms Studies of Equilibrium Sorption of Zn 2+ Unto Phosphoric Acid Modified Rice Husk, IOSR J. Appl. Chem. 3 (2012) 38–45. https://doi.org/10.9790/5736-0313845.

[192] F. Togue Kamga, Modeling adsorption mechanism of paraquat onto Ayous (Triplochiton scleroxylon) wood sawdust, Appl. Water Sci. 9 (2019) 1–7. https://doi.org/10.1007/s13201-018-0879-3.

[193] A. Papadopoulou, I.P. Román, A. Canals, K. Tyrovola, E. Psillakis, Fast screening of perfluorooctane sulfonate in water using vortex-assisted liquid-liquid microextraction coupled to liquid chromatography-mass spectrometry, Anal. Chim. Acta. 691 (2011) 56–61. https://doi.org/10.1016/j.aca.2011.02.043.

[194] M. Ye, M. Sun, F.O. Kengara, J. Wang, N. Ni, L. Wang, Y. Song, X. Yang, H. Li, F. Hu, X. Jiang, Evaluation of soil washing process with carboxymethyl-β-cyclodextrin and carboxymethyl chitosan for recovery of PAHs/heavy metals/fluorine from metallurgic plant site, J. Environ. Sci. (China). 26 (2014) 1661–1672. https://doi.org/10.1016/j.jes.2014.06.006.

[195] Z. Zou, R. Qiu, W. Zhang, H. Dong, Z. Zhao, T. Zhang, X. Wei, X. Cai, The study of operating variables in soil washing with EDTA, Environ. Pollut. 157 (2009) 229–236. https://doi.org/10.1016/j.envpol.2008.07.009.

[196] C. Wang, L. Zhu, C. Zhang, A new speciation scheme of soil polycyclic aromatic hydrocarbons for risk assessment, J. Soils Sediments. 15 (2015) 1139–1149. https://doi.org/10.1007/s11368-015-1083-9.

[197] E. Mousset, D. Huguenot, E.D. Van Hullebusch, N. Oturan, G. Guibaud, G. Esposito, M.A. Oturan, Impact of electrochemical treatment of soil washing solution on PAH degradation efficiency and soil respirometry, Environ. Pollut. 211 (2016) 354–362. https://doi.org/10.1016/j.envpol.2016.01.021.

[198] T.C. Egbosiuba, A.S. Abdulkareem, A.S. Kovo, E.A. Afolabi, J.O. Tijani, M. Auta, W.D. Roos, Ultrasonic enhanced adsorption of methylene blue onto the optimized surface area of activated carbon: Adsorption isotherm, kinetics and thermodynamics, Chem. Eng. Res. Des. 153 (2020) 315–336. https://doi.org/10.1016/j.cherd.2019.10.016.

[199] S. Cheng, L. Zhang, H. Xia, J. Peng, J. Shu, C. Li, X. Jiang, Q. Zhang, Adsorption behavior of methylene blue onto waste-derived adsorbent and exhaust gases recycling, RSC Adv. 7 (2017) 27331–27341. https://doi.org/10.1039/c7ra01482a.

[200] C.H. Marvin, A. Berthiaume, D.A. Burniston, L. Chibwe, A. Dove, M. Evans, L.M. Hewitt, P. V. Hodson, D.C.G. Muir, J. Parrott, P.J. Thomas, G.T. Tomy, Polycyclic aromatic compounds in the Canadian Environment: Aquatic and terrestrial environments, Environ. Pollut. 285 (2021) 117442. https://doi.org/10.1016/j.envpol.2021.117442.

[201] J. Ding, J. Cong, J. Zhuo, S. Gao, Polycyclic aromatic hydrocarbon biodegradation and extracellular enzyme secretion in agitated and stationary cultures of Phanerochaete chrysosporium, J. Environ. Sci. 20 (2008) 88–93. https://doi.org/10.1016/S1001-0742(08)60013-3.

[202] F. Gomez, M. Sartaj, Field scale ex-situ bioremediation of petroleum contaminated soil under cold climate conditions, Int. Biodeterior. Biodegrad. 85 (2013) 375–382. https://doi.org/10.1016/j.ibiod.2013.08.003.

[203] F. Gomez, M. Sartaj, Optimization of field scale biopiles for bioremediation of petroleum hydrocarbon contaminated soil at low temperature conditions by response surface methodology (RSM), Int. Biodeterior. Biodegrad. 89 (2014) 103–109. https://doi.org/10.1016/j.ibiod.2014.01.010.

[204] E. Mirzaee, S. Gitipour, M. Mousavi, S. Amini, Optimization of total petroleum hydrocarbons removal from Mahshahr contaminated soil using magnetite nanoparticle catalyzed Fenton-like oxidation, Environ. Earth Sci. 76 (2017). https://doi.org/10.1007/s12665-017-6484-1.

[205] A.A. Befkadu, Q. Chen, Surfactant-Enhanced Soil Washing for Removal of Petroleum

Hydrocarbons from Contaminated Soils: A Review, Pedosphere. 28 (2018) 383–410. https://doi.org/10.1016/S1002-0160(18)60027-X.

[206] R. López-Vizcaíno, C. Sáez, P. Cañizares, M.A. Rodrigo, The use of a combined process of surfactant-aided soil washing and coagulation for PAH-contaminated soils treatment, Sep. Purif. Technol. 88 (2012) 46–51. https://doi.org/10.1016/j.seppur.2011.11.038.

[207] USEPA, Compendium of Methods for the Determination of Toxic Organic Compounds in Ambient Air, Compendium Method TO-13A: Determination of Polycyclic Aromatic Hydrocarbons (PAHs) in Ambient Air Using Gas Chromatography/Mass Spectrometry (GC/MS), Cent. Environ. Res. Inf. Off. Res. Dev. U.S. Environ. Prot. Agency Cincinnati, OH 45268. II (1999) 78.

[208] J. Liu, J. Chen, L. Jiang, X. Yin, Adsorption of mixed polycyclic aromatic hydrocarbons in surfactant solutions by activated carbon, J. Ind. Eng. Chem. 20 (2014) 616–623. https://doi.org/10.1016/j.jiec.2013.05.024.

[209] Q. Hu, Z. Zhang, Application of Dubinin–Radushkevich isotherm model at the solid/solution interface: A theoretical analysis, J. Mol. Liq. 277 (2019) 646–648. https://doi.org/10.1016/j.molliq.2019.01.005.

[210] M. Lončarski, V. Gvoić, M. Prica, L. Cveticanin, J. Agbaba, A. Tubić, Sorption behavior of polycyclic aromatic hydrocarbons on biodegradable polylactic acid and various nondegradable microplastics: Model fitting and mechanism analysis, Sci. Total Environ. 785 (2021). https://doi.org/10.1016/j.scitotenv.2021.147289.

[211] E.M. Nigri, A. Bhatnagar, S.D.F. Rocha, Thermal regeneration process of bone char used in the fluoride removal from aqueous solution, J. Clean. Prod. 142 (2017) 3558–3570. https://doi.org/10.1016/j.jclepro.2016.10.112.

[212] S.J. Tshemese, W. Mhike, S.M. Tichapondwa, Adsorption of phenol and chromium (VI) from aqueous solution using exfoliated graphite: Equilibrium, kinetics and thermodynamic studies, Arab. J. Chem. 14 (2021) 103160. https://doi.org/10.1016/j.arabjc.2021.103160.

[213] S. Yurdakal, C. Garlisi, L. Özcan, M. Bellardita, G. Palmisano, (Photo)catalyst characterization techniques: Adsorption isotherms and BET, SEM, FTIR, UV-Vis, photoluminescence, and electrochemical characterizations, 2019. https://doi.org/10.1016/B978-0-444-64015-4.00004-3.

[214] K.S.W. Sing, R.T. Williams, Physisorption hysteresis loops and the characterization of

nanoporous materials, Adsorpt. Sci. Technol. 22 (2004) 773–782. https://doi.org/10.1260/0263617053499032.

[215] K.S.W. Sing, D.H. Everett, R.A.W. Haul, L. Moscou, R.A. Pierotti, J. Rouquerol, T. Siemieniewska, Reporting Physisorption Data for Gas/Solid Systems with Special Reference to the Determination of Surface Area and Porosity, Pure Appl. Chem. 57 (1985) 603–619. https://doi.org/10.1351/pac198557040603.

[216] A. Amani, P. York, H. De Waard, J. Anwar, Molecular dynamics simulation of a polysorbate 80 micelle in water, Soft Matter. 7 (2011) 2900–2908. https://doi.org/10.1039/c0sm00965b.

[217] Z.S. Liu, M.Y. Wey, C.L. Lin, Simultaneous control of acid gases and PAHs using a spray dryer combined with a fabric filter using different additives, J. Hazard. Mater. 91 (2002) 129–141. https://doi.org/10.1016/S0304-3894(01)00380-6.

[218] Z.-S. Liu, Control of PAHs from Incineration by Activated Carbon Fibers, J. Environ. Eng. 132 (2006) 463–469. https://doi.org/10.1061/(asce)0733-9372(2006)132:5(463).

[219] M. Mortazavi, M. Baghdadi, N.H. Seyed Javadi, A. Torabian, The black beads produced by simultaneous thermal reducing and chemical bonding of graphene oxide on the surface of amino-functionalized sand particles: Application for PAHs removal from contaminated waters, J. Water Process Eng. 31 (2019) 100798. https://doi.org/10.1016/j.jwpe.2019.100798.

[220] S. Wu, F. Liang, D. Hu, H. Li, W. Yang, Q. Zhu, Determining the Critical Micelle Concentration of Surfactants by a Simple and Fast Titration Method, Anal. Chem. 92 (2020) 4259–4265. https://doi.org/10.1021/acs.analchem.9b04638.

[221] M. Ishiguro, L.K. Koopal, Surfactant adsorption to soil components and soils, Adv. Colloid Interface Sci. 231 (2016) 59–102. https://doi.org/10.1016/j.cis.2016.01.006.

[222] K. Urum, T. Pekdemir, M. Çopur, Surfactants treatment of crude oil contaminated soils, J. Colloid Interface Sci. 276 (2004) 456–464. https://doi.org/10.1016/j.jcis.2004.03.057.

[223] M.S. Kuyukina, I.B. Ivshina, S.O. Makarov, L. V. Litvinenko, C.J. Cunningham, J.C. Philp, Effect of biosurfactants on crude oil desorption and mobilization in a soil system, Environ. Int. 31 (2005) 155–161. https://doi.org/10.1016/j.envint.2004.09.009.

[224] G. Newcombe, M. Drikas, R. Hayes, Influence of characterised natural organic material on activated carbon adsorption: II. Effect on pore volume distribution and adsorption of 2-

methylisoborneol, Water Res. 31 (1997) 1065–1073. https://doi.org/10.1016/S0043-1354(96)00325-9.

[225] J.E. Kilduff, A. Wigton, Sorption of TCE by humic-preloaded activated carbon: Incorporating size- exclusion and pore blockage phenomena in a competitive adsorption model, Environ. Sci. Technol. 33 (1999) 250–256. https://doi.org/10.1021/es980321z.